CORSO DI DOTTORATO DI RICERCA IN ELETTRONICA APPLICATA

XXXII CICLO DEL CORSO DI DOTTORATO

NEW INSTRUMENTAL APPROACHES FOR QUANTITATIVE ASSESSMENT OF BIOMECHANICAL RISK IN OCCUPATIONAL FIELD

PhD Student: Tiwana Varrecchia

Tutors:
Prof.ssa Silvia Conforto
Prof. Maurizio Schmid

Coordinator: Prof. Enrico Silva

ABSTRACT

This PhD project deals with the study of new instrumental approaches for quantitative assessment of biomechanical risk in occupational field.

Worker health is an issue of fundamental importance in the ergonomic field: it is a duty to protect and guarantee the health of workers, in particular those exposed to occupational risk factors. In this context, of particular interest are the work-related musculoskeletal disorders (WMSDs) which represent the most common disorder in the occupational field and the main cause of absence from work in the industrialized world. During my PhD work I focused on two main groups of WMSDs: work-related low-back disorders (WLBDs), mainly caused by manual lifting tasks, and work-related neck and upper limb disorders (WRNULDs), mainly caused by computer use and use of touch screen devices that require static neck and shoulder posture or forward head posture.

Previously, in the attempt to reduce the risk of WMSDs several methods have been developed, accepted by the international literature and used in the workplace. Specifically, regarding WLBDs, the National Institute for Occupational Safety and Health (NIOSH) published the Revised NIOSH Lifting Equation (RNLE), an approach widely used throughout the world to assess two-handed manual lifting demands but cannot be used in all work conditions. Regarding WRNULDs, there are few quantitative studies for work activities associated with use of computer and touch screen devices. Indeed, the majority of studies is founded on the questionnaire to evaluate self-reported pain, discomfort at the neck, at the shoulder and at the upper extremity and muscle fatigue due to the daily use of computer and touch screen devices.

Therefore, the risk assessment methods currently used for WLBDs and WRNULDs have different limitations that inhibit their applicability to all work activities; hence the idea of using an instrumental and quantitative approach to evaluate the biomechanical risk in any work environment

improving the risk assessment, adapting it to all the work conditions and overcoming the limits of the current standardized methods. Particularly, it is useful to introduce quantitative indices related to biomechanical risk because when the risk factors are analysed by means of quantitative methods, the possibility of identifying the relationship between pathologies and risk increases significantly. Furthermore, thanks to the technological advances that have allowed the development of miniaturized and non-invasive devices, such as the sEMG and wearable sensors, it will be possible to provide a method of assessing the biomechanical commitment applicable directly in the field without interfering with the work activity. Indeed, these devices can be performed both in the laboratory and in the workplace allowing the estimation of biomechanical risk in real-time providing a direct feedback to the end-user who would be constantly monitored directly while at work. That quantitative approach could allow to prevent and reduce the onset of these disorders but also the reintegration of workers affected by these and other disorders.

Therefore, I tried to introduce quantitative approaches to evaluate biomechanical risk of certain work activities estimating the biomechanical commitment required by these activities with a computerized multifactorial motion analysis system (kinematics, kinetics and surface electromyography) and with new methodologic approaches to analyse muscle activity of weak and noisy myoelectric signals. Thesis' results show that these instrumental approaches could be used to classify the risk. Particularly, regarding WLBDs, this thesis dealt with biomechanical risk assessment during lifting tasks, showing that kinematic features (i.e. lifitng energy consumption or jerk) and time and frequency sEMG features (max, average rectified value, mean and median frequency) have been seen significantly change in relation to the risk levels during these activities and they also correlate with spinal load variables (force and moment) in the L5-S1 region. Furthermore, the erector spinae longissimus was identified as the most sensitive trunk muscle with respect to changes in the lifting conditions. Additionally, these kinematic and sEMG features have been used as input

variables of artificial neural networks for the prediction of WLBDs during lifting tasks. This approach has been proved to be able to improve the biomechanical risk estimation suggesting that an IMU/Inertial sensor or sEMG based lifting recognition tool using these features and designed according to the revised RNLE lends itself to the estimation of biomechanical risk. These instrumental methods could be integrated with methods already used for biomechanical risk assessment (i.e. NIOSH protocol) or used when the standardized methods cannot be used due to the equation and parameters restrictions.

Moreover, my thesis' work also dealt with weak and noisy signals allowing to quantify the muscle activity during some typical work activities that cause WRNULDs (i.e. use of computer and mobile touch screen devices by office workers). Indeed, the muscles involved in these work activities are often difficult to analyse being the signals produced by these muscles weak and noisy myoelectric signals which are characterized by low amplitudes, low firing rate, low number of recruited motor units and low signal to noise ratio. Two methods tested on synthetic and semisynthetic signals were developed so highlighting the possibility to identify the muscle activation also in these conditions evaluating biomechanically some work activities that aren't evaluable with classical methods.

Therefore, the use of new innovative technologies for biomechanical risk assessment is only at its initial stage, but this process seems to be unstoppable, as it is happening in all the other areas of medicine and beyond. Obviously, it will be necessary for any validation to follow evidence-based medicine/policy/legislation multistep scientific approaches by designing rigorous laboratory and epidemiologic studies, by replicating them by independent research groups and by systematically evaluating them through transparent review processes. I am however convinced that, even if such use should fail in ergonomic practice, the huge knowledge that will derive from its experimentation

will allow the optimization of the current standardized methods or the developments of the new ones.

KEYWORDS

Work related musculoskeletal disorders (WMSDs)

Biomechanical risk assessment

Kinematics

Kinetics

Surface electromyography (sEMG)

Inertial measurement units (IMUs)

High density Surface electromyography (HD-sEMG)

PUBLICATIONS

International Journal Papers

1. Applied Science: “Lifting activity assessment using kinematic features and neural networks”; **T. Varrecchia**, C. De Marchis, F. Draicchio, M. Schmid, S. Conforto, A. Ranavolo; 2020.
2. Biomedical Signal Processing and Control: “Generalization of a wavelet-based algorithm to adaptively detect activation intervals in weak and noisy myoelectric signals”; **T. Varrecchia**, C. D'anna, M. Schmid, S. Conforto; 2020.
3. Cerebellum: “The working life of people with degenerative cerebellar ataxia”; A. Ranavolo, M. Serrao, **T. Varrecchia**, C. Casali, A. Filla, A. Roca, A. Silvetti, C. Marcotulli, B. M. Rondinone, S. Iavicoli, F. Draicchio; 2019.
4. Human Movement Science: “Common and specific gait patterns in people with varying anatomical levels of lower limb amputation and different prosthetic components”; **T. Varrecchia**, M. Serrao, M. Rinaldi, A. Ranavolo, S. Conforto, C. De Marchis, A. Simonetti, I. Poni, S. Castellano, A. Silvetti, A. Tatarelli, L. Fiori, C. Conte, F. Draicchio; 2019.
5. Biomedical Signal Processing and Control: “Using the frequency signature to detect muscular activity in weak and noisy myoelectric signals”; C. D’Anna, **T. Varrecchia**, M. Schmid, S. Conforto; 2019.
6. Journal of Electromyografy and Kinesiology: “Global lower limb muscle coactivation during walking at different speeds: relationship between spatio-temporal, kinematic, kinetic, and energetic parameters”; **T. Varrecchia**, M. Rinaldi, M. Serrao, F. Draicchio, C. Conte, S. Conforto, M. Schmid, A. Ranavolo; 2018.
7. International Journal of Environmental Research and Public Health: “Wearable Monitoring Devices for Biomechanical Risk Assessment at Work: Current Status and Future Challenges-A Systematic Review.” A. Ranavolo, F. Draicchio, **T. Varrecchia**, A. Silvetti, S. Iavicoli; 2018.
8. International Journal of Industrial Ergonomics: “Surface electromyography for risk assessment in work activities designed using the “revised NIOSH lifting equation”. A. Ranavolo, **T. Varrecchia**, S. Iavicoli, A. Marchesi, M. Rinaldi, M. Serrao, S. Conforto, M. Cesarelli, F. Draicchio; 2018.
9. European Journal of Sport Science: “Biomechanical characterization of the Junzuki karate punch: indexes of performance”; M. Rinaldi, Y. Nasr, G. Atef, F. Bini, **T. Varrecchia**, C. Conte, G. Chini, A. Ranavolo, F. Draicchio, F. Pierelli, M. Amin, F. Marinozzi, M. Serrao; 2018.
10. International Journal of Industrial Ergonomics: “Lifting activity assessment using surface electromyographic features and neural networks”; **T. Varrecchia**, C. De Marchis, M. Rinaldi, F. Draicchio, M. Serrao, M. Schmid, S. Conforto, A; 2018.
11. Clinical Biomechanics: “Increased lower limb muscle coactivation reduces gait performance and increases metabolic cost in patients with hereditary spastic paraparesis”; autori: **M. Rinaldi**, A. Ranavolo, S. Conforto, G. Martino, F. Draicchio, C. Conte, T. Varrecchia, F. Bini, C. Casali, F. Pierelli, M. Serrao; 2017.
12. Industrial Health: “Mechanical lifting energy consumption in work activities designed by means of the “revised NIOSH lifting equation”; autori: A. Ranavolo, **T. Varrecchia**, M. Rinaldi, A. Silvetti, M. Serrao, S. Conforto, F. Draicchio; 2017.
13. PLOSONE: “Gait patterns in patients with hereditary spastic paraparesis””; M. Serrao, M. Rinaldi, A. Ranavolo, F. Lacquaniti, G. Martino, L. Leonardi, C. Conte, **T. Varrecchia**, F. Draicchio, G. Coppola, C. Casali, F. Pierelli; 2016.

International Conference Papers

1. 41st Annual International Conference of the IEEE Engineering in Medicine and Biology Society (EMBC), 2019; "Wearable-based temporal parameters of gait in circuitous routes under dual-task conditions"; C. Caramia, D. Bibbo, C. D'Anna, C. De Marchis, S. Ranaldi, **T. Varrecchia**, S. Conforto, M. Schmid.
2. ISPGR 2019 Edinburgh Scotland 30 Giugno-4 Luglio 2019; "Global lower limb coactivation during gait in patients with cerebellar ataxia"; M. Serrao, L. Fiori, **T. Varrecchia**, A. Tatarelli, A. Ranavolo, F. Draicchio, C. Conte, C. Casali.
3. ISEK International Society of Electrophysiology and Kinesiology, University College Dublin, 29 Giugno-02 Luglio 2018 "Kinetic and kinematic patterns for prosthetic gait analysis"; S. Conforto, M. Serrao, **T. Varrecchia**, M. Rinaldi.
4. 2018 IEEE International Symposium on Medical Measurements & Applications, 11-13 Giugno 2018, Roma: "Effect of different smartphone uses on posture while seating and standing"; C. D'Anna, **T. Varrecchia**, D. Bibbo, F. Orsini, M. Schmid, S. Conforto.
5. 2018 IEEE International Symposium Medical Measurements & Applications, 11-13 Giugno 2018, Roma: "Muscle activity detection in pathological, weak and noisy myoelectric signals"; **T. Varrecchia**, C. D'Anna, A. Scorza, S. Andrea Sciuto, S. Conforto.
6. 8th International Conference on Applied Human Factors and Ergonomics. AHFE 2017, 17-21 Luglio 2017, California, USA: "Comparison of two post office workstation layouts by means of an optoelectronic motion analysis system"; autori: 3. A. Silvetti, A. Ranavolo, **T. Varrecchia**, M. Rinaldi, G. Chini, A. Marchesi, F. Draicchio.

National Conference Papers

1. XX Congresso SIAMOC Bologna 9-12 October 2019: "The role of trunk on human locomotion: damper, generator or perturbator?"; M. Rinaldi, **T. Varrecchia**, A. Ranavolo, F. Draicchio, S.F. Castiglia, F. Pierelli, M. Serrao.
2. XX Congresso SIAMOC Bologna 9-12 October 2019: "Artificial neural networks for staging the gait deficit in Parkinson disease"; **T. Varrecchia**, A. Ranavolo, M. Rinaldi, F. Draicchio, SF. Castiglia, F. Pierelli, C. Conte M. Serrao.
3. XX Congresso SIAMOC Bologna 9-12 October 2019: "Impairment of global lower limb muscle coactivation during walking in cerebellar ataxias"; L. Fiori, A. Ranavolo, **T. Varrecchia**, F. Draicchio, A. Tatarelli, C. Conte, C. Casali, M. Serrao.
4. XX Congresso SIAMOC Bologna 9-12 October 2019: "Gait harmonic structure of walking in patients with neurological gait disorders"; A. Tatarelli, A. Ranavolo, **T. Varrecchia**, F. Draicchio, L. Fiori, C. Conte, C. Casali, M. Iosa, M. Serrao.
5. XIX Congresso SIAMOC Firenze 3-6 Ottobre 2018; "Wearable sensor use for assessing walking dynamic balance in gait ataxia: comparisons between different stability indexes"; G. Chini, M. Serrao, A. Ranavolo, **T. Varrecchia**, C. Conte, C. Casali, F. Pierelli, F. Draicchio.
6. SIN XLIX Congresso SIN Roma, 27-30 Ottobre 2018: "The role of trunk in neurological gait disorders: damper, generator or perturbator?"; M. Rinaldi, M. Serrao, **T. Varrecchia**, C. Conte, A. Ranavolo, F. Draicchio, C. Casali, F. Pierelli.
7. SIN XLIX Congresso SIN Roma, 27-30 Ottobre 2018: "Global lower limb co-activation in patients with cerebellar ataxia"; **T. Varrecchia**, M. Serrao, L. Fiori, M. Rinaldi, A. Ranavolo, C. Conte, F. Draicchio, C. Casali, F. Pierelli.
8. SIN XLIX Congresso SIN Roma, 27-30 Ottobre 2018: "Gait harmonic structure of walking in patients with neurological gait disorders"; **T. Varrecchia**, M. Serrao, A. Tatarelli, M. Rinaldi, C. Conte, A. Ranavolo, F. Draicchio, C. Casali, F. Pierelli.

9. Sixth National Congress of Bioengineering, 25-27 Giugno 2018, Milano: “Muscle activity detection in weak and noisy myoelectric signals”; **T. Varrecchia**, C. D’Anna, M. Schmid, S. Conforto.
10. 48° Congresso SIN Napoli, 14-17 Ottobre 2017: “The working life of people with degenerative cerebellar ataxia”; **T. Varrecchia**, A. Ranavolo, C. Casali, A. Filla, A. Silvetti, F. Pirelli, M. Rinaldi, C. Conte, G. Chini, A. Roca, C. Marcotulli, F. Draicchio, M. Serrao.
11. 48° Congresso SIN Napoli, 14-17 Ottobre 2017: “Predictors of gait improvement in patients with Parkinson's disease after rehabilitation”; G. Chini, M. Serrao, G. Caramanico, M. Rinaldi, **T. Varrecchia**, C. Conte, E. Sinibaldi, G. Monari, F. Pierelli.
12. 48° Congresso SIN Napoli, 14-17 Ottobre 2017: “Increased lower limb muscle coactivation and its relationship with gait performance and metabolic cost in patients with hereditary spastic paraparesis”; M. Rinaldi, M. Serrao, A. Ranavolo, C. Conte, **T. Varrecchia**, G. Chini, C. Casali, F. Pierelli.
13. 48° Congresso SIN Napoli, 14-17 Ottobre 2017: “Trunk-lower limb coordination pattern during gait in patients with ataxia”; C. Conte, P. Caliandro, C. Iacovelli, C. Casali, A. Ranavolo, G. Chini, M. Rinaldi, **T. Varrecchia**, L. Padua, F. Pierelli, M. Serrao.
14. XVIII Congresso SIAMOC Torino, 4-7 Ottobre 2017: “Analisi Cinematica del Cammino in Amputati per la Valutazione Funzionale della Stabilità Dinamica”; M. Guaitolini, C. De Marchis, M. Rinaldi, **T. Varrecchia**, G. Chini, A. Silvetti, M. Serrao, A. Ranavolo, M. Schmid, F. Draicchio, S. Conforto.
15. XVIII Congresso SIAMOC Torino, 4-7 Ottobre 2017: “Controllo motorio modulare dell’arto controlaterale nel cammino di amputati trans-femorali S. Ranaldi, C. De Marchis, M. Rinaldi, **T. Varrecchia**, A. Marchesi, A. Silvetti, M. Serrao, A. Ranavolo, M. Schmid, S. Conforto.
16. XI Congresso Nazionale SIE Napoli, 16-18 novembre 2016: “Analisi Cinematica di una postazione di interfaccia cliente/operatore”; A. Silvetti, A, Ranavolo, **T. Varrecchia**, M. Rinaldi, G. Chini, A. Marchesi, F. Draicchio.

TABLE OF CONTENTS

CHAPTER I

1. INTRODUCTION AND PURPOSE OF THE STUDY

Worker health is an issue of fundamental importance in the ergonomic field: it is a duty to protect and guarantee the health of workers, in particular those exposed to occupational risk factors [1].

In this context, of particular interest are the work-related musculoskeletal disorders (WMSDs) which represent the most common disorder in the occupational field and the main cause of absence from work in the industrialized world [2-4]. The two main groups of WMSDs are work-related low-back disorders and upper limb disorders (WLBDs e UL-WMSDs). Studies on this topic [5] have shown that WLBDs are mainly caused by manual lifting tasks while UL-WMSDs are caused by repeated movements of the upper limbs.

In recent years, among WMSDs, work-related neck and upper limb disorders (WRNULD) are increasingly common. Particularly, biomechanical, physiological and psychophysical evidences suggest that static neck and shoulder posture or forward head posture, such as that frequently assumed by office workers, as a possible risk factor in WRNULD [6]. These disorders are mainly caused by increasing computer use and use of touch screen devices which may be used in various non-traditional workstations and postures [7].

Previously, in the attempt to reduce the risk of WMSDs while handling materials, handling people in the healthcare sector or while maintaining fixed postures, several methods have been developed, accepted by the international literature and used in the workplace.

Specifically, in an attempt to prevent and reduce the risk of WLBDs, a growing effort has been made over the past three decades to identify work associated with a high risk of low back disorders (LBD) and to evaluate the effectiveness of ergonomic interventions [2,4,8]. Particularly,

the National Institute for Occupational Safety and Health (NIOSH) published the Revised NIOSH Lifting Equation (RNLE), a pioneering and noteworthy approach widely used throughout the world by safety and health practitioners to assess two-handed manual lifting demands [5,8-9]. This approach is also suggested by the International Standard ISO 11228-1 and part of the technical report 12-295 [10].

To reduce the risk of UL-WMSDs, different methods have been developed to identify high-risk jobs of UL-WMSDs. The International Standard ISO 11228-3 and part of the technical report 12-295 suggest, among other methods, the use of the OCRA checklist [11] to assign a level of risk to the performed task.

As regard WRNULD, there are few studies quantifying the musculoskeletal exposures through mathematical model or laboratory measurements [7]. Indeed, the majority of studies is founded on the questionnaire to evaluate self-reported pain, discomfort at the neck, at the shoulder and at the upper extremity and muscle fatigue due to the daily use of computer and touch screen devices [7]. There aren't quantitative approaches for reduce or prevent WRNULD caused by work activities associated with use of computer and touch screen devices because the muscles involved in these work activities are often difficult to analyze. Indeed, the involved muscles produce weak and noisy myoelectric signals that are characterized by amplitudes lower than 5% of the Maximal Voluntary Contraction (MVC), and they are generally associated with a low firing rate (i.e. 8-12 pulses per second, pps), a low number of recruited motor units (i.e. 50-100 MU)).

The risk assessment methods currently used for UL-WMSDs or WLBDs have different limitations that inhibit their applicability to all work activities [12-18]; hence the idea of using an instrumental and quantitative approach to evaluate the biomechanical risk in any work environment. Particularly, it is useful to introduce quantitative indices related to biomechanical risk because when the risk factors are analyzed by means of quantitative methods, the possibility of

identifying the relationship between pathologies and risk increases significantly [10]. Furthermore, thanks to the technological advances that have allowed the development of miniaturized and non-invasive devices, such as the sEMG and wearable sensors, it will be possible to provide a method of assessing the biomechanical commitment applicable directly in the field without interfering with the work activity. In particular, sEMG is widely used in ergonomics, because it can be performed both in the laboratory and in the workplace [19], but inertial sensors in recent years are also finding different applications in this field [20-21].

This approach could allow to prevent and reduce the onset of these disorders but also the reintegration of workers affected by these and other disorders.

Therefore, the aim of this research project is to introduce quantitative approaches to evaluate biomechanical risk of certain work activities estimating the biomechanical commitment required by these activities with a computerized multifactorial motion analysis system (kinematics, kinetics and surface electromyography) and with new methodologic approaches to analyze muscle activity of weak and noisy myoelectric signals.

Thesis outline

Chapter II: describes the work-related musculoskeletal disorders and the both the traditional and new instrumental methods used for risk assessment.

Chapter III: describes studies based on kinematic, kinetic data and neural networks for risk assessment during lifting activities.

Chapter IV: describes studies based on sEMG features and neural networks for risk assessment during lifting activities.

Chapter V: describes the assessment of fatiguing lifting activities using inertial measurement units, bipolar and high-density sEMG in both healty subjects and people with low back pain.

Chapter VI: describes biomechanical assessment in works associated to WRNULD.

Chapter VII: methodological aproches for the detection of muscular activity for signals characterized by low amplitude and low signal-to-noise ratio – weak and noisy – that is a challenge in biomedical data processing.

Chapter VIII: general conclusions of this PhD work.

BIBLIOGRAPHY

1. D.Lgs. 81/08
2. Buckle, P. 2005. “Ergonomics and Musculoskeletal Disorders: Overview.” Occupational Medicine 55(3): 164–167.
3. da Costa, B.R. and E.R. Vieira. 2010. “Risk factors for work-related musculoskeletal disorders: A systematic review of recent longitudinal studies.” American Journal of Industrial Medicine 53: 285–323.
4. Palmer, K.T., E.C. Harris, C. Linaker, M. Barker, W. Lawrence, C. Cooper and D. Coggon. 2012. “Effectiveness of Community- and Workplace-Based Interventions to Manage Musculoskeletal-Related Sickness Absence and Job Loss: A Systematic Review.” Rheumatology (Oxford) 51(2): 230–242.
5. NIOSH. 1981. Work practices guide for manual lifting. NIOSH Technical Report No. 81-122 (U.S. Dept. of Health and Human Services, National Institute for Occupational Safety and Health Cincinnati, OH).
6. Szeto GP, Straker L, Raine S. A field comparison of neck and shoulder postures in symptomatic and asymptomatic office workers. Appl Ergon. 2002 Jan;33(1):75-84.
7. Toh SH, Coenen P, Howie EK, Straker LM. The associations of mobile touch screen device use with musculoskeletal symptoms and exposures: A systematic review. PLoS One. 2017 Aug 7;12(8):e0181220. doi: 10.1371/journal.pone.0181220.
8. Waters, T.R., V. Putz-Anderson and A. Garg. 1994. “Applications Manual for the Revised NIOSH Lifting Equation.” Cincinnati, OH: U.S. Department of Health and Human Services.
9. Waters, T.R., V. Putz-Anderson, A. Garg and L.J. Fine. 1993. “Revised NIOSH Equation for the Design and Evaluation of Manual Lifting Tasks.” Ergonomics. 36 (7): 749–776.
10. Dempsey, P.G., A. Burdorf, F.A. Fathallah, G.S. Sorock and L. Hashemi. 2001. “Influence of measurement accuracy on the application of the 1991 NIOSH equation.” Applied Ergonomics 32(1): 91-99.
11. Occhipinti E, Colombini D. 2004. “The OCRA method: updating of reference values and prediction models of occurrence of work-related musculo-skeletal diseases of the upper limbs (UL-WMSDs) in working populations exposed to repetitive movements and exertions of the upper limbs.” La Medicina del Lavoro. 95(4):305-19.
12. Marras WS, Fine LJ, Ferguson SA, Waters TR. The effectiveness of commonly used lifting assessment methods to identify industrial jobs associated with elevated risk of low-back disorders. Ergonomics. 1999; 42(1): 229-245.
13. Dempsey PG. Usability of the revised NIOSH lifting equation. Ergonomics. 2002; 45(12): 817-828.
14. Dempsey PG, Fathallah FA. Application issues and theoretical concerns regarding the 1991 NIOSH equation asymmetry multiplier. Int J Ind Ergon. 1999; 23: 181-191.
15. Elfeituri FE, Taboun SM. An evaluation of the NIOSH Lifting Equation: a psychophysical and biomechanical investigation. Int J Occup Saf Ergon. 2002; 8(2): 243-258.
16. Karwowski W, Brokaw N. Implications of the proposed revisions in a draft of the revised NIOSH lifting guide (1991) for job redesign: A field study. 1992. In Proceedings of the 36th Annual Meeting of the Human Factors Society (pp.659–663). Santa Monica, CA, USA: Human Factors Society.
17. Lavender SA, Li YC, Natarajan RN, Andersson GB. Does the asymmetry multiplier in the 1991 NIOSH lifting equation adequately control the biomechanical loading of the spine?. Ergonomics. 2009; 52(1): 71-79.
18. Ranavolo A, Varrecchia T, Rinaldi M, Silvetti A, Serrao M, Conforto S, Draicchio F. Mechanical lifting energy consumption in work activities designed by means of the "revised NIOSH lifting equation". Ind Health. 2017 Oct 7; 55(5): 444-454.
19. Gazzoni, M. 2010. Multichannel Surface Electromyography in Ergonomics: Potentialities and Limits. Human Factors and Ergonomics in Manufacturing & Service Industries. 20(4): 255–271.
20. Sprager, S. and M.B. Juric, 2015. “Inertial Sensor-Based Gait Recognition: A Review.” Sensors (Basel) 15 (9): 22089-127.

21. Taborri, J., E. Palermo, S. Rossi and P. Cappa. 2016. “Gait Partitioning Methods: A Systematic Review.” Sensors (Basel) 16 (1).

CHAPTER II

2. WORK RELATED MUSCULOSKELETAL DISORDERS AND RISK ASSESSMENT

Musculoskeletal disorders (MSDs) include a wide range of inflammatory and degenerative conditions affecting the muscles, tendons, ligaments, joints, peripheral nerves, cartilages and spinal discs. Body regions most commonly involved are the low back, neck, shoulder, forearm and hand. MSDs have multiple risk factors, both non-occupational and occupational [1]. In this first chapter the causes and incidence of work-related musculoskeletal disorders (WMSDs) are described to give a detailed explanation of this problem that cause suffering and disability among workers. We focused our attention on work-related low back disordes (WLBDs) and work-related neck and upper limb disorders (WRNULD).

Particularly, as regards WLBDs, a revision of the state of art is done to understand the limitations of methods used to identify high risk jobs and to propose a new instrumental approach designed to prevent and therefore cut down the injury phenomenon (see 1.1).

As regard WRNULD, we analyse the exponential growth of the use of mobile handheld devices, including touchscreen smartphone, tablet and keypad phones [2]. Particularly, I highlighted the presence of few quantitative studies regarding the relashionship between WRNULD and work activities associated with use of computer and touch screen devices, introducing the possibility to study, with specific methods, the weak and noisy myoelectric signals of the muscles involved in these work activities (see 1.2).

Furthermore, the necessity to introduce instrumental approacches to evaluate biomechanical risks related to these work activities must be underlined (see 1.3).

2.1 WORK-RELATED LOW BACK DISORDES (WLBDs): LIFTING ACTIVITY

2.1.1 Epidemiology

According to the National Institute for Occupational Satefy and Health (NIOSH), several epidemiological studies have demonstrated evidence of a cause between physical exertion at work and WMSDs. They are the reason of an impaired work capacity and are defined as multi-factorial disorders among workers [1].

Since WMSDs are growing and the burden is likely to become an even more serious threat to occupational health, there has been an increasing effort in recent years to investigate the causes of WMSDs and to take action to prevent them. Furthermore, WMSDs, as well as being a personal problem leading to long and serious disability that have substantial impact on quality of life, are also considered a social issue because of their high incidence, in terms of cost, on the national health system and on the employment sphere, i.e. lost of productivity, sickness absence and job loss [3-6]. Annual incidence of WMSDs accounts for a third of all occupational disorders estimated in the USA, the Nordic countries and Japan, and for 23% in the European Union [7-8]. The cost of WMSDs was estimated to be 17 billion pounds in 2009 in the UK, 38 billion euros in 2002 in Germany, 26 billion Canadian dollars in 1998 in Canada and 215 billion dollars in the USA [9]. In Italy, WMSDs are the most frequent disorders, with almost 31.000 complaints being made in 2011. Their overall percentage is rising, with a steady increase from 40% in 2007 to 66% in 2011 [10]. Furthermore, several studies indicated gender differences in the prevalence of WMSD with higher risk of developing these disorders for the women than their male counterparts [11-14]. The women and men differ in terms of the types of injuries they experience, their symptoms, or level of disability in relation to WMSDs [12, 15,16] due to physiological differences in the gener i.e. in relation to

perception of pain [17], fatigability [18], tendon properties [19], hormonal differences (Sullivan), anthropometry and muscular entities [20].

WMSDs include work-related low back disorders (WLBDs), which are mainly caused by manual lifting tasks and are the most common and costly musculoskeletal problem [21]. WLBDs and injuries attributed to manual lifting activities continue as one of the leading occupational health and satefy issues facing preventive medicine [5]. WLBDs can occur when spinal load exceeds tissue tolerance [22]. National standards advising against spinal compression in excess of 6400 N [23]. One of the mechanisms increasing the spinal load is the simultaneous activation (co-activation) of many of the main muscle groups of the trunk during dynamic liftings [24].

WLBDs also can occur by direct trauma, a single exertion ('overexertion') or potentially as the result of multiple exertions. Several other work-related factors including pushing or pulling activities, repetitive tasks, excessive force, awkward and/or sustained postures, prolonged sitting and standing extreme postures, and whole-body vibrations are also associated with development of WLBDs and impairment. Finally, scientific literature highlights that work-related psychological stress and lifestyle factors also may increase the risk of WLBP and the subsequent risk of prolonged impairment or disability [6]. Psychosocial factors, appropriate medical treatment, and job demands may be particularly important in influencing the transition of acute low back pain to chronic disabling pain [5].

WLBDs account for almost 20% of all workplace injuries and illness, for almost 25% of workers' yearly compensation expenses and for almost 25% of all lost work days, with a yearly prevalence of about 18% [25, 26]. In Italy, over 11,000 out of 31,000 complaints related to all WMSDs involve WLBDs, with a threefold increase being recorded over a 5-year observation period [10]. In Italy, diseases of the intervertebral discs show an incidence grewing systematically going through, year after year, from almost 11% in 2007 (over 3 thousand complaints on total of almost 28 thousand)

to 24% in 2011 (over 11 thousand complaints on total of almost 46 thousand) [10]. In particular, the proportion of the population exposed to ergonomic risk factors for WLBDs is 87% according to the Global Burden of Disease 2016 [27].

2.1.2 State of the art

To reduce the risk of WLBDs while lifting materials, several methods have been developed in field of surveillance studies to identify high-risk jobs that will probably be associated with an elevated risk of LBD and to evaluate the effectiveness of potential ergonomic interventions.

Among the methods used by safety and health practitioners to asses two-handed manual lifting demands, the Revised National Institute for Occupational Safety and Health (NIOSH) Lifting Equation (RNLE) [5-6] is widely used in overall the world to prevent or reduce the occurrence of lifting-related LBD because it provided an empirical method for computing a weight limit for manual lifting.

Historically, the National Institute for Occupational Safety and Health (NIOSH) has recognized the problem of work-related back injuries and published the Work Practices Guide for Manual Lifting (WPG) in 1981. The NIOSH WPG contained: i) a summary of the lifting-related literature before 1981; ii) analytical procedures and a lifting equation for calculating a recommended weight for specified two-handed, symmetrical lifting tasks; iii) an approach for controlling the hazards of low back injury from manual lifting [28].

The pioneering original 1981 equation, developed to assist safety and health practitioners in evaluating lifting demands in the sagittal plane [29], could only be applied to a limited number of lifting tasks, namely sagittal lifting tasks. So, it was revised and expanded in 1991 to be applied to a larger percentage of lifting tasks.

In 1985, NIOSH convened an ad hoc committee of experts who reviewed the current literature on lifting, including the NIOSH WPG. The ad hoc committee recommended criteria for defining the

lifting capacity of healthy workers and they used the criteria to formulate the revised lifting equation.

The 1991 lifting equation (for this thesis, the revised 1991 NIOSH lifting equation will be identified simply as 'the revised NIOSH lifting equation, (RNLE)) reflects new findings, provides methods for evaluating asymmetrical lifting tasks, objects with less than optimal hand-container couplings, and offers new procedures for evaluating a larger range of work durations and lifting frequencies than the earlier equation [6].

The objective of RNLE is to prevent or reduce the occurrence of lifting-related back injuries among workers and to reduce other musculoskeletal disorders associated with some lifting tasks such as shoulder or arm pain [5-6].

RNLE is based on three criteria (biomechanical, physiological, and psychophysical) derived from the scientific literature and combined judgment of experts from the fields of biomechanics, psychophysics, and work physiology [5-6].

In general, the criteria chosen by the NIOSH *ad hoc committees* were used as a basis to develop an equation for determining a recommended weight limit for a specific task. The recommended weight limit for a task represents a load value that nearly all healthy workers can lift over a substantial period of time without an increased risk of developing lifting-related LBP. Several criteria were used to develop the equation because each lifting task imposes different biomechanical and physiological requirements on the worker. As a result, the limiting factor or criteria in each lifting task may vary.

The concept behind the RNLE is to start with a recommended weight that is considered safe for an 'ideal' lift and then reduce the weight as the task becomes more stressful. RNLE predicts a Recommended Weight Limit (RWL) defined, for a specific set of task conditions, as the weight of the load that nearly all healthy workers (workers who are free of adverse health conditions that would

increase their risk of musculoskeletal injury) could perform over a substantial period of time without an increased risk of developing lifting-related low back pain (LBP) [28].

The RWL compared to the weight of lift in the task of interest, yields a lifting index (LI). RWL is an equation in which a constant load is mediated (reduced) by several multipliers based on measured parameters (*See Appendix A*):

$$RWL = LCxHMxVMxDMxAMxFMxCM$$

The measured parameters (Figure 2.1) that define the level of physical stress associated with specific characteristic of a lifting task are:

- Horizontal Location (H): is measured from the mid-point of the line joining the inner ankle bones to a point projected on the floor directly below the mid-point of the hand grasps;
- Vertical Location (V): is the distance of the hands above the floor;
- Vertical Travel Distance (D): is the absolute value of the difference between the vertical heights at the destination and origin of the lift;
- Asymmetry Angle (A): is defined by the location of the load relative to the worker's mid-sagittal plane;
- Lifting frequency (F): refers to the average number of lifts made per minute, as measured over a 15-minute period;
- Coupling quality: classifies the quality of the hand-to-object coupling [5-6].

The RWL is the principal product of the RNLE. The RWL is defined for a specific set of task conditions as the weight of the load that nearly all healthy workers could perform over a substantial period of time (e.g., up to 8 hours) without an increased risk of developing lifting-related LBP. By healthy

workers, we mean workers who are free of adverse health conditions that would increase their risk of musculoskeletal injury [5].

The LI is an index that provides a relative estimate of the level of physical stress associated with a particular manual lifting task. The estimate of the level of physical stress is defined by the relationship of the actual weight of the load lifted (L) and the recommended weight limit [5].

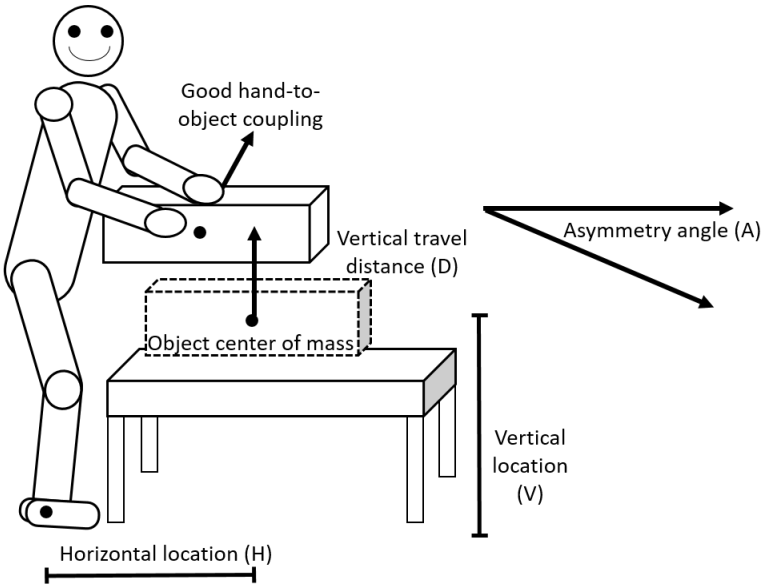

Figure 2.1. *Graphic Representation of NIOSH Parameters.*

LI is calculated dividing the actual object load lifted by the RWL:

$$\mathrm{LI} = \frac{\text{Load Weight}}{\text{Recommended Weight Limit}} = \frac{\mathrm{L}}{\mathrm{RWL}}$$

The aim of the RNLE approach is to design tasks such that the LI is less than 1.0. In fact, LI values greater than 1.0 but lower than 3.0 are assumed to represent tasks posing risk for some fraction of the worker population while LI values greater than 3.0 are referred to highly stressful lifting tasks implying an elevated risk of work-related injury for many workers (Table 2.1).

Lifting Index Value	**Exposure level**
LI≤1	Acceptable
1<LI≤2	Moderate level of risk
2<LI≤3	High level of risk
LI>3	Very high level of risk

Table 2.1. *Interpretation of Lifting Index values (ISO/TR 12295 2014).*

The legislation deals with the activity of manual handling of loads. In decree 81/08 the norms of Title VI shall apply to work activities of manual handling of loads involving risks to workers of biomechanical overload disorders, especially back injury. In this title there are two important definitions:

- *manual handling operations*: transporting or supporting of a load, by one or more workers, including lifting, putting down, pushing, pulling, carrying or move a load, which, for their characteristics or as a result of unfavorable ergonomic conditions, involve risks of biomechanical overload disorders, particularly of back injury;
- *biomechanical overload disorders*: disorders of the musculoskeletal structures, muscle-tendon and nerve vascular.

2.1.3 Niosh: RNLE strengths and restrictions

The LI has been shown to be a valid indicator of the risk of WLBDs for manual lifting [20]. In particular, its strength lies in the fact that the risk of WLBDs increases significantly as the LI increase from 1.0 to 3.0 with a statistically significant odd ratio (OR) occurring when $1 < LI \leq 2$ and when $2 < LI \leq 3$ [30-31].

The RNLE does, however, also have some weaknesses [32] that have been clearly summarized in a paper by Dempsey [33]. These include the fact that the parameters and equation upon which the

RNLE is based restrict its usability. Indeed, the value ranges of some of the RNLE parameters are so stringent as to exclude many existing manual lifting tasks [34-37], with approximately 35% of the lifting tasks having at least one parameter outside the accepted ranges [33]. Moreover, the equation should not be applied to a number of conditions [5], including lifting: with one hand, for over eight hours, while seated or kneeling, in a restricted work space, unstable objects, with high speed motion, while carrying, pushing, or pulling, with wheelbarrows or shovels, with an unreasonable foot-floor coupling, and in unfavorable environments (i.e. temperature out of the range 19-26° C). Approximately 63% of workers perform lifting tasks that are in contrast with the assumptions made when the RNLE was developed. Some of the aforementioned issues are partially, though never exhaustively, addressed in the Technical Report TR 12295 [38]. Other critical aspects are the misidentification of jobs [31-32] and the accuracy of the RNLE [28, 32].

2.1.4 From semi-quantitative to quantitative approach

To overcome these restrictions that reduced the applicability of the NIOSH Lifting Equation, comes the need to move from a this semi-quantitative to a quantitative approach.

The developing of an instrumental-based tool built on data acquired in perfectly controlled lifting conditions could be helpful in expanding the knowledge that is the basis and directly supports the NIOSH methods. Indeed, when the risk factors are analyzed by the use of quantitative methodologies for exposure assessment, the ability to identify relationship between LBD and risk occurrence increases significantly [33]. Given today's technologic advances, it is now possible to describe exposure to physical risk factors with a degree of accuracy that has not been previously available [32]. The development of a kinematic and surface electromiographic (sEMG)-based tool built on data acquired in perfectly controlled lifting conditions (from LI=0.5 to LI=3) could increase the chances to well identify any significant relationship with LBD. Parameters extracted from sEMG,

acquired during the execution of LI=1 and LI=3 lifting tasks, could be used as reference indexes in identifying the risk of the lifting task. Moreover, these sEMG indices, if well parameterized on sex, age, work experience, lifting type (lifting and lowering), speed, *one hand-jobs*, lifting while seated or kneeling, lifting in a restricted work space, *lifting unstable objects*, lifting while carrying, pushing or pulling, lifting with wheelbarrows or shovels, lifting with unreasonable foot-floor coupling, *lifting in an unfavorable environment*, could be used in a larger number of lifting tasks. sEMG is capable of quantify muscular involvement caused by lifting tasks and could be helpful in expanding the knowledge about NIOSH methods. sEMG [39-40], relevant in ergonomics because it can be used both in the laboratory and at a workplace in the field [41-43], is one of the most important objective and non-invasive approaches offering direct information on muscle involvement.

Furthermore, the possibility to use these technologies connected to electronic smart devices (smartphones, phablets, tablets and smartwatches) via wireless protocols such as Wi-Fi and Bluetooth, would allow a simplified analysis in the worker-centered environments and distributed computing environments.

2.2 WORK-RELATED NECK AND UPPER LIMB DISORDERS (WRNULD): WEAK AND NOISY MYOELECTRIC SIGNALS

In the last twenty years the use of mobile handheld devices, including touchscreen smartphone, tablet and keypad phones, has grown exponentially, for both adolescents and adults. Recent surveys have shown that the users spend approximately more than three hours daily [2] on their mobile device to text, read e-mail, surf the internet and game (excluding voice activities). These data are expected to continue to increase in the next years showing an important social change: due to their portability and simplicity of use, these devices are recently introduced in education, in healthcare and also in various working environments.

The effect of an intensive and daily use of mobile hand-held devices – smartphones and tablets, in particular – on one's health is still a matter of research: while several reviews [44-45] have deeply investigated the association between electromagnetics field exposure and some non-specific symptoms such as fatigue, sleep disturbance, headache and earache, few studies have targeted the relationship between the daily use of smartphones and modifications to motor outcomes (such as alterations of gait patterns while walking [46]); in particular, posture taken when using touch-screen devices has been investigated together with the potential associated risks to develop musculoskeletal complaints and disorders [47-48]. Moreover, since children extensively use digital devices, the topic regarding possible alterations to the development of motor and stance control mechanisms [49-51] is worth being investigated.

Most studies in this research area make use of questionnaires to evaluate self-reported pain, discomfort at the neck, at the shoulder and at the upper extremity and muscle fatigue. Among these, Berolo et al. [2] used a questionnaire to collect some self-reported measures of smartphone use and symptoms of pain on a population of university students and observed a relationship between the use of a mobile device and some symptoms of the upper extremity and neck. Hakala et al. [52] found that the use of the smartphone for more than five hours daily was associated with neck-shoulders pain, while the effect of sustained static postures and repetitive movements of the finger has been investigated by Barr et al. [53]. Xie and colleagues [54] showed that the participants to their study felt a neck discomfort after using a smartphone for more than ten minutes when they were sitting.

While several studies have been based on kinematic analysis of some tasks to deal with a functional assessment (see for example [55]), the musculoskeletal exposure of head and trunk districts has been rarely studied through mathematical models or laboratory measurements (e.g. motion analysis systems, electro-goniometers): Hansraj [56] developed a mathematical model to simulate the effect of the neck tilt on the cervical spine, and showed that the equivalent weight suffered by

the spine depends on the neck angle, so becoming a potential cause of cervical pathology. Lee et al. [57], evaluated head flexion during common smartphone tasks showing that the messaging produced the highest effect on the neck tilt. Guan et al. [58] investigated gender differences in the cervical posture when using mobile phone. Ning et al. [59] explored the kinematics of the cervical spine while typing and showed a high level of risk to develop neck pain. Other experimental studies have also shown the postural difference between natural standing and the posture assumed while focussing upon the smartphone. Only one study analysed head flexion while using a smartphone in sitting compared to standing [60] and indecisive results have been found about the effect of the task on the neck and trunk posture.

The limited evidence regarding the relationship between mobile handheld device and musculoskeletal symptoms and exposures, due to few studies, does not permit the development of clinical management and ergonomics guidelines to facilitate prevention strategies.

When studying how reducing or preventing WRNULD caused by work activities associated with use of computer and touch screen devices, quantitative approaches based on sEMG activity could be usefull but they are missing expecially because the muscles involved in these work activities are often difficult to analyze. Indeed, the involved muscles produce weak and noisy myoelectric signals. These signals are characterized by a low activity level due to low firing rate, low number of motor units recruited, low activation threshold and very low signal-noise ratio (SNR) [61]. In this context, in this thesis I focused my attention on these signals trying to introduce some methodological approaches that can allow to analyze the muscles involved in these work activities.

2.3 QUANTITATIVE APPROCHES FOR BIOMECHANICAL RISK ASSESSMENT

As highlighted in the work “Wearable Monitoring Devices for Biomechanical Risk Assessment at Work: Current Status and Future Challenges-A Systematic Review.” (Ranavolo A, Draicchio F,

Varrecchia T, et al. 2018.) pubblished on *International Journal of Environmental Research and Public Health,* in recent years, wearable sensors have been used for quantitative instrumental-based biomechanical risk assessments in the prevention of work-related musculoskeletal disorders (WMSDs). The past approaches have without doubt facilitated prevention activities during the last decades by improving occupational health and safety of people at work but, on the other hand, need a significant update based on two main aspects. First, the standardized methods commonly used for biomechanical risk assessment are still mainly based on observational and subjective approaches [62-65] and don't include instrumentation-based tools. Second, the recent widespread use of robots, automation and mechanization in industry for the reduction of the physical effort has modified manual handling work activities. One of the key technologies driving this epochal change, the human-robot collaboration (HRC) technology [66-67], is invading several areas of the industry and small-medium enterprises. The nascent nature of HRC in the workplace conceives the safe coexistence and interaction of workers and robots within the same environment allowing a significant transformation of the current static automation paradigms into adaptive, flexible and reconfigurable ones. In particular, the presence of the most advanced remotely controlled robot, occupational collaborative robots [68] and wearable trunk and upper-limb exoskeletons [69-72] will assist more and more workers in performing their tasks reducing their exposure to the associated physical demands.

In view of this new workplace setup there are some questions to ask: are the standardized biomechanical risk assessment methods able to take into account all these new factors? Are the most recent electronic wearable technologies used for biomechanical risk assessment? And again, can they be considered the answer to the aforementioned advanced "Industry 4.0" manufacturing solutions? The authors of this review propose that while advances in wearable wireless sensor networking and ubiquitous computing have paved the way for new possibilities in sport performance measures [73-

75] and clinical applications [76-78], today their potential for biomechanical risk assessment is still largely underexploited and the state of the art lags dramatically behind the expectations. The hypothesis underlying in this chapter is that the most innovative wearable technologies and electronic smart devices such as smartphones and tablets may improve the biomechanical risk assessment by adapting it to all the work conditions and overcoming the limits of the current standardized methods. For instance, intelligent work environments [79] may represent the new scenario in which smart wearable sensors with computational capabilities and network connection are sensitive, responsive, adaptive and transparent [80] to workers' movements allowing online, real-time monitoring of work activities.

Thus, these devices, without interfering with the typical movements performed by workers at the workplace thanks to the miniaturization process and wireless protocols, would allow the estimation of biomechanical risk in real-time providing a direct feedback to the end-user who would be constantly monitored directly at work. In this way, the workers could modify their movements during the execution of work tasks thereby reducing and preventing their exposure to the risk of WMSDs.

To shed light on this issue, the aim of this chapter was, through a literature research, to describe recent implementations of wearable sensors for quantitative instrumental-based biomechanical risk assessments in the prevention of WMSDs. To do this, we have provided: an explanation of how wearable sensors work and measurements are performed, with particular attention to inertial measurement units (IMUs), hand-held dynamometers and grip force devices, and surface electromyography (sEMG) sensors (see 1.3.1); a description of quantitative instrumental-based biomechanical risk assessment methods, which have proved themselves significant for physicians, ergonomists and researchers. These proposed tools have been analyzed for: (i) direct instrumental evaluations [81-83] providing real-time measures of risk of exposure, requiring simple hardware

setup and allowing easy analysis and interpretation of data by workers (see 1.3.2); (ii) rating standard methods for biomechanical risk assessment (see 1.3.3).

2.3.1 IMUs, Hand-Held Dynamometers and Grip Force Devices, sEMG Sensors: How They Are Made and Measure

Movement analysis systems allow the quantification of motor functions, motor abilities, pathological conditions, compensatory motor strategies and improvements due to rehabilitation treatments and ergonomic interventions. However, these systems can be easily used only within the laboratory and more difficult in the field. This difficulty has led to the development, in the last decade, of accurate and reliable wearable human body sensor-based tools for easy human motion analysis directly in the workplace. The main factor allowing the abovementioned use has been, without doubt, the miniaturization of devices which has allowed huge benefits over traditional approaches. Other factors are wireless connectivity, light weight, small-size, low power consumption, portability, low-cost, comfort, and the possibility to monitor subjects remotely and to provide feedback to the end-user [84-89].

Among wearable human body sensors, inertial measurement units (IMUs), dynamometers and surface electromyography (sEMG) sensors allow a detailed estimation (compared to traditional observational methods) of kinematics, kinetics and muscle behaviors without interfering with the typical movements performed by workers in the workplace [90-91].

In experimental settings, IMUs, dynamometers and sEMG sensors are placed and fixed on the appropriate body segments to measure joint angles, forces and muscle behaviors, respectively. All the sensors are commonly synchronized for data alignment in time [92]. Connection is always performed by implementing one of two wireless protocols: Wi-Fi or Bluetooth. The former has an increased power consumption, but a greater transmission speed and distance with respect to the

latter. The sampling frequency of these sensors varies between 50 and 1000 Hz while the minimum number of bit is 12 [93].

2.3.2 Direct Instrumental Evaluations

Several papers have proposed instrumental-based tools for biomechanical risk classification without using measured/calculated indices as input to standardized methods. Instrumental approaches based on wearable sensors have been used to classify lifting tasks into low and high risk categories. In a very recent study [94], IMUs and sEMG sensors have been used to monitor trunk inclination and trapezius and erector spinae muscle activity, respectively, during the execution of several types of lifting tasks with different weights, horizontal distance and technique executed by male office workers. The method proposed in this study allows, with an acceptable accuracy, the automatic identification of the risk levels associated with the lifting activities. Indeed, the lifting tasks were characterised by a feature vector composed of the 90th, 95th or 99th percentile of sEMG activity level and trunk inclinations during the task. Linear Discriminant Analysis and a subject-specific threshold scheme were applied and lifting tasks were classified. The authors highlighted how the strength of this study lies on its objective instrumental approach based on subject-specific thresholds and on the possibility to complement the current standardized approaches usually used to detect biomechanical hazard.

Furthermore, muscle coactivation has deeply been investigated [95] because it, being a neuromuscular pattern needed to stabilize the trunk [96], represents one of the causal pathways for WLBDs. The behavior of the cervical and lumbar spine has also been investigated in complex multiplanar dynamic motions including lifting and pushing [97]. sEMG has been used to develop a sEMG-based multi-muscle coactivation index that resulted usable to continuously assess the neuromuscular effort and significantly sensitive to several factors. In particular, the higher the

speed, complexity of the motion and head control are, the higher the coactivation index value is. Also, in this case this simple approach has been proposed to be used for ergonomic assessments.

Another tool developed to calculate the simultaneous activation of trunk muscles is the time-varying multi-muscle co-activation index (TMCi) which includes a sigmoid-weighting factor dependent on relative differences between muscles that do not rely on a priori definitions of agonist or antagonist behavior [21]. This index was evaluated during the execution of lifting task in controlled conditions considering trunk muscles [21]. It has been shown that heavier lifting conditions resulted in higher TMCi values and that significant correlations exist between the TMCi and other agonist–antagonist methods.

Manual lifting has also been assessed by using muscle fatigue estimation. In a recent review regarding this issue a list of methods was given, though the authors concluded that there are still many gaps to be filled and further studies are needed to find better fatigue indices and improved techniques [98].

Besides lifting activities, wearable sensors have been used for direct instrumental evaluations in handling of low loads during high frequency activities. For instance, local myoelectric manifestation of muscle fatigue [98] has been estimated in several conditions to investigate several groups of workers. Kinematic and sEMG assessments have also been performed in biomechanical evaluation of supermarket cashiers before and after a redesign of the checkout counter, in analysis of post office employees' workstations and in manual handling on a supermarket greengrocery shelf [99-101].

Finally, the usefulness of wearable sensors has also been investigated in many work tasks which require intensive and repetitive production of forces on the upper extremities in manipulating external loads, wrists, palms, fingers and tendons [102-103]. In these cases, the role of wearable sensors, in most cases hand-held dynamometers devices, is to measure the normal and shear forces

created between fingers and handles to assess muscle integrity and to determine the level of any strength deficits [104] associated to clinical physical examination tests (i.e., the diagnosis of shoulder pain [105]). A wearable, unobtrusive, wireless and accurate system (Activity Tracking with Body Area Network) has been designed to operate autonomously and to quantitatively measure postures and body motions of workers. This system is meant to be used by workers to autonomously monitor themselves on actual job sites over long periods of time. Different working processes in a wood workshop have been evaluated by using three accelerometers and two microphones and by correlating the worker's motion and frequency and intensity of sounds [107]. IMUs were also used in several work activities such as car assembly, hammering, screwing and drilling [107]. In construction activities IMUs [98-99] and sEMG has been used to monitor lifting and holding loads activities to detect potential sources of WMSDs at neck [110] lower back levels [111].

2.3.3 Risk Assessment in the Context of Rating of Standard Methods

As done for direct instrumental evaluations, in this section tentative ratings of standard methods using wearable technologies are analyzed.

An innovative "on-body wireless sensors network"-based approach for real-time ergonomic assessment in industrial manufacturing has been proposed by Vignais and colleagues [112]. The sensor network was composed by IMUs and goniometers and the body posture (joint angles) was assessed by using a rigid, ten segments, twenty degrees of freedom biomechanical model. IMUs were placed bilaterally on the upper arm and forearms, on the head, trunk (on the chest) and pelvis (on the sacrum). Goniometers were placed on the hands and forearms to measure wrist motions. Angle values were used as input within the Rapid Upper Limb Assessment (RULA) method, whose global and local scores were continuously computed by a mobile processing unit (a standard laptop) and fed back to the user via a see-through head-mounted display.

Moreover, a real-time body sensors network composed by IMUs and sEMG sensors has also been used in real-time to monitor workers by measuring muscular efforts and postures (upper limbs have been modeled as a 7-DoF kinematic chain) for WMSD prevention according to the RULA index and the Strain Index (SI) [74]. The accuracy, expressed as the number of correct assessments (with respect to those performed by two human evaluators) of the system was 95% for RULA and 45% for SI, indicating that the body sensor network is able to give a RULA score estimation congruent to the one given by the human evaluators. As far as the SI score is concerned, the system gives a score congruent to the evaluators' evaluation in almost the 50% of the cases.

sEMG has also been used for complementing the RULA scoring system [113] and as an alternative to the visual inspection according to the BORG scale. It is in fact demonstrated that the two assessments are strongly correlated [114]. An example of the latter application has been studied by Cabeças [115] where sEMG was used as an alternative to observational methods in computing the SI score. The authors concluded that, once appropriate trigger levels for the muscular activation are defined, sEMG is a valid alternative to visual inspection in SI computation. This is true in particular when efforts are not clearly associated to hand/wrist movements and when non-cyclical high-frequency activities are assessed.

BIBLIOGRAPHY

1. da Costa, B.R. and E.R. Vieira. 2010. “Risk factors for work-related musculoskeletal disorders: A systematic review of recent longitudinal studies.” American Journal of Industrial Medicine 53: 285–323.
2. S. Berolo, RP. Wells, and B.C. Amick III, "Musculoskeletal symptoms among mobile hand-held device users and their relationship to device use: a preliminary study in a Canadian university population," Applied Ergonomics vol. 42, no.2, pp.371-378, 2011.
3. Buckle, P. 2005. “Ergonomics and Musculoskeletal Disorders: Overview.” Occupational Medicine 55(3): 164–167.
4. Palmer, K.T., E.C. Harris, C. Linaker, M. Barker, W. Lawrence, C. Cooper and D. Coggon. 2012. “Effectiveness of Community- and Workplace-Based Interventions to Manage Musculoskeletal-Related Sickness Absence and Job Loss: A Systematic Review.” Rheumatology (Oxford) 51(2): 230–242.
5. Waters TR, Putz-Anderson V, Garg A (1994) Applications Manual for the Revised NIOSH Lifting Equation. Cincinnati, OH: U.S. Department of Health and Human Services.
6. Waters TR, Putz-Anderson V, Garg A and Fine LJ (1993) Revised NIOSH Equation for the Design and Evaluation of Manual Lifting Tasks. Ergonomics 36 No. 7, 749–776.
7. Punnett, L., and D. H. Wegman. 2004. “Work-related Musculoskeletal Disorders: The Epidemiologic Evidence and the Debate.” Journal of Electromyography and Kinesiology, 14 (1): 13–23.
8. EFILWC (European Foundation for the Improvement of Living and Working Conditions). 2007. “Fourth European Working Conditions Survey.” Dublin: European Foundation for the Improvement of Living and Working Conditions, ISBN 92-897-0974-X.
9. Hussey, L., S. Turner, K. Thorley, R. McNamee, and R. Agius. 2012. “Work-related Sickness Absence as Reported by UK General Practitioners.” Occupational Medicine, 62 (2): 105–111.
10. INAIL, Italian Worker’s Compensation Authority. Annual Report. Part IV. Statistics, Accidents and Occupational Diseases. 2016. Available online: https://www.inail.it/cs/internet/docs/alg-relazionedel-presidente-appendice-statistica-2016pdf.pdf (accessed on 5 December 2017).
11. Messing, K. (1998). One-eyed science: Occupational health and women workers. Philadelphia, PA: Temple University.
12. Nordander, C., Ohlsson, K., Balogh, I., Rylander, L., Palsson, B., & Skerfving, S. (1999). Fish processing work: The impact oftwo sex dependent exposure profiles on musculoskeletal health. Occupational and Environmental Medicine, 56, 256-264.
13. Treaster, D. & Burr, D. (2004). Gender differences in prevalence of upper extremity muscloskeletal disorders. Ergonomics, 47,495-526.
14. Vroman, K., & MacRae, N. (2001). Non-work factors associated with musculoskeletal extremity disorders in women: Beyond the work environment. Work, 17,3-9.
15. Dahlberg, R., Karlqvist, L., Bildt, C., & Nykvist, K. (2004). Do work technique and musculoskeletal symptoms differ between men and women performing the same type of work tasks? Applied Ergonomics, 35, 521-529.
16. Strazdins, L., & Bammer, G. (2004). Women, work and musculoskeletal health. Social Science and Medicine, 58,997-1005.
17. Fillingim RB, King CD, Ribeiro-Dasilva MC, Rahim-Williams B, Riley JL, III. Sex, gender, and pain: a review of recent clinical and experimental findings. J Pain 2009 May;10(5):447-85.

18. 18.Hunter SK. Sex differences in human fatigability: mechanisms and insight to physiological responses. Acta Physiol (Oxf) 2014 Apr;210(4):768-89.
19. Sullivan BE, Carroll CC, Jemiolo B, Trappe SW, Magnusson SP, Dossing S, et al. Effect of acute resistance exercise and sex on human patellar tendon structural and regulatory mRNA expression. J Appl Physiol (1985) 2009 Feb;106(2):468-75.
20. Johansen T, Samani A, Antle D, Côté JN, Madeleine P. Gender effects on the coordination of subdivisions of the trapezius muscle during a repetitive box-folding task. Eur J Appl Physiol 2013;113(1):175-82.
21. Ranavolo A, Mari S, Conte C, Serrao M, Silvetti A, Iavicoli S, Draicchio F. A new muscle co-activation index for biomechanical load evaluation in work activities. Ergonomics. 2015; 58(6):966-79. http://doi:10.1080/00140139.2014.991764.
22. McGill SM. 1999. "The biomechanics of low back injury: Implications on current practices in industry and the clinic." Journal of Biomechanics, 30:465–75.
23. Granata KP, Marras WS (1995) An EMG-assisted model of trunk loading during free-dynamic lifting. J Biomech 28 No. 11, 1309-1317.
24. Marras, W. S., and G. A. Mirka. 1993. "Electromyographic Studies of the Lumbar Trunk Musculature During the Generation of Lowlevel Trunk Acceleration." Journal of Orthopaedic Research, 11 (6): 811–817.
25. NSC (National Safety Council). 1990. Accident Facts. Chicago, IL: NSC.
26. Guo, H. R., S. Tanaka, W. E. Halperin, and L. L. Cameron. 1999. "Back Pain Prevalence in US Industry and Estimates of Lost Workdays." American Journal of Public Health, 89 (7): 1029–1035.
27. GBD 2016 Risk Factors Collaborators. Global, regional, and national comparative risk assessment of behavioural, environmental and occupational, and metabolic risks or clusters of risks, 1990–2016: A systematic analysis for the Global Burden of Disease Study 2016. Lancet 2017, 16, 390, 1345–1422.
28. Waters, T.R., Lu M. L., and E. Occhipinti. 2007. "New procedure for assessing sequential manual lifting jobs using the revised NIOSH lifting equation". Ergonomics, 50:1761–1770.
29. NIOSH, 1981.Work practices guide for manual lifting. NIOSH Technical Report No. 81-122 (U.S. Dept. of Health and Human Services, National Institute for Occupational Safety and Health Cincinnati, OH).
30. Waters, T.R., M.L. Lu, L.A. Piacitelli, D. Werren, and J.A. Deddens. 2011. "Efficacy of the revised NIOSH lifting equation to predict risk of low back pain due to manual lifting: expanded cross-sectional analysis." Journal of Occupational Environmental Medicine, 53(9):1061-7.
31. Sesek R., Gilkey D., Drinkaus P., Bloswick D.S., and R. Herron. 2003. "Evaluation and quantification of manual materials handling risk factors." International Journal of Occupational Safety and Ergonomics, 9(3):271-87.
32. Marras WS, Fine LJ, Ferguson SA, Waters TR. The effectiveness of commonly used lifting assessment methods to identify industrial jobs associated with elevated risk of low-back disorders. Ergonomics. 1999; 42(1): 229-245.
33. Dempsey PG. Usability of the revised NIOSH lifting equation. Ergonomics. 2002; 45(12): 817-828.
34. Elfeituri FE, Taboun SM (2002) An evaluation of the NIOSH Lifting Equation: a psychophysical and biomechanical investigation. Int J Occup Saf Ergon 8 No. 2, 243-258.
35. Dempsey PG, Fathallah FA (1999) Application issues and theoretical concerns regarding the 1991 NIOSH equation asymmetry multiplier. Int J Ind Ergon 23, 181-191.
36. Lavender SA, Li YC, Natarajan RN, Andersson GB (2009) Does the asymmetry multiplier in the 1991 NIOSH lifting equation adequately control the biomechanical loading of the spine? Ergonomics 52 No. 1, 71-79.
37. Wang M, Garg A, Chang Y, Shin Y, Yeh W, Lee C (1998) The relationship between low back discomfort ratings and the NIOSH lifting index. Hum Factors 40, 509–515.

38. ISO/TR 12295. 2014. “Application document for ISO standards on manual handling (ISO 11228-1, ISO 11228-2 and ISO 11228-3) and static working postures (ISO 11226)”. Ergonomics.
39. Merletti, R., A. Botter, A. Troiano, E. Merlo, and M.A. Minetto. 2009. “Technology and instrumentation for detection and conditioning of the surface electromyographic signal: State of the art.” Clinical Biomechanics, 24, 122–134
40. Zwarts M.J., and D.F. Stegeman. 2003.” Muscle Nerve, 28(1):1-17. Review.
41. Gazzoni, M. 2010. Multichannel Surface Electromyography in Ergonomics: Potentialities and Limits. Human Factors and Ergonomics in Manufacturing & Service Industries. 20(4): 255–271.
42. Hägg GM, Luttmann A, Jäger M (2000) Methodologies for evaluating electromyographic field data in ergonomics. J Electromyogr Kinesiol 10 No. 5, 301-312. Review.
43. Kumar S, Mital A (1996) Electromyography in ergonomics. London, Taylor and Francis.
44. E. Valentini, G. Curcio, F. Moroni, M. Ferrara, L. De Gennaro, M. Bertini, “Neurophysiological effects of mobile phone electromagnetic fields on humans: a comprehensive review,” Bioelectromagnetics, vol. 28, no. 6, pp. 415-432, 2007.
45. M. Röösli, P. Frei, E. Mohler, K. Hug, “Systematic review on the health effects of exposure to radiofrequency electromagnetic fields from mobile phone base stations,” Bulletin of the World Health Organization, vol.88, no. 12, pp. 887-896, 2010.
46. C. Caramia, I. Bernabucci, C. D'Anna, C. De Marchis, M. Schmid, “Gait parameters are differently affected by concurrent smartphone-based activities with scaled levels of cognitive effort,” PloS one, vol.12, no. 10, 2017.
47. Y. Xie, G. Szeto, J. Dai, “Prevalence and risks factors associated with musculoskeletal complaints among users of mobile handheld devices: A systematic review,”, Applied Ergonomics, vol. 59, pp. 132-142, 2017
48. S.H Toh, P. Coenen, E.K Howie, L.M Straker, “The associations of mobile touch screen device use with musculoskeletal symptoms and exposures: A systematic review,”Plos one, vol. 12, no. 10, 2017.
49. C. D’Anna, M. Schmid, A. Scorza, SA Sciuto, L. Lopez, S. Conforto, “Time-to-boundary function to study the development of upright stance control in children,” Open Biomedical Engineering Journal, vol.11, pp. 49-58, 2017.
50. M. Schmid, S. Conforto, L. Lopez, T. D'Alessio, “Cognitive load affects postural control in children,” Experimental Brain Research, vol. 179, no. 3, pp. 375-385, 2007.
51. M. Schmid, S. Conforto, L. Lopez, P. Renzi, T. D'Alessio, “The development of postural strategies in children: A factorial design study,” Journal of NeuroEngineering and Rehabilitation, vol. 2, no. 29, 2005.
52. P.T. Hakala, A.H. Rimpela, L.A. Saarni, J.J. Salminen, “frequent computer- related activities increase the risk of neck- sholulder and low back pain in adolescents,” Adolescent health, vol. 16, no.5, pp.536-541, 2006.
53. A.E. Barr, M.F. Barbe, B.D. Clark, “Work-related musculoskeletal disorders of the hand and wrist: epidemiology pathophysiology, and sensorimotor changes,” J. Orthp. Sports Phys. Ther., vol.34, no. 10, pp. 610-627, 2004.
54. Y. Xie, G.P. Szeto, J. Dai, P. Madeline, “A comparison of muscle activity in using touchscreen smartphone among young people with and without chronic neck-shoulder pain,” Ergonomics, vol.59, no.1, pp. 61-72, 2016.
55. C. D'Anna, A. Scorza, M. Schmid, F. Orsini, A.S. Sciuto, S. Conforto, S. Scena, “A preliminary study on the validation of an automatic measurement method for functional reach assessment by stereophotogrammetry,” 2017 IEEE International Instrumentation and Measurement Technology Conference, Proceedings, 2017.

56. K.K. Hansraj, "Assessment of stresses in the cervical spine caused by posture and position of the head," Surg Technol Int, vol. 25, pp. 277-9, 2004.
57. M. Lee, et al., “The effects of smartphone use on upper extremity muscle activity and pain threshold,” Journal of physical therapy science, vol. 27, no. 6, pp. 1743-1745, 2015.
58. X. Guan et al., “Gender difference in mobile phone use and the impact of digital device exposure on neck posture,” Ergonomics, vol. 59, no.11, pp. 1453-1461, 2016.
59. X. Ning, Y. Huang, B. Hu, A.D. Nimbarte, “Neck kinematics and muscle activity during mobile device operations,” International Journal of Industrial Ergonomics, vol. 48, pp. 10-15, 2015.
60. S. Lee, H. Kang, G. Shin, “Head flexion angle while using a smartphone,” Ergonomics, vol. 58, no.2, pp. 220-226, 2015.
61. Merlo, D. Farina, R. Merletti, A fast and reliable technique for muscleactivity detection from surface EMG signals, IEEE Trans. Biomed. Eng. 50 (3) (2003) 316–323.
62. Eliasson, K.; Palm, P.; Nyman, T.; Forsman, M. Inter- and Intra- Observer Reliability of Risk Assessment of Repetitive Work without an Explicit Method. Appl. Ergon. 2017, 62, 1–8.
63. Valero, E.; Sivanathan, A.; Bosché, F.; Abdel-Wahab, M. Musculoskeletal disorders in construction: A review and a novel system for activity tracking with body area network. Appl. Ergon. 2016, 54, 120–130.
64. Peppoloni, L.; Filippeschi, A.; Ruffaldi, E.; Avizzano, C.A. (WMSDs issue) A novel wearable system for the online assessment of risk for biomechanical load in repetitive efforts. Int. J. Ind. Ergon. 2016, 52, 1–11.
65. Takala, E.P.; Pehkonen, I.; Forsman, M.; Hansson, G.A.; Mathiassen, S.E.; Neumann, W.P.; Sjøgaard, G.; Veiersted, K.B.; Westgaard, R.H.; Winkel, J. Systematic Evaluation of Observational Methods Assessing Biomechanical Exposures at Work. Scand. J. Work. Environ. Health 2010, 36, 3–24.
66. Vieweg, H. An Introduction to Mechanical Engineering: Study on the Competitiveness of the EU Mechanical Engineering Industry; Within the Framework Contract of Sectoral Competitiveness Studies [Electronic Resource]; European Commission: Brussels, Belgium, 2012.
67. ISO 8373. Robots and Robotic Devices—Vocabulary; ISO: Geneva, Switzerland, 2012.
68. Saito, T.; Hoshi, T.; Ikeda, H.; Okabe, K. Global harmonization of safety regulations for the use of industrial robots-permission of collaborative operation and a related study by JNIOSH. Ind. Health 2015, 53, 498–504.
69. Huysamen, K.; de Looze, M.; Bosch, T.; Ortiz, J.; Toxiri, S.; O’Sullivan, L.W. Assessment of an active industrial exoskeleton to aid dynamic lifting and lowering manualhandling tasks. *Appl. Ergon.* 2018, *68*, 125–131.
70. Weston, E.B.; Alizadeh, M.; Knapik, G.G.; Wang, X.; Marras, W.S. Biomechanical evaluation of exoskeleton use on loading of the lumbar spine. *Appl. Ergon.* 2018, *68*, 101–108.
71. de Looze, M.P.; Bosch, T.; Krause, F.; Stadler, K.S.; O’Sullivan, L.W. Exoskeletons for industrial application and their potential effects on physical work load. *Ergonomics* 2016, *59*, 671–681.
72. Bosch, T.; van Eck, J.; Knitel, K.; de Looze, M. The effects of a passive exoskeleton on muscle activity, discomfort and endurance time in forward bending work. *Appl. Ergon.* 2016, *54*, 212–217.
73. Camomilla, V.; Bergamini, E.; Fantozzi, S.; Vannozzi, G. Trends Supporting the In-Field Use of Wearable Inertial Sensors for Sport Performance Evaluation: A Systematic Review. *Sensors (Basel)* 2018, *18*, 873.
74. Chambers, R.; Gabbett, T.J.; Cole, M.H.; Beard, A. The use of wearable microsensors to quantify sport-specific movements. *Sports Med.* 2015, *45*, 1065–1081.
75. Parkka, J.; Ermes, M.; Korpipaa, P.; Mantyjarvi, J.; Peltola, J.; Korhonen, I. Activity classification using realistic data from wearable sensors. Information Technology in Biomedicine. *IEEE Trans.* 2006, *10*, 119–128.
76. Johansson, D.; Malmgren, K.; Alt Murphy, M. Wearable sensors for clinical applications in epilepsy, Parkinson’s disease, and stroke: A mixed-methods systematic review. *J. Neurol.* 2018, *265*, 1740–1752.

77. Shanahan, C.J.; Boonstra, F.M.C.; Cofré Lizama, L.E.; Strik, M.; Moffat, B.A.; Khan, F.; Kilpatrick, T.J.; van der Walt, A.; Galea, M.P.; Kolbe, S.C. Technologies for Advanced Gait and Balance Assessments in People with Multiple Sclerosis. *Front. Neurol.* 2018, *8*, 708.
78. Bensona, L.C.; Clermonta, C.A.; Bošnjaka, E.; Ferber, R. The use of wearable devices for walking and running gait analysis outside of the lab: A systematic review. *Gait Posture* 2018, *63*, 124–138.
79. Chan, M.; Estève, D.; Fourniols, J.Y.; Escriba, C.; Campo, E. Smart wearable systems: Current status and future challenges. *Artif. Intell. Med.* 2012, *56*, 137–156.
80. Cook, D.J.; Augusto, J.C.; Jakkula, V.R. Ambient intelligence: Technologies, applications, and opportunities. *Pervasive Mob. Comput.* 2009, *5*, 277–298.
81. Spyropoulos, E.; Chroni, E.; Katsakiori, P.; Athanassiou, G. A quantitative approach to assess upper limb fatigue in the work field. *Occup. Ergon.* 2013, *11*, 45–57.
82. David, G. Ergonomic methods for assessing exposure to risk factors for workrelated musculoskeletal disorders. *Occup. Ergon.* 2005, *55*, 190–199.
83. Søgaard, K.; Laursen, B.; Jensen, B.R.; Sjøgaard, G. Dynamic loads on the upper extremities during two different floor cleaning methods. *Clin. Biomech.* 2001,*16*, 866–879.
84. Wang, Q.; Markopoulos, P.; Yu, B.; Chen, W.; Timmermans, A. Interactive wearable systems for upper body rehabilitation: A systematic review. *J. Neuroeng. Rehabil.* 2017, *14*, 20.
85. Cuesta-Vargas, AI.; Galán-Mercant, A.; Williams, J.M. The use of inertial sensors system for human motion analysis. *Phys. Ther. Rev.* 2013, *15*, 462–473.
86. Ullah, S.; Higgins, H.; Braem, B.; Latre, B.; Blondia, C.; Moerman, I.; Saleem, S.; Rahman, Z.; Kwak, K.S. A comprehensive survey of wireless body area networks. *J. Med. Syst.* 2012, *36*, 1065–1094.
87. Fong, D.; Chan, Y.Y. The use of wearable inertial motion sensors in human lower limb biomechanics studies: A systematic review. *Sensors* 2010, *10*, 11556–11565.
88. Breen, P.P.; Nisar, A.; Olaighin, G. Evaluation of a single accelerometer based biofeedback system for real-time correction of neck posture in computer users. In Proceedings of the IEEE Engineering in Medicine and Biology Society Annual International Conference, Minneapolis, MN, USA, 2–6 September 2009; pp. 7269–7272.
89. Roetenberg, D.; Luinge, H.; Slycke, P. *Xsens MVN: Full 6DOF Human Motion Tracking Using Miniature Inertial Sensors*; Technical Report; Xsens Technologies B.V.: Enschede, The Netherlands, 2009.
90. injury risk factors in challenging work environments: An evaluation of cost and feasibility. *Am. J. Ind. Med.* 2007, *50*, 687–696.
91. Mogk, J.P.; Keir, P.J. Prediction of forearm muscle activity during gripping. *Ergonomics* 2006, *49*, 1121–1130.
92. Iosa, M.; Picerno, P.; Paolucci, S.; Morone, G. Wearable inertial sensors for human movement analysis. *Expert Rev. Med. Devices* 2016, *13*, 641–659.
93. Rodríguez-Martín, D.; Pérez-López, C.; Samà, A.; Català, A.; Moreno Arostegui, J.M.; Cabestany, J.; Mestre, B.; Alcaine, S.; Prats, A.; Cruz Crespo, M.; Bayés, À. A Waist-Worn Inertial Measurement Unit for Long-Term Monitoring of Parkinson's Disease Patients. *Sensors (Basel)* 2017, *17*, 827.
94. Brandt, M.; Madeleine, P.; Samani, A.; Jakobsen, M.D.; Skals, S.; Vinstrup, J.; Andersen, L.L. Accuracy of identification of low or high risk lifting during standardized lifting situations. *Ergonomics* 2018, *61*, 710–719.
95. Le, P.; Best, T.M.; Khan, S.N.; Mendel, E.; Marras, W.S. A review of methods to assess coactivation in the spine. *J. Electromyogr. Kinesiol.* 2017, *32*, 51–60.
96. Granata, K.P.; Marras, W.S. Cost-benefit of muscle cocontraction in protecting against spinal instability. *Spine (Phila PA 1976)* 2000, *25*, 1398–1404.

97. Andersen, K.S.; Christensen, B.H.; Samani, A.; Madeleine, P. Between-day reliability of a hand-held dynamometer and surface electromyography recordings during isometric submaximal contractions in different shoulder positions. *J. Electromyogr. Kinesiol.* 2014, *245*, 579–587.
98. Stark, T.; Walker, B.; Phillips, J.K.; Fejer, R.; Beck, R. Hand-held dynamometry correlation with the gold standard isokinetic dynamometry: A systematic review. *PM R* 2011, *3*, 472–479.
99. Silvetti, A.; Mari, S.; Ranavolo, A.; Forzano, F.; Iavicoli, S.; Conte, C.; Draicchio, F. Kinematic and electromyographic assessment of manual handling on a supermarket green- grocery shelf. *Work* 2015, *51*, 261–271.
100. Draicchio, F.; Silvetti, A.; Forzano, F.; Iavicoli, S.; Ranavolo, A. Kinematic analysis of post office employees' workstations. *Work* 2012, *41* (Suppl. 1), 2012–2016.
101. Draicchio, F.; Trebbi, M.; Mari, S.; Forzano, F.; Serrao, M.; Sicklinger, A.; Silvetti, A.; Iavicoli, S.; Ranavolo, A. Biomechanical evaluation of supermarket cashiers before and after a redesign of the checkout counter. *Ergonomics* 2012, *55*, 650–669.
102. Kadefors, R.; Areskoug, A.; Dahlman, S.; Kilbom, Å.; Sperling, L.; Wikström, L.; Oster, J. An approach to ergonomics evaluation of hand tools. *Appl. Ergon.* 1993, *24*, 203–211.
103. National Research Council. *Musculoskeletal Disorders and the Workplace*; National Academy Press: Washington, DC, USA, 2001.
104. Constant, C.R.; Murley, A.H.G. A clinical method of functional assessment of the shoulder. *Clin. Orthop. Relat. Res.* 1987, *214*, 160–164.
105. Cadogan, A.; Laslett, M.; Hing, W.; McNair, P.; Williams, M. Reliability of a new hand-held dynamometer in measuring shoulder range of motion and strength. *Manu. Ther.* 2011, *16*, 97–101.
106. Lukowicz, P.; Ward, J.A.; Junker, H.; Stger, M.; Trster, G.; Atrash, A.; Starner, T. Recognizing workshop activity using body worn microphones and accelerometers. In *Pervasive Computing*, Ferscha, A., Mattern, F., Eds.; No. 3001 in Lecture Notes in Computer Science; Springer: Berlin/Heidelberg, Germany, 2004; pp. 18–32.
107. Zappi, P.; Lombriser, C.; Stiefmeier, T.; Farella, E.; Roggen, D.; Benini, L.; Trster, G. Activity recognition from on-body sensors: Accuracy-power trade-off by dynamic sensor selection. In *Wireless Sensor Networks*, Verdone, R., Ed.; Vol. 4913 of Lecture Notes in Computer Science; Springer: Berlin/Heidelberg, Germany, 2009; pp. 17–33.
108. Yan, X.; Li, H.; Li A.R., Zhang, H. Wearable IMU-based real-time motion warning system for construction workers' musculoskeletal disorders prevention. *Autom. Constr.* 2017, *74*, 2–11.
109. Lee, J.A.; Li, N.; Haines, C.S.; Kim, K.J.; Lepró, X.; Ovalle-Robles, R.; Kim, S.J.; Baughman, R.H. Electrochemically Powered, Energy-Conserving Carbon Nanotube Artificial Muscles. *Adv. Mater.* 2017, *29*, doi:10.1002/adma.201700870.
110. Nimbarte, A.D.; Aghazadeh, F.; Ikuma, L.H.; Harvey, C.M. Neck disorders among construction workers: Understanding the physical loads on the cervical spine during static lifting tasks. *Ind. Health* 2010, *48*, 145–153.
111. Jia, B.; Kim, S.; Nussbaum, M.A. An EMG-based model to estimate lumbar muscle forces and spinal loads during complex, high-effort tasks: Development and application to residential construction using prefabricated walls. *Int. J. Ind. Ergon.* 2011, *41*, 437–446.
112. Vignais, N.; Miezal, M.; Bleser, G.; Mura, K.; Gorecky, D.; Marin, F. Innovative system for real-time ergonomic feedback in industrial manufacturing. Appl. Ergon. 2013, 44, 566–574.
113. Perez-Duarte, F.; Lucas-Hernandez, M.; Matos-Azevedo, A.; Sanchez-Margallo, J.; Díaz-Güemes, I.; Sanchez-Margallo, F. Objective analysis of surgeons ergonomy during laparoendoscopic single-site surgery through the use of surface electromyography and a motion capture data glove. *Surg. Endosc.* 2014, *28*, 1314–1320.

114. Jones, T.; Kumar, S. Comparison of ergonomic risk assessment output in four sawmill jobs. *Int. J. Occup. Saf. Ergon.* 2010, *16*, 105–111.
115. Cabeças, J.M. The risk of distal upper limb disorder in cleaners: A modified application of the strain index method. *Int. J. Ind. Ergon.* 2007, *37*, 563–571.

CHAPTER III

3. KINEMATIC, KINETIC DATA AND NEURAL NETWORKS FOR RISK ASSESSMENT DURING LIFTING ACTIVITY

Recently, in order to overcome equation and parameter restrictions [1-8], to increase the accuracy and minimize job misidentification [1,9] and to enhance the ability to identify the relationship between WLBDs and risk factors [10], wearable monitoring devices have been proposed for biomechanical risk assessment [11]. The use of these instrumental techniques has been facilitated by the enormous technological advances that led to increased measurement accuracy, device miniaturization, and more efficient connections via wireless protocols (i.e. Wi.Fi and Bluetooth).

Among the instrumental and quantitative approaches proposed to evaluate different tasks and classify the biomechanical risk, those based on artificial neural networks (ANNs) are particularly promising [12-13]. An ANN is a mathematical model that represents a distributed adaptive system built using multiple interconnecting processing elements (neurons) and mimics the behavior of real neuronal networks. In layered ANNs, the neurons are distributed in several layers: each neuron receives signals processed and transmitted by neurons in the preceding layer and in turn processes and transmits them to the next layer. ANNs are used in many fields of research (psychology, robotics, biology, computer science, ergonomics) due to their ability to adapt, learn, generalize, organize, or cluster data. For the WLBD problem the predictive capacity of this model has been proven to be greater than that achieved by statistical methods [14]. Researchers who attempted to

use ANNs to predict the risk of developing WLBDs, have performed many tests with different topological configurations in terms of number of neurons and hidden layers to determine the most appropriate network architecture. The ANN approaches proposed by Zurada et al. [11] and Chen et al. [12-13], aimed at classifying the risk (low-risk and high-risk), according to the associated likelihood of causing WLBDs, using mechanical parameters associated with risk factors (e.g. lift rate, peak twist velocity average, peak moment, peak sagittal angle, peak lateral velocity maximum) as input signals.

An instrumental-tool to evaluate the biomechanical risk during lifting activities could be based on kinematic measurements: kinematic features as ANN input could predict the risk levels during the execution of controlled lifting tasks expressed in terms of LI identified by the NIOSH equation [15-16] in a controlled environment.

Particularly, the considered kinematic parameters are:

1) the mechanical lifting energy consumption (LEC) in relation to the center of mass (CoM) of the system involved in the lifting task. Mechanical energy consumption, previously used in both normal [17-18] and abnormal gait patterns [19-20], provides information on the mechanical energy consumed by the whole skeletal muscle system during the movement task. Higher values are indicative of greater energy expenditure. We hypothesize that this parameter may be used as an index that is sensitive to the LI and is closely related to the compression and shear forces at the L5-S1 joint.
2) The jerk parameter as index of smoothness of movement.

It may be possible to study this approach in the laboratory by means of optoelectronic systems [21-24] and apply it to indoor and outdoor work environments by means of wearable sensors [25]. Indeed, the recent development of microelectromechanical systems, such as inertial measurement

units (IMUs) (i.e. combined accelerometers and gyroscopes), has paved the way for some noteworthy scientific breakthroughs that may be applied to a range of research areas [26-27].

In this thesis a research study was carried on to: i) calculate the Lifting Energy Consumption (LEC) during the execution of controlled lifting tasks designed on the basis of the RNLE and with an increasing lifting index (LI=l, LI=2 and LI=3); ii) verify the sensitivity of LEC to the risk level and to evaluate its relationship with forces at the L5-S1 joint; iii) verify the sensitivity of kinematic data to the risk level and to test whether machine-learning techniques (ANNs) used for mapping kinematic features on LI levels can lead to a reliable biomechanical risk estimation.

In this chapter, text and figures have been taken from or adapted from the articles "Mechanical lifting energy consumption in work activities designed by means of the "revised NIOSH lifting equation"" [2017, *Industrial Health]*, and "Lifting activity assessment using kinematic features and neural networks" [the work has been submitted on *Applied Science]* which were co-authored by me.

3.1 MATERIALS AND METHODS

3.1.1 Subjects

Twenty male subjects (mean age 33.30±7.39 years, height 1.80±0.07 m, body mass index (BMI) 24.37±2.67 kg/m^2) were enrolled in the study (see **Table 3.1**). The workers had no history of musculoskeletal disorders, upper limb, lower limb and trunk surgery, or orthopedic and neurological diseases. All the participants gave their informed consent to the study, which complied with the Helsinki Declaration and was approved by the local ethics committee.

Subject	Age range	Sex	Weight [kg]	Height [m]
S1	30-40	Male	68	1.71
S2	30-40	Male	85	1.84
S3	40-50	Male	94	1.85
S4	20-30	Female	52	1.58
S5	20-30	Female	57	1.58
S6	40-50	Male	92	1.73
S7	40-50	Male	76	1.76
S8	20-30	Female	54	1.6
S9	40-50	Female	50	1.64
S10	20-30	Male	80	1.86
S11	20-30	Male	72	1.82
S12	30-40	Female	50	1.62
S13	20-30	Female	52	1.68
S14	20-30	Male	73	1.78

S15	20-30	Male	82	1.77
S16	40-50	Female	57	1.63
S17	30-40	Male	58	1.68
S18	20-30	Male	85	1.95
S19	40-50	Male	75	1.78
S20	30-40	Male	85	1.84

Table 3.1. *Summary of subjects enrolled in the study with place experiments and tasks performed.*

3.1.2 Kinematic and kinetic recordings

An eight infrared cameras (sampling frequency 340 Hz) optoelectronic motion analysis system (SMART-DX 6000 System, BTS, Milan, Italy) was used to detect the movements of 33 spherical markers (15 mm in diameter) covered with aluminum powder reflective material placed over the spinous processes of the seventh and tenth cervical vertebrae, suprasternal notch (between the clavicular notches), sternum, sacrum and, bilaterally, over the temple, posterior-superior parietal bone, acromion, olecranon, ulnar styloid and radial processes, head of the third metacarpal bone, anterior superior iliac spine, great trochanter, lateral femoral condyle, fibula head, lateral malleoli, metatarsal head and heel [28-30] (Figure 3.1). Four markers were also placed over the 4 vertexes of a load consisting of a plastic crate (**Figure 3.1**). Acquisitions were performed using Smart Capture software (BTS, Milan, Italy).

The analysis is based on the recognition and three-dimensional reconstruction of passive markers positioned on the anatomical landmarks (**Figure 3.1** (A)) using a kinematic model (**Figure 3.1** (B)).

Ground reaction forces were acquired by using four dynamometric platforms embedded in the floor. Data was sampled at 680 Hz (P 6000, BTS, Milan, Italy).

Data acquisition from the infrared cameras and force platforms was integrated and synchronized.

3.1.3 Experimental Procedures

The subjects were asked to perform some lifting tasks in a movement analysis laboratory (**Figure 3.2**), a quiet room with normal indoor lighting and temperature. The environmental data in the laboratory were collected using a portable multi-channel (sampling frequency 0.033 Hz) data logger (Lsi – Lastem, Babuc A, Permenugo, Italy). Air temperature and relative humidity were 23.30±0.95 °C and 40.60±5.03 % respectively.

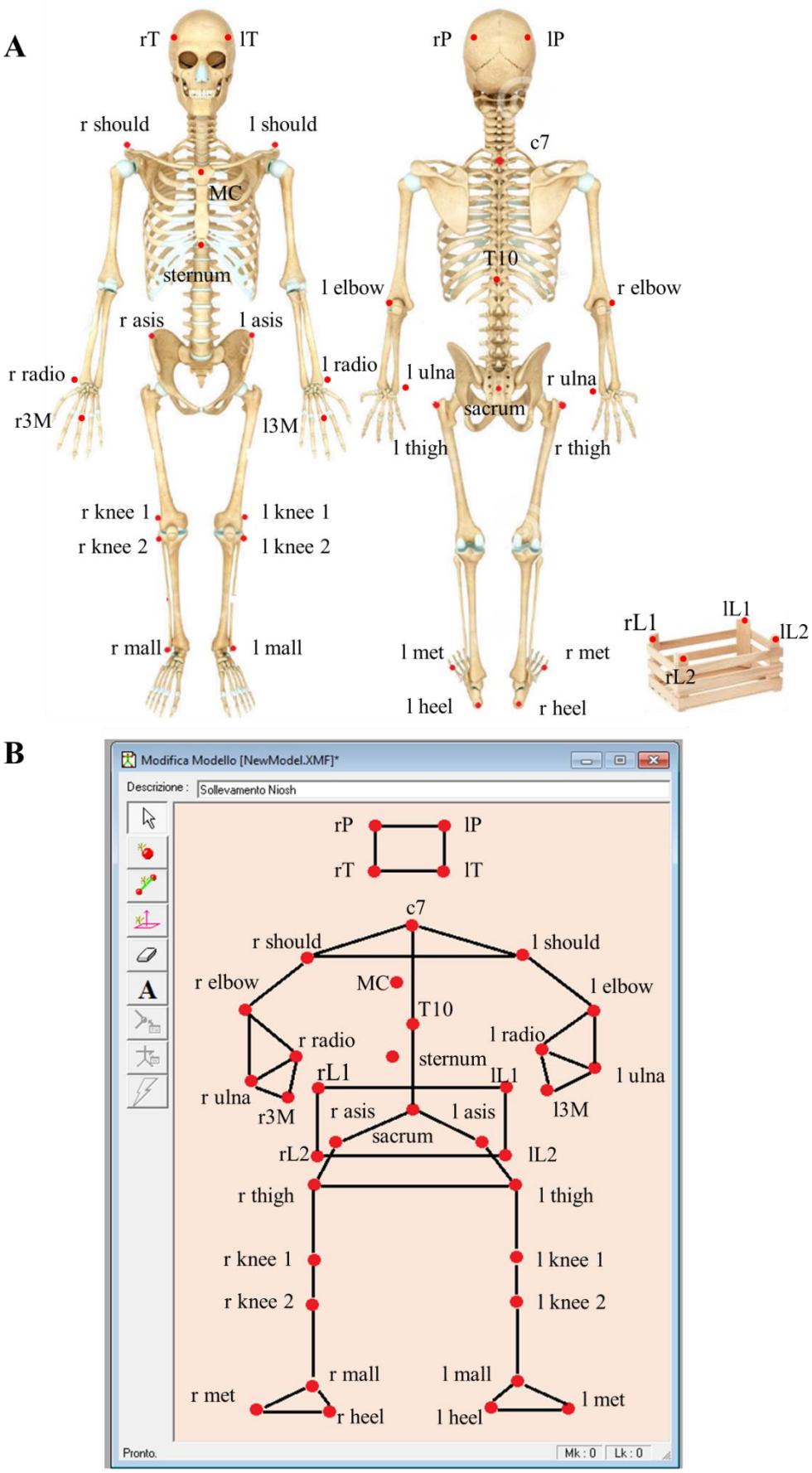

Figure 3.1. *Anatomical and load marks (A) and kinematic model (B) used in the study.*

Spatial accuracy after the calibration procedure was 0.2 mm in the x, y and z dimensions. A global reference system (GRS) in the laboratory was adopted in accordance with the International Society of Biomechanics [31-32].

The subjects were asked to perform the manual material lifting task standing in a neutral body position and lifting a plastic crate with handles using both hands in three different lifting conditions, according to the RNLE [16]. The six lifting conditions were chosen in order to obtain LI values of 1, 2 and 3. The task factors were arbitrarily chosen among a large number of combinations to have these three fixed LI values. **Table 3.2** shows, for each lifting condition, the values of the load weight (L), horizontal (H) and vertical (V) locations, vertical travel distance (D), asymmetry angle (A) and lifting frequency (F), as well as the corresponding values of the multipliers. The hand-to-object coupling was defined as "good" for all three lifting conditions. Each participant was required to perform a total of 30 trials (5 repetitions X 6 lifting tasks). The order of each condition was randomly assigned.

Figure 3.2. *Structure of gait analysis laboratory used for the experiments.*

Task	LC (kg)	H (cm)	HM	V (cm)	VM	D (cm)	DM	A (°)	AM	F (lift/min)	FM	C	CM	L (kg)	RWL	LI
A	23 kg	25	1	75	1	25	1	30	**0.9**	≤2	1	good	1	20.7	**20.7**	**1**
B	23 kg	25	1	75	1	25	1	0	1	≤2	1	good	1	23	23	
C	23 kg	50	0.5	75	1	25	1	30	0.9	≤2	1	good	1	20.7	10.35	**2**
D	23 kg	50	0.5	75	1	25	1	0	1	≤2	1	good	1	23	11.5	
E	23 kg	60	0.42	30	0.87	45	0.92	0	0.9	≤2	1	good	1	20.9	6.96	**3**
F	23 kg	63	0.4	30	0.87	45	0.92	0	1	≤2	1	good	1	22.09	7.36	

Table 3.2. *For each task (A, B, C, D, E and F), the values of the load weight (L), the horizontal (H) and vertical (V) locations, the vertical travel distance (D), the asymmetry angle (A), the lifting frequency (F) and the hand-to-object coupling (C) and the corresponding values of the multipliers and recommended weight limit (RWL).*

Fig 3.3. *Experimental set-up and four representative subjects who performed the lifting tasks.*

3.1.4 Data analysis

The tracking procedure and data computing were performed by Smart Tracker (BTS, Milan, Italy), Smart Analyzer (BTS, Milan, Italy) and Matlab (version 8.0.0.783, MathWorks, Natick, MA, USA) software.

3.1.4.1 Lifting cycle detection

A reconstruction of the tridimensional position of each marker, from the images of each camera, is necessary to process data (**Figure 3.4**). This procedure is carried out through the software SMART Tracklab (BTS, Milan, Italy), which allows you to apply the anatomical model (in our case our Lifting Model, **Figure 3.1 (B)** and match the individual points of this scheme to the markers detected in the acquisition assigning them a specific label (labeling).

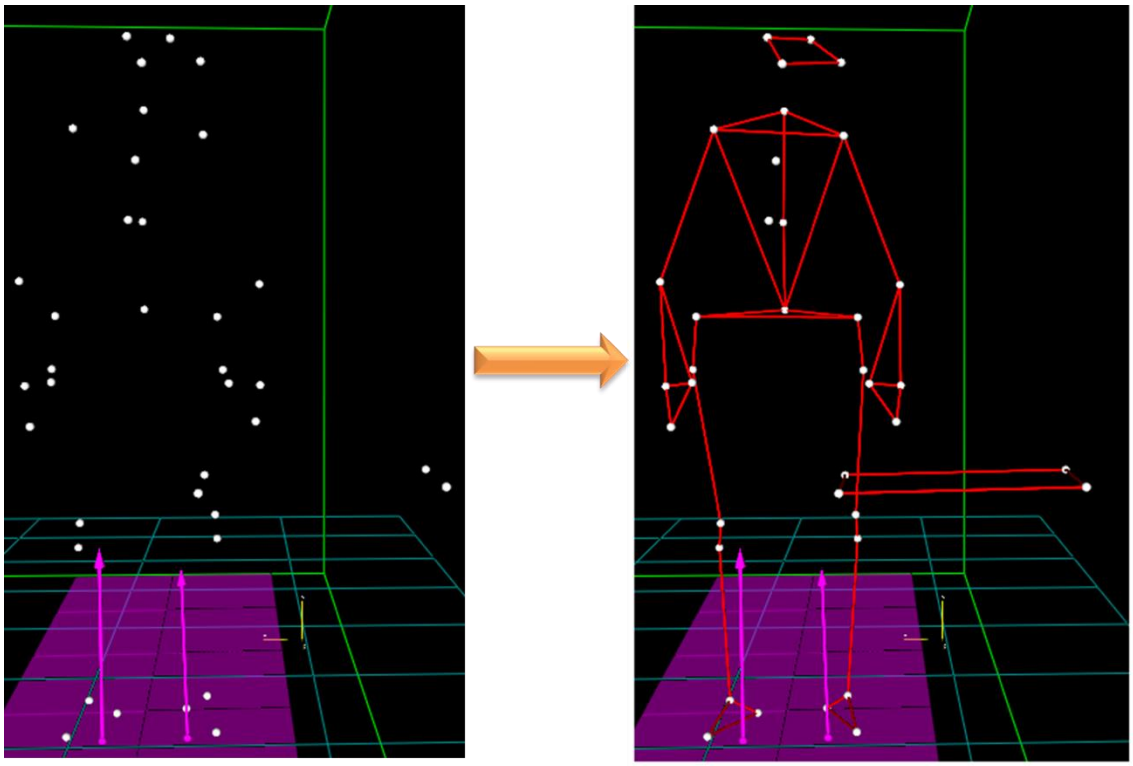

Figure 3.4. *Reconstruction of the 3D position of each marker and tracking procedure.*

After rebuilding the 3D position of each marker at each instant of time, next step is to calculate their trajectory (tracking), from which it is possible to estimate the joint kinematics and, consequently, the relative position and orientation of the reference system with respect to the bone segment

under examination. The operation of tracking is the first stage of data processing: it represents the logical connection of two successive frames, so as to identify the time curve of each single marker. Thus, from the trajectories of the markers, the kinematic speed and acceleration are obtained by derivation. In this step, you can also assign a label to force signals from the platform, displayed as a vector with the origin in the center of pressure and magnitude and direction equal to the vector sum of the three components of force.

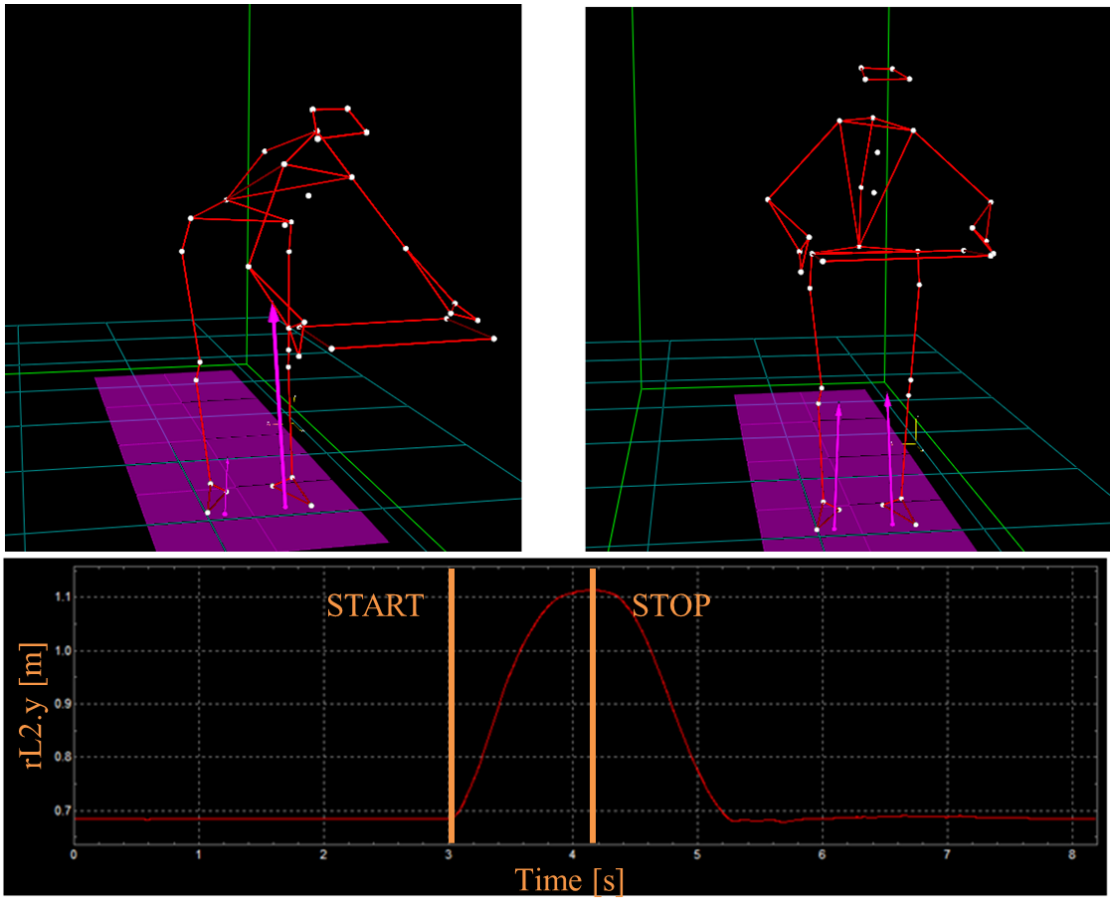

Figure 3.5. *Start and Stop of Lifting.*

Then, the vertical displacement and velocity of one of the four markers placed over the vertexes of the crate were evaluated. Velocities were obtained by applying finite difference derivatives and a Butterworth filtered 4-Hz cut-off low-pass frequency. The onset of the lifting task was defined as the time point at which the crate marker velocity exceeded the velocity threshold by 0.025 m/s on the vertical axis. Termination of the lifting task was defined as the point on the graph at which the

crate marker velocity fell below the velocity threshold in the opposite direction. So, we have defined the Start and Stop of trials and calculated the lifting duration (**Figure 3.5**). Kinematic and kinetic data were time normalized to the duration of the lifting tasks and reduced to 101 samples using a polynomial procedure.

3.1.4.2 CoM calculation

We calculated three different CoM values referring respectively to the load (CoM_L), the multi-segment upper body model (head, trunk, upper arms, forearms and hands) and load together (CoM_{Upp+L}) as well as to the whole body (multi-segment upper body model, pelvis, thighs, shanks and feet) and load together (CoM_{Tot}). In all the three cases, the CoM was computed as the centroid of a set of elements composed by n body segments and the load. The computation was carried on by considering kinematic and anthropometric data together with the body segment parameters [30, 33-34], according to the weighted average of the individual body segments' center of mass [28, 35].

$$CoM_x = \frac{1}{m}\sum_{i=1}^{n} x_i * m_i \; ; \qquad CoM_y = \frac{1}{m}\sum_{i=1}^{n} y_i * m_i \; ; \qquad CoM_z = \frac{1}{m}\sum_{i=1}^{n} z_i * m_i$$

where CoM_x, CoM_y and CoM_z are, respectively, the instantaneous x, y and z components of the CoM position, m is the mass of the system being considered (load, upper body+load and whole body+load, respectively), n is the number of parts being considered (*n=1, n=9 and n=16*, respectively), x_i, y_i and z_i are the components of the CoM position of the i_{th} part, and m_i is the mass of the i_{th} segment or load.

3.1.4.3 *Lifting energy consumption (LEC)*

For each of the CoMs calculated, the kinetic energy (E_k) during the lifting tasks was calculated as the sum of the kinetic energy on the x (E_{kx}), y (E_{ky}) and z (E_{kz}) axes as follows:

$$E_k = E_{kx} + E_{ky} + E_{kz} = \frac{1}{2}m\left(v_x^2 + v_y^2 + v_z^2\right)$$

where m and v_x, v_y and v_z are, respectively, the mass and velocity components on x, y and z of the CoM being considered. Furthermore, the potential energy (E_p) was calculated using the following equation:

$$E_p = mgh$$

where *h* is the vertical (y) component of the CoM of the system being considered and g is the acceleration of gravity.

Lastly, the mechanical energy (E_M) was calculated as the sum of E_k and E_p. For each CoM, the difference between maximum and minimum values of each E_k, E_p and E_M within the lifting cycle were considered as LEC (LEC_k, LEC_p and LEC_M, respectively). In particular, we calculated LEC_{k_L}, LEC_{p_L}, and LEC_{M_L} for CoM_L, LEC_{k_Upp+L}, LEC_{p_Upp+L} and LEC_{M_Upp+L} for CoM_{Upp+L}, and LEC_{k_Tot}, LEC_{p_Tot} and LEC_{M_Tot} for CoM_{Tot}.

3.1.4.4 Jerk

The flexion-extension angles of trunk, elbow and knee were evaluated using the kinematic data. The jerk value, that is the rate of change of acceleration and represents the third derivative of position/angle [m/ s^3 or degrees/s^3]) [36], was calculated for the trunk (J_{trunk}), elbow (J_{elbow}) and knee (J_{knee}) angles ([degrees/s^3]).

Then we computed the jerk square mean (JSM) values for trunk (JSM_{trunk}), elbow (JSM_{elbow}) and knee (JSM_{knee}), defined as follows:

$$JSM = \frac{1}{n}\sum_{i=1}^{n} J_i$$

where J_i is the jerk and n is the number of data points (101). The JSM is an index of smoothness of movement: the lower the Jerk is, the smoother the movements are [36].

3.1.4.5 Force calculation

According to the multi-segment upper body model, the net forces (F_{L5-S1}) at the L_5-S_1 joint were calculated, in the local reference system (LRS) placed on the trunk in which the y' axis is oriented as the vector C7-sacrum and $x' - z'$ represents the orthogonal plane to y, by using the following formula [37]:

$$F_{L5-S1} = -\sum_{j=1}^{q} F_j - \sum_{i=1}^{p} m_i g + \sum_{i=1}^{p} m_i a_i$$

where q is the number of external forces, F_j is the j_{th} external force, p is the number of body segments being considered, m_i and a_i are respectively the mass [29-30] and the acceleration of the i_{th} segment.

In this LRS, the components of F_{L5-S1} on the y' axis and the $x' - z'$ plane were called compression ($Fcompr_{L5-S1}$) and shear ($Fshear_{L5-S1}$) forces, respectively.

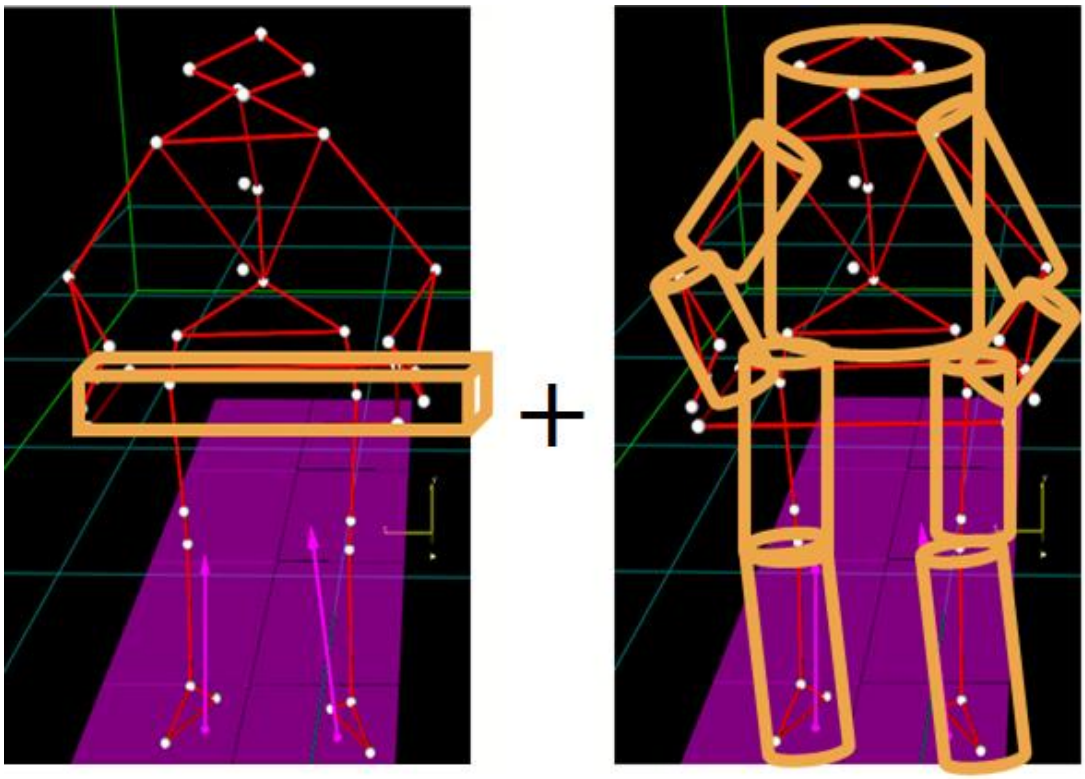

Figure 3.6. *Representation of the human body with different cylinders and representation of load with parallelepiped.*

3.1.4.6 Selection of the neural networks (chosen machine-learning technique) and mapping of kinematic features on LI levels

A neural network approach (ANNs) was used to estimate the biomechanical risk in terms of LI on the basis of kinematic features. We used feedforward ANNs trained using different feature combinations. The networks differ in the topology showing different numbers of hidden layers (HL) and different numbers of neurons (N) in each HL. The output set (OS) consisted of an orthogonal coding of the three LI levels: L1 = [1 0 0], L2 = [0 1 0], and L3 = [0 0 1]. The entire system is schematically described in the **Figure 3.7**.

The number of hidden layers varied in the range of 1–3, while the number of neurons in each HL varied based on the number of nodes N in the first hidden layer (N_{HL1}); N was set to three different values (12, 20 and 50, respectively), and the number of nodes in the other hidden layers (when defined) was 1/2 and 1/3 of N for the second (N_{HL2}) and third (N_{HL3}) hidden layer, respectively. Thus, the combination of HL and N nodes in the first HL led to the following nine different network architectures ([dim(SET) N_{L1} OS], [dim(SET) N_{L1} N_{L2} OS], [dim(SET) N_{L1} N_{L2} N_{L3} OS]): [dim(SET) 12 3], [dim(SET) 20 3], [dim(SET) 50 3], [dim(SET) 12 6 3], [dim(SET) 20 10 3], [dim(SET) 50 25 3], [dim(SET) 12 6 4 3], [dim(SET) 20 10 7 3], and [dim(SET) 50 25 17 3], where dim(SET) defines the size of the ANN input layer (depending on the number of features).

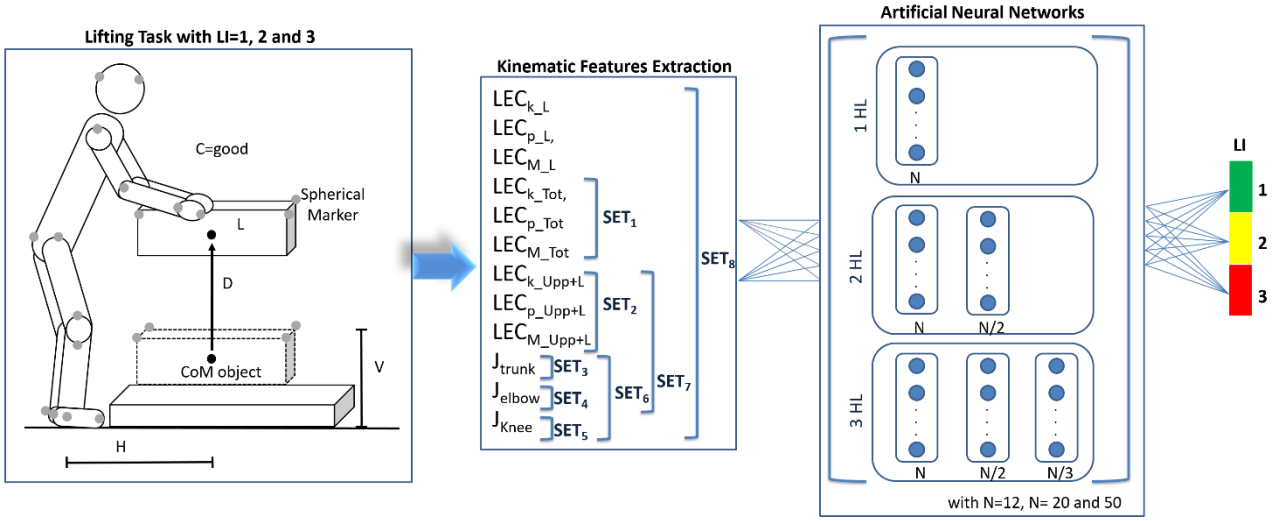

Figure 3.7. *A schematic description of the lifting task and artificial neural network method used to map*

kinetic features on the Lifting Index (1, 2, and 3) levels. C, hand-to-object coupling; D, vertical travel distance; H, horizontal location; L, load weight; V, vertical location; N, number of nodes in the first hidden layer (HL).

Eight different training sets were used: SET_i, i=1,…8 (**Figure 3.7**). Each set was defined as a combination of different kinematic features derived by different parts of the body.

SET_1 contained data derived from CoM of all body (LEC_{k_Tot}, LEC_{p_Tot} and LEC_{M_Tot}), SET_2 contained data derived from CoM of upper body and load (LEC_{k_Upp+L}, LEC_{p_Upp+L} and LEC_{M_Upp+L}), SET_3 contained only jerk data derived from lower limb (J_{knee}), SET_4 contained only jerk data derived from upper limb (J_{elbow}), SET_5 contained only jerk data derived from trunk (J_{trunk}), SET_6 contained all data derived from jerk (J_{knee}, J_{elbow}, J_{trunk}), SET_7 data derived from upper body and load (LEC_{k_Upp+L}, LEC_{p_Upp+L}, LEC_{M_Upp+L}, J_{elbow} and J_{trunk}) and SET_8 data derived from all body and load (all extracted features).

Networks were trained with a supervised approach using the Levenberg-Marquardt back-propagation algorithm [38]. The training was stopped when at least one of the following conditions was met: 1000 iterations, 10^{-6} mean square error, or six consecutive fails on the validation set.

Each of the nine network topologies was trained ten times for each of the 8 training sets so as to obtain a total of 720 trained ANNs. Each training was performed by using a random 10% of samples as the validation set and a random 10% as the testing set. This approach was used in order to verify the repeatability of our results. For each trained network, a confusion matrix was calculated based on the real LI and the one estimated on the randomly extracted testing set.

The mean 3 × 3 confusion matrix was then obtained by averaging the confusion matrixes of the trained ANNs. A performance parameter (P) was calculated as the mean (%) of the elements on the diagonal of the mean confusion matrix, where 100% indicates the absence of misclassifications.

3.1.4.7 Statistical analysis

All the analyses were performed using SPSS 17.0 software (SPSS Inc. Chicago, IL, USA). The Shapiro-Wilk and Kolmogorov-Smirnov test were used to analyze the normal distribution of the data. For each LEC and for each J, we performed a one-way repeated-measures ANOVA to determine whether there were any significant differences between the three risk levels. Post-hoc analyses were performed using a paired t test with Bonferroni's corrections when significant differences were observed in the ANOVA. The Pearson test was used to investigate any correlations between $LEC_{k,}$ LEC_p and LEC_M and the forces.

As regard statistical analysis of ANNs performance, we performed a three-way ANOVA test (with SET, L, N as factors) to determine possible significant effects on ANN performance caused by the listed factors. Post-hoc analysis with Bonferroni's corrections were performed when significant differences were observed in the ANOVA results. The statistical significance was set for p values < 0.05.

3.2 RESULTS

3.2.1 Kinematic feature analysis

A description of the vertical displacements of the three CoMs considered, E_k, E_p and E_M during the execution of the lifting tasks in the three conditions is provided in **Figure 3.8**: the qualitative analysis of energy expenditure revealed differences in both the E_p and E_M curves among the three lifting conditions (**Figure 3.8 (D)** and **Figure 3.8 (E)**) for each CoM considered. **Figure 3.9** shows the means and standard deviation values of LEC.

As reported in **Table 3.3**, the repeated measures ANOVA revealed a significant effect of the lifting condition on LEC_p and LEC_M for all the CoMs considered. Statistically significant effects were also detected for LEC_{k_Upp+L} and LEC_{k_Tot}. Particularly, post hoc analysis showed significant differences (all

p<0.001) between each pair of lifting conditions for LEC_p and LEC_M for all the CoMs considered and also for LEC_{k_Upp+L}. Furthermore, as regard LEC_{k_Tot} significant differences were found between each pair of lifting conditions (LI=1 vs LI=2: p=0.001; LI=1 vs LI=3: p= 0.005; LI=2 vs LI=3: p=0.021).

The results of the correlation analysis between each LEC with $Fcompr_{L5-S1}$, $Fshear_{L5-S1}$ (scatter plots, regression line, correlation coefficients and p values) are reported in **Figure 3.10**. Particularly, the correlation analysis highlighted i) a strong correlation (r>0.7) between each LEC relating to CoM_{Upp+L} and $Fshear_{L5-S1}$, ii) a moderate correlation (0.3<r<0.7) between each LEC relating to CoM_{Upp+L} and $Fcompr_{L5-S1}$, iii) a moderate correlation (0.3<r<0.7) between each LEC relating to CoM_{Tot} and only $Fshear_{L5-S1}$, iv) a strong correlation (r>0.7) between LEC_{p_L} and LEC_{M_L} and $Fshear_{L5-S1}$, v) a moderate correlation (0.3<r<0.7) between LEC_{p_L} and LEC_{M_L} and $Fcompr_{L5-S1}$.

As regards J, for J_{trunk} significant differences (p<0.05) were found between LI=1 vs LI=2 and between LI=1and LI=3, for J_{elbow} significant differences (p<0.05) were found between LI=1 vs LI=3 and between LI=2 and LI=3 and for J_{knee} significant differences were found between each pair of lifting conditions (*p*<0.05 for LI=1 vs LI=2 and LI=2 vs LI=3; *p* <0.001 for LI=1 vs LI=3; see **Figure 3.11**).

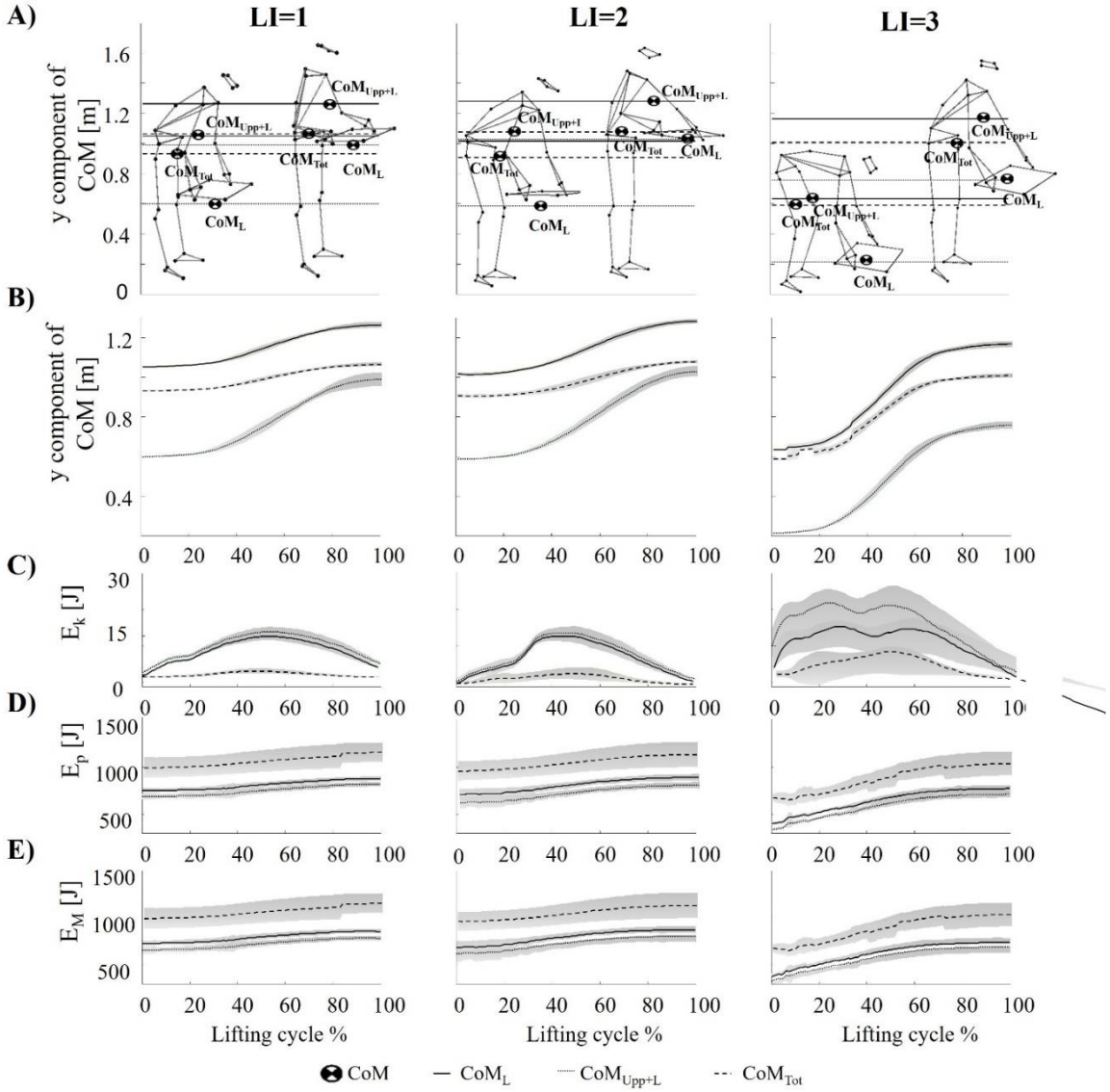

Figure 3.8. *A qualitative description in a representative subject of vertical displacements of CoM_L, CoM_{Upp+L} and CoM_{Tot} (B) (in meters), E_k (C), E_p (D) and E_M (E) (in Joule) for each CoM investigated during the execution of the three lifting conditions (LI=1, LI=2 and LI=3). Black curves represent the mean values, with the SDs of the means shown in grey. Data are normalized to the lifting cycle duration and reduced to 101 samples over the cycle.*

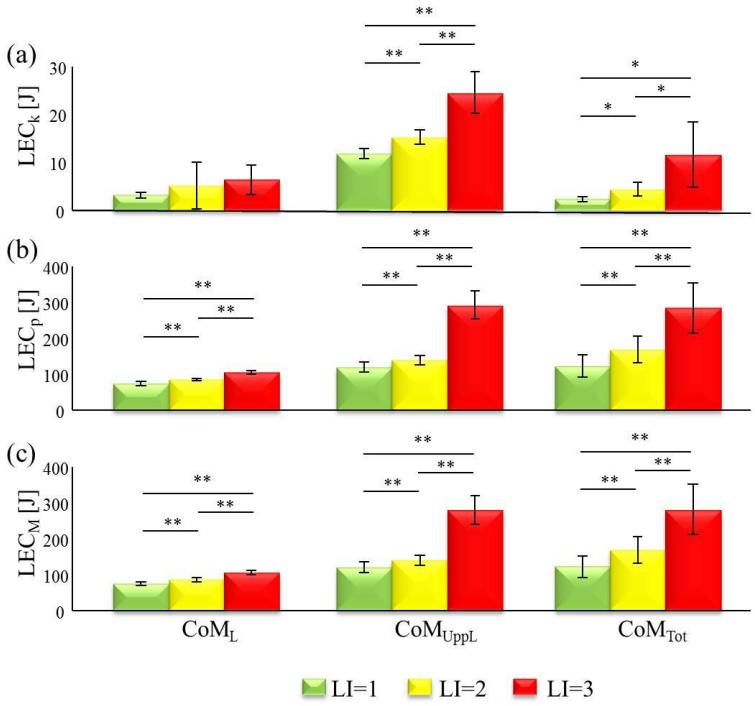

Figure 3.9. Means and standard deviations of the LEC_k (a), LEC_p (b) and LEC_M (c) calculated while performing manual material lifting tasks in the three different conditions (LI=1, LI=2 and LI=3) for the three CoMs (CoM_L, CoM_{Upp+L}, CoM_{Tot}). * and ** Significant differences at the post hoc analysis with $p<0.05$ and $p<0.001$ respectively.

		CoM_L	**CoM_{Upp+L}**	**CoM_{Tot}**
LEC_k	F	3.847	73.469	16.043
	df	1.118	1.081	1.047
	p	0.075	**<0.001**	**0.003**
LEC_p	F	150.992	173.479	65.755
	df	1.349	1.027	1.049
	p	**<0.001**	**<0.001**	**<0.001**
LEC_M	F	126.454	146.276	67.219
	df	1.154	1.012	1.050
	p	**<0.001**	**<0.001**	**<0.001**

Table 3.3. *The F, df and p-values of the repeated-measures ANOVA considering the L_k, L_p, and L_M in the three lifting conditions for the CoM_L, CoM_{Upp+L} and CoM_{Tot}. Bold type indicates statistical significance.*

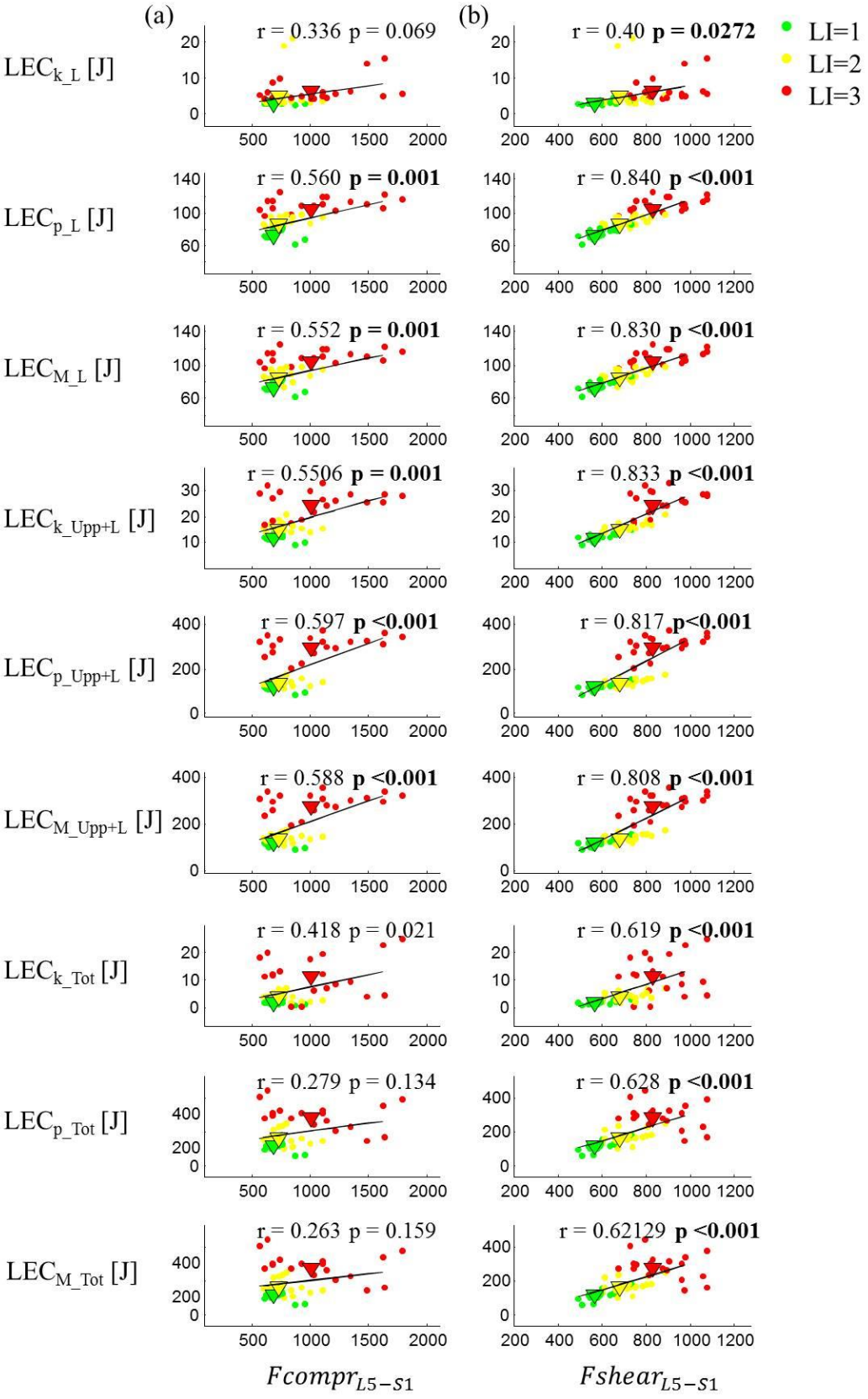

Figure 3.10. *Correlation between the LEC_{k_L}, LEC_{p_L}, LEC_{M_L}, LEC_{k_Upp+L}, LEC_{p_Upp+L}, LEC_{M_Upp+L}, LEC_{k_Tot}, LEC_{p_Tot} and LEC_{M_Tot} and the maximum values of $Fcomp_{L5-S1}$ (a) and $Fshear_{L5-S1}$ (b). Each plot contains 60 points,*

which correspond to the 20 subjects performing the three different lifting conditions (LI=1, LI=2 and LI=3). Green, yellow and red triangles represent the mean of the twenty points for each lifting condition. Each plot shows the r and p values. Bold type indicates statistical significance.

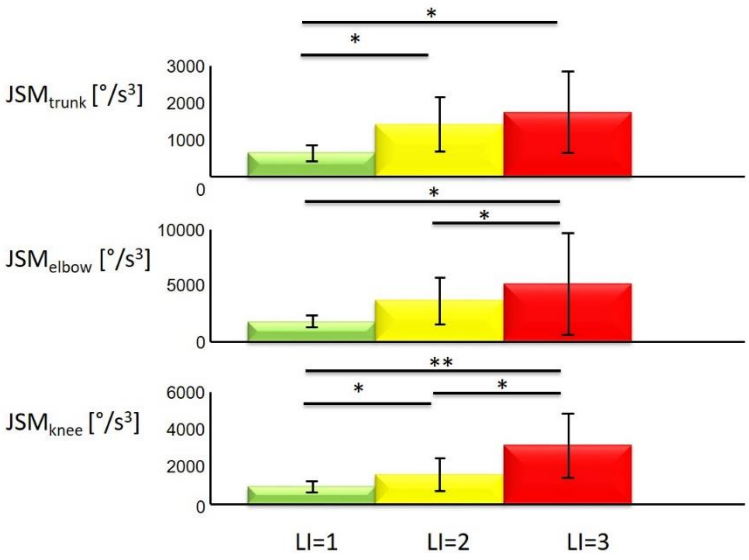

Figure 3.11. Means and standard deviations of the jerk square mean (JSM) values evaluated considering angles of trunk, elbow and knee while performing manual material lifting tasks in the three different conditions (LI=1, LI=2 and LI=3) and statistical significance (* means $p<0.05$; ** means $p<0.001$).

3.2.2 Mapping of kinematic features on LI levels

The results of the detection expressed as P (mean ± SD) for each combination of HL and N, for each of the nine architectures of the ANNs, and with different training sets are reported in **Figure 3.12**. Furthermore, **Figure 3.12** shows also the best confusion matrix for each SET (confusion matrix with highest value of P).

Three-way ANOVA showed significant effects of the training set (df=7; F=174.01; $p<0.001$), N (df=2; F=6.07; p=0.002) and HL (df=2; F=5.2; p=0.01) on the performance.

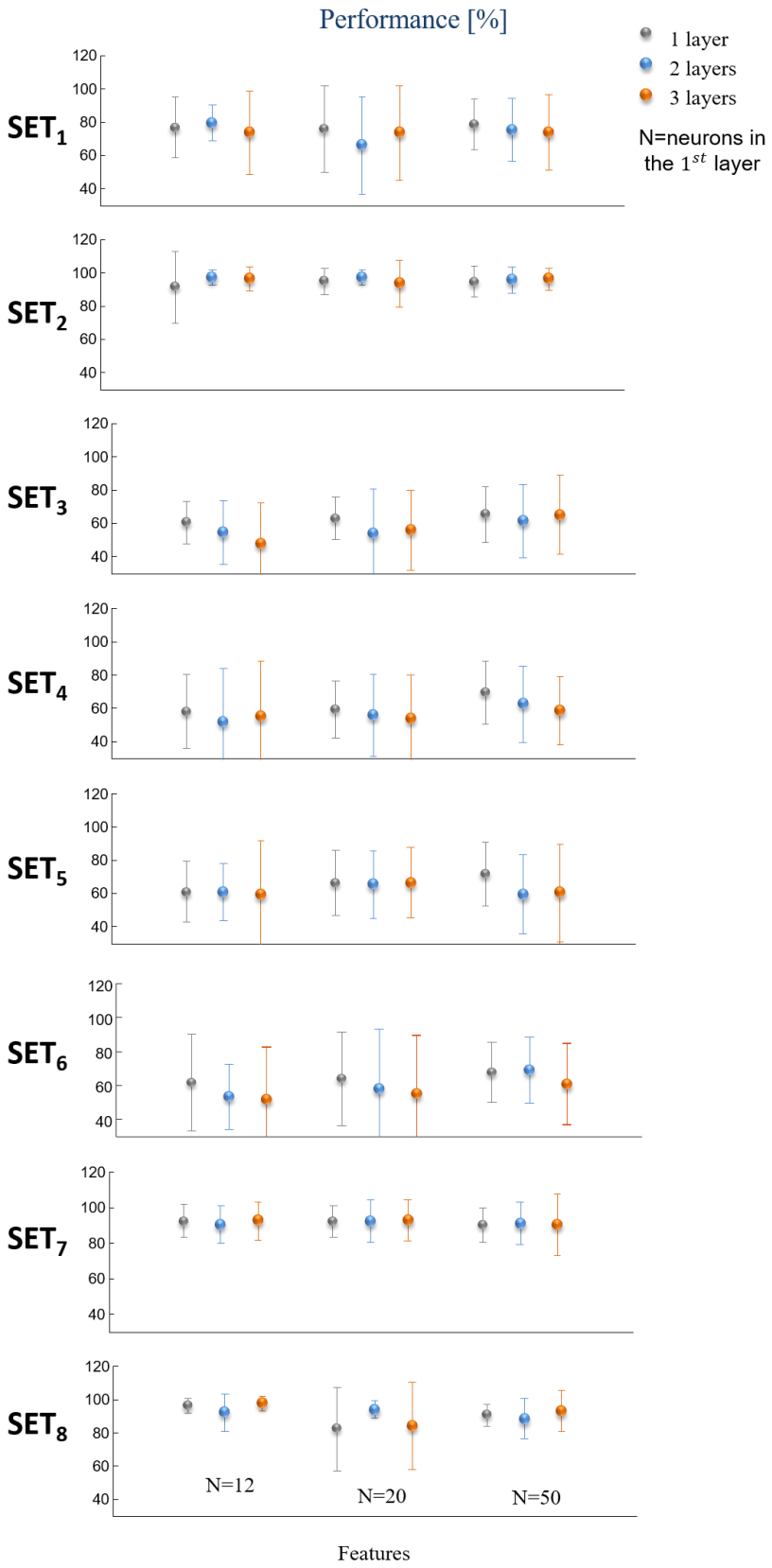

Real LI

Estimated LI

N=12 L=1	1	2	3
1	98.8%	0.2%	0%
2	19.8%	80.2%	0%
3	0%	19.9%	90.1%

Estimated LI

N=12 L=1	1	2	3
1	100%	0%	0%
2	0%	100%	0%
3	0%	0%	100%

Estimated LI

N=50 L=1	1	2	3
1	79.3%	20.7%	0%
2	9.9%	79.8%	10.3%
3	10.3%	38.9%	50.8%

Estimated LI

N=50 L=1	1	2	3
1	100%	0%	0%
2	9.8%	70%	20.2%
3	9.6%	10.2%	80.2%

Estimated LI

N=50 L=1	1	2	3
1	90.1%	9.9%	0%
2	9.8%	90.2%	0%
3	10.3%	9.7%	80%

Estimated LI

N=20 L=2	1	2	3
1	90.2%	9.8%	0%
2	10.1%	89.9%	0%
3	0%	9.6%	90.4%

Estimated LI

N=50 L=1	1	2	3
1	100%	0%	0%
2	0%	100%	0%
3	0%	0%	100%

Estimated LI

N=12 L=1	1	2	3
1	100%	0%	0%
2	0%	100%	0%
3	0%	0%	100%

Figure 3.12. Performance of artificial neural networks considering different features (SET_i, i=1,…8). Nine different architectures of neural networks were represented by varying the numbers of

hidden layers (1, 2, or 3) and the numbers of neurons in each hidden layer based on the numbers of nodes N in the first hidden layer. For each SETi, the best mean confusion matrix was reported.

Particularly, significant differences ($p<0.05$) emerged from post-hoc analysis comparing SET_1 with all SET; comparing SET_2 with SET_3, SET_4, SET_5, SET_6; comparing SET_3 with SET_1, SET_2, SET_7, SET_8; comparing SET_4 with SET_1, SET_2, SET_7, SET_8; comparing SET_5 with SET_1, SET_2, SET_7, SET_8; comparing SET_6 with SET_1, SET_2, SET_7, SET_8; comparing SET_7 with all SET excepted SET_2; comparing SET_8 with all SET excepted SET_2. As regards N, particularly significant differences ($p<0.05$) emerged from post-hoc analysis comparing N=12 and N=50 and comparing N=20 and N=50 As regards HL, no significant differences ($p>0.05$) emerged from post-hoc analysis. In general, SET_2, SET_7 and SET_8 showed higher mean values of performance with lower standard deviations (**Figure 3.12**).

3.3 DISCUSSIONS AND CONCLUSIONS

In this study, energy consumption, the forces at the L_5-S_1 joint and the relationship among these parameters were investigated during the execution of lifting tasks designed in such a way as to exert a growing biomechanical load using the RNLE. Furthermore, ANNs and kinematic data have been used to classify the biomechanical risk. The feed-forward ANNs were trained with different training sets, numbers of hidden layers, and numbers of neurons in each hidden layer using as input LEC indices and Jerk. The training set were selected considering different combinations of the body segments necessary to extract kinematic features (i.e. only upper body, only upper limb, total body, etc.).

The rationale behind this investigation is that an instrumental tool based on kinematic data may be used as risk assessment method to combine with the NIOSH protocol.

Qualitative analysis of the results revealed differences in both the E_p and E_M curves among the three lifting conditions for each CoM considered and in E_k curves for the CoMs referred to the upper-body

and whole body multi-segments systems (**Figure 3.8**). Furthermore, a significant effect of the lifting condition was found on each lifting energy consumption for the CoM_{Upp+L} and CoM_{Tot} and also on LEC_P and LEC_M in relation to the CoM referring to the load (**Figure 3.9**).

This is likely to be due to the fact that CoM_{Upp+L} and CoM_{Tot} take into account the dynamic of subject body during the execution of the lifting tasks and are, consequently, more sensitive to the RNLE factors that influence the risk level. By contrast, CoM_L is influenced above all by the motor strategy at the end effectors (hands), and does not take into account the dynamic of subject body during the execution of the lifting tasks. Indeed, for a given L, an equal D and different LI, CoM_L might not yield any differences in lifting energy consumption because the total movement dynamic would not be considered in the same way as for CoM_{Upp+L} and CoM_{Tot}, nor would the relevance of the other RNLE factors be considered, i.e. H and A.

The results also highlighted that lifting energy consumption grew significantly with the LI and that all the lifting condition pairs are discriminated (**Table 3.3** and **Figure 3.9**): these trends indicate that the lifting energy consumption correctly represents the greater energetic requirements due to the increased level of physical stress, and thus suggest that lifting energy consumption may be used as a risk assessment biomechanical index. In particular, it may be possible to use each lifting energy consumption related to CoM_{Upp+L} and COM_{Tot} to correctly interpret low-, medium- and high-risk jobs. Certainly, the validity of lifting energy consumption method depends on the lifting conditions we set so depending on the multipliers of RNLE equation. On the other hand, findings of this study show the presence of a significant effect of LI on lifting energy consumption calculated by considering CoM_{Upp+L} and CoM_{Tot}, even if obtained within the boundaries of our experimental setup. These results allow us to comprehend that lifting energy consumption, although calculated by a different equation with respect to LI, is sensitive to the RNLE factors and to the risk level because centers of mass are linked to the dynamic body geometry during the execution of the lifting tasks.

The above considerations are supported by the correlation analysis (**Figure 3.10**), which highlights a close relationship i) between each lifting energy consumption and $Fshear_{L5-S1}$ and $Fcompr_{L5-S1}$ when we considered the CoM_{Upp+L}, ii) between each lifting energy consumption and only $Fshear_{L5-S1}$ when we considered CoM_{Tot} and iii) between LEC_{p_L} and LEC_{M_L} and both the forces $Fshear_{L5-S1}$ and $Fcompr_{L5-S1}$. In particular, these findings point to the need to calculate the CoM_{Upp+L} for the lifting energy consumption analysis. For against a low correlation between LEC_k and forces was detected when we considered CoM_L. From a global point of view, mechanical energy expenditure during the execution of lifting tasks is always closely related to the shear forces because spinal loads are affected by lifting dynamics, i.e. flexed lifting [39].

The experimental data allowed to identify the lifting energy consumption indices that are sensitive to an increasing LI (LI=l, LI=2 and LI=3) designed on the basis of the RNLE. These indices would be particularly useful as an instrumental risk assessment method if referred to the set of conditions studied to support the NIOSH protocol or to evaluate a varied range of conditions in which the NIOSH protocol cannot be used (lifting with one hand, for over eight hours, while seated or kneeling, in a restricted work space, unstable objects, while carrying, pushing or pulling, with wheelbarrows or shovels, in high speed motion, with unreasonable foot-floor coupling, in an unfavourable environment).

In literature, there are many studies considering the mechanical energy consumption and/or the body energy consumption [40,41] during lifting tasks. Furthermore, a linear relationship between mechanical work and body energy consumption was found in different activities [42-44]. Particularly, in lifting tasks, for the same increase in absolute mechanical work there is a higher increase in body energy consumption for positive compared with negative work [44].

This relationship strengthens the choice of the index to risk assessment during lifting task. Certainly, the mechanical energy consumption method is easier to apply in work environments than the body

energy consumption. In fact, measurements of oxygen consumption (VO_2) are generally carried out by using a portable system for pulmonary gas exchange measurement. In this kind of measurement, the subject needs to wear a mask that can interfere with the working activities and can introduce psychological stress in the works [45].

Indeed, once these indices have been identified in the laboratory in controlled lifting conditions by means of the optoelectronic system, they could be applied in indoor and outdoor work environments by means of IMUs. In addition to being able to measure single- or multi-point motion trajectories of single or multiple body segments of the subject during the movement task, IMUs have become widely used in all activities that address complex motion analysis because of their interconnectivity, light weight, small size, low power consumption, portability and low cost. Moreover, since IMUs are included in smart devices (i.e. smartphones and tablets), which are now used in every walk of life, inertial sensor-based movement recognition has attracted increasing interest in a number of research fields, including biomechanics [46-52]. Such research might lead to an IMU-based lifting recognition tool built on data acquired in controlled lifting conditions that would increase the likelihood of detecting the risks associated with WLBDs.

For instance, a LEC-based lifting recognition tool could be designed by considering one criterion of risk classification based on LEC_M, as shown in **Figure 3.13**.

The LEC-based lifting recognition tool was built considering: low risk jobs as the interval between 0 and [mean+SD of LI=1] (all values under [mean-SD of LI=1] were associated with low risk jobs); medium risk jobs as the interval between [mean-SD of LI=2] and [mean+SD of LI=2]; high risk jobs as the interval between [mean-SD of LI=3] and [mean+SD of LI=3]. The values included in two different intervals or in any interval (grey histogram in **Figure 3.13**), represent ranges for which it is not possible to make a choice because they should be associated with two different types of risk jobs. Values above the high-risk zone indicate very high-risk jobs (purple histogram in **Figure 3.13**).

In particular, LEC_{M_L} values within the range 0-[mean+SD of LI=1], [mean-SD of LI=2]-[mean+SD of LI=2] and [mean-SD of LI=3]-[mean+SD of LI=3] indicate low- (green histogram), medium- (yellow histogram) and high- (red histogram) risk jobs, respectively (**Figure 3.13** (a)). Instead, as regards LEC_{M_Upp+L} and LEC_{M_Tot} values within the range 0-[mean-SD of LI=2], [mean+SD of LI=1]-[mean+SD of LI=2] and [mean-SD of LI=3]-[mean+SD of LI=3] indicate low-, medium- and high- risk jobs, respectively (**Figure 3.13** (b and c)). Others ranges for which it is not possible to make a choice are shown as grey histograms. Finally, values above the red zone indicate very high-risk jobs (purple histogram).

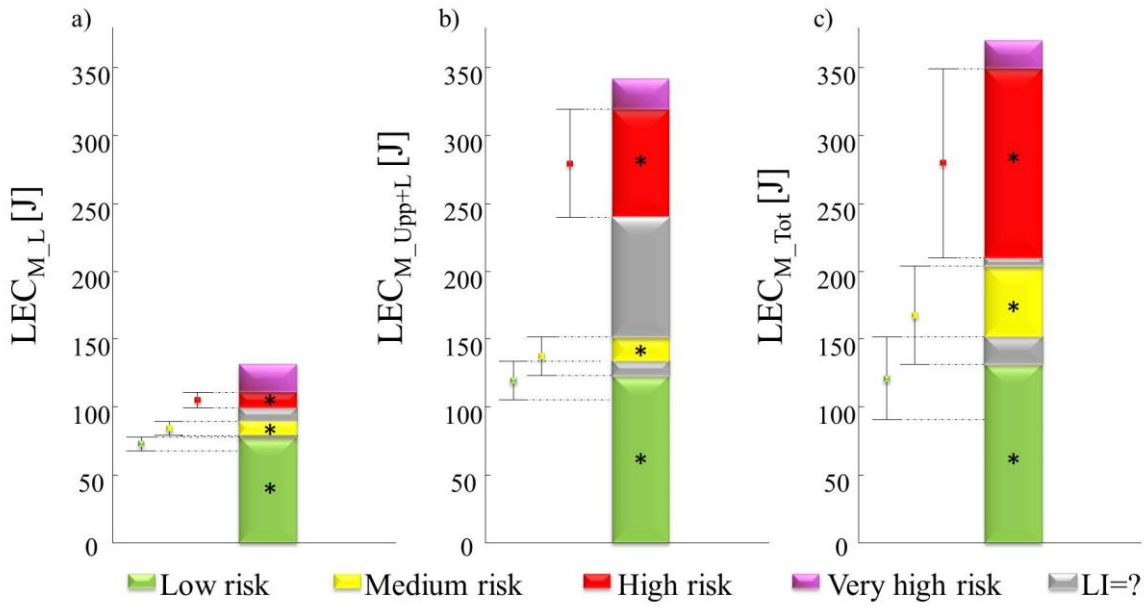

Figure 3.13. An IMU-based lifting recognition tool designed by considering one criterion of risk classification (LEC_{M_L} (a) or LEC_{M_Upp+L} (b) or LEC_{M_Tot} (c)). The error bars represent the mean ± SD values.

Furthermore, findings of this study show that a quantitative machine-learning approach based on ANNs and kinematic data is able to predict the biomechanical risk in lifting activities. A proper combination of kinematic features and network architectures can lead to a good classification. In particular, the training sets, the numbers of hidden layers, and the numbers of neurons in each hidden layer influence the ANNs performance. The best performances were obtained by using SET_2

(containing data derived from upper body and load), SET_7 (containing data derived from upper body, load and smoothness) and SET_8 (containing data derived from the whole body and load and smoothness).

ANNs trained by using SET_2 show a high performance. However, SET_2 takes into account the kinematic behavior of the multi-segment upper body (head, trunk, upper arms, forearms and hands) and load together (CoM_{Upp+L}) and it could fail in presence of human-robot collaboration (HRC) technologies such as wearable assistive devices worn by the workers. For instance, the use of a spinal exoskeleton could strongly reduce the muscle effort without modifying the lifting kinematics, thus implying a misclassification.

This limit linked to the use of HRC technologies could be completely eliminated, or at least greatly reduced, by using SET_7 and SET_8. Both SETs allow the best performance with the advantage to take into account also information about the smoothness of the motion, the only index that, unlike the other kinematic indices, could be sensitive to the use of assistive devices, changing it when the worker wears them.

Among these, SET_7 shows a reliable performance also in terms of variability, meaning that biomechanical risk estimation using this specific SET is reliable and repeatable at the same time.

Furthermore, it is worth highlighting that errors never imply misclassification between LI=1 and LI=3 that represent the lowest and the highest risk classes respectively, and this constitutes a desired and acceptable behavior of an LI classifier.

Moreover, it has been shown that the best performance is almost always obtained with only one hidden layer (see **Figure 3.12**), and the increase of the network complexity does not improve the risk estimation. This aspect is of importance when dealing with applications in real scenarios using wearable sensors, since the reduced network complexity lowers the overall computational cost needed to train the ANNs.

3.3.1 Limitations and future developments

One limitation of this method may be its suitability for the assessment of composite or sequential [53] manual lifting jobs in which the lifting tasks are significantly different. Another limitation of this study is the use of only male workers; indeed, gender aspects are important, and they may lead to different results.

This study may be developed further by: i) widening the range of lifting task types with the same LI but changing the multiplier values; ii) testing also lifting conditions with LI values lower than 1, between 1 and 2, and between 2 and 3; iii) analyzing changes in the criteria selected due to temperature and humidity, sex, age, work experience, etc. The study could also be extended by using, in addition to the optoelectronic motion analysis system, wearable inertial sensors during manual material lifting tasks in the laboratory in different lifting conditions.

The study could also be extended by using wearable inertial sensors during manual material lifting tasks in the laboratory in different lifting conditions to compare the results obtained using the optoelectronic system with those provided by inertial sensors, thereby validating and strengthening the applicability of this method in indoor and outdoor work environments. An instrumental lifting recognition tool could be further implemented by using surface electromyography-based indices that would provide additional criteria of classification and enhance the power of the test.

BIBLIOGRAPHY

1. Marras, W.S.; Fine, L.J.; Ferguson, S.A.; Waters; T.R. The effectiveness of commonly used lifting assessment methods to identify industrial jobs associated with elevated risk of low-back disorders. *Ergonomics* **1999,** *42 (1)*, 229-245. http://doi: 10.1080/001401399185919
2. Lavender, S.A.; Li, Y.C.; Natarajan, R.N.; Andersson, G.B. Does the asymmetry multiplier in the 1991 NIOSH lifting equation adequately control the biomechanical loading of the spine? *Ergonomics* **2009**, *52 (1)*, 71-79.
3. Dempsey, P.G. Usability of the revised NIOSH lifting equation. *Ergonomics* **2002**, *45 (12)*, 817-828.
4. Elfeituri, F.E.; Taboun, S.M. An evaluation of the NIOSH Lifting Equation: a psychophysical and biomechanical investigation. *Int J Occup Saf Ergon* **2002**, *8 (2)*, 243-258.
5. Dempsey, P.G.; Fathallah FA. Application issues and theoretical concerns regarding the 1991 NIOSH equation asymmetry multiplier. *Int J Ind Ergon* **1999**, *23*, 181-191.
6. Wang, M.; Garg, A.; Chang, Y.; Shin, Y.; Yeh, W.; Lee, C. The relationship between low back discomfort ratings and the NIOSH lifting index. *Hum Factors* **1998**, *40*, 509–515.
7. Nussbaum, M.; Chaffin, D.; Page, G. A biomechanical investigation of the asymmetric multiplier in the revised NIOSH lifting equation. In Proceedings of the Human Factors and Ergonomics Society 39th Annual Meeting (709–713). Santa Monica, CA, USA: Human Factors and Ergonomics Society.
8. Karwowski, W.; Brokaw N. Implications of the proposed revisions in a draft of the revised NIOSH lifting guide (1991) for job redesign: A field study," In Proceedings of the 36th Annual Meeting of the Human Factors Society, pp.659–663, Santa Monica, CA, USA: Human Factors Society. **1995**.
9. Sesek, R.; Gilkey, D.; Drinkaus, P.; Bloswick, D.S.; Herron, R. Evaluation and quantification of manual materials handling risk factors. *Int J Occup Saf Ergon* **2003**, *9 (3)*, 271-287.
10. Dempsey, P.G.; Burdorf, A.; Fathallah, F.A. Sorock, G.S., Hashemi, L. Influence of measurement accuracy on the application of the 1991 NIOSH equation. *Appl Ergon* **2001** *32 (1)*, 91-99.
11. Zurada, J.; Karwowski, W.; Marras, W.S. A neural network-based system for classification of industrial jobs with respect to risk of low back disorders due to workplace design. *Appl Ergon* **1997**, *28(1),* 49-58.
12. Chen, C.L.; Kaber, D.B.; Dempsey, P.G. A new approach to applying feedforward neural networks to the prediction of musculoskeletal disorder risk. *Appl Ergon* **2000**, *31*, 269-282.
13. Chen, C.L.; Kaber, D.B.; Dempsey, P.G. Using feedforward neural networks and forward selection of input variables for an ergonomics data classification problem. *Hum Factors Ergon Manuf* **2004**, *14(1)*, 31-49. http://doi:10.1002/hfm.10052
14. Asensio-Cuesta, S.; Diego-Mas, J.A.; Alcaide-Marzal J. Applying generalised feedforward neural networks to classifying industrial jobs in terms of risk of low back disorders * *International Journal of Industrial Ergonomics* **2010**, *40*, 629-635
15. Waters, T.R.; Putz-Anderson, V.; Garg, A.; Fine, L.J. Revised NIOSH Equation for the Design and Evaluation of Manual Lifting Tasks. *Ergonomics*, **1993**, *36 (7)*, 749–776.
16. Waters, T.R., Putz-Anderson, V.; Garg, A. Applications Manual for the Revised NIOSH Lifting Equation. Cincinnati, OH: U.S. Department of Health and Human Services. **1994.**
17. Cavagna GA, Thys H, Zamboni A (1976) The sources of external work in level walking and running. J Physiol 262 No. 3, 639-657.
18. Cavagna GA, Willems PA, Legramandi MA, Heglund NC (2002) Pendular energy transduction within the step in human walking. J Exp Biol 205 No. 21, 3413-3422.
19. Detrembleur C, Dierick F, Stoquart G, Chantraine F, Lejeune T (2003) Energy cost, mechanical work, and efficiency of hemiparetic walking. Gait Posture 18 No. 2, 47-55.
20. Don R, Serrao M, Vinci P, Ranavolo A, Cacchio A, Ioppolo F, Paoloni M, Procaccianti R, Frascarelli F, De Santis F, Pierelli F, Frascarelli M, Santilli V (2007) Foot drop and plantar flexion failure determine different gait strategies in Charcot-Marie- Tooth patients. Clin Biomech 22 No. 8, 905-916.
21. Della Croce U, Leardini A, Chiari L, Cappozzo A (2005) Human movement analysis using stereophotogrammetry. Part 4: assessment of anatomical landmark misplacement and its effects on joint kinematics. Gait Posture 21 No. 2, 226-237, Review.
22. Leardini A, Chiari L, Della Croce U, Cappozzo A (2005) Human movement analysis using stereophotogrammetry. Part 3. Soft tissue artifact assessment and compensation. Gait Posture 21 No. 2, 212-225, Review.

23. Chiari L, Della Croce U, Leardini A, Cappozzo A (2005) Human movement analysis using stereophotogrammetry. Part 2: instrumental errors. Gait Posture 21 No. 2, 197-211, Review.
24. Cappozzo A, Della Croce U, Leardini A, Chiari L (2005) Human movement analysis using stereophotogrammetry. Part 1: theoretical background," Gait Posture 21 No. 2, 186-196, Review.
25. Gómez-Galán M, Pérez-Alonso J, Callejón-Ferre ÁJ, López-Martínez J. (2017) Musculoskeletal disorders: OWAS review. Ind Health.
26. Taborri J, Palermo E, Rossi S, Cappa P (2016) Gait Partitioning Methods: A Systematic Review. Sensors 16 No. 1.
27. Sprager S, Juric MB (2015) Inertial Sensor-Based Gait Recognition: A Review. Sensors 15 No. 9, 22089-22127.
28. Gutierrez-Farewik EM, Bartonek A, Saraste H (2006) Comparison and evaluation of two common methods to measure center of mass displacement in three dimensions during gait. Hum Mov Sci 25, 238-256.
29. Rab G, Petuskey K, Bagley A (2002) A Method for Determination of Upper Extremity Kinematics. Gait Posture 15 No. 2, 113–119.
30. Davis III RB, Õunpuu S, Tyburski D, Gage JR (1991) A gait analysis data collection and reduction technique. Hum Mov Sci 10, 575–587.
31. Wu G, Siegler S, Allard P, Kirtley C, Leardini A, Rosenbaum D, M. Whittle M, D'Lima DD, Cristofolini L, Witte H, Schmid O, Stokes I (2002) Standardization and Terminology Committee of the International Society of Biomechanics. ISB Recommendation on Definitions of Joint Coordinate System of Various Joints for the Reporting of Human Joint Motion. Part I. Ankle, Hip, and Spine. J Biomech 35 No. 4, 543–548.
32. Wu G, van der Helm FC, Veeger HE, Makhsous M, Van Roy P, Anglin C, Nagels J, Karduna AR, McQuade K, Wang X, Werner FW, Buchholz B (2005) International Society of Biomechanics. ISB Recommendation on Definitions of Joint Coordinate Systems of Various Joints for the Reporting of Human Joint Motion. Part II. Shoulder, Elbow, Wrist and Hand. J Biomech 38 No. 5, 981–992.
33. Zatsiorsky VM, Seluyanov VN, Chugunova LG (1990) Methods of determining mass-inertial characteristics of human body segments. In G.G. Chernyi & S.A. Regirer, Contemporary Problems of Biomechanics, 272-291.
34. De Leva P (1996) Adjustments to Zatsiorsky-Seluyanov's segment inertia parameters J Biomech 29 No. 9, 1223-1230.
35. Winter DA (1990) Biomechanics and Motor Control of Human Movement New York: Wiley.
36. Sakata, K.; Kogure, A.; Hosoda, M.; Isozaki, K.; Masuda, T.; Morita, S. Evaluation of the age-related changes in movement smoothness in the lower extremity joints during lifting. *Gait Posture* **2010**, *31(1)*, 27-31. doi: 10.1016/j.gaitpost.2009.08.239.
37. Plamondon A, Gagnon M, Desjardins P (1996) Validation of two 3-D segment models to calculate the net reaction forces and moments at the L5/S1 joint in lifting. Clin Biomech 11 No. 2, 101-110.
38. Rumelhart, D.E.; Hinton, G.E.; Williams, R.J. Learning internal representations by error propagation, In Parallel Distributed Processing, Cambridge, MA: MIT Press. **1986**, *1*, 318-362.
39. Granata KP, Marras WS (1995) An EMG-assisted model of trunk loading during free-dynamic lifting. J Biomech 28 No. 11, 1309-1317.
40. de Looze MP, Bussmann JB, Kingma I, Toussaint HM (1992) Different methods to estimate total power and its components during lifting. J Biomech 25(9), 1089-1095.
41. Li KW, Yu RF, Han XL (2007) Physiological and psychophysical responses in handling maximum acceptable weights under different footwear--floor friction conditions. Appl Ergon 38(3), 259-65.
42. Burdett RG, Skrinar GS, Simon SR (1983) Comparison of mechanical work and metabolic energy consumption during normal gait. J Orthop Res 1(1), 63-72.
43. Cotes JE, Meade F (1960) The energy expenditure and mechanical energy demand in walking. Ergonomics 3, 97-119.
44. De Looze MP, Toussaint HM, Commissaris DA, Jans MP, Sargeant AJ (1994) Relationships between energy expenditure and positive and negative mechanical work in repetitive lifting and lowering. J Appl Physiol 77(1), 420-6.
45. Horwat F, Meyer JP, Malchaire J (1988) Validation of a new pocket computer assisted method for metabolic rate estimation in field studies. Ergonomics 31(8), 1155–1164.
46. Fong DTP, Chan YY (2010) The use of wearable inertial motion sensors in human lower limb biomechanics studies: a systematic review. Sensors 10 No. 12, 11556-1165.
47. Tao W, Liu T, Zheng R, Feng H (2012) Gait Analysis Using Wearable Sensors. Sensors 12, 2255–2283.
48. Whittle MW (2008) Gait Analysis: An Introduction. 4th ed. Butterworth-Heinemann, Elsevier: Edinburgh, UK.
49. Favre J, Aissaoui R, Jolles B, de Guise J, Aminian K (2009) Functional calibration procedure for 3D knee joint angle description using inertial sensors J Biomech 42, 2330–2335.
50. Liu T, Inoue Y, Shibata K (2009) Development of a wearable sensor system for quantitative gait analysis. Measurement 42, 978–988.

51. Klucken J, Barth J, Kugler P, Schlachetzki J, Henze T, Marxreiter F, Kohl Z, Steidl R, Hornegger J, Eskofier B, Winkler J (2013) Unbiased and Mobile Gait Analysis Detects Motor Impairment in Parkinson's Disease. PLoS ONE 8 No. 2.
52. Muro-de-la Herran A, García-Zapirain B, Méndez-Zorrilla A (2014) Gait Analysis Methods: An Overview of Wearable and Non-Wearable Systems, Highlighting Clinical Applications. Sensors 14, 3362–3394.
53. Waters TR, Dick RB, Davis-Barkley J, Krieg EF (2007) A cross-sectional study of risk factors for musculoskeletal symptoms in the workplace using data from the General Social Survey (GSS). J Occup Environ Med 49, 172–184.

CHAPTER IV

4. SEMG FEATURES AND NEURAL NETWORKS FOR RISK ASSESSMENT DURING LIFTING ACTIVITY

As highlighted in the previous chapter, to overcome NIOSH restrictions, there is a need to move from a semi-quantitative to a quantitative assessment of the risks posed by a lifting task.

Surface electromyography (sEMG) has been widely demonstrated as a technique for improving human movement analysis; sEMG has been shown to provide significant information from time and frequency domain features [1-3]. Several features extracted from the sEMG signal have a neurophysiological correlation, mainly for what concerns the amount of neural drive to muscle, the kind of recruited fibers and the muscle fiber conduction velocity [4]: for example, the muscle co-activaction index [5], the root mean square, the averaged rectified value [1], and the median or mean frequency [2], have been successfully and widely used in ergonomics, both in the laboratory and at the workplace.

Based on the previous considerations, sEMG features as artificial neural networks (ANNs) input have been used for predicting LBDs expressed in terms of LI during the execution of controlled lifting tasks.

The sEMG activity from a variety of trunk muscles was recorded with the following aims: 1) to identify the most sensitive trunk muscles with respect to changes in lifting conditions based on the selected sEMG features; 2) to evaluate the relationship between the indices extracted by identified muscles and forces (F_{L5-S1}) and moments (M_{L5-S1}) at the L5-S1 joint. 3) to test whether machine-learning techniques (ANNs) used for mapping time and frequency sEMG features on LI levels can improve the biomechanical risk estimation. Indeed, techniques such as sEMG for risk assessment

could be integrated with methods already used for the biomechanical risk assessment, with the aim of quantifying the risk also when the RNLE cannot be applied. In addition, this integrated approach could overcome one of the main limits of RNLE, consisting in jobs misidentification based on risk [6].

Furthermore, the possibility to implement the integrated approach on electronic smart devices (smartphones, phablets, tablets and smartwatches) would allow a simplified analysis in the workplace as compared to the analysis based on mechanical factors control.

In this chapter, text and figures have been taken from or adapted from the articles "Surface electromyography for risk assessment in work activities designed using the "revised NIOSH lifting equation"" [2018, *International Journal of Industrial Ergonomics]*, and "Lifting activity assessment using surface electromyographic features and neural networks" [2018, *International Journal of Industrial Ergonomics*] which were co-authored by me".

4.1 STUDY N°1: SURFACE ELECTROMYOGRAPHY FOR RISK ASSESSMENT IN WORK ACTIVITIES DESIGNED USING THE RNLE

The aims of this study were: to identify surface electromyography (sEMG)-based indices of trunk muscles acquired during the execution of lifting tasks designed using the revised NIOSH lifting equation and featuring a progressively increasing lifting index (LI); to study changes of these indices in relation to the LI; to evaluate the relationship between the identified indices and forces (F_{L5-S1}) and moments (M_{L5-S1}) at the L5-S1 joint.

4.1.1 Materials and Methods

4.1.1.1 Subjects

Twenty male subjects (mean age 33.30±7.39 years, height 1.80±0.07 m, body mass index (BMI) 24.37±2.67 kg/m^2) were recruited in the study (the subjects' sample is the same of 3.1.1).

4.1.1.2 Kinematic, kinetic and electromyographic recordings

The kinematic and kinetic data were recording as in 3.1.2. Furthermore, a 16-channel Wi-Fi transmission surface electromyograph (FreeEMG300 System, BTS, Milan, Italy) was used to acquire the surface myoelectric signals at a sampling rate of 1000 Hz. After skin preparation, bipolar Ag/AgCl surface electrodes (diameter 2 cm, H124SG Kendall ARBO, Tyco healthcare, Neustadt/Donau, Germany), prepared with electroconductive gel, were placed over the muscle belly in the direction of the muscle fibers (distance of 2 cm between the center of the electrodes) according to the European recommendations for surface electromyography [7] and the atlas of muscle innervation zones [8]. Twelve bipolar electrodes were placed bilaterally on the erector spinae longissimus (ESL), erector spinae iliocostalis (ESI), multifidus (M), latissimus dorsi (LD), rectus abdominis superior (RAS) and rectus abdominis middle (RAM) muscles (**Figure 4.1**). The first four muscles were chosen because of their role as trunk extensors, the last two because of their role as flexors.

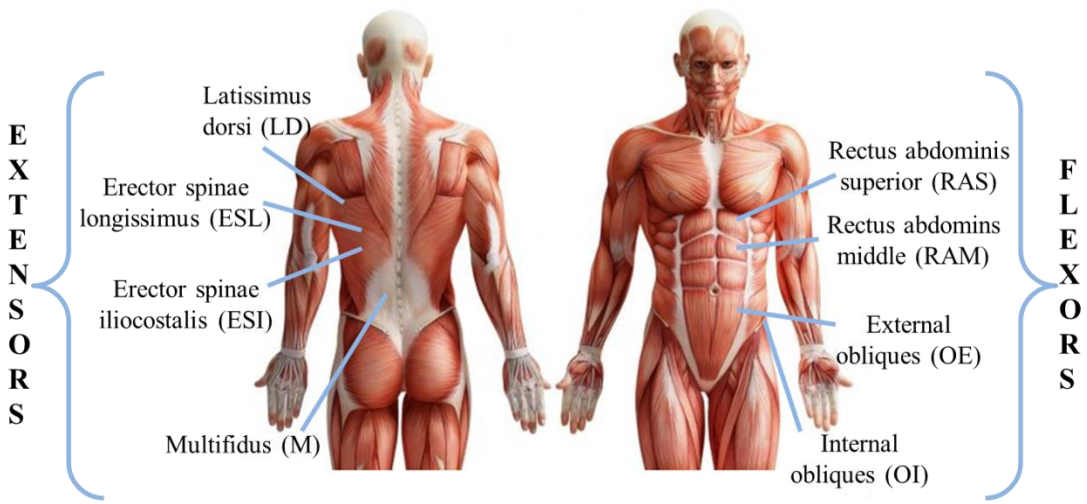

Figure 4.1. *Muscles recorded by EMGs.*

Data acquisition from the optoelectronic cameras, dynamometric platforms and surface electromyography were integrated and synchronized. Particularly, all the data were managed by a unique data station which collected them. Optoelectronic cameras and force platforms were

connected via Ethernet while the sEMG system via Wi-Fi. The synchronization was guaranteed by a unique internal clock that manages optoelectronic, kinetic and sEMG signals by means of a high-quality synchronization protocol for networked devices [9].

4.1. 1.3 Experimental Procedures

The experimental procedures were the same of in 3.1.3.

4.1.1.4 Data analysis

The Lifting Cycle definition was performed as in 3.1.4.1 then the following kinematic and electromioraphic parameters were taken in the account.

Force and moment calculation

The net reaction forces (F_{L5-S1}) and moments (M_{L5-S1}) at the L_5-S_1 joint were calculated in the GRS according to the dynamic multi-segment upper body model (hands, forearms, arms, head and trunk) using the formulas in 3.1.4.5 and the following formula [10]:

$$M_{L5-S1} = -\sum_{j=1}^{n}\left(r_j - r_{L5-S1}\right) x\, F_j$$

$$-\sum_{i=1}^{p}(r_i - r_{L5-S1})\, x\, m_i g \; + \sum_{i=1}^{p}(r_i - r_{L5-S1})\, x\, m_i a_i \; + \sum_{i=1}^{p}\frac{d}{dt}(I_i\omega_i)$$

where: n is the number of external forces; F_j is the j_{th} external force; p is the number of body segments considered; g is the acceleration of gravity; r_j is the position of the j_{th} external force; r_{L5-S1} is the position of the L_5-S_1 joint; r_i, m_i a_i, I_i, and ω_i are the position of the centre of mass, the mass [10-11], the acceleration, the moment of inertia and the angular velocity of the i_{th} segment, respectively. The moments of inertia Ii were calculated by modelling the overall system as follows: one cylinder for the trunk and head, two cylinders for the right and left upper arms, two cylinders

for the right and left forearms and hands and one parallelepiped for the load. The formulas used for the calculation of the I_i are reported below:

$$I_i = \frac{1}{2} m_i \left(3 \left(\frac{d_i}{2} \right)^2 + {h_i}^2 \right)$$

$$I_i = \frac{1}{12} m_l (d_l^2 + h_l^2)$$

where m_i is the mass of the i_{th} segment, h_i and d_i are the height and diameter of the i_{th} cylinder, while m_l is the mass of the load, h_l and d_l are the height and depth of the parallelepiped.

The projections of F_{L5-S1} on the y axis and on x- z plane were called longitudinal ($Flong_{L5-S1}$) and transversal ($Ftrans_{L5-S1}$) forces, respectively. We also considered F_{L5-S1} in a local reference system (LRS) on the trunk in which the y' axis is oriented as the vector C7-sacrum and x'-z'represents the orthogonal plane to y'. In this LRS, the components of F_{L5-S1} on the y' axis and the x'-z' plane were called compression ($Fcompr_{L5-S1}$) and shear ($Fshear_{L5-S1}$) forces, respectively.

sEMG parameters

Before the time normalization was performed, sEMG signals were processed as follows:

- the iMVC and the sEMG raw data of each lifting trial were band-pass filtered using a fourth-order Butterworth filter between 20 and 450 Hz, in order to reduce motion artifacts and other components of high frequency noise and to remove the ECG artefacts from all the trunk muscles [12-13];
- subsequently, to extract the envelope of muscle activity, full-wave rectification of signals was performed and low-pass filtering using a fourth-order Butterworth filter at 5 Hz [14] was applied;
- the rectified and filtered sEMG data related to each lifting trial were expressed as a percentage of the sEMG peak value [7, 15-17] calculated as the mean of the maximum values detected for

each of the two iMVCs [7, 17-21]. In detail we normalized the sEMG amplitude to a 0–100% range through dividing the instantaneous amplitude by the value obtained when performing a maximum voluntary contraction in static conditions.

From the elaborated sEMG signals of each lifting trial, in order to characterize differences in the sEMG activity between different conditions, we computed the average rectified value (ARV), the root mean square (RMS) and the maximum value (Max) within the cycle. ARV and RMS were calculated as follows:

$$ARV = \frac{1}{101}\sum_{k=0}^{100} sEMG_k$$

$$RMS = \sqrt{\frac{1}{101}\sum_{k=0}^{100} sEMG_k^2}$$

where $sEMG_k$ is the k_{th} sample value of the envelope of each muscle. Furthermore, the simultaneous activation of the trunk muscles (co-activation) was calculated by considering the time-varying multi-muscle co-activation function (TMCf) proposed by Ranavolo and colleagues [5]:

$$TMCf(d(k),k) = \left(1 - \frac{1}{1+e^{-12(d(k)-0.5)}}\right).\frac{\left(\sum_{m=1}^{M} sEMG_m(k)/(100xM)\right)^2}{max_{m=1\ldots M}[sEMG_m(k)]}$$

where d(k) is the mean of the differences between each pair of $sEMG_m(k)$, M is the number of muscles considered in the analysis, $sEMG_m$ is the sEMG signal of the m_{th} muscle. As co-activation indices, the area of total TMCf ($TMCf_{Area}$) and the maximum ($TMCf_{Max}$) within the cycles were considered. We calculated the TMCf, $TMCf_{Area}$ and $TMCf_{Max}$ by considering all twelve trunk muscles (TMCf_12, $TMCf_{Area}$_12 and $TMCf_{Max}$_12) as well as only four trunk muscles (right and left ESL and right and left RAS; TMCf_4, $TMCf_{Area}$_4 and $TMCf_{Max}$_4) to verify the possibility to reduce the number of muscles included in the analysis to simplify the acquisition protocol. The data from the ten lifting

tasks (5 repetitions for symmetric and 5 repetitions for asymmetric tasks) for each condition (LI=1, 2 and 3) were averaged for each subject.

4.1.1.5 Statistical Analysis

All the analyses were performed using SPSS 17.0 software (SPSS Inc. Chicago, IL, USA). The Shapiro-Wilk and Kolmogorov–Smirnov test were used to analyze the normal distribution of the data. For each lifting condition and for each parameter, a parametric paired samples t-test was applied to detect any differences between the right and left muscles and between co-activations calculated with both twelve and four muscles. We performed a one-way repeated-measures ANOVA to determine whether there was any significant difference between the three low back pain risk levels. Post-hoc analyses, with Bonferroni's corrections, were performed when significant differences were observed in the ANOVA. The Pearson test was used to investigate any correlation between each of the sEMG parameters and forces and moments. The Pearson test was also used to investigate the correlations between each of the sEMG parameters (ARV, RMS, $TMCf_{Area}$_12, $TMCf_{Max}$_12, $TMCf_{Area}$_4 and $TMCf_{Max}$_4) and the LI levels. A p value of less than 0.05 was considered statistically significant.

4.1.2. Results

No statistical differences emerged between the right and left muscles in any of the sEMG parameters, ARV, RMS or Max (all $p>0.05$). Thus, the results were pooled across sides.

The repeated measures ANOVA revealed a significant effect of the LI on ARV and Max for all the muscles except RAM, and on RMS for ESL, ESI and LD (**Table 4.1**).

Table 4.2 shows the p-values of the paired *t* test with Bonferroni's corrections for the ARV, RMS and Max of all the muscles investigated, which highlight the differences between pairs of LI. Significant differences and means with standard deviations are shown in **Figure 4.2**.

		ESL	ESI	M	LD	RAS	RAM
ARV	F	33.404	9.044	15.874	11.923	31.268	5.120
	df	2	2	2	2	2	2
	p	**<0.001**	**0.002**	**<0.001**	**0.001**	**<0.001**	**0.017**
RMS	F	24.003	8.851	15.791	21.894	30.552	5.139
	df	2	2	2	2	2	2
	p	**<0.001**	**0.002**	**<0.001**	**<0.001**	**<0.001**	0.077
Max	F	53.850	24.501	17.256	7.307	13.053	1.906
	df	2	2	2	2	2	2
	p	**<0.001**	**<0.001**	**<0.001**	**0.006**	**<0.001**	0.181

Table 4.1. *The F, df and p-values of the repeated measures ANOVA considering the ARV, RMS and Max in the three lifting conditions (LI=1, LI=2 and LI=3) for the six muscles ESL, ESI, M, LD, RAS and RAM. Bold type indicates statistical significance.*

	LI	ESL	ESI	M	LD	RAS	RAM
ARV	1 vs 2	**0.001**	**<0.001**	**0.001**	**0.002**	**0.004**	0.226
	1 vs 3	**<0.001**	**0.019**	**0.003**	**0.017**	**<0.001**	0.143
	2 vs 3	**0.017**	0.482	0.971	0.086	**0.003**	0.130
RMS	1 vs 2	**0.006**	**<0.001**	**0.001**	**<0.001**	**0.004**	.
	1 vs 3	**0.001**	**0.020**	**0.003**	**0.002**	**<0.001**	.
	2 vs 3	**0.019**	0.485	0.959	0.555	**0.004**	.
Max	1 vs 2	**0.001**	**<0.001**	**0.002**	**0.006**	0.689	.
	1 vs 3	**<0.001**	**0.001**	**0.003**	0.066	**0.011**	.
	2 vs 3	**0.002**	0.113	0.476	0.271	**0.018**	.

Table 4.2. *The p-values of the paired t test with Bonferroni's corrections between pairs of different LI levels for the ARV, RMS and Max for the six muscles ESL, ESI, M, LD, RAS and RAM. Bold type indicates statistical significance.*

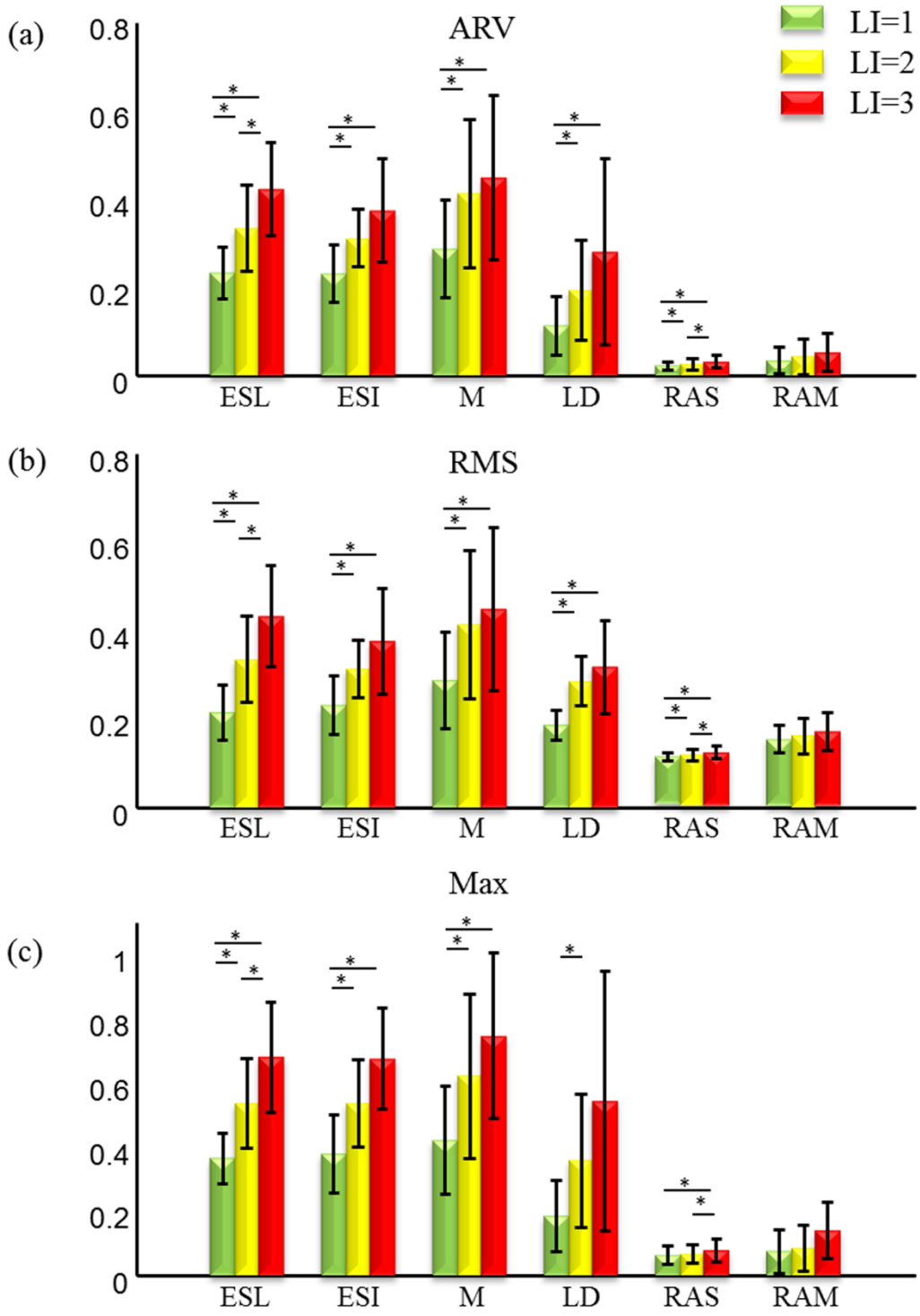

Figure 4.2. Surface electromyographic parameters of the trunk muscles

*Means and standard deviations of 20 subjects' ARV (a), RMS (b) and Max (c) of the bilateral trunk muscles ESL, ESI, M, LD, RAS and RAM, while performing manual lifting tasks of three low back pain risk levels (LI=1, 2 and 3). N=20 for each lifting risk level. * Significant differences at post hoc analysis.*

As regards the co-activation indices in each lifting task with same LI, no significant differences were observed either between $TMCf_{Area}$_12 and $TMCf_{Area}$_4 (p=0.626) or between $TMCf_{Max}$_12 and $TMCf_{Max}$_4 (p=0.352).

The repeated measures ANOVA revealed a significant effect of the LI on $TMCf_{Area}$_12 and $TMCf_{Area}$_4 (F=36.642, df=1.504, p<0.001 and F=23.756, df=1.742, p<0.001 respectively) and $TMCf_{Max}$_12 and $TMCf_{Max}$_4 (F=47.717, df=1.323, p<0.001 and F=79.055, df=1.310, p<0.001 respectively). When investigating differences in co-activation between pairs of the 3 low back pain risk levels, significant differences were observed in both $TMCf_{Area}$ and $TMCf_{Max}$ between LI 1 and 2 ($TMCf_{Area}$_12: p=0.001; $TMCf_{Area}$_4: p=0.007; $TMCf_{Max}$_12: p<0.001; $TMCf_{Max}$_4: p<0.001), LI 2 and 3 ($TMCf_{Area}$_12: p=0.008; $TMCf_{Area}$_4: p=0.027; $TMCf_{Max}$_12: p=0.010; $TMCf_{Max}$_4: p=0.001) and LI 1 and 3 ($TMCf_{Area}$_12: p<0.001; $TMCf_{Area}$_4: p=0.001; $TMCf_{Max}$_12: p<0.001; $TMCf_{Max}$_4: p<0.001). Mean and SD values and significant differences are shown in **Figure 4.3**.

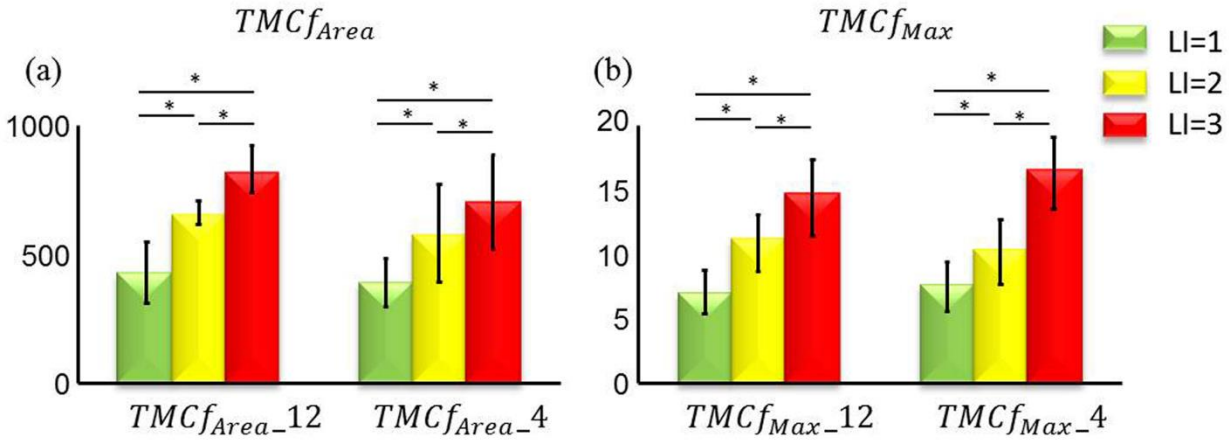

Figure 4.3. *$TMCf_{Area}$ (a) and $TMCf_{Max}$ (b) calculated while performing manual material lifting trials in the three different conditions (LI=1, LI=2 and LI=3) for all the muscles investigated ($TMCf_{Area}$_12 and $TMCf_{Max}$_12) and for right and left ESL and RAS ($TMCf_{Area}$_4 and $TMCf_{Max}$_4). N=20 for each lifting risk level. * Significant difference at post hoc analysis.*

A qualitative description of a representative subject of F_{L5-S1} and M_{L5-S1}, the trunk flexion-extension, sEMG activity and TMCf_12 during the execution of the lifting tasks in the different lifting conditions (LI=1, 2 and 3) is provided in **Figure 4.4**. This figure shows mean curves (with shaded SDs)

of combined 10 trials of different lifting tasks (no lift asymmetry and lift asymmetry) with the same LI for one subject sample.

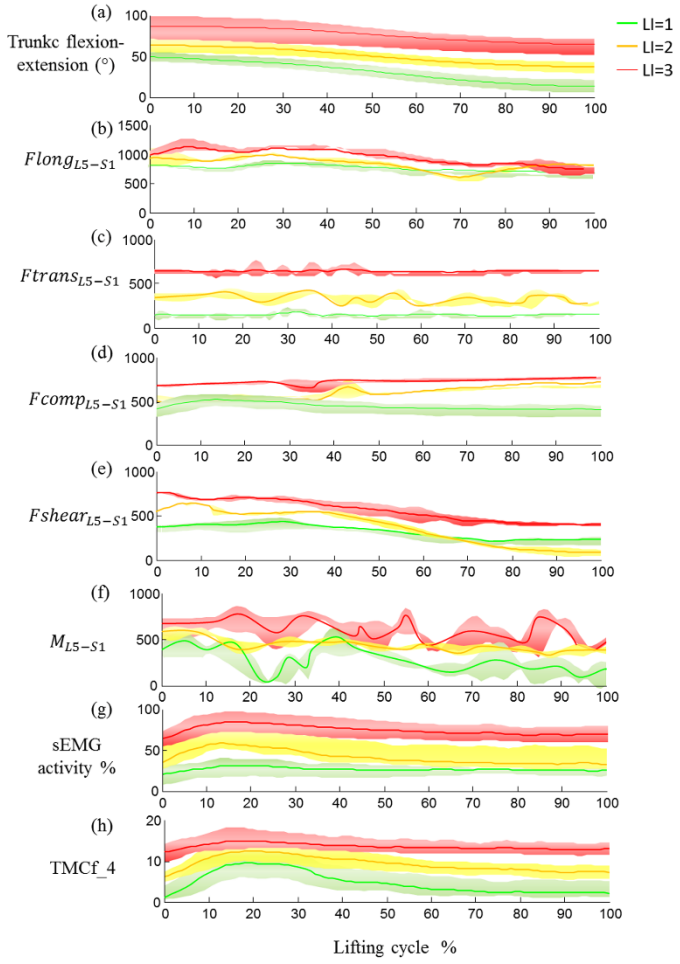

Figure 4.4. *A qualitative description of a representative subject of the trunk flexion-extension (a),* $Flong_{L5-S1}$ *(b),* $Ftrans_{L5-S1}$ *(c),* $Fcomp_{L5-S1}$ *(d),* $Fshear_{L5-S1}$ *(e),* M_{L5-S1} *(f), sEMG activity (g) and* $TMCf_{Max}\_12$ *(h) during the execution of the lifting tasks in the three different conditions (LI=1, LI=2 and LI=3). Curves represent the mean values with shaded SDs. Data are normalized to the lifting duration and reduced to 101 samples over the cycle.*

Figure 4.5 illustrates correlations between $Flong_{L5-S1}$, $Ftrans_{L5-S1}$, $Fcomp_{L5-S1}$, $Fshear_{L5-S1}$ and M_{L5-S1} and the sEMG parameters (ARV, RMS, Max, $TMCf_{Area}\_12$, $TMCf_{Max}\_12$, $TMCf_{Area}\_4$ and $TMCf_{Max}\_4$). Each plot contains 60 points, which correspond to the 20 subjects performing the different lifting conditions (points represent LI=1, 2 and 3). Triangles represent the mean of the twenty points for each lifting condition (LI=1, 2 and 3). This figure also shows the r and p values.

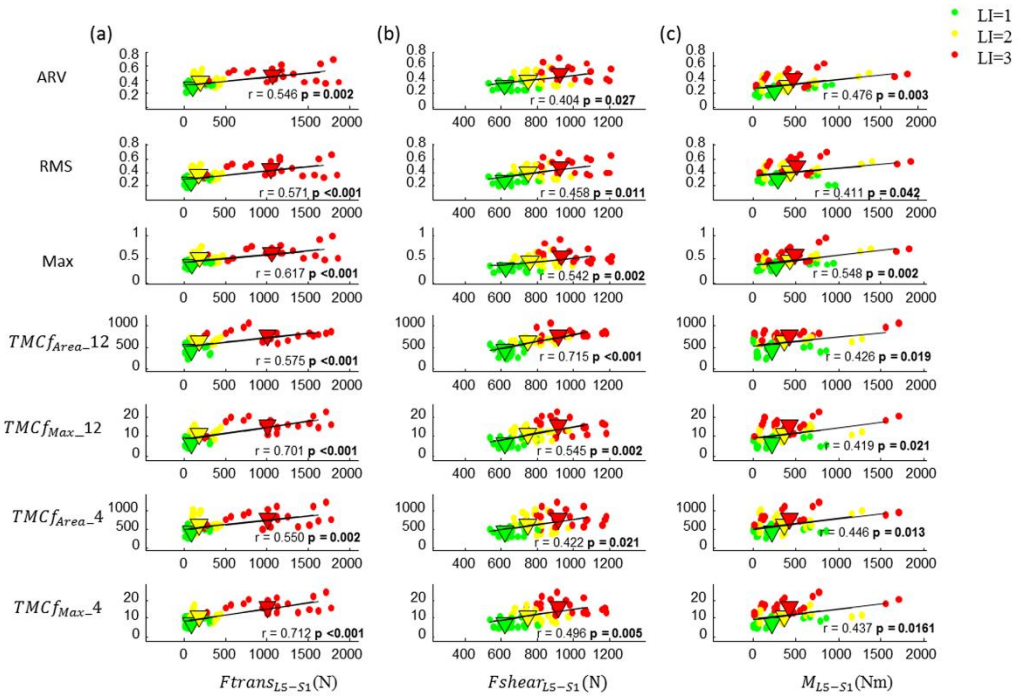

Figure 4.5. Correlation between the ARV, RMS, Max (all calculated on ESL), $TMCf_{Area}\_12$, $TMCf_{Max}\_12$, $TMCf_{Area}\_4$ and $TMCf_{Max}\_12$ and the maximum values of $Ftrans_{L5-S1}$ (a), $Fshear_{L5-S1}$ (b) and M_{L5-S1}, (c). The number of sample size is 60. Each plot contains 60 points, which correspond to the 20 subjects performing the lifting tasks in the three different conditions (LI=1, LI=2 and LI=3). Triangles represent the mean of the twenty points for each lifting condition. Each plot shows the r and p values. Bold type indicates statistical significance.

Table 4.3 shows the r and p values of the Pearson test carried out between each of the sEMG parameters (ARV, RMS, $TMCf_{Area}\_12$, $TMCf_{Max}\_12$, $TMCf_{Area}\_4$ and $TMCf_{Max}\_4$) and the LI levels.

	R	p
LI vs ARV	0,608	**< 0.001**
LI vs RMS	0,687	**< 0.001**
LI vs Max	0,844	**< 0.001**
LI vs TMCfArea_12	0,828	**< 0.001**
LI vs TMCfMax_12	0,803	**< 0.001**
LI vs TMCfArea_4	0,643	**< 0.001**
LI vs TMCfMax_4	0,800	**< 0.001**

Table 4.3. *The r and p-values of the Pearson test carried out between each of the sEMG parameters, ARV, RMS (all calculated on ESL), $TMCf_{Area}\_12$, $TMCf_{Max}\_12$, $TMCf_{Area}\_4$ and $TMCf_{Max}\_4$ and the LI levels. Bold type indicates statistical significance.*

4.1 3 Discussions and Conclusions

In this study, the sEMG activities of the trunk extensor and flexor muscles and forces and moments at the L_5-S_1 joint during the execution of three-dimensional dynamic lifting trials designed using the RNLE were investigated. In particular, three lifting conditions with a progressively increase of LI (LI=1, LI=2 and LI=3) were analyzed. A correlation analysis was also performed between the sEMG parameters and forces and moments at the L_5-S_1 joint, hypothesizing that a quantitative sEMG-based Lifting Risk Recognition Tool can be used as a risk assessment method in association with the NIOSH protocol. sEMG has previously been used in sEMG-assisted models and methods developed for continuous estimates of low back compression during whole-body free dynamic lifting [22-23]. Ranavolo and colleagues [5] showed that the sEMG-based indices, particularly co-activation values, increased with LI increment. Furthermore, Le et al. [24] developed an EMG-based coactivation index for the lumbar spine to assess complex dynamic tasks (i.e. task ergonomics) and to develop rehabilitation strategy.

Furthermore, sEMG is increasingly being applied in ergonomic investigations throughout the world [1] thanks to miniaturization process and the introduction of wireless probes.

The results of this study did not reveal any differences, in any of the lifting conditions, between the right and left trunk muscle sEMG activities. Indeed, even though the analysis took into account both symmetrical and asymmetrical tasks, no differences emerged between the right and left sides of the trunk in the ARV, RMS or Max calculated on the same muscles.

No differences between right and left side in asymmetric tasks with the same LI, may be caused by the small 30 degree asymmetry angle. This finding suggests that, for symmetric and asymmetric tasks (with small 30 degree asymmetry angle), an instrumental sEMG-based tool designed for risk assessment purposes could take into consideration a halved number of trunk muscles parameters (six instead of twelve).

Furthermore, the statistical analysis performed on our data highlighted that the ARV and Max, calculated for all the trunk extensor muscles and for the flexor muscle RAS, are influenced by the risk levels and that they significantly increased with the LI (**Table 4.1** and **Figure 4.2**). Similar findings were observed for the RMS of the ESL, ESI and LD. These trends show that the ARV, RMS and Max are reliable indicators of the greater muscle involvement resulting from the increased level of physical stress. In particular, when we compared the three different lifting conditions (LI 1 versus 2, 1 versus 3 and 2 versus 3), the ESL proved to be the only trunk extensor muscle for which every ARV, RMS and Max amplitude parameter discriminates each of pairs with different LI level (**Table 4.2** and **Figure 4.2**). The ARV and RMS of the flexor muscle RAS were found to be the parameters that discriminate each of the risk level pairs. With a view to further reducing the number of muscles to be acquired, these findings suggest that the ESL and RAS may be used to correctly interpret low-, medium- and high-risk jobs. Indeed, it may be possible to calculate the ARV, RMS and Max for the ESL, and the ARV alone for RAS, to obtain reliable results, thereby restricting the analysis required to only two muscles. Obviously, the attained results, as well as the possibility of reducing the number of muscles to be acquired to only two muscles, must be strengthened by other experiments in which the same values of LI (LI=1, 2 and 3) are obtained based on other several combinations of multiplier values (i.e. by exploring higher values of asymmetry). The appropriateness of the ARV, RMS and Max as sEMG signal amplitude estimators has previously also been reported in the scientific literature [1, 15, 25]. The ARV and RMS are linearly related in case of a Gaussian signal distribution and provide an overall estimate of the muscle activity within the cycle. The ARV is widely used because of its high precision [25] and linear relationship to force [26], and the RMS because of its direct relationship to signal power [27]. The Max provides a local estimate of sEMG activity related to the maximal effort of the muscle within the cycle. In the light of these considerations, we

think that the ARV and RMS could be particularly useful to discriminate globally the low-, medium- and high-risk jobs.

The systematic increased activity of both the extensor and flexor muscles of the trunk related to an increasing LI is congruous with the need for improved spinal stability achieved by recruiting antagonistic co-activation (**Figure 4.3**) [5, 22-23,28-30]. Unfortunately, co-activation contributes to a reduction in the net moments at the L_5-S_1 joint and to a 12-18% increase of the spinal load, which in turn increases the risk of LBDs [5, 22, 27]. However, trunk muscle co-activation is generally recruited to balance the risk of injury associated with tissue overload and the risk of spinal instability. We calculated the co-activation by using TMCf [5] and considering both twelve and four muscles (right and left ESL and RAS). The statistical inference made on the co-activation indices $TMCf_{Area}$ and $TMCf_{Max}$ did not reveal any differences between $TMCf_{Area}$_12 and $TMCf_{Area}$_4 or between $TMCf_{Max}$_12 and $TMCf_{Max}$_4. These findings indicate that it may be possible to reduce the number of muscles included in the analysis, focusing on only the ESL and RAS, though it would be necessary to acquire data from both the right and left sides in this case. Like some of the sEMG parameters, $TMCf_{Area}$ and $TMCf_{Max}$ increased significantly in parallel with the risk levels (**Figure 4.3**), thereby showing that these indices also correctly represent the greater co-activation resulting from the increased level of physical stress. The post-hoc analysis performed on $TMCf_{Area}$ and $TMCf_{Max}$ also showed that the algorithm used to calculate the co-activation discriminates all the pairs with different LI (1 versus 2, 1 versus 3 and 2 versus 3). This result suggests, as it has previously been recommended [5], that the co-activation index should be included in the construction of any sEMG-based Lifting Risk Recognition Tool.

Lastly, the Pearson test highlighted a moderate linear correlation between some sEMG parameters considered and some kinetic variables at the L_5-S_1 joint level. In more detail, the Max correlates with all the longitudinal ($p=0.037$), transversal, compression ($p=0.041$) and shear forces and moments

(**Figure 4.5**). This indicates that the maximum value of the ESL activity detected within the lifting cycle mildly correlates with the factors that damage the L_5-S_1 joint and that a higher Max value corresponds to an increased load at the L_5-S_1 joint (**Figure 4.5**). The other parameters, i.e. the ARV, RMS, $TMCf_{Area}$ and $TMCf_{Max}$, correlate with $Ftrans_{L5-S1}$, $Fshear_{L5-S1}$ and M_{L5-S1}, though not with $Flong_{L5-S1}$, and $Fcompr_{L5-S1}$ (**Figure 4.5**). The lack of any correlation between the sEMG parameters and longitudinal and compression forces is probably due to the fact that lifting trials generate spinal loads that are influenced by lifting dynamics (i.e. flexed liftings) [22]. An increased LI may be a function of the trunk flexion (**Figure 4.4** a)) and of the transverse force component. **Figure 4.4** shows the kinematics (trunk flexion-extension), kinetics (forces and moments at L_5-S_1 joint) and electromyography in the cycle of a representative subject. These curves strengthened the obtained results. Indeed, the figure clearly shows that trunk flexion-extension, $Flong_{L5-S1}$, $Ftrans_{L5-S1}$, $Fcompr_{L5-S1}$, $Fshear_{L5-S1}$, M_{L5-S1}, sEMG activity and co-activation increase with increasing LI.

Moreover, it also shows that the forces that most clearly represent the risk levels are $Ftrans_{L5-S1}$ and $Fshear_{L5-S1}$, which are those that correlate most closely with the other parameters investigated.

The experimental data support the proposed hypothesis by demonstrating that a sEMG-based lifting risk recognition tool based on the ARV and/or RMS and/or Max (calculated on ESL) and TMCf, as well as the instrumental tool based on kinematic measurements (see chapter 3) would serve as an extremely useful instrumental risk assessment method if referred to the set of conditions studied.

According to our experimental setup, a sEMG-based Lifting Risk Recognition Tool could be designed in a number of ways, one of which is to consider one (i.e. RMS or Max or $TMCf_{Max}$_4), two (i.e. RMS and Max) or three (i.e. RMS, Max and $TMCf_{Max}$_4) criteria of risk classification, as shown in **Figure 4.6** and **4.7**.

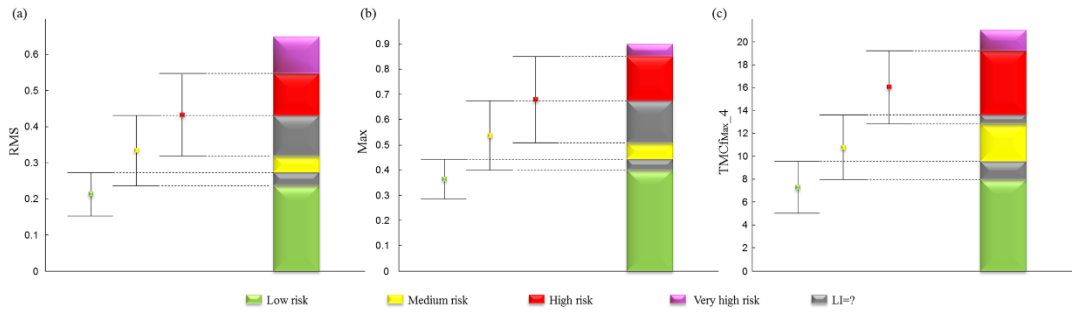

Figure 4.6. *A sEMG-based Lifting Risk Recognition Tool designed by considering one criterion of risk classification: RMS (a), Max (b) or TMCf$_{Max}$_4 (c). Low-, medium- and high- risk jobs are recognized by error bars (in the left side of each panel). Real low-, medium-, high and very high-risk jobs are identified by histograms. LI=? histograms denote ranges for which it is not possible to make a choice of risk jobs.*

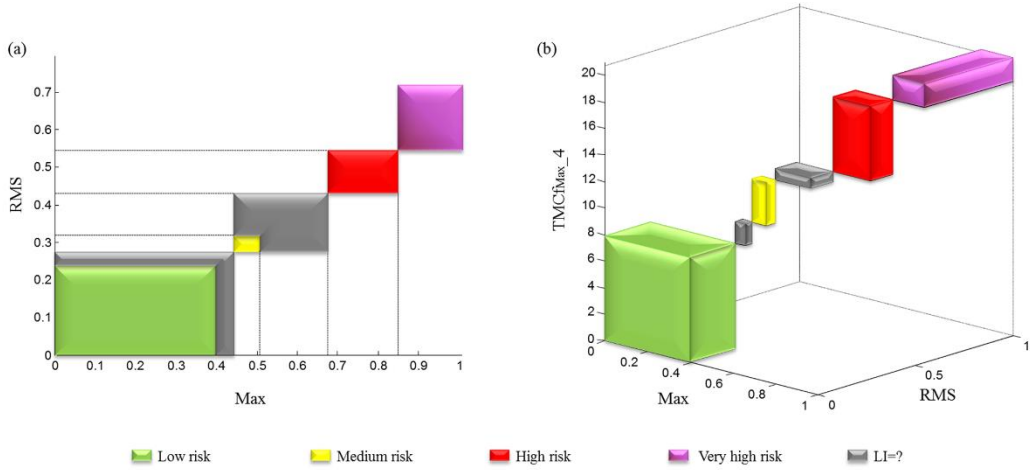

Figure 4.7. *A sEMG-based Lifting Risk Recognition Tool designed by considering two and three criteria of risk classification: RMS-Max (a) and RMS-Max-TMCf$_{Max}$_4 (b). Areas and volumes associated to low-, medium- and high- risk jobs are built according to the criterion used in the definitions of intervals in* ***Figure 4.6****.*

The Lifting Risk Recognition Tool was built considering: low risk jobs as the interval between 0 and [mean+SD of LI=1] (all values under [mean-SD of LI=1] were associated with low risk jobs); medium risk jobs as the interval between [mean-SD of LI=2] and [mean+SD of LI=2]; high risk jobs as the interval between [mean-SD of LI=3] and [mean+SD of LI=3]. The values included in two different intervals or in any interval (LI=? in **Figure 4.6**), represent ranges for which it is not possible to make a clear choice because they should be associated with two different type of risk jobs. Whereas values above the high risk zone indicate very high-risk jobs (LI=Very high-risk in **Figure 4.6**).

In particular, considering one criterion based on RMS (**Figure 4.6** (a)) or TMCf$_{Max}$_4 (**Figure 4.6** (c)), values within the range 0-[mean-SD of LI=2], [mean+SD of LI=1]-[mean-SD of LI=3] and [mean+SD

of LI=2]-[mean+SD of LI=3] indicate real low-(LI=1 in **Figure 4.6**), medium-(LI=2 in **Figure 4.6**) and high-(LI=3 in **Figure 4.6**) risk jobs, respectively. Values included in two intervals ([mean-SD of LI=2]-[mean+SD of LI=1] and [mean-SD of LI=3]-[mean+SD of LI=2]) represent ranges for which it is not possible to make a clear choice. As regards Max (**Figure 4.6** (b)), values within the range 0-[mean-SD of LI=2], [mean+SD of LI=1]-[mean+SD of LI=2] and [mean-SD of LI=3]-[mean+SD of LI=3] indicate real low-(LI=1 in **Figure 4.6**), medium- (LI=2 in **Figure 4.6**) and high-(LI=3 in **Figure 4.6**) risk jobs, respectively. Values included in two intervals ([mean-SD of LI=2]-[mean+SD of LI=1]) and values not included in any intervals ([mean+SD of LI=2]-[mean-SD of LI=3]) represent ranges for which it is not possible to make a clear choice.

Methods with two and three criteria of classification should adopt different areas and volumes, as shown in **Figure 4.7**. Values of two (**Figure 4.7** (a)) or three (**Figure 4.7** (b)) parameters are reported on the axes in order to build areas and volumes associated to low-, medium- and high- risk jobs according to the definitions of intervals of above mentioned. It goes without saying that the power of the approach, defined as the ability of the test to detect an effect, if any effect does exist, would increase in parallel with the number of risk classification criteria.

4.1.3.1 Limitations and developments

A possible limitation of this method may be its application to the assessment of composite or sequential [31, 32] manual lifting jobs in which there are significant differences in lifting trials performed concurrently or in which workers rotate between a series of manual lifting rotation slots or elements. Furthermore, EMG-based indices would be considered as frequency-independent and single-task. This limitation may, however, be regarded as negligible because although the mechanical load on the body is not the only causative factor, it is likely to be by far the most important [1]. Another limitation of this approach is the impossibility to acquire all the trunk muscles involved in the lifting task, which would yield a more detailed analysis. Indeed, European

Recommendations for Surface Electromyography [7] and the atlas of muscle innervation zones [8] do not allow the internal and external abdominal obliques to be recorded, as has previously been done in other studies [33]. The technical limitations of the study are largely related to the sEMG approach, and include the presence of crosstalk muscle signals, electrode-skin impedance, noise and other problems linked to the electrode location, size, configuration and distance [34]. To minimize these problems, the European Recommendations for Surface Electromyography [7] and the atlas of muscle innervation zones [8] as references were used. Finally, another limitation of this study is the use of only male workers, although gender aspects are important, and they may lead to different results.

This study could be further developed by: i) enlarging the sample recruited; ii) widening the range of lifting task types with the same LI but changing the multiplier values; iii) testing lifting trials with LI values lower than 1, between 1 and 2, and between 2 and 3; iv) analyzing the choice criteria changes due to lifting while seated or kneeling, in a restricted work space, unstable objects, with high speed motion, with unreasonable foot-floor coupling, temperature and humidity, work experience, sex, age, etc. For instance, a faster lifting pace increases the demands made on trunk muscle recruitment above all in the initial phase [35].

Finally, as already done in other studies, task and evaluation methods [36-37], a real-time body sensors network including IMUs and sEMG sensors could be tested to monitor workers during lifting activities by measuring muscular efforts and postures for WLBDs prevention according to the RNLE.

4.2 STUDY N°2: LIFTING ACTIVITY ASSESSMENT USING SURFACE ELECTROMYOGRAPHIC FEATURES AND NEURAL NETWORKS

The aims of this work were to: 1) identify the most sensitive trunk muscles with respect to changes in lifting conditions based on the selected sEMG features and 2) test whether machine-learning

techniques (artificial neural networks) used for mapping time and frequency sEMG features on LI levels can improve the biomechanical risk assessment.

4.2.1 Materials and Methods

4.2.1.1 Subjects

Ten male participants (mean age = 32.50 ± 7.63 years, body mass index [BMI] = 25.00 ± 2.57 kg/m^2) were recruited in the study. The participants had no history of musculoskeletal disorders; upper-limb, lower-limb, or trunk surgery; orthopedic or neurological diseases; vestibular system disorders; visual impairments; or back pain. All participants provided informed consent prior to participating in the study, which complied with the Helsinki declaration. No information regarding the expected results was provided to avoid bias.

4.2.1.2 Data recordings

An optoelectronic motion analysis system (SMART-DX 6000 System, BTS, Milan, Italy) consisting of eight infrared cameras (sampling frequency, 340 Hz) was used to track the movements of one spherical marker (15-mm diameter) covered with an aluminum powder reflective material placed over the vertex of a load consisting of a plastic crate.

Surface myoelectric signals were acquired as in 4.1.1.2.

Data acquired from the optoelectronic cameras and surface electromyography were synchronized.

4.2.1.3 Experimental Procedures

The experimental procedures were the same of in 3.1.3 with the Task B, D and F of **Table 3.2**.

4.2.1.4 Data analysys

The Lifting Cycle definition was performed as in 3.1.4.1. Then the sEMG signals were processed as follows: the iMVC and the sEMG raw data of each lifting task were band-pass filtered using a fourth-

order Butterworth filter of 30–400 Hz to reduce artifacts and other components of high-frequency noise [12, 13].

From these signals, analyses of time and frequency domains were performed.

As regards time domain, from the processed sEMG signals of each lifting task (see 4.1.1.4), the Max and the ARV within the cycle where calculated to characterize differences in the sEMG activity among the different lifting conditions.

As regards, frequency domain, using the band-pass filtered sEMG data recorded during lifting tasks and iMVC, the power spectral density was estimated by using the Yule-Walker's approach on the signal portion recorded during the detected lifting cycle: the autoregressive parameters were estimated using Levinson Durbin recursion with a model order p = 15 [38]. For each muscle, the mean frequency (MNF), defined as the gravity center frequency of the power spectrum (it gives information on physiological phenomena that occur in the muscle during contraction) of the signal, was calculated as:

$$MNF = \frac{\int_0^\infty f * P(f)df}{\int_0^\infty P(f)df}$$

and the median frequency (MDF), which divides the spectrum into two parts of equal power:

$$\int_0^{MDF} P(f)df = \int_{MDF}^\infty P(f)df = \frac{1}{2}\int_0^\infty P(f)df.$$

where P(f) is the power spectral density and f is the frequency vector.

For each muscle, both MNF and MDF related to the lifting tasks were normalized to the MNF_{MVC} and MDF_{MVC} calculated from the iMVC power spectral densities for each participant, respectively.

4.2.1.5 Statistical analysis of sEMG features

All of the statistical analyses were performed using SPSS 17.0 software (SPSS Inc., Chicago, IL, USA). The Shapiro-Wilk and Kolmogorov-Smirnov tests were used to analyze the normality of the data. For each muscle, we performed one-way repeated-measures analysis of variance (ANOVA) to determine whether LI levels determine significant changes in time and frequency features. Post-hoc analyses were performed using a paired *t*-test with Bonferroni's corrections when significant differences were observed in the ANOVA results. p values < 0.05 were considered statistically significant. Furthermore, for each lifting condition and feature, we applied a parametric paired-samples t-test to detect any differences between the right and left muscles.

4.2.1.6 Selection of the neural networks (chosen machine-learning technique) and mapping of sEMG features on LI levels

A neural network approach based on sEMG features was used to estimate the biomechanical risk in terms of LI. To reach this objective in a parsimonious and computationally efficient way, ANNs were trained using only the most significant features/muscles identified in the analysis described in the previous paragraph 2.6. All of the trained networks are feedforward ANNs that were trained using different feature combinations. The networks differ in the topology showing different numbers of hidden layers and different numbers of neurons in each hidden layer. The output set (OS) consisted of an orthogonal coding of the three LI levels: L1 = [1 0 0], L2 = [0 1 0], and L3 = [0 0 1]. The entire system is schematically described in the **Figure 4.8**.

The number of hidden layers varied in the range of 1–3, while the number of neurons in each hidden layer varied based on the number of nodes N in the first hidden layer (N_{L1}); N was set to two different values (20 and 50, respectively), and the number of nodes in the other hidden layers (when defined) was 1/2 and 1/3 of N for the second (N_{L2}) and third (N_{L3}) hidden layer, respectively. Thus,

the combination of L layers and N nodes in the first hidden layer led to the following six different network architectures ([dim(SET) N_{L1} OS], [dim(SET) N_{L1} N_{L2} OS], [dim(SET) N_{L1} N_{L2} N_{L3} OS]): [dim(SET) 20 3], [dim(SET) 50 3], [dim(SET) 20 10 3], [dim(SET) 50 25 3], [dim(SET) 20 10 7 3], and [dim(SET) 50 25 17 3], where dim(SET) defines the size of the ANN input layer (depending on the number of sEMG features).

Six different training sets were used: SET_i, i=1,…6. Each set was defined as a combination of different sEMG features. SET_1 contained only time features (ARV and Max), SET_2 contained only frequency features (MNF and MDF), and SET_3 contained both time and frequency features. SET_4, SET_5, and SET_6 were defined in the same way as SET_1, SET_2, and SET_3 but contained one additional feature related to the participants' BMI. Networks were trained with a supervised approach using the Levenberg-Marquardt back-propagation algorithm [39]. The training was stopped when at least one of the following conditions was met: 1000 iterations, 10^{-6} mean square error, or six consecutive fails on the validation set.

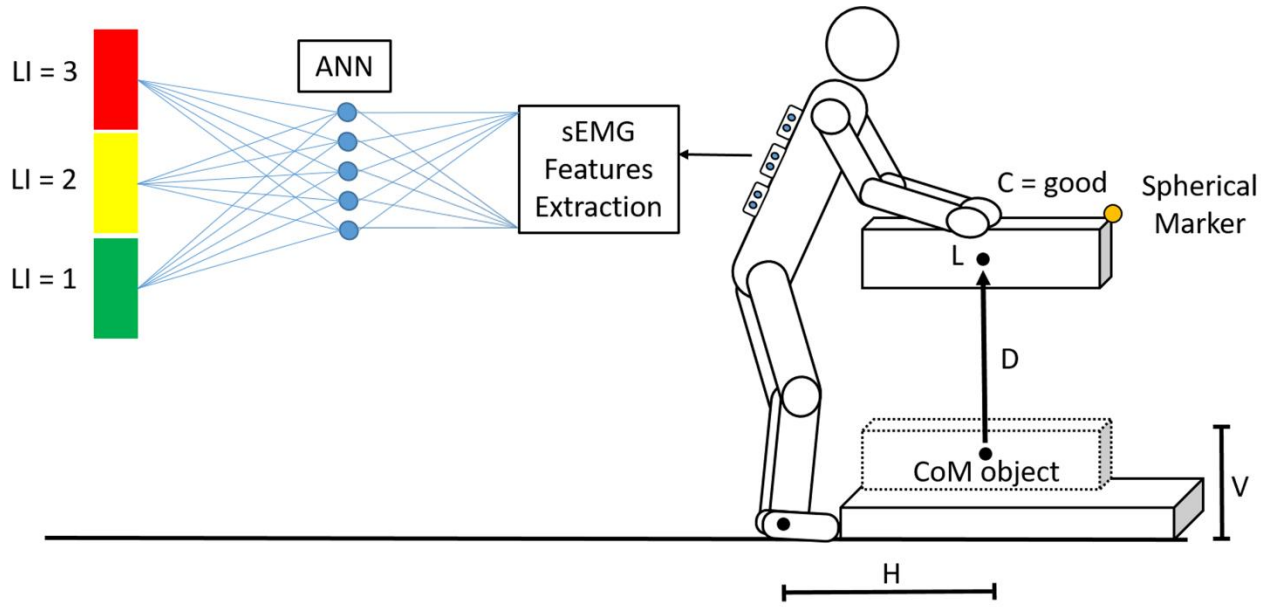

Figure 4.8. *A schematic description of the lifting task and artificial neural network method used to map surface electromyography features on the Lifting Index (1, 2, and 3) levels.*
C, hand-to-object coupling; D, vertical travel distance; H, horizontal location; L, load weight; V, vertical location.

Each of the six network topologies was trained ten times for each of the six training sets so as to obtain a total of 360 trained ANNs. Each training was characterized by a different random initialization (i.e. weights and bias values), and by using a random 10% of samples as the validation set and a random 10% as the testing set. This approach was used in order to verify the repeatability of our results. For each trained network, a confusion matrix was calculated based on the real LI and the one estimated on the randomly extracted testing set.

The mean 3 × 3 confusion matrix was then obtained by averaging the confusion matrixes of the trained ANNs. A performance parameter (P) was calculated as the mean (%) of the elements on the diagonal of the mean confusion matrix, where 100% indicates the absence of misclassifications.

4.2.1.8 Statistical analysis of ANNs performance

We performed a three-way ANOVA test (with training set, L, N as factors) to determine possible significant effects on ANN performance caused by the listed factors. Post-hoc analysis with Bonferroni's corrections were performed when significant differences were observed in the ANOVA results. P values < 0.05 were considered statistically significant.

4.2.2 Results

4.2.2.1 Time and frequency feature analysis

The repeated-measures ANOVA revealed a significant effect of LI on ARV and Max for all muscles except RAM on both sides. A significant effect of LI was also observed on both MNF and MDF for ESL, M, and RAM on both sides (**Table 4.4**).

Table 4.5 shows the p values of the paired *t*-test with Bonferroni's corrections for ARV, Max, MNF, and MDF of all the investigated muscles, which highlight the differences between pairs of LI. Significant differences and means with standard deviations of the ESL are shown in **Figure 4.9**.

From **Table 4.5** emerges that the most significant difference between pairs of LI (1 versus 2, 1 versus 3, 2 versus 3) is explained by right and left ESL. Since no statistically significant differences were found between the right and left muscles in any of the sEMG features ($p > 0.05$), the following results will refer only to the right ESL (**Figure 4.9**). For what concerns ANNs, based on the results of the statistical analysis, the size of the corresponding input layer was 2 for SET_1 and SET_2, 4 for SET_3, 3 for SET_4 and SET_5, and 5 for SET_6.

		RIGHT						LEFT					
		ESL	**ESI**	**M**	**LD**	**RAS**	**RAM**	**ESL**	**ESI**	**M**	**LD**	**RAS**	**RAM**
Max	F	149.027	7.490	6.653	11.579	7.147	2.782	56.869	24.394	11.844	17.889	8.685	1.124
	df	2	2	2	2	2	2	2	2	2	2	2	2
	p	**<0.001**	**0.004**	**0.007**	**0.001**	**0.005**	0.089	**<0.001**	**<0.001**	**0.001**	**<0.001**	**0.002**	0.320
ARV	F	39.122	6.668	5.978	13.427	28.705	2.431	28.014	5.203	15.789	14.556	17.330	2.824
	df	2	2	2	2	2	2	2	2	2	2	2	2
	p	**<0.001**	**0.007**	**0.010**	**<0.001**	**<0.001**	0.116	**<0.001**	**0.016**	**<0.001**	**<0.001**	**<0.001**	0.051
MNF	F	60.557	0.359	55.692	1.040	0.995	3.042	48.995	1.291	14.177	1.107	1.519	11.759
	df	2	2	2	2	2	2	2	2	2	2	2	2
	p	**<0.001**	0.703	**<0.001**	0.374	0.389	0.052	**<0.001**	0.299	**<0.001**	0.352	0.246	**0.001**
MDF	F	39.056	1.027	30.902	1.405	1.263	2.999	31.095	0.711	10.903	0.340	2.490	8.191
	df	2	2	2	2	2	2	2	2	2	2	2	2
	p	**<0.001**	0.341	**<0.001**	0.271	0.298	0.105	**<0.001**	0.504	**0.004**	0.716	0.056	**0.003**

Table 4.4. *The F, df and p-values of the repeated measures ANOVA considering the Max, ARV, MNF and MDF in the three lifting conditions (LI=1, LI=2 and LI=3) for the twelve muscles bilaterally. Bold type indicates statistical significance. Max, maximum value; ARV, average rectified value; MNF, mean frequency; MDF, median frequency; LI, Lifting Index; ESL, erector spinae longissimus; ESI, erector spinae iliocostalis; M, multifidus; LD, latissimus dorsi; RAS, rectus abdominis superior; RAM, rectus abdominis middle muscles.*

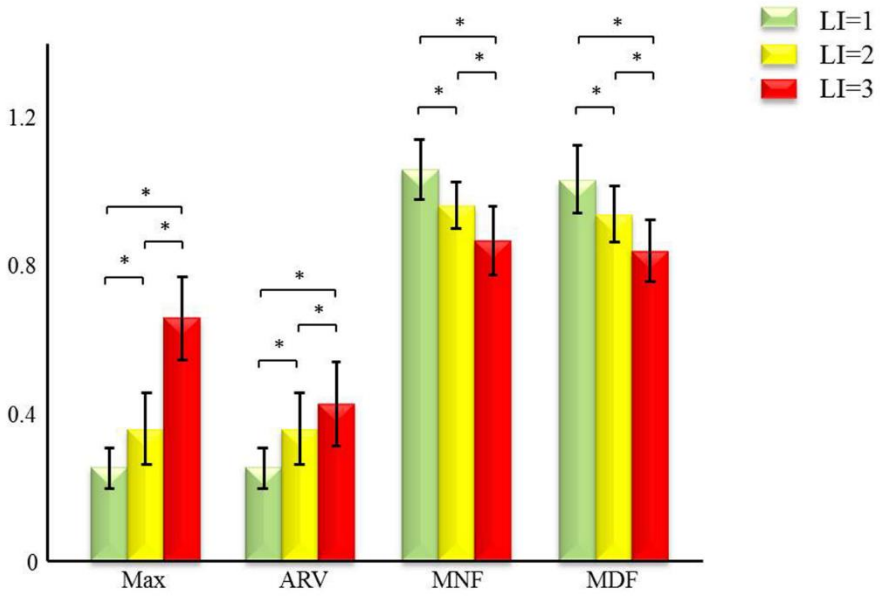

Figure 4.9. *Means and standard deviations of time (ARV and Max) and frequency (MNF and MDF) features related to right erector spinae longissimus (ESL) during the manual lifting tasks with three LI levels. *Significant differences on post-hoc analysis. ARV, average rectified value; Max, maximum value; MNF, mean frequency; MDF, median frequency; ESL, erector spinae longissimus; LI, Lifting Index.*

		RIGHT						LEFT					
	LI	ESL	ESI	M	LD	RAS	RAM	ESL	ESI	M	LD	RAS	RAM
Max	1 vs 2	**<0.001**	**0.001**	**0.012**	**0.002**	0.849	-	**<0.001**	**0.001**	**0.001**	**0.002**	0.128	-
	1 vs 3	**<0.001**	0.058	**0.008**	**0.017**	**0.047**	-	**<0.001**	**<0.001**	**0.009**	**0.003**	**0.030**	-
	2 vs 3	**<0.001**	1.000	1.000	0.257	**0.007**	-	**0.005**	0.109	0.255	0.722	0.082	-
ARV	1 vs 2	**<0.001**	**<0.001**	0.102	**0.009**	**0.001**	-	**0.001**	**0.001**	**<0.001**	**0.001**	**0.001**	-
	1 vs 3	**<0.001**	0.093	**0.015**	**0.014**	**<0.001**	-	**<0.001**	0.202	**0.007**	**0.007**	**0.003**	-
	2 vs 3	**0.035**	1.000	1.000	**0.041**	**0.012**	-	**0.048**	1.000	1.000	0.799	0.069	-
MNF	1 vs 2	**<0.001**	-	0.004	-	-	-	**0.001**	-	0.162	-	-	0.480
	1 vs 3	**<0.001**	-	**<0.001**	-	-	-	**<0.001**	-	**0.007**	-	-	**0.016**
	2 vs 3	**0.003**	-	**<0.001**	-	-	-	**<0.001**	-	**0.002**	-	-	**0.012**
MDF	1 vs 2	**0.002**	-	**0.025**	-	-	-	**0.032**	-	0.504	-	-	1.000
	1 vs 3	**<0.001**	-	**<0.001**	-	-	-	**<0.001**	-	**0.014**	-	-	**0.020**
	2 vs 3	**0.001**	-	**<0.001**	-	-	-	**0.001**	-	**0.001**	-	-	**0.035**

Table 4.5. *The p-values of the paired t test with Bonferroni's corrections between pairs of different LI levels for the Max, ARV, MNF and MDF for the twelve muscles bilaterally. Bold type indicates statistical significance. Max, maximum value; ARV, average rectified value; MNF, mean frequency; MDF, median*

frequency; LI, Lifting Index; ESL, erector spinae longissimus; ESI, erector spinae iliocostalis; M, multifidus; LD, latissimus dorsi; RAS, rectus abdominis superior; RAM, rectus abdominis middle muscles.

4.2.2.2 Mapping of sEMG features on LI levels

Three-way ANOVA showed significant effects of multiple factors on the performances considering training set ($p<0.001$), L ($p<0.001$) and N ($p<0.001$).

Significant differences ($p<0.001$) emerged from post-hoc analysis when comparing each topology performance when trained with SET_1, SET_2 and SET_3 with the corresponding topology performance when trained with SET_4, SET_5 and SET_6. Further details are reported in the following paragraphs.

Mapping with time features

The results of the detection expressed as P (mean ± SD) for each combination of L and N, for each of the six architectures of the ANNs, and with SET_1 (only time features) and SET_4 (time features and BMI) as training sets are reported in **Figure 4.10**. SET_4 shows higher performance values ($P_{(L=1, N=20)}$=72.17±5.76; $P_{(L=1, N=50)}$=75.30±4.87; $P_{(L=2, N=20)}$=75.24±5.70; $P_{(L=2, N=50)}$=77.44±5.13; $P_{(L=3, N=20)}$=75.20±5.55; $P_{(L=3, N=50)}$=76.64±4.21) than SET_1 ($P_{(L=1, N=20)}$=64.80±6.47; $P_{(L=1, N=50)}$=67.94±4.62; $P_{(L=2, N=20)}$=66.34±5.58; $P_{(L=2, N=50)}$=67.80±6.79; $P_{(L=3, N=20)}$=66.15±7.78; $P_{(L=3, N=50)}$=66.38±5.63) suggesting that BMI information leads to a higher predictive value for the ANNs.

Mapping with frequency features

The results of the detection expressed as P (mean ± SD) for each of the six ANN architectures, with SET_2 (with only frequency features) and SET_5 (with frequency features and BMI) as training sets, are reported in **Figure 4.10**. Regarding the frequency analysis, BMI features, in addition to frequency features in the input set, slightly improved the network performance (SET_5: $P_{(L=1, N=20)}$=67.07±4.98; $P_{(L=1, N=50)}$=74.33±5.07; $P_{(L=2, N=20)}$=67.37±7.01; $P_{(L=2, N=50)}$=75.10±4.84; $P_{(L=3, N=20)}$=70.61±6.38; $P_{(L=3, N=50)}$=74.48±5.04; SET_2: $P_{(L=1, N=20)}$=63.43±3.72; $P_{(L=1, N=50)}$=64.10±4.45; $P_{(L=2, N=20)}$=62.55±5.87; $P_{(L=2, N=50)}$=63.37±4.47; $P_{(L=3, N=20)}$=65.10±2.63; $P_{(L=3, N=50)}$=64.34±4.50). Furthermore, the network

configuration with three layers and 50 neurons in the first layer led to higher P values than the other architectures.

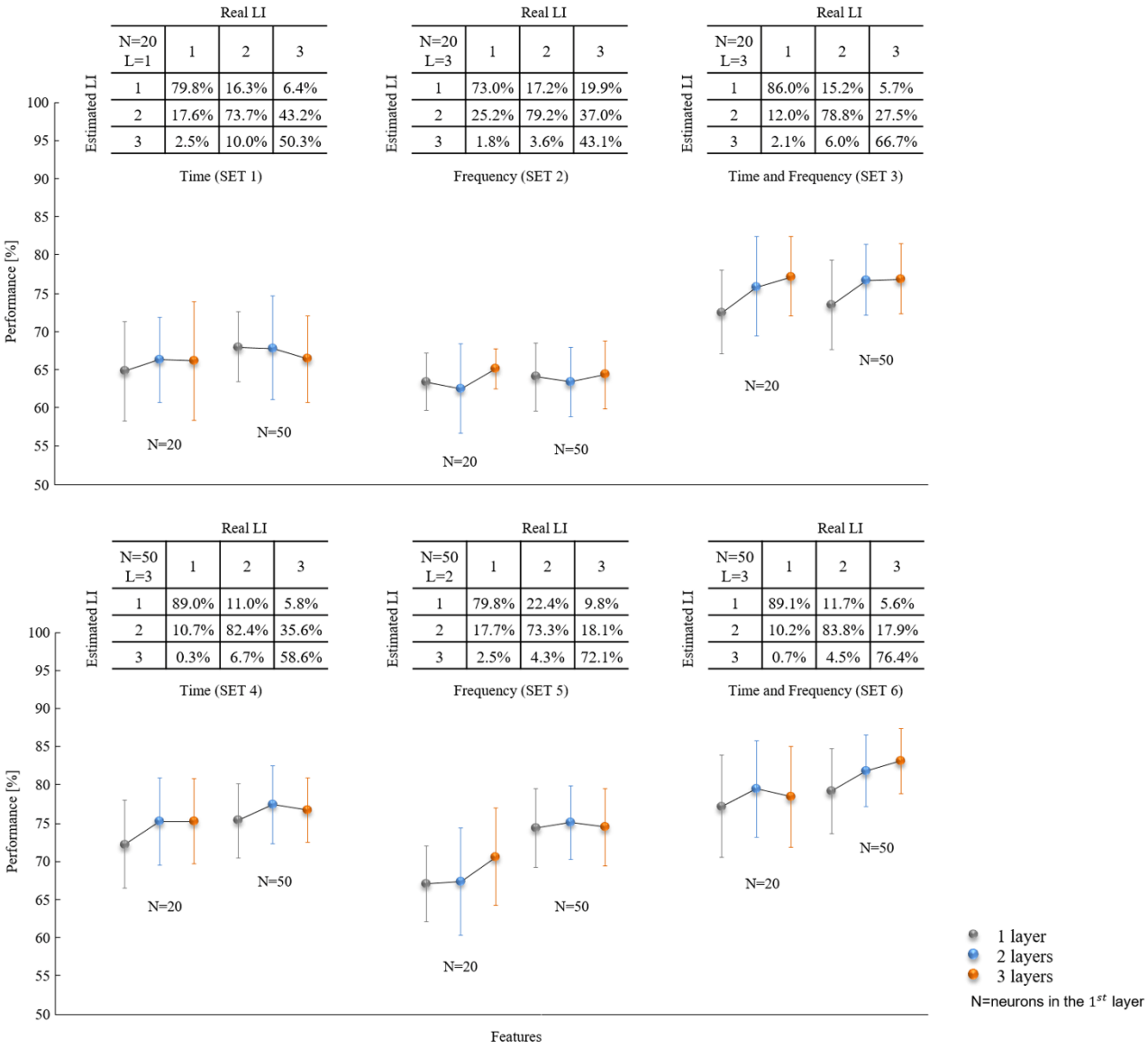

Figure 4.10. *Performance of artificial neural networks considering only time features (ARV and Max), only frequency features (MNF and MDF), and both time and frequency features. One additional feature related to the participants' BMI was considered for each combination of different kinds of sEMG features. Six different architectures of neural networks were represented by varying the numbers of hidden layers (1, 2, or 3) and the numbers of neurons in each hidden layer based on the numbers of nodes N in the first hidden layer. For each SET$_i$, the best mean confusion matrix was reported. ARV, average rectified value; BMI, body mass index; Max, maximum value; MDF, median frequency; MNF, mean frequency; sEMG, surface electromyography.*

Multi-domain mapping

For each of the six network architectures, considering SET_3, which contained frequency and time features, and SET_6, which contained time, frequency, and BMI features, the performances (P = mean ± SD) for each combination of L and N are reported in **Figure 4.10**. SET_6 ($P_{(L=1, N=20)}$=77.19±6.72; $P_{(L=1, N=50)}$=79.13±5.52; $P_{(L=2, N=20)}$=79.42±6.26; $P_{(L=2, N=50)}$=81.83±4.67; $P_{(L=3, N=20)}$=78.45±6.55; $P_{(L=3, N=50)}$=83.10±4.28) performed better than SET_3 ($P_{(L=1, N=20)}$=72.51±5.49; $P_{(L=1, N=50)}$=73.50±5.86; $P_{(L=2, N=20)}$=75.83±6.52; $P_{(L=2, N=50)}$=76.74±4.59; $P_{(L=3, N=20)}$=77.15±5.16; $P_{(L=3, N=50)}$=75.90±4.61). In particular, the best network configuration is composed of three layers and 50 neurons in the first hidden layer with SET_6 as the input set.

4.2.3 Discussions and Conclusions

In this study, the sEMG activities of the trunk extensor and flexor muscles during the execution of three-dimensional dynamic lifting trials designed using the RNLE were investigated. Starting from lifting tasks with a specific LI identified by the NIOSH equation [32] in a controlled environment, each above-mentioned lifting task was characterized in terms of biomechanical risk using the sEMG features analysis. The results obtained in this work from sEMG time and frequency features are significantly related to LI for specific trunk muscles. Based on these findings, a quantitative machine-learning approach based on artificial neural networks was used to predict the biomechanical risk directly from sEMG features, showing that proper combinations of input features and network architectures can lead to good classification results.

4.2.3.1 Neuromechanical aspects related to the findings

Three lifting conditions with a progressive increase of LI (LI = 1, LI = 2, and LI = 3) were analyzed and the statistical analysis performed on the data highlighted that the ARV, Max, MNF, and MDF are

reliable indicators of the greater involvement of erector spinae longissimus muscle and different muscle fiber recruitment strategies. The study results did not reveal any differences in any of the lifting conditions between the right and left trunk muscles regardless of dominant side. This finding suggests that an instrumental sEMG-based tool, designed for risk assessment purposes, could consider a halved number of trunk muscles (six instead of twelve). In particular, when comparing the three different lifting conditions (LI 1 versus 2, 1 versus 3, and 2 versus 3), the ESL proved to be the only trunk extensor muscle for which every feature (ARV, Max, MNF, and MDF) was able to significantly discriminate each pair of LI (**Table 4.5** and **Figure 4.9**).

This result might indicate that ESL is a functional muscle with high sensitivity to the risk conditions during lifting and largely contributes to the different phases of the analyzed task. The erector spinae muscles are described as extensors of the trunk that remained relaxed during the initial lifting of the weight and became vigorously active when the weight was lifted. This activity continued with diminishing intensity until the upright position was reached. Its proper activation is critical to maintain trunk posture without pain and further injury to complete the movement [40].

With the aim of further reducing the number of muscles to be acquired, these findings suggest that the ESL may be used to correctly classify low, medium-, and high-risk jobs/lifting tasks. Indeed, it may be possible to calculate the ARV, Max, MNF, and MDF for the ESL to obtain reliable results, thereby reducing the required analysis to only one muscle.

4.2.3.2 Use of machine-learning for automatic LI classification

The sEMG features in the time and frequency domains were successfully used to classify human motor activities in different applications. The use of ARV and Max as sEMG signal amplitude estimators as well as MDF and MNF as sEMG frequency features have also been reported previously in the scientific literature [1, 16, 25, 41].

The potentially complex function linking sEMG time and frequency features to LI levels justifies the use of machine-learning techniques for the identification of the input-output relationship. For this reason, a neural network approach has been used to solve this problem and thus classify different biomechanical risks associated with lifting tasks.

Zurada et al. [42] and Chen et al. [43-44] used ANN approaches to predict musculoskeletal disorder risks by analyzing work activities and using mechanical variables representing potentially risky factors for developing LBDs as input. In our study, to reach this objective in a parsimonious and computationally efficient way, neural networks were trained using only sEMG features extracted from a single muscle (right ESL) coming from the analysis of all of the recorded muscles with the advantage of having information on the neurophysiological signal strictly related to the mechanical outcome.

All the networks are feed-forward neural networks trained with different training sets, numbers of hidden layers, and numbers of neurons in each hidden layer. Considering SET_4 as the input set, which contained time features with the additional feature related to the BMI, the results in terms of classification accuracy suggest that the neural network is more powerful than the one obtained considering SET_1 as the input set, containing only time features without BMI (**Figure 4.10**). This result suggests that BMI correction helps neural network performance, indicating that a sole amplitude normalization of sEMG data is insufficient. Indeed, the experimental protocol was defined according to the RNLE (equation (1)) which does not take into account the anthropometric features of the participants when defining the parameters (i.e. load constant is always 23 kg independently from anthropometric features) and the subject-specific link between the amount of muscular activation and the lifted load. Participants with a significantly different BMI might have a substantially different MVC, so that the percentage of muscular activity for performing the same task might not be indicative of the biomechanical risk.

The frequency analysis results (**Figure 4.10**) confirm the importance of considering the BMI and frequency features (SET_5) to estimate the biomechanical risk in terms of LI. These results seem to suggest that, since BMI influences fiber recruitment, as changes in muscle activity are influenced by BMI values [45], using frequency features in combination with BMI values helps improve classification power.

The combination of both time and frequency features (SET_3) led to significantly higher performance than SET_1 and SET_2 (**Figure 4.10**). Furthermore, considering the additional feature of BMI as input (SET_6), the predictive power of the networks significantly increased with respect to the other input sets (**Figure 4.10**). SET_6 showed the best results with a network architecture of three hidden layers and 50 neurons composing the first hidden layer. This result suggests that, when using only multi-domain features, more complex network architectures lead to an improved biomechanical risk classification during lifting tasks.

From a general point of view, it is worth highlighting that errors never imply misclassification between LI 1 and LI 3 that represent the least and riskiest situations. Particularly, considering that SET_6 showed the best performance, the real LI = 1 is well recognized for 89.1% and is misclassified with LI = 3 accounting for only 0.7%, while the real LI = 3 is correctly recognized for 76.4%, and it is misclassified with LI = 1 accounting for only 5.6%, which constitutes a desired and acceptable behavior of the LI classifier.

4.2.3.3 Limitations

The possibility of reducing the number of muscles to only one must be certified by another experimental setup in which the same values of LI (LI = 1, 2, or 3) are created playing with different combinations of parameters as defined in the RNLE equation. For instance, asymmetrical tasks could

imply the presence of differences in sEMG features between the right and left sides of the body. This could lead to a generalization of the used approach for practical application on the field.

In the experimental set-up, the effect of muscle fatigue on the sEMG features was not considered. Indeed, the muscle fatigue phenomenon might occur after a prolonged or repetitive working activity characterized by high lifting frequencies, while our lifting task has a very low frequency (≤2 lifts/min) and is executed in a short period of time. The change of sEMG time and frequency features with the development of muscle fatigue [46] might require real-time adaptation of the classifier.

BIBLIOGRAPHY

1. Hägg GM, Luttmann A, Jäger M (2000) Methodologies for evaluating electromyographic field data in ergonomics. J Electromyogr Kinesiol **10 No. 5**, 301-312. Review.
2. Kumar S, Mital A (1996) Electromyography in ergonomics. London, Taylor and Francis.
3. Gazzoni M (2010) Multichannel Surface Electromyography in Ergonomics: Potentialities and Limits. Human Factors and Ergonomics in Manufacturing & Service Industries. **20 No. 4**, 255–271.
4. Farina D, Fosci M, Merletti R. Motor unit recruitment strategies investigated by surface EMG variables. J Appl Physiol. 2002; 92(1): 235-247.
5. Ranavolo A, Mari S, Conte C, Serrao M, Silvetti A, Iavicoli S, Draicchio F. A new muscle co-activation index for biomechanical load evaluation in work activities. Ergonomics. 2015; 58(6):966-79. http://doi:10.1080/00140139.2014.991764.
6. Marras WS, Fine LJ, Ferguson SA, Waters TR. The effectiveness of commonly used lifting assessment methods to identify industrial jobs associated with elevated risk of low-back disorders. Ergonomics. 1999; 42(1): 229-245.
7. Hermens HJ, Freriks B, Disselhorst-Klug C, Rau G (2000) Development of Recommendations for SEMG Sensors and Sensor Placement Procedures. J Electromyogr Kinesiol 10 No. 5, 361–374.
8. Barbero M, Merletti R, Rainoldi A (2012) editors. Atlas of Muscle Innervation Zones: Understanding Surface Electromyography and Its Applications, New York, Springer.
9. IEEE 1588 Standard for a Precision Clock Synchronization Protocol, 2002.
10. Plamondon A, Gagnon M, Desjardins P (1996) Validation of two 3-D segment models to calculate the net reaction forces and moments at the L5/S1 joint in lifting. Clin Biomech **11 No. 2**, 101-110.
11. Zatsiorsky VM, Seluyanov VN, Chugunova LG (1990) Methods of determining mass-inertial characteristics of human body segments. In G.G. Chernyi & S.A. Regirer, Contemporary Problems of Biomechanics, 272-291.
12. Butler HL, Newell R, Hubley-Kozey CL, Kozey JW. The Interpretation of Abdominal Wall Muscle Recruitment Strategies Change when the Electrocardiogram (ECG) is Removed from the Electromyogram (EMG). J Electromyogr Kinesiol. 2009; 19(2): 102–113. http://doi:10.1016/j.jelekin.2007.10.004.
13. Drake JD, Callaghan JP (2006) Elimination of electrocardiogram contamination from electromyogram signals: An evaluation of currently used removal techniques. J Electromyogr Kinesiol **16 No. 2**, 175-187.
14. Winter DA (2009) Biomechanics and motor control of human movement. Fourth Edition University of Waterloo, Waterloo, Ontario, Canada. John Wiley & Sons, Inc.
15. Mirka GA (1991) The quantification of EMG normalization error. Ergonomics **34 No. 3**, 343–352.
16. Staudenmann D, Roeleveld K, Stegeman DF, van Dieën JH (2010) Methodological aspects of SEMG recordings for force estimation--a tutorial and review. J Electromyogr Kinesiol 20 No. 3, 375-387.
17. Burden A (2010) How should we normalize electromyograms obtained from healthy participants? What we have learned from over 25 years of research. J Electromyogr Kinesiol 20 No. 6, 1023-1035.
18. Ball N, Scurr J (2010) An assessment of the reliability and normalization of tests used to elicit reference muscular actions for electromyographical normalization. J Electromyogr Kinesiol **20 No. 1**, 81-88.
19. Burden A, Bartlett R (1999) Normalisation of EMG amplitude: an evaluation and comparison of old and new methods. Med Eng Phys 21 No. 4, 247-257.
20. Marras WS, Davis KG (2001) A non-MVC EMG normalization technique for the trunk musculature: Part 1. Method development. J Electromyogr Kinesiol **11 No. 1**, 1-9.
21. Marras WS, Davis KG, Maronitis AB (2001) A non-MVC EMG normalization technique for the trunk musculature: Part 2. Validation and use to predict spinal loads. J Electromyogr Kinesiol **11 No. 1**, 11-18. 2001).
22. Granata KP, Marras WS (1995) An EMG-assisted model of trunk loading during free-dynamic lifting. J Biomech **28 No. 11**, 1309-1317.

23. Granata KP, Marras WS (2000) Cost-Benefit of Muscle Cocontraction in Protecting Against Spinal Instability. Spine **25 No. 11**, 1398–1404.
24. Le, P, Aurand A, Walter BA, Best TM, Khan SN, Mendel E, Marras WS (2017) Development of a lumbar EMG-based coactivation index for the assessment of complex dynamic tasks. Ergonomics, 1-9.
25. Merletti R, Knaflitz M, De Luca CJ (1990) Myoelectric manifestations of fatigue in voluntary and electrically elicited contractions. J Appl Physiol **69 No. 5**, 1810–1820.
26. Solomonow M, Baratta R, Shoji H, D'Ambrosia RD (1986) The myoelectric signal of electrically stimulated muscle during recruitment: an inherent feedback parameter for a closed-loop control scheme. IEEE Transactions on Biomedical Engineering **33 No. 8**, 735–745.
27. De Luca CJ. The use of surface electromyography in biomechanics. J Appl Biomech. 1997; 13(2): 135–163.
28. Gardner-Morse MG, Stokes IA (1998) The Effects of Abdominal Muscle Coactivation on Lumbar Spine Stability. Spine **23**, 86–92.
29. Granata KP, Orishimo KF (2001) Response of trunk muscle coactivation to changes in spinal stability. J Biomech **34 No. 9**, 1117-1123.
30. Hodges PW, Richardson CA (1996) Inefficient Muscular Stabilization of the Lumbar Spine Associated with Low Back Pain: A Motor Control Evaluation of Transverses Abdominis. Spine **21**, 2640–2650.
31. Waters TR, Dick RB, Davis-Barkley J, Krieg EF (2007) A cross-sectional study of risk factors for musculoskeletal symptoms in the workplace using data from the General Social Survey (GSS). J Occup Environ Med **49**, 172–184.
32. Waters TR, Putz-Anderson V, Garg A (1994) Applications Manual for the Revised NIOSH Lifting Equation. Cincinnati, OH: U.S. Department of Health and Human Services.
33. Mientjes MI, Norman RW, Wells RP, McGill SM (1999) Assessment of an EMG-based method for continuous estimates of low back compression during asymmetrical occupational tasks. Ergonomics **42 No. 6**, 868-879.
34. Merletti R, Parker PJ (2004) Electromyography: Physiology, Engineering, and Non-invasive Applications. Hoboken, Wiley-IEEE Press.
35. Yoon J, Shiekhzadeh A, Nordin M (2012) The effect of load weight vs. pace on muscle recruitment during lifting. Appl Ergon **43 No. 6**, 1044-1050.
36. Peppoloni L, Filippeschi A, Ruffaldi E, Avizzano CA (2016) (WMSDs issue) A novel wearable system for the online assessment of risk for biomechanical load in repetitive efforts. Int J Ind Ergon. **52,** 1-11.
37. Vignais, N, Miezal M, Bleser G, Mura K, Gorecky D, Marin F (2013) Innovative system for real-time ergonomic feedback in industrial manufacturing. Appl Ergon **44 No.** 4, 566-574.
38. Farina D, Merletti R. Comparison of algorithms for estimation of EMG variables during voluntary isometric contractions. J Electromyogr Kinesiol. 2000; 10(5): 337-349. Review.
39. Rumelhart, DE, Hinton GE and Williams RJ. Learning internal representations by error propagation, In Parallel Distributed Processing, Cambridge, MA: MIT Press. 1986; 1: 318-362.
40. Floyd WF, Silver PH. The function of the erectores spinae muscles in certain movements and postures in man. J Physiol. 1955; 129(1): 184-203.
41. Phinyomark A, Limsakul C, Phukpattaranont P. A Novel Feature Extraction for Robust EMG Pattern Recognition. J. Comput. 2009; 1(1): 2151-9617. http://dx.doi.org/10.3109/03091902.2016.1153739
42. Zurada, J.; Karwowski, W.; Marras, W.S. A neural network-based system for classification of industrial jobs with respect to risk of low back disorders due to workplace design. *Appl Ergon* **1997**, *28(1),* 49-58.
43. Chen, C.L.; Kaber, D.B.; Dempsey, P.G. A new approach to applying feedforward neural networks to the prediction of musculoskeletal disorder risk. *Appl Ergon* **2000**, *31*, 269-282.
44. Chen, C.L.; Kaber, D.B.; Dempsey, P.G. Using feedforward neural networks and forward selection of input variables for an ergonomics data classification problem. *Hum Factors Ergon Manuf* **2004**, *14(1)*, 31-49. http://doi:10.1002/hfm.10052
45. Bollinger LM. Potential contributions of skeletal muscle contractile dysfunction to altered biomechanics in obesity. Gait Posture. 2017; 56: 100-107. doi: 10.1016/j.gaitpost.2017.05.003.
46. Conforto, T. D'Alessio, Real time monitoring of muscular fatigue fromdynamic surface myoelectric signals using a complex covariance approach,Med. Eng. Phys. 21 (4) (1999) 225–234.

CHAPTER V

5. ASSESSMENT OF FATIGUING LIFTING ACTIVITY USING INERTIAL MEASUREMENT UNITS, BIPOLAR AND HIGH-DENSITY sEMG IN BOTH HEALTY SUBJECTS AND PEOPLE WITH LOW BACK PAIN

In several studies carried on during this thesis work kinematic (see chapter 3) and surface electromyography (sEMG) (see chapter 4) indices extracted from signals acquired during the execution of lifting tasks and analysed via machine-learning techniques (artificial neural networks, (see chapter 4), have been used to classify the biomechanical risk. Findings of these studies show how the instrumental-based indices are positively correlated with unitary increments of LI (Lifting Index calculated by using the revised NIOSH lifting equation, [1,2]) and compression and shear forces at the lumbar and sacral level of the spine (5^{th} lumbar and 1^{st} sacral vertebra). These results suggest a promising use of Inertial Measurement Units (IMUs) and sEMG sensors in developing instrumental-based risk assessment tools in either the laboratory or workplace.

However, the quantitative indices, introduced in the previous studies, would be considered as frequency-independent and single-task without considering, among the others, fatigue phenomenon. The measurement of sEMG parameters to estimate muscle fatigue have been hypothesized to take into account the effect of lifting frequencies and fatigue on the risk classes.

Furthermore, the previous studies dealt with healthy subjects without considering what's happen when the worker are people affected by low back pain: can they perform lifting task? Which are the limitations for them? Is the biomechanical risk different for them?

Indeed, numerous studies have shown changes in trunk muscle activation in LBP, during walking [3-4], repetitive arm movements [5] and unexpected multidirectional translation perturbations [6]. Falla and collegues [7] showed that LBP alters (reducing the variability of muscle activity) the normal adaptation of lumbar erector spinae muscle activity to exercise, which was observed when pain-free individuals performed a repetitive lifting task.

Thus, in this study conducted in collaboration with the University of Birmingham (where I spent 6 months of my PhD period), I tried: 1) to define biomechanical risk classes parametrized by frequency; 2) to compare the parameter in two population of subjects: healthy subjects (HS) and subjects with low back pain (LBP).

In the following paragraphs the methodology of this study and the first results are reported.

5.1 MATERIALS AND METHODS

5.1.1 Subjects

15 healthy and physically active subjects (HS) and 8 subjects with low back pain (LBPS) were recruited in this study according with the following inclusion and exclusion criteria.

Inclusion criteria:

- Both females and males are eligible for the study.
- The age range will be restricted to 18- 60 years to limit age effects on physical measures of the lumbar region.
- Healthy and LBP participants must have the capacity to give the consent at his/her own will.
- Pain-free participants will be included if they have no relevant history over the last three years of back or lower limb pain or injury that limited their function and/or required treatment from a health profession.

- Individuals with LBP will be considered for the study.

The following definition for Non Specific Low Back Pain (NSLBP) is low back pain which is not related to serious pathology and/or does not have a specific cause (also known as simple or mechanical low back pain). Chronic refers to a sub type where back pain problem may have persisted at least 3 months and has resulted in pain on at least half the days in the past 6 months. If possible, participants should be willing to refrain from analgesic medication on the day of testing.

Exclusion criteria:

- Concurrent systemic, rheumatic or neuro-musculoskeletal disorders which may confound testing or being currently pregnant.
- Radicular low back pain or pain related to trauma, fractures, spinal stenosis.
- Participants with higher doses of opioids (> 30 mg of morphine equivalent dose) will be excluded.

Participants under active management of LBP by a GP, consultant or therapists (physiotherapist, osteopath, chiropractor) less than 3 months before enrolment.

All the participants gave their informed consent prior to take part in the study, which was complied with the Helsinki Declaration and it was approved by the local ethics committee. No information regarding the expected results will provide in order to avoid biasing the results.

Two different analysis were conducted: first only the HS were analyzed to discriminate the levels of LI (see paragraph 5.2); then a subgroup of 8 HS (age-sex matched with LBPS) was selected to compare the 2 groups of subjects aiming to discriminate the level of risk but also understand how it changes when back pain is present (see paragraph 5.3).

5.1.2 Questionnaires data

Questionnaires data were obtained from the participants using REDCap system. Both HS and LBP completed the SF-36 Health Survey [8], the Depression, Anxiety, Stress Scales (DASS) [9] and the International Physical Activity Questionnaires (IPAQ) [10]. Futhremore the Numeric Rating Scale on Low Back Pain intensity and duration, the Pain Catastrophizing Scale (PCS) [11], the Oswestry Disability Index [12], the Fear Avoidance Believe Questionnaire [13] and Tampa Scale of Kinesiophobia [14] were completed by LBP. Additionally, LBP reported the area where the pain is felt by completing a pain drawing through sketch software on an iPad. They drew the area of habitual pain in the first session, and the pain before to start the acquisition and after the acquisition in each session. Finally, the Visual Analogue Scale (VAS) was used to rate the pain in low back. It was used in both Healthy Controls and LBP after the experimental session and before the session and each minute during lifting task in LBP.

5.1.3 Experimental procedures

The experimental procedure is schematized in the following **Figure 5.1**. The participants performed lifting tasks in three different lifting conditions chosen to obtain the Lifting Index (LI) values of 1, 2, and 3 according to the Revised National Institute for Occupational Safety and Health (NIOSH) Lifting Equation (RNLE) [2].

Table 5.1 shows, for each lifting condition, the values of the load weight (L), the horizontal (H) and vertical (V) locations, the vertical travel distance (D), the asymmetry angle (A), the lifting frequency (F) and the corresponding values of the multipliers (HM, VM, DM, AM, FM, CM). The hand-to-object coupling was defined “good” for all 3 lifting tasks. The frequency parameter is (FM) <1 in the calculation of LI. Tasks were performed with the subjects standing in a neutral body position and lifting a plastic crate (34x29x13) with handles using both hands in three different lifting conditions.

The subjects performed the lifting tasks in three different sessions organised on three different days, one for each LI. The different lifting trials were randomly executed across the three sessions. The three sessions were 78 hours apart and conducted at the same time of the day for each subject to avoid confounding effects due to fatigue or daily habits.

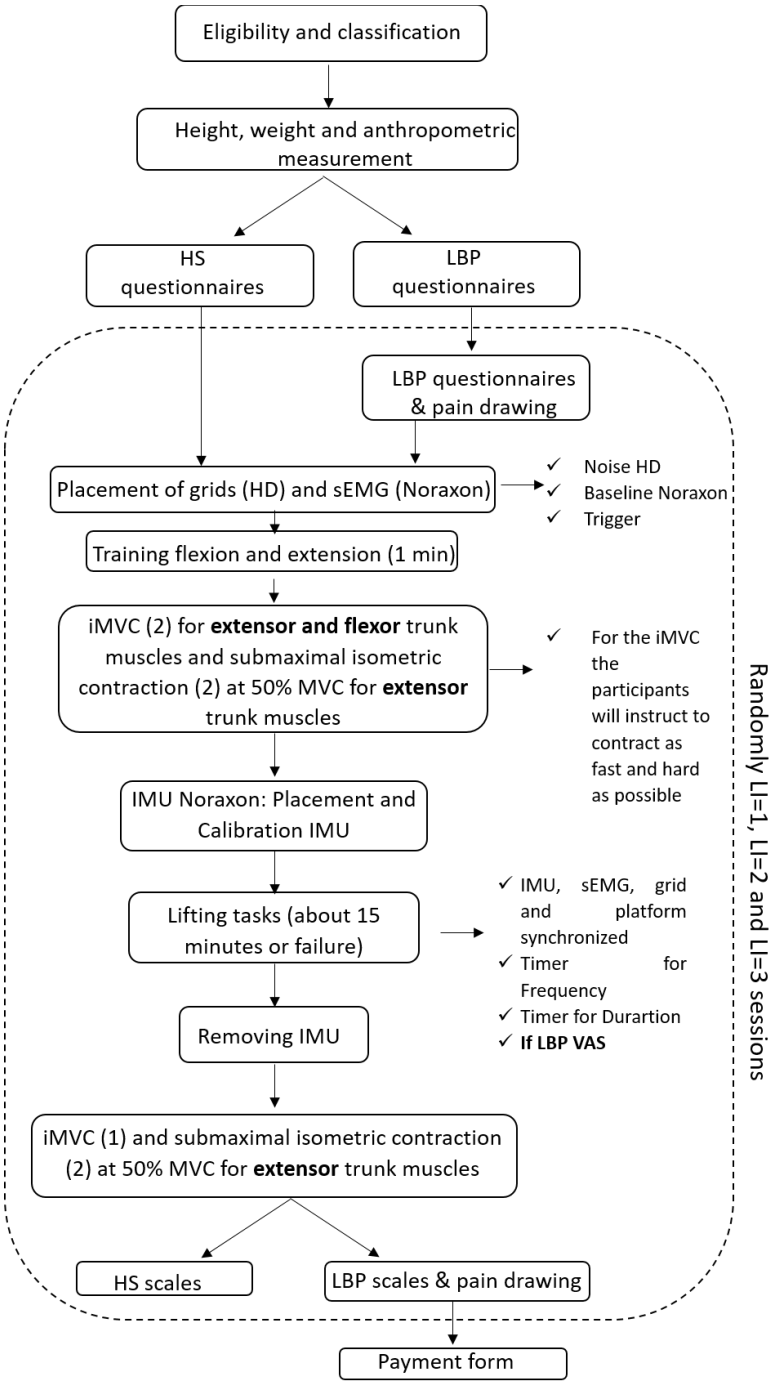

***Figure 5.1**. Experimental procedure.*

Task	LC (kg)	H (cm)	HM	V (cm)	VM	D (cm)	DM	A (°)	AM	F (lift/min)	FM	C	CM	L (kg)	RWL	LI
A	23	44	0,57	75	0,99	40	0,93	0	1	4	0,83	good	1	10	15	**1**
B	23	44	0,57	75	0,99	40	0,93	0	1	11	0,41	good	1	10	7,5	**2**
C	23	44	0,57	75	0,99	40	0,93	0	1	15	0,28	good	1	10	5	**3**

Table 5.1. *For each task (A, B, and C), the values of the load weight (L), the horizontal (H) and vertical (V) locations, the vertical travel distance (D), the asymmetry angle (A), the lifting frequency (F) and the hand-to-object coupling (C) and the corresponding values of the multipliers (HM, VM, DM, AM, FM, CM), the recommended weight limit (RWL) and the lifting index (LI).*

The lifting tasks duration were 15 minutes or until exhaustion of the subject. The number of repetitions was determined by the frequency parameter used to obtain the specific LI of the session. We used a timer to monitor the duration of lifting and an acoustic feedback to monitor the frequency of tasks.

In each of the 3 sessions, before the lifting tasks, the subjects performed specific exercises to record the isometric maximum voluntary contractions (iMVCs) for both flexor and extensor trunk muscles. Particularly, subjects were seated comfortably on an isokinetic dynamometer (Biodex System 3, Biodex Medical Systems Inc., Shirley, NY, USA) in an adjustable chair with their trunk reclined to 90°. iMVC contractions were exerted two times, each over a period of 5 s for [15]. These trials were separated by 2 min of rest.

After the MVC measurement, 4 minutes of rest were provided. Then, for ES, the highest MVC value were used as a reference for the definition of the submaximal force levels, expressed in each of the three experimental sessions as 50% of the MVC measured during the same session. The contraction at 50% was sustained for 20 s and it was performed 2 times per session and the 2 repetitions were separated by 4 min of rest to avoid confounding fatiguing effects. In each trial, the subjects received visual feedback of their force, which was displayed as a trapezoid with 5 s ramps and with 20 s hold-phase durations (see **Figure 5.2**).

In each of the 3 sessions, after the lifting tasks, as soon as possible (to see the fatigue effect), the subjects performed iMVCs for extensor trunk muscles in the same way performed before the task but only 1 repetition was performed. 4 minutes of rest were provided after the MVC measurement. Then, considering the highest MVC value in the exercise after the lifting task, 2 repetitions of the contraction at 50% of iMVC were sustained for 20 s and they were separated by 4 min of rest in the same way used before the lifting task.

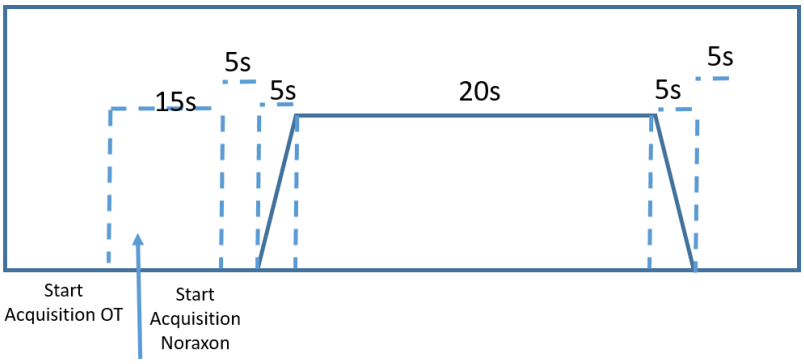

Figure 5.2. *Trapezoidal feedback for 50% of MVC.*

5.1.4 Kinematic, kinetic and electromyographic recordings

5.1.4.1 Kinematic recording

MyoMotion Reseach inertial sensors were used to acquire movements of the following body segments (**Figure 5.3**): the head (in the middle of the back of the head), upper thoracic (below C7 along the spinal cord, but high enough not to be affected by upper trapezius muscle movement), lower thoracic (on the spinal cord at approximately L1/T12, the strap belt on the front body side positioned on lower ribs), pelvic (bony area of sacrum), right arm (half of humerus bone) and right forearm (half of ulna/radio bone). One IMU was placed also on the load (z axis in vertical direction).

Calibration was carried out in an upright position of the subject in order to determine the value of the 0° angle in the joints studied. Sampling frequency for the inertial sensors was set at 200 Hz.

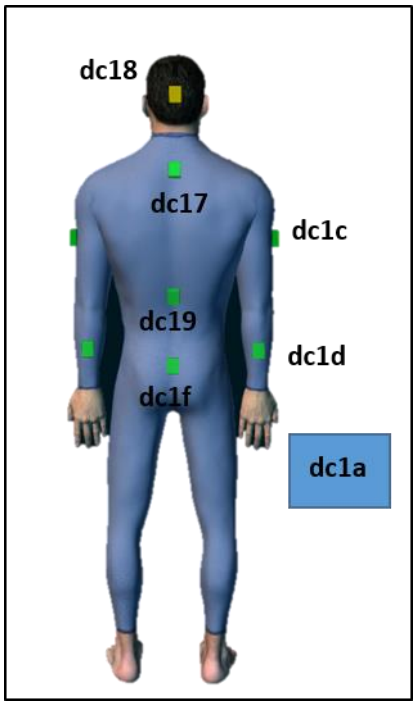

Figure 5.3. *IMUs position.*

5.1.4.2 Kinetic recording

Nintendo Wii Balance Board (rectangular in shape; weighs 3.5 kilograms; capable of supporting up to 150 kg; powered by four AA batteries allowing for 60 hours of operation, **Figure 5.4**), was used to acquires forces and Center of Pressure (CoP) during lifting task.

The Balance board was released in 2007 as an accessory to the Wii console, but now it is being used as an instrumental tool in many research projects [16]: the board operates similarly to a force plate by containing four transducers (strain gauges) in each of the four cylindrical legs (**Figure 5.4**) that assess force distribution and the resultant movements in COP.

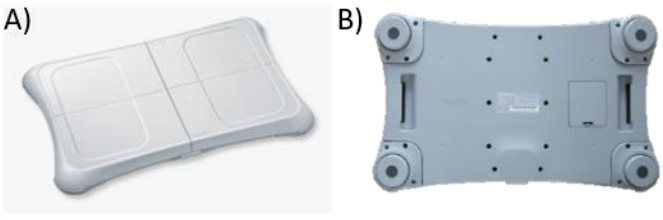

Figure 5.4. *The Nintendo Wii Balance Board: frontal side (A) and dorsal side with the four legs each with a transducer.*

Open source code from the University of Colorado's Neuromechanics Lab was utilized as the base of the code to acquire the data. The interface involves the Wii Balance Board communicating with a PC via Bluetooth and a computer program written in MATLAB.

It has the capabilities to display the CoP collected by the Wii Balance Board in real time, as well as the capability to record the CoP data. To run the program, the board must be calibrated by placing an object with a known weight on it and then entering the weight in kilograms into the appropriate window. The object is then removed, and the interface appears as seen in **Figure 5.5**.

The interface lists the location of the CoP, the force sensed by each quadrant, and information regarding time for recording. The white grid (**Figure 5.5**), represents the top platform of the Wii Balance Board. The x and y axes are the length and width, respectively, of the active part of the board with the origin located at the center of board. The center of the board is physically marked on the Wii Balance Board by lines differentiating the four panels. When the board senses a load, a red cursor appears in the white graph area. The size of the cursor is proportional to the amount of the load.

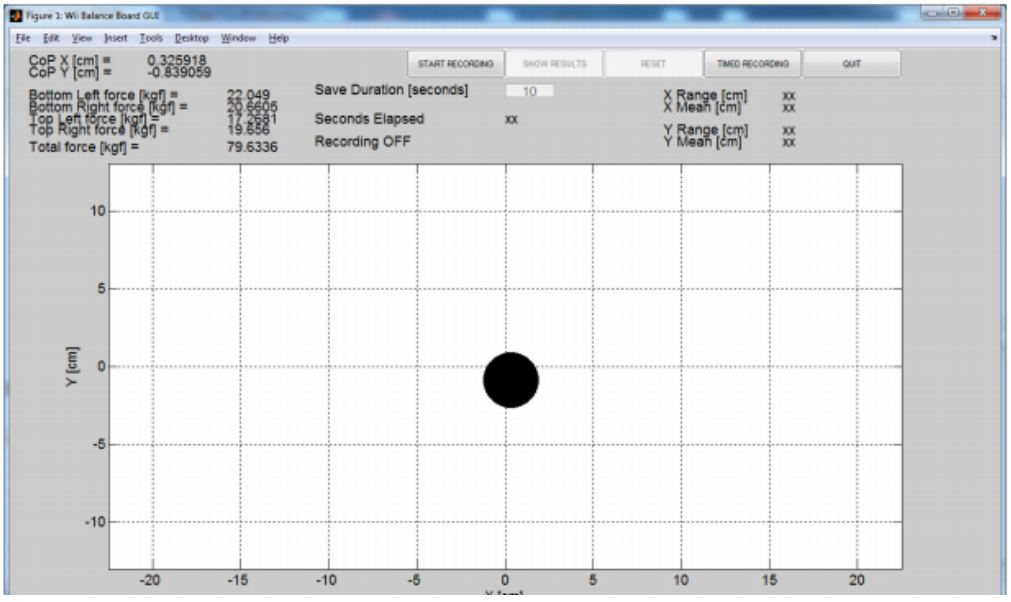

Figure 5.5. *Balance Board Interface.*

5.1.4.3 Bipolar and HD sEMG recording

Muscle activity were acquired via 8 wireless bipolar sEMG amplifiers (Ultimium EMG system, Noraxon, USA Inc. Scottsdale, AZ) bilaterally from the rectus abdominis superior (RAS), external oblique (EO), latissimus dorsi (LD) and erector spinae longissimus (ESL). Bipolar AgCl electrodes for EMG measurements were placed following guidelines provided by the SENIAM project [17-18].

High Density superficial electromyography (HD-sEMG, OTBioelettronica, Torino, Italy) were acquired via two 64 channels grids placed 2.5 cm away from the spinous process, between the 2rd and 5th lumbar vertebra (**Figure 5.6**) [7,19].

The grid consisted of 13 rows and 5 columns of electrodes (1-mm diameter, 8-mm interelectrode distance in both directions), with one electrode absent from the upper right corner (**Figure 5.6**). The position corresponding to the missing electrode was used as the origin of the coordinate system to define the electrode location.

Prior to the application of electrodes, the skin in the region lateral to the lumbar spine was prepared by shaving the area if needed and then applying an abrasive paste (SPES Medica, Italy), and finally washing and drying the region. The electrodes were prepared by applying a thin custom double-sided adhesive foam pad

to the electrode grid (SPES Medica, Genoa, Italy). The cavities of the electrode grids were then filled with an electroconductive paste (SPES Medica).

Reference electrodes were placed on prepared skin over the sacrum, posterior and anterior superior iliac spines.

The EMG signals were amplified (128-channel surface EMG amplifier, OT Bioelettronica; #3 dB bandwidth 10-500 Hz) by a factor of 2000 and sampled at 2048 Hz.

A Biodex System 3 dynamometric device (Biodex, USA) was used to acquire the peak torque during iMVCs and submaximal isometric contraction at 50% MVC before and after the lifting activity.

All the acquisition devices were synchronised together during lifting tasks and during iMVC with a trigger signal generete by MyoSync (Noraxon) (**Figure 5.7**).

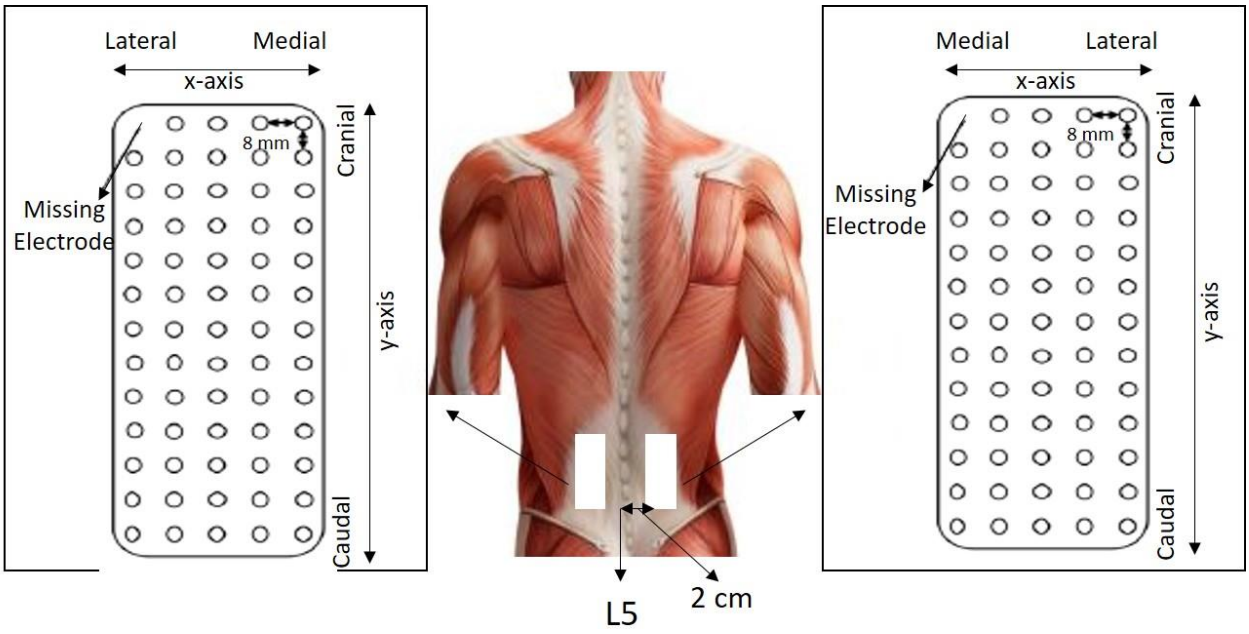

Figure 5.6. *Description of the approximate positioning of the HDEMG grids 2.5 cm lateral to the L5 spinous process on the lumbar ES of the participant and a schematic of the electrode grids showing the x- and y-axes, reference electrode and inter-electrode distance.*

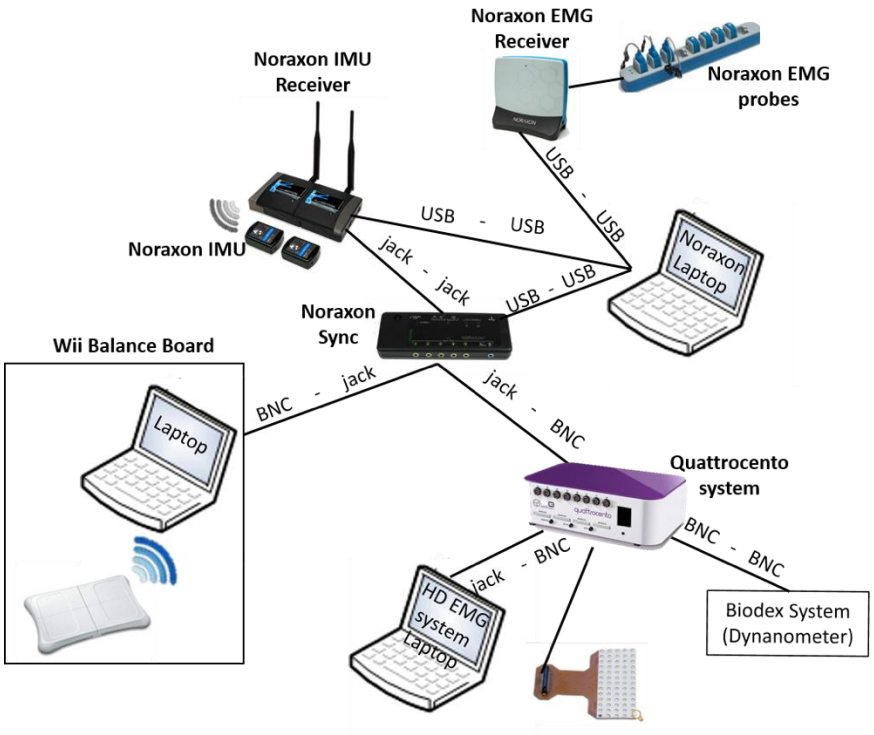

Figure 5.7. *Hardware setup.*

5.1.5 Data Analysis

After acquisition, data were processed using Matlab (version 8.0.0.783; MathWorks, Natick, MA, USA) software.

Kinematic, kinetic and electromyographic data during lifting task were normalized to the duration of the lifting, lowering and whole (lifting+cycle) cycles. The data were interpolated to 100 samples for lifting cycle and 100 for lowering cycle using a polynomial procedure.

5.1.5.1 Lifting and lowering cycles detection

The vertical displacement and velocity of the IMU placed over the load were calculated. To estimate vertical velocity and displacement, the filtered acceleration of IMU load (3th order low-pass Butterworth filtered by applying a 10Hz cut-off frequency) is integrated one and two times respectively, and the drift is corrected assuming that before and after lifting the vertical acceleration and speed are zero (**Figure 5.8**).

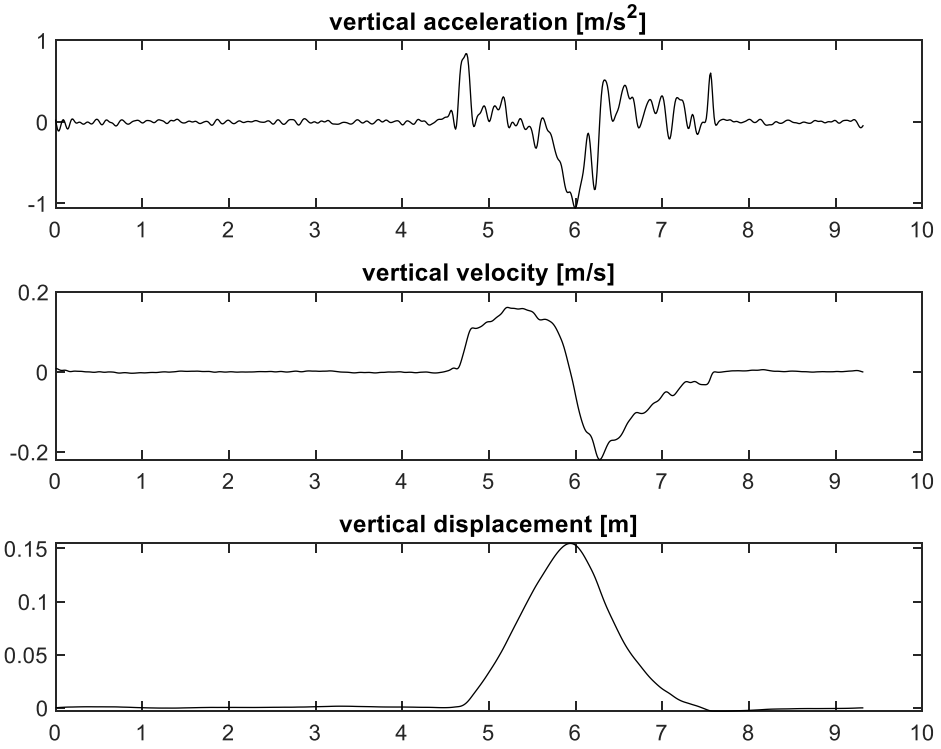

Figure 5.8. *Accerelation, vertical displacement and velocity of the IMU placed over the load.*

The onset of the lifting task was defined as the time point at which the IMU load velocity exceeded a velocity threshold of 0.025 m/s on the vertical axis. Termination of the lifting task was defined as the maximum point on the graph of the vertical displacement of IMU load (z axis). Termination of lowering cycle was defined as the point on the graph at which the IMU load velocity fell below the velocity threshold in the opposite direction after the minimum value (See **Figure 5.9**).

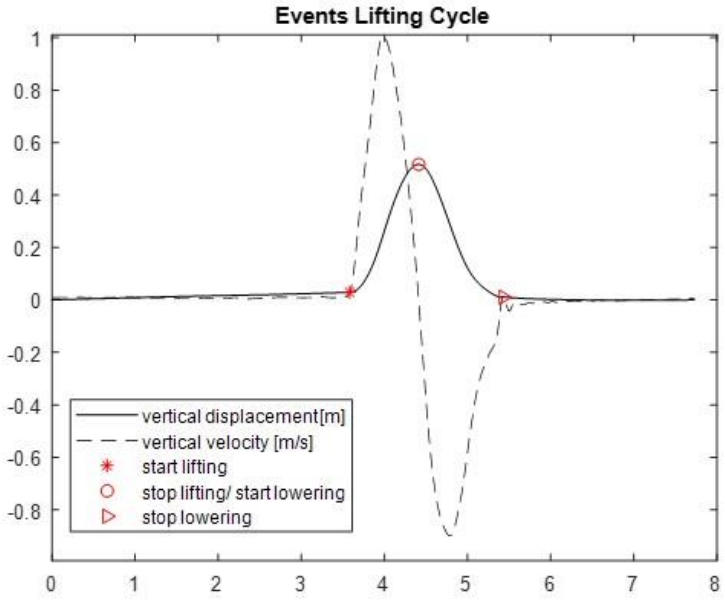

Figure 5.9. *Cycles definition.*

After cycles definition, cross-correlation analysis between each curve of elbow flexion-extension (see 2.5.2) and mean curve of elbow flexion-extension was applied to delete some cycles (**Figure 5.10**). Particularly, if the cross-correlation of mean curve and the single curve was less than 0.9 the curve was deleted.

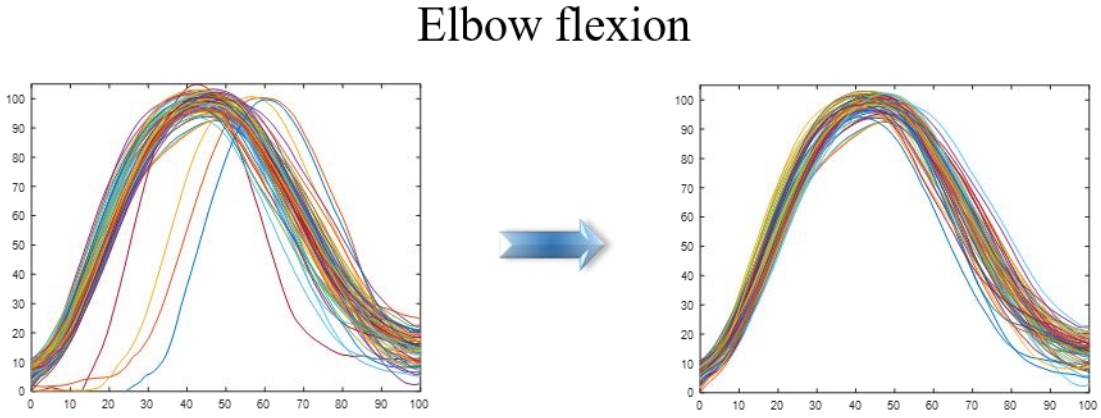

Figure 10. *Cross-correlation between the cycle.*

5.1.5.2 Kinematic data

Joint Angles

Anatomical angles for cervical segment, lumbar segment, thoracic segment, pelvis and right shoulder joint in the three planes (frontal, sagittal, and transverse) and the right elbow joint angle in the sagittal plane were extracted from Noraxon Software.

From these variables, we derived the Range of Motion (RoM) at each joint or segment, defined as the difference between the maximum and minimum value during the lifting cycles.

Acceleration and Jerk

Starting from the accelerations acquired from each sensor during the lifting tasks, we evaluated the stability parameters: the RMS of each component of the acceleration, the RMS of the acceleration magnitude ($RMS_{acceleration}$) and the RMS of the jerk (i.e. the derivative of the acceleration) magnitude (RMS_{jerk}) [20].

5.1.5.3 Kinetic data

Starting from CoP data (**Figure 5.11**), the following parameters were calculated:

- COP length: represents the total trajectory in mm followed by the COP from its initial position to its maximal position;

- Total excursion of the COP: is defined as the total distance travelled by the COP over the course of the trial duration;
- COP velocity: represents the total distance travelled by the COP over time.

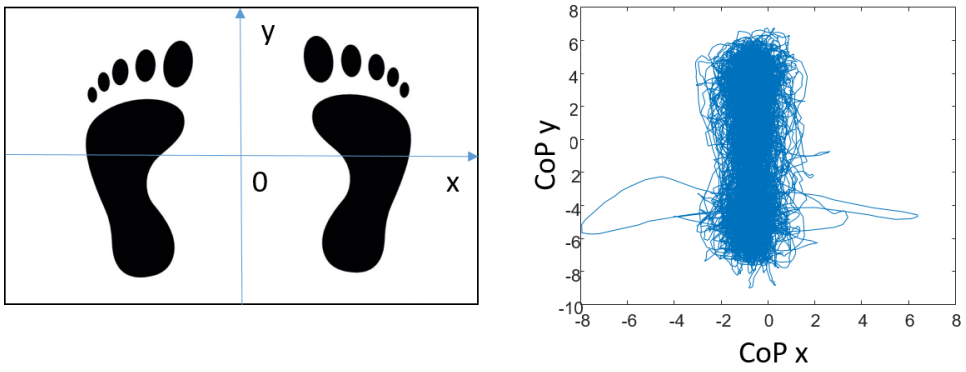

***Figure 5.11**. The feet position on Balance Board and an example of CoP acquisition.*

5.1.5.4 Bipolar sEMG processing

The sEMG signals were processed as follows: the iMVC and the sEMG raw data of each lifting task were band-pass filtered using a fourth-order Butterworth filter of 20–400 Hz to reduce artifacts and other components of high-frequency noise [21-22]. From these signals, the analysis of time and frequency domains was performed.

Time domain features

As regards time domain, from the processed sEMG signals of each lifting task, the average rectified value (ARV), the root mean square (RMS) and the maximum value (Max) within the cycle where calculated to characterize differences in the sEMG activity among the different lifting conditions (see 4.1.1.4 for details).

CoA and FWHM

To characterize timing and duration of the the sEMG curves, the center of activity (CoA) and the full width at half maximum (FWHM) were calculated. The CoA of the sEMG waveform during the cycle

was calculated using circular statistics [23]. It was evaluated as the angle of the vector (1st trigonometric moment) that points to the center of mass of that circular distribution using the following formulas:

$$A = \sum_{i}^{T} \cos\theta_i \times EMG_i$$

$$B = \sum_{i}^{T} \sin\theta_i \times EMG_i$$

$$CoA = \tan^{-1}(B/A)$$

Where θ is one of 100/200 samples (lifting or lowering/whole) of EMG converted to a common angular scale in radians by:

$$\alpha = \frac{2\pi x}{k}$$

where x is the representation of the data in the original scale, α is its angular direction and k is the total number of steps (100/200) on the scale that x is measured in. The EMG and the CoA were plotted in polar coordinates (polar direction denoted the phase of the gait cycle, with angle θ that varies from 0 to 360°).

The FWHM for EMG waveform was calculated as the sum of the durations of the intervals in which the EMG activity exceeded the half of its maximum:

$$FWHM = \sum_j \Delta t_j.$$

Particularly for each subject, the FWHM for the EMG curve of each trunk muscles considering the lifting cycle, the lowering cycle and the whole cycle, were extracted.

Co-activation function

Furthermore, the simultaneous activation of the trunk muscles (co-activation) was also computed by considering the time-varying multi-muscle co-activation function (TMCf) proposed by Ranavolo and colleagues [23] (see 4.1.1.4 for details).

Frequency domain features

As regards the frequency domain, using the band-pass filtered sEMG data recorded during lifting tasks and iMVC, only for extensor muscle, the power spectral density was estimated [24] and for each muscle, we computed the mean frequency (MNF) and the median frequency (MDF) (see 4.1.1.4 for details).

For each muscle, both MNF and MDF related to the lifting tasks were normalized, to the MNF_{MVC} and MDF_{MVC} calculated from the iMVC spectra for each participant, respectively.

5.1.5.5 HD EMG system data

Before data analysis, the EMG signals were digitally band-pass filtered in the frequency bandwidth 10–350 Hz (2nd order Butterworth filter).

Fifty-nine bipolar EMG signals were obtained from each grid (12 longitudinal bipolar recordings in each column except the first column of the grid, which had 11 electrode pairs).

Spatial distribution of muscle activity before, during and after lifting task

Then, to characterize the spatial distribution of muscle activity, the following variables were extracted from the 59 bipolar signals. Mean power spectral frequency (MF) and root mean square (RMS) values were computed from each bipolar recording from adjacent, nonoverlapping signal epochs of 0.5 second duration, as described in [25]. For graphical representation, the 59 values were

interpolated by a factor of 8, but only the original values were used for data processing and statistical analysis.

The individual RMS and MNF values for each bipolar signal were averaged to produce the mean RMS and MNF values across the grid. The RMS values for each bipolar signal were used to create a topographical map of ES activity. This map was used to determine the location of the x- and y-coordinates of the centroid as described previously [26-28]. Particularly, the two coordinates of the center of gravity of the root mean square map (Gx and Gy for the lateral–medial and cranial–caudal direction, respectively) are defined as:

$$G_x = \frac{1}{RMS_{total}} \sum_{i=1}^{59} RMS_i x_i \; G_y = \frac{1}{RMS_{total}} \sum_{i=1}^{59} RMS_i y_i$$

where RMS_{total} is the sum of RMS values, RMS_i is the RMS value at the ith position which corresponds to the coordinates (x_i, y_i). The center of gravity corresponds to the point where the 59 RMS values are concentrated on average. The power spectrum for mean frequency estimation was computed with Welch periodogram with Hanning window and no zero-padding [29].

To characterize heterogeneity in spatial EMG potential distribution at individual torque levels, coefficient of variation (CoV) and modified entropy were used in the present study. CoV was defined as the quotient of standard deviation among 59 RMS and averaged value of 59 RMS at a torque level. Modified entropy of the spatial distribution of EMG amplitude was calculated for 59 RMS values (in space) of single differential signals computed over a 500 ms epoch taken at 50% of MVC.

As done by Farina et al. [30] in a previous work, modified entropy was defined as entropy of the signal power, that is

$$E = -\sum_{i=1}^{59} p(i)^2 log_2 p(i)^2$$

where p(i) is the square of the RMS value of channel i divided by the sum of the squares of all the 59 RMS values, at the given force level. Therefore, $p(i)^2$ represents the normalized power of each channel. It is E = 0 when all the p(i) are zero except one and is maximal and equal to $\log_2 59 = 5.884$ when the p(i) values are identical and equal to 1/59 (all channels have the same energy). Increase in CoV and decrease in modified entropy, respectively, mean an increase of heterogeneity in the spatial EMG potential distribution within an electrode grid.

Correlation coefficients were calculated from the 59 pairs of RMS values at the same regions between 20% of MVC and those of all other torque levels to compare the spatial EMG potential distribution pattern. Decrease of correlation coefficient indicates a change in spatial EMG potential distribution pattern [31].

The RMS and MF were expressed as a percentage relative to the initial value (first minute of the task) [7]. These parameters were evaluated during submaximal contractions before and after the lifting task and during lifting task within each lifting cycle (see "Lifting cycle detection" paragraph).

5.2 RESULTS ON 15 HS

5.2.1 Characteristics of subjects and questionnaires

The characteristic of the investigated sample is reported in **Table 5.2** while the values of VAS and Borg scale at the end of each session are reported in **Table 5.3**.

Characteristic	Control (N=15)
Age (years)	27.87±3.98
Gender (female)	9
Height (m)	1.68±0.09
Weight (kg)	71.88±14.01
BMI (kg/m^2)	25.26±3.21
SF-36 (Total)	119.88±6.61

Table 5.2. *Subjects' characteristics.*

scale	LI	Control
VAS at the end of session	1	0.69±1.44
	2	4±10.83
	3	7.64±17.49
Borge Scale at the end of session	1	7.44±1.55
	2	9.44±2.71
	3	10.19±2.66

Table 5.3. *Pain and fatigue scale of the subjects.VAS, visual analogue scale (0-100); LI, Lifting Index. Values are presented as mean ± SD.*

5.2.2 Kinematic Angles

Figure 5.12 shows the mean curves ($\pm$ SD) for each lifting condition of anatomical angles for cervical segment, lumbar segment, thoracic segment, pelvis and right shoulder joint in the three planes and the right elbow joint angle in the sagittal plane during the lifting (100 samples) and lowering cycles (100 samples).

5.2.3 RMS of acceleration and Jerk

Figure 5.13 shows the means and standard deviation values of RMS of acceleration and jerk for each IMU and for each LI considering lifting cycles, lowering cycles and whole cycles (lifting+lowering).

The repeated measures ANOVA revealed a significant effect of the LI on all parameters ($p<0.05$) except RMS_{acc_z} of Forearm and RMS_{acc_z}, $RMS_{acc\_magnitude}$ and RMS_{jerk} of Load.

The significant differences of post hoc analysis between the pair of lifting conditions are shown in **Figure 5.13**.

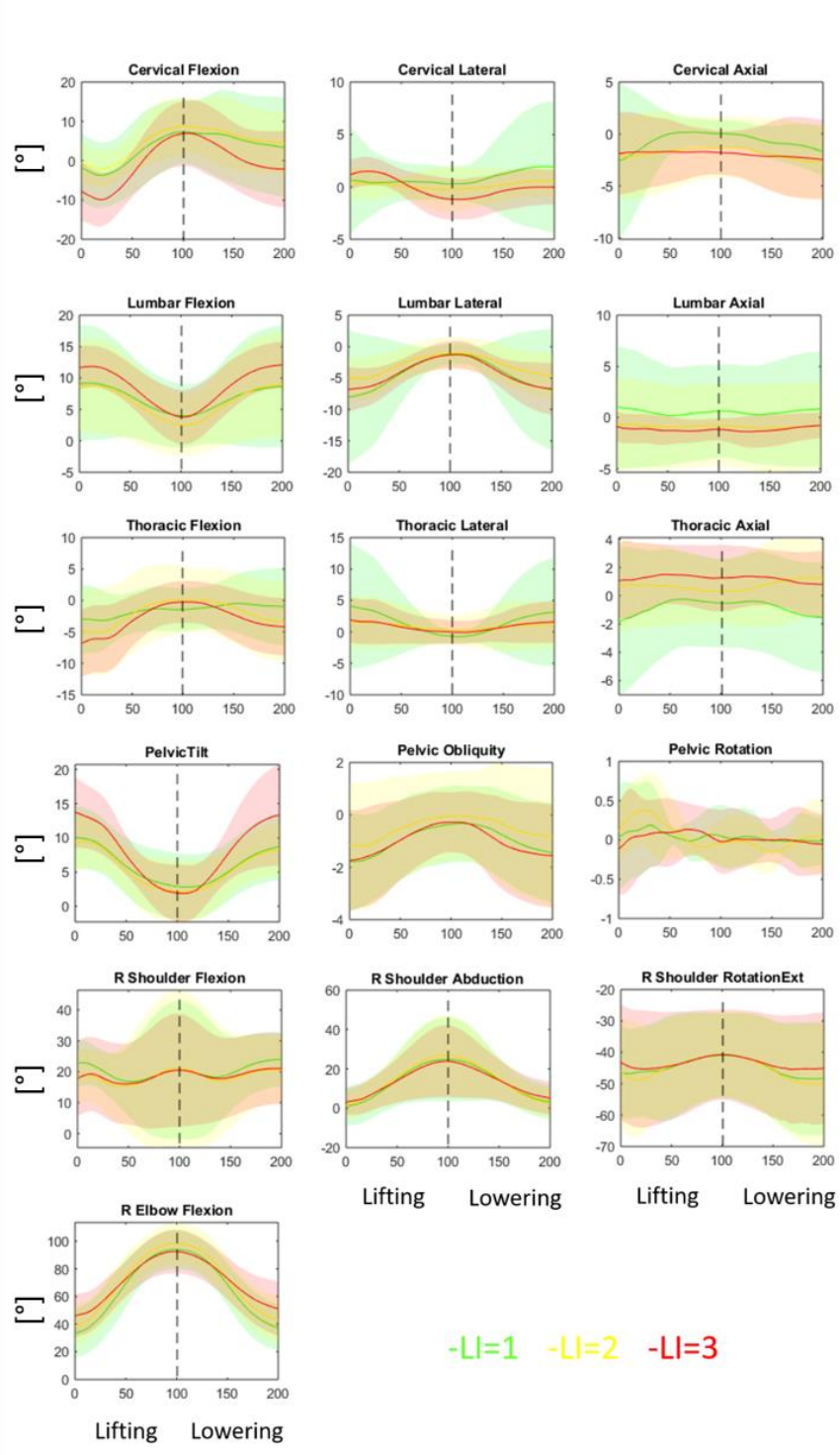

Figure 5.12. *Kinematic curves.*

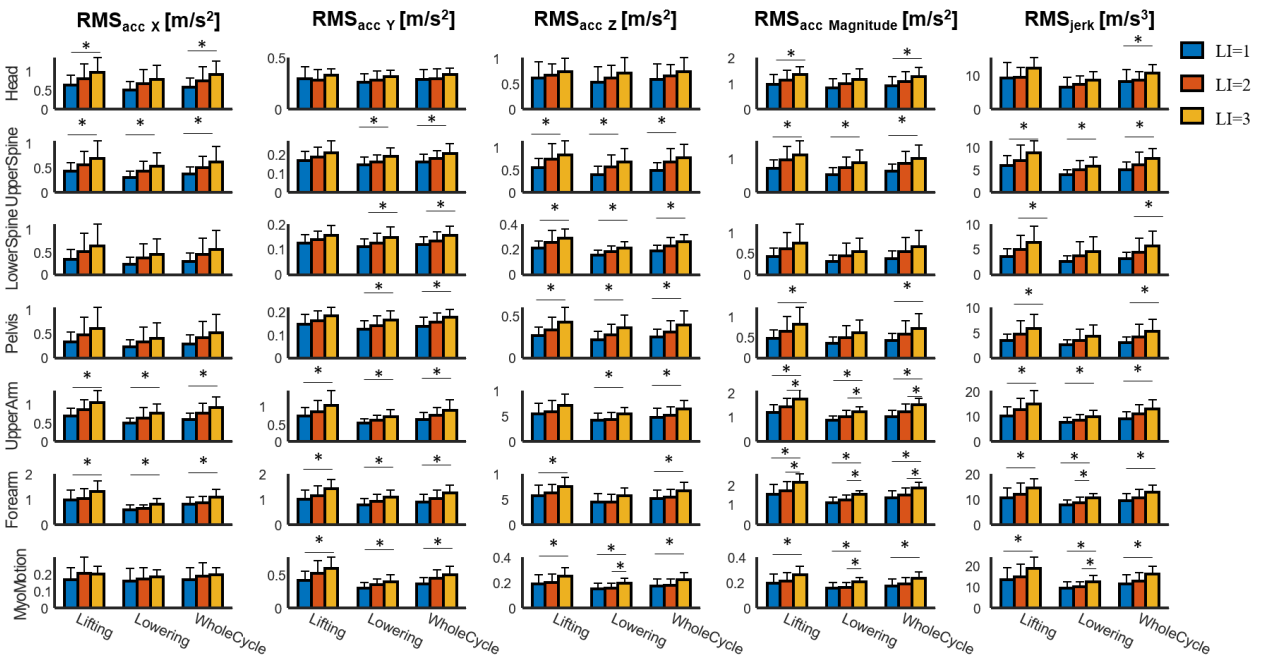

Figure 5.13. *Mean and standard deviation values of RMS of acceleration and jerk for each IMU and for each LI considering lifting cycles, lowering cycles and whole cycles.*

5.2.4 CoP

Figure 5.14 shows the mean curves ($\pm$ SD) for each lifting condition of x and y coordinations of CoP and forces (4 transductor) during the lifting (100 samples) and lowering cycles (100 samples).

Figure 5.15 shows the means and standard deviation values of COP length, Total excursion of the COP and COP velocity for each LI considering lifting cycles, lowering cycles and whole cycles (lifting+lowering).

Two-way ANOVA showed significant effects on CoP excursion caused by LI ($p < 0.05$) and phase ($p < 0.05$). The statistical significance of post hoc analysis is reported on **Figure 5.15**.

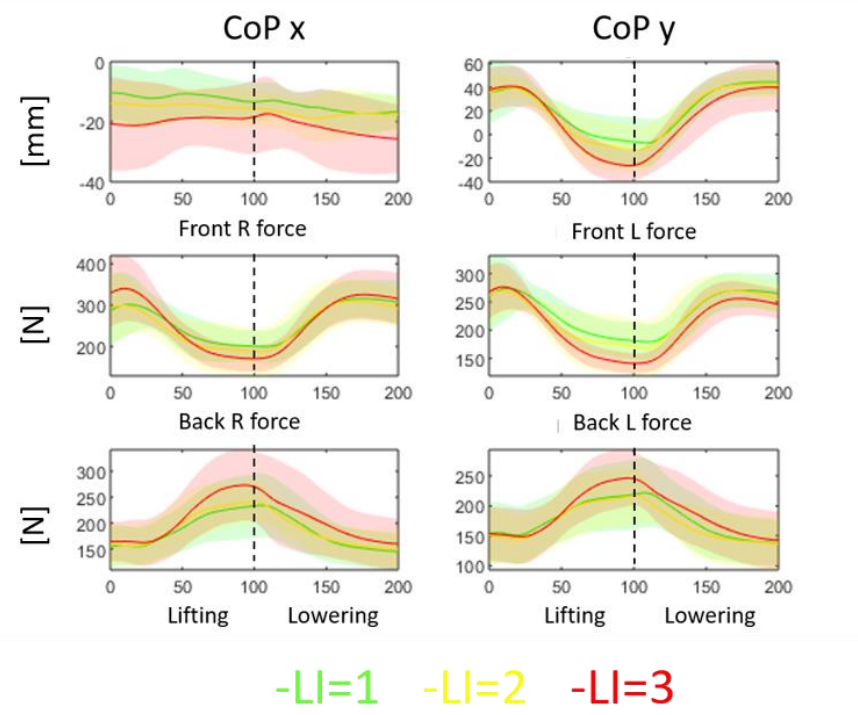

Figure 5.14. *Mean and standard deviation of the curves of CoP in the anteroposterior and medio-lateral directions and of the curves on the four transductor of Balance Board.*

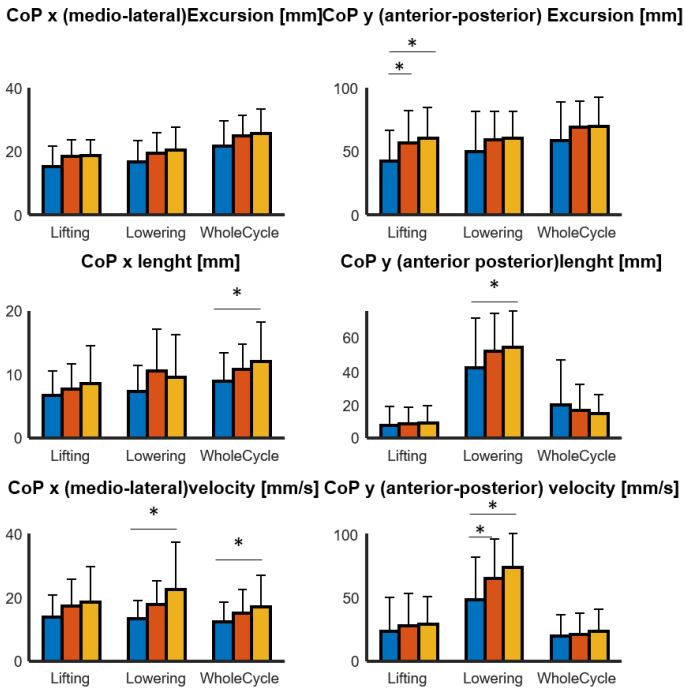

Figure 5.15. *Mean and Standard deviation of COP, COP length, Total excursion of the COP and COP velocity for each LI considering lifting cycles, lowering cycles and whole cycles (lifting+lowering).*

5.2.5 Bipolar sEMG

Figure 5.16 shows an example of the EMG signals for each acquired muscle: the raw data (in blue), the envelopes (in red) and the events (red, green and blue vertical lines are the start and stop of lifting phase and the stop of lowering phase) are reported. **Figure 5.17** shows the mean envelopes ($\pm$ SD) for each lifting condition of right and left trunk muscles during the lifting (100 samples) and lowering cycles (100 samples). In the following paragraphs the parameters extracted starting from these envelope: the means in each minute normalized with the value in the first minute were considered.

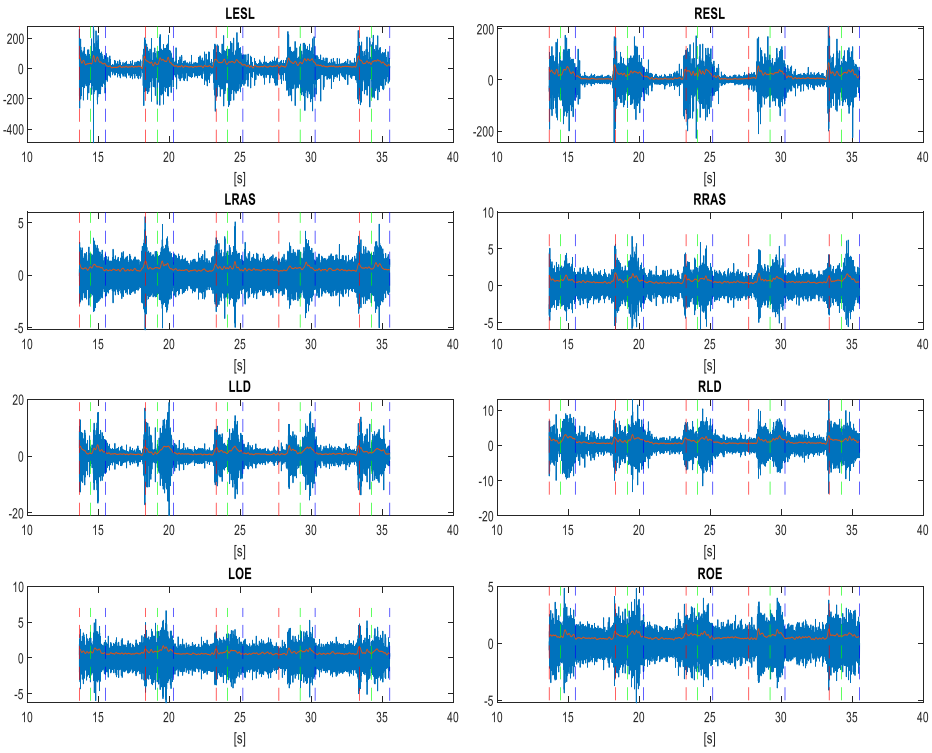

Figure 5.16. *An example of raw sEMG signals of right and left trunk muscles during the lifting task. RESL and LESL: right and left erector spinae longissimus; RLD and LLD: right and left latissimus dorsi; RRAS and LRAS: right and left rectus abdominis superior; REO and LEO: right and left external oblique.*

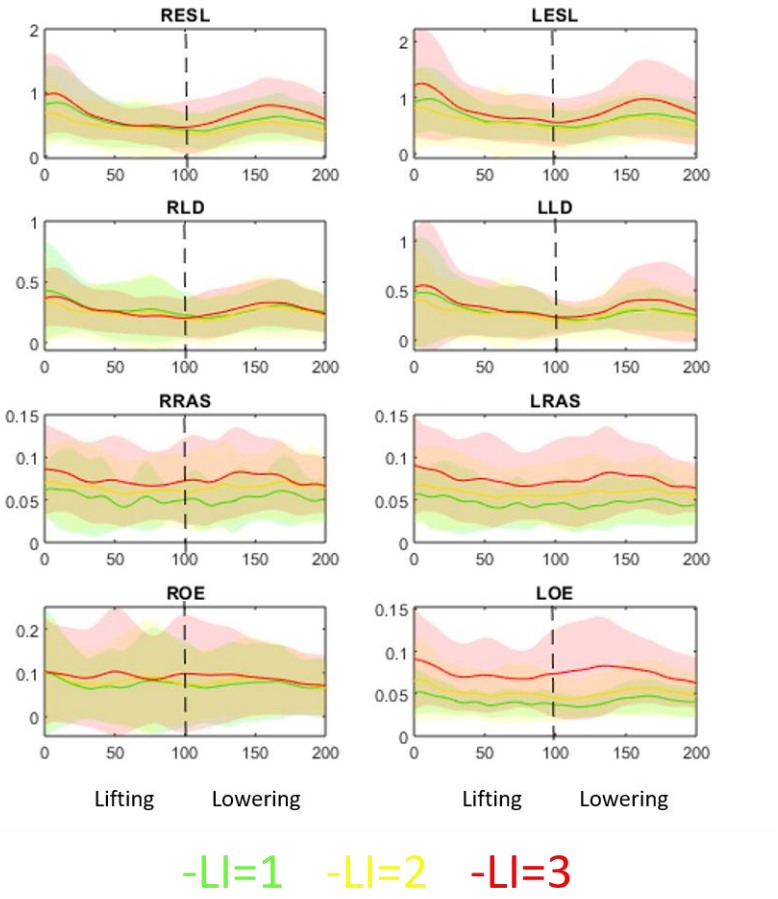

Figure 5.17. *Mean envelopes (± SD) for each lifting condition of right and left trunk muscles during the lifting (100 samples) and lowering cycles (100 samples). RESL and LESL: right and left erector spinae longissimus; RLD and LLD: right and left latissimus dorsi; RRAS and LRAS: right and left rectus abdominis superior; REO and LEO: right and left external oblique.*

5.2.5.1 Lifting: mean in each minute normalized with the value in the first minute

Time domain features

Since no statistically significant differences were found between the right and left muscles in any of the sEMG features ($p > 0.05$), the following results are referred considering the two sides togheter.

Figure 5.18 shows the means and standard deviation values of RMS (A), ARV (B) and Max (C) of ESL and LD muscles for each LI considering lifting cycles, lowering cycles and whole cycles (lifting+lowering).

Figure 5.19 shows the means and standard deviation values of RMS (A), ARV (B) and Max (C) of RAS and EO muscles for each LI considering lifting cycles, lowering cycles and whole cycles (lifting+lowering).

These values are the mean during each minute normalized by the mean in the 1st minute of lifting task.

Two-way ANOVA showed significant effects of multiple factors on sEMG parameters considering training LI ($p < 0.05$), and phase ($p < 0.05$).

The statistical significance of post hoc analysis are reported on **Figures 5.18** and 5.**19.**

Co-activation function

Figure 5.20 shows the means and standard deviation values of $TMCf_{Area}$ for each LI considering lifting cycles, lowering cycles and whole cycles (lifting+lowering).

These values are the mean during each minute normalized by the mean in the 1st minute of lifting task.

Two-way ANOVA showed significant effects of multiple factors considering LI ($p < 0.05$) and considering phase ($p < 0.05$). The statistical significance of post-hoc analysis is reported on **Figure 5.20**.

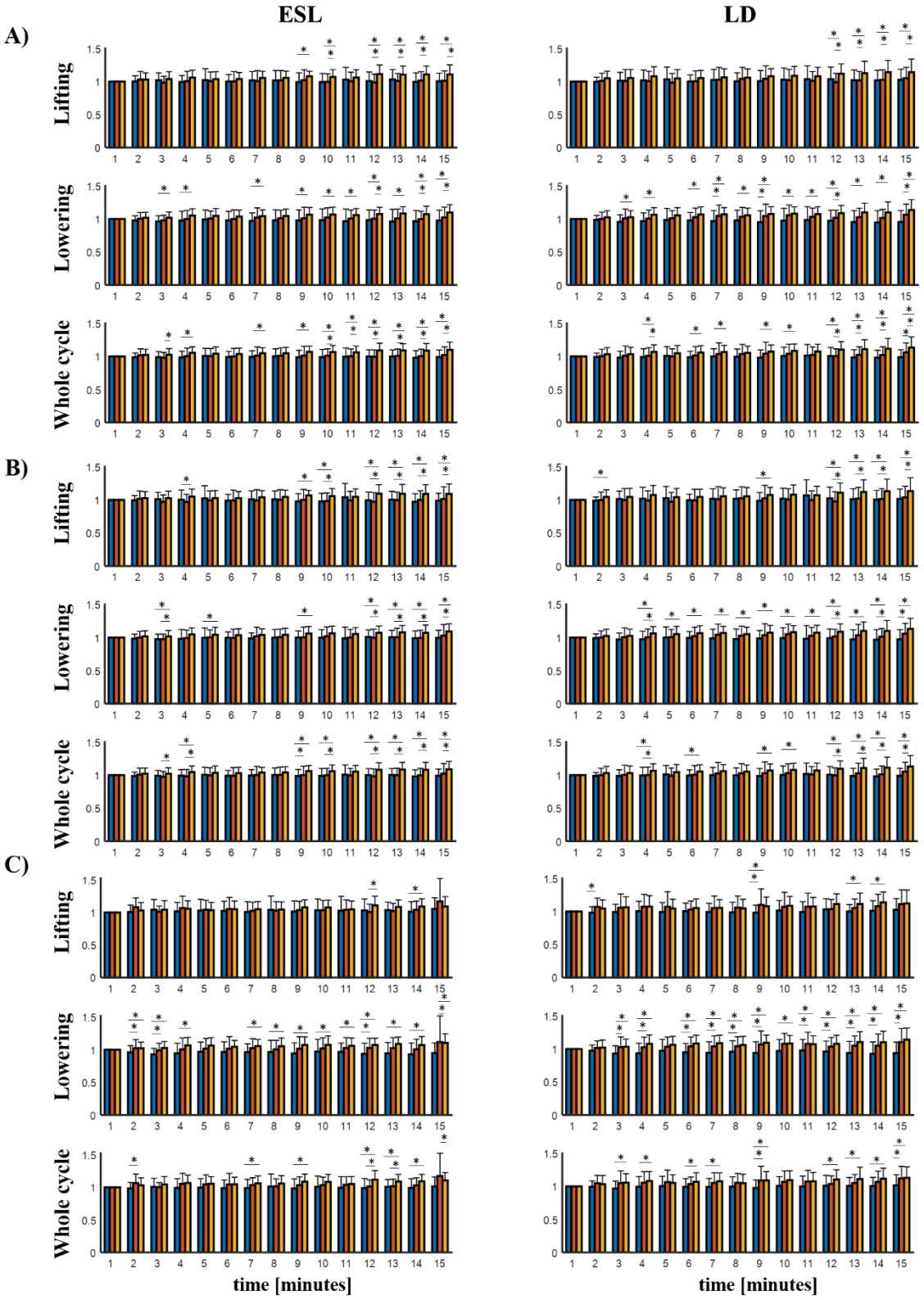

Figure 5.18. *Mean and standard deviation values of RMS (A), ARV (B) and Max (C) of ESL and LD for each LI considering lifting cycles, lowering cycles and whole cycles. *statistical significance.*

F

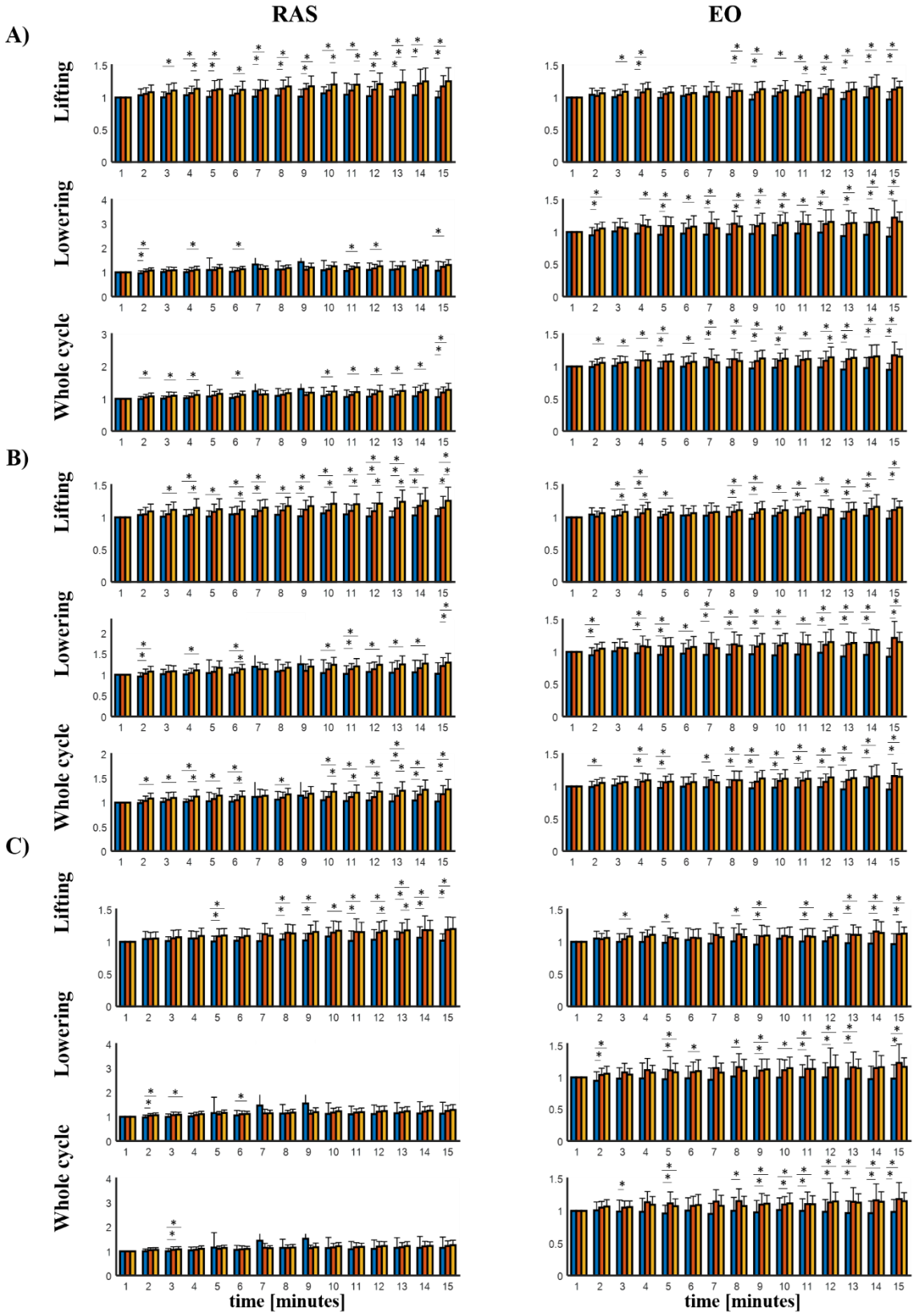

Figure 5.19. *Mean and standard deviation values of RMS (A), ARV (B) and Max (C) of RAS and EO for each LI considering lifting cycles, lowering cycles and whole cycles. *statistical significance.*

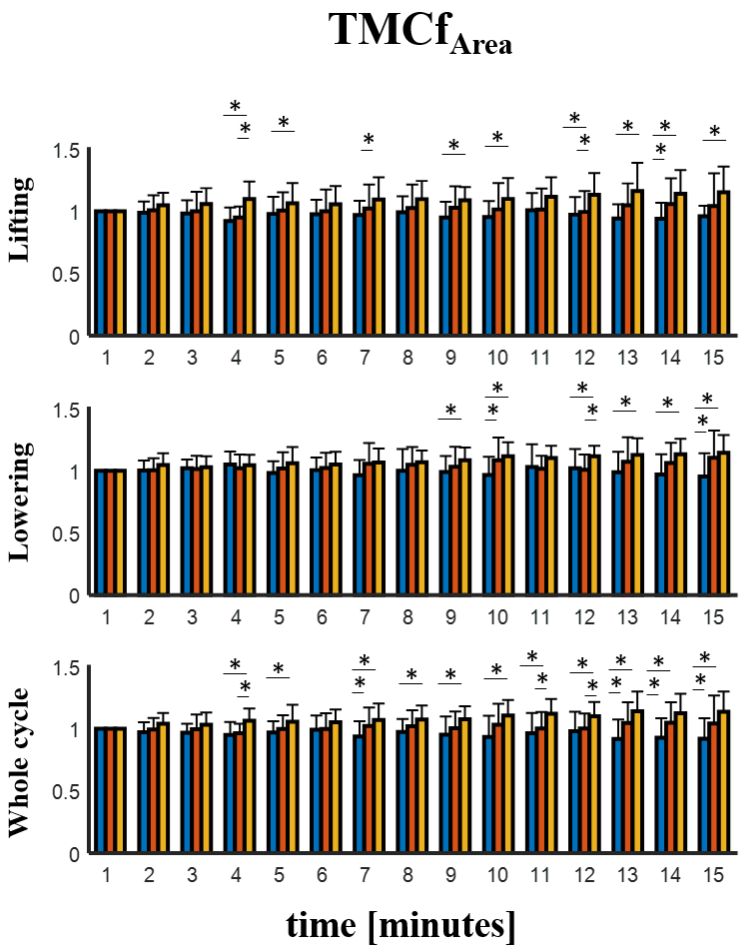

Figure 5.20. *Mean and standard deviation values of $TMCf_{Area}$ for each LI considering lifting cycles, lowering cycles and whole cycles. *statistical significance.*

Frequency domain features

Figure 5.21 shows the means and standard deviation values of MNF (A) and MDF (B) of ESL and LD, muscles for each LI considering lifting cycles, lowering cycles and whole cycles (lifting+lowering). These values are the mean during each minute normalized by the mean in the 1st minute of lifting task.

The statistical significance of post-hoc analysis is reported on **Figure 5.21.**

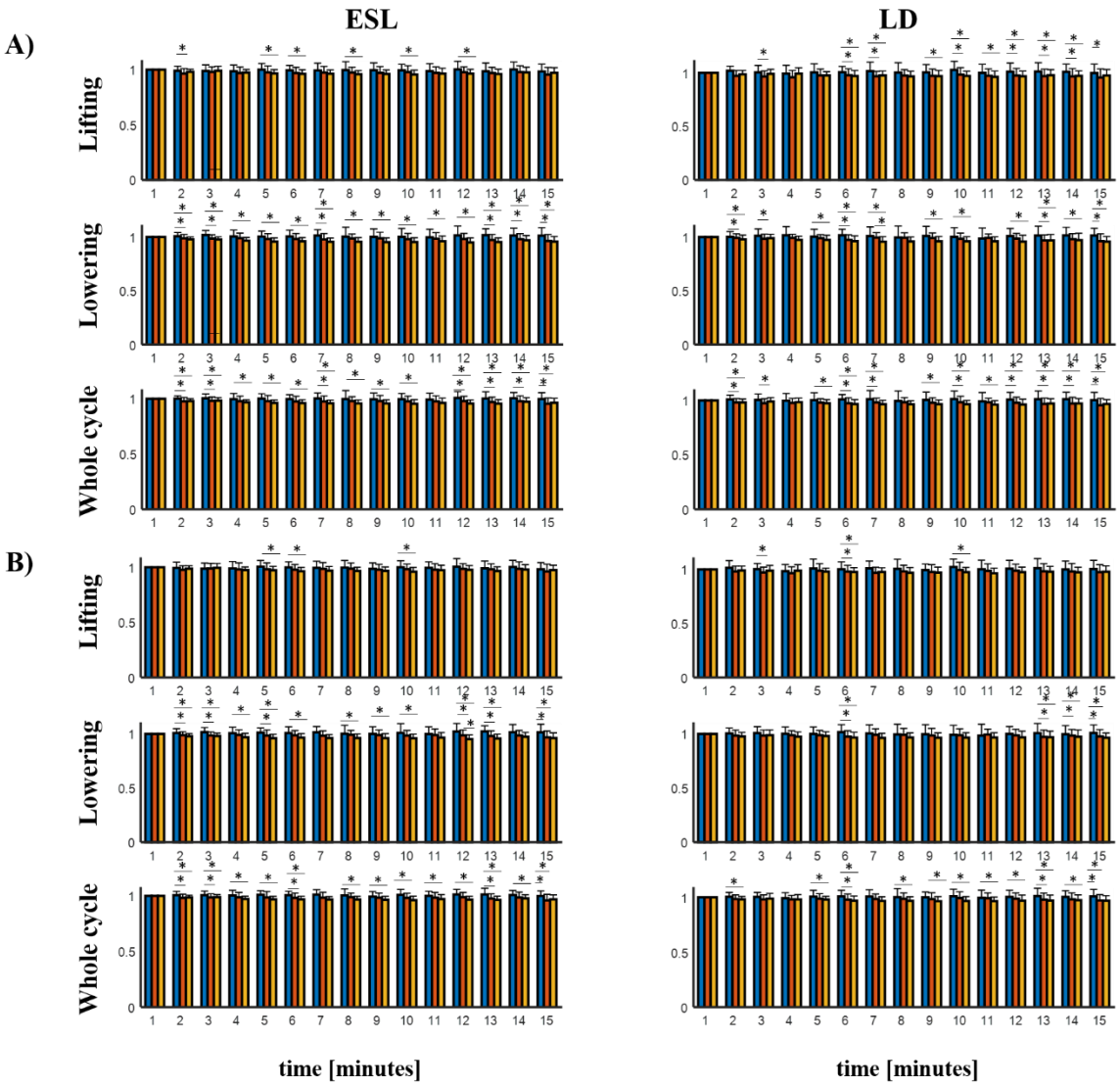

Figure 5.21. *Mean and standard deviation values of MNF (A) and MDF (B) of ESL and LD for each LI considering lifting cycles, lowering cycles and whole cycles. *statistical significance.*

5.2.5.2 MVC pre and post lifting tasks

Figure 5.22 shows the delta for Max and FMD between 50% MVC pre and post lifting tasks. No significant statistical differences were found.

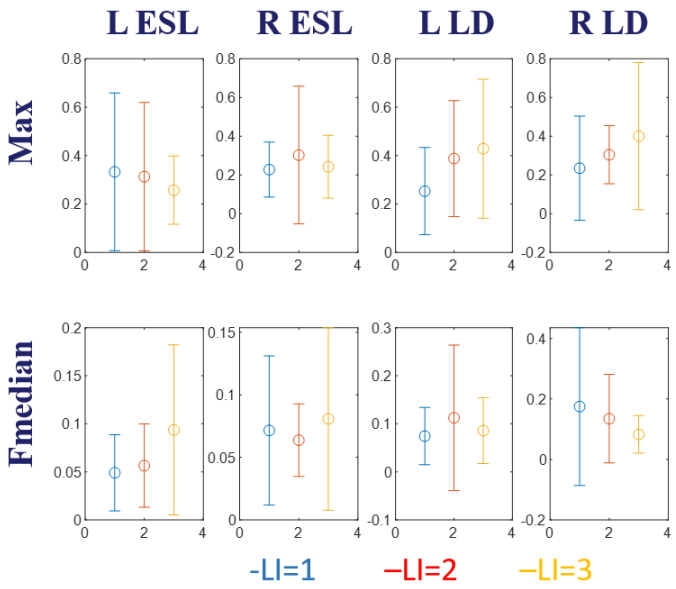

Figure 5.22. *delta for Max and FMD between 50% MVC pre and post lifting tasks.*

5.2.6 HD sEMG

5.2.6.1 Lifting: mean in each minute normalized by the value in the first minute

Since no statistically significant differences were found between the right and left muscles in any of the HD sEMG features ($p > 0.05$), the following results will refer considering the two side together.

Figure 5.23 shows the means and standard deviation values of RMS and MNF of ESL for each LI considering lifting cycles, lowering cycles and whole cycles (lifting+lowering). These values are the mean during each minute normalized by the mean in the 1st minute of lifting task.

The statistical significances are reported in **Figure 5.23.**

For x and y coordinate of baricenter, Entropy, CV RMS and Correlation Coefficient RMS of ESL no significant differences were found.

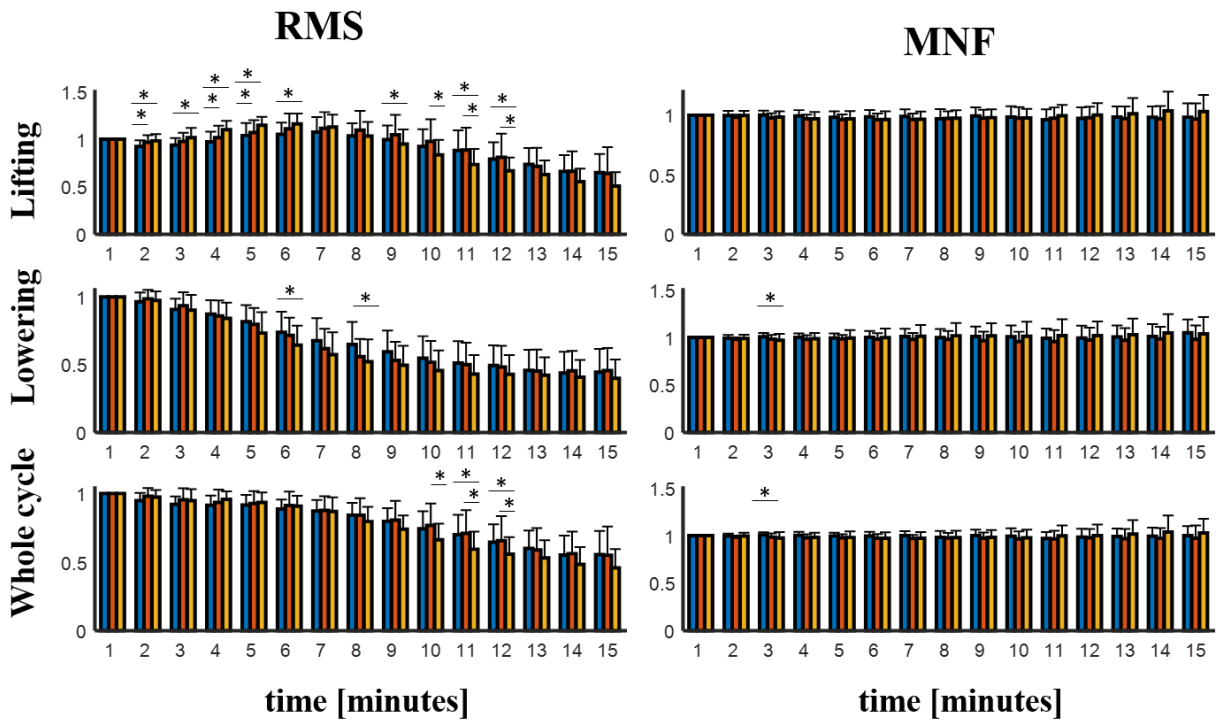

Figure 5. 23. *Mean and standard deviation values of RMS and MNF of HD-sEMG for each LI considering lifting cycles, lowering cycles and whole cycles. *statistical significance.*

5.2.6.2 MVC pre and post lifting tasks

Figure 5.24 shows an example of RMS topographical maps of the EMG amplitude.

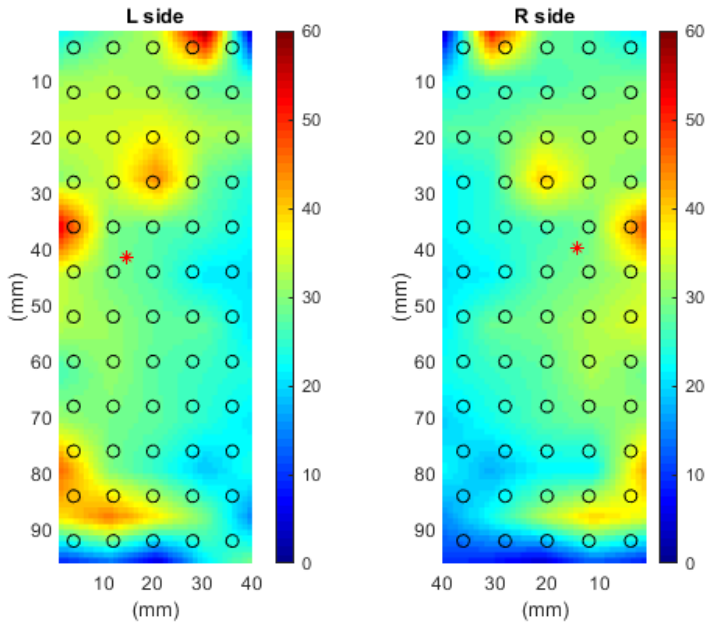

Figure 5.24. *Representative RMS topographical maps for one HS participant during the 50 %MVC test. The centriod is depicted by * and the scale is indicated in μV.*

RMS, MNF, Entropy, CV RMS, Correlation Coefficient, x and y coordinate of baricenter, CV Torque during 50% of MVC for each LI are shown in **Figure 5.25**. The statistical differences are reported in the **Figure 5.25**.

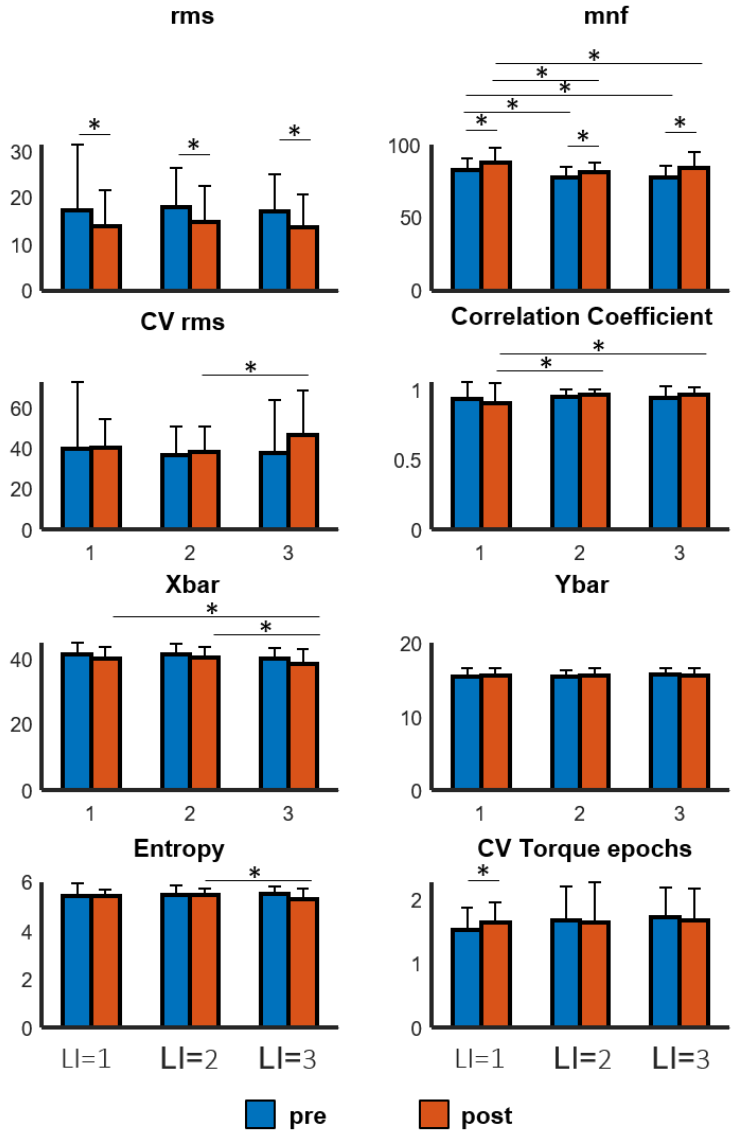

Figure 5.25. *HD sEMG parameters for Erector Spinae Muscles in Healty subjects.*

5.3. RESULTS ON 2 MATCHED GROUPS: HS AND LBP

5.3.1 Characteristics of subjects and questionnaires

The 2 groups are matched for age and gender. The **Table 5.4** reports the characteristics of the 2 matched groups while the values of VAS and Borg scale at the end of each session are reported in **Table 5.5**.

Characteristic	LBP (n=8)	Control (n=8)
Age (years)	25.17±6.43	25.25±6.43
Gender (female)	4	4
Height (m)	1.68±0.06	1.71±0.10
Weight (kg)	65.38±13.82	74.75±11.99
BMI (kg/m^2)	23.21±4.39	25.38± 2.45
Oswestry Disability Score (%)	15.39±9.81	
Duration of pain (years)	3.45±3.07	
SF-36 (Total)	113±8.01	121.5±3.16
TSK	36.88±4.97	
PCS	8.88.±7.48	

Table 5.4. *Baseline characteristics of the LBP and control groups.*
n, number of subjects; LBP, low back pain; SF-36, Short-Form-36 Health Survey; TSK, Tampa Scale for Kinesiophobia; PCS, Pain Catastrophizing Scale. Values are presented as mean ± SD.

scale	LI	LBP (n=8)	Control (n=8)
VAS baseline	1	36.5±21.46	
	2	21.38±8.94	
	3	23.75±14.01	
VAS at the end of session	1	42.25±28.48	1.14±1.77
	2	45.71±11.70	2±2.51
	3	45.37±17.02	5.42±7.72
Borge Scale at the end of session	1	10.13±2.47	7.75±3.10
	2	13.13±1.96	9.37±1.60
	3	13.5±2.78	10.5±2.73

Table 5.5. *Pain and fatigue scale of the LBP and control groups. VAS, visual analogue scale (0-100); LI, Lifting Index. Values are presented as mean ± SD.*

A two-way ANOVA test with LI and subjects (LBP vs Control) as factors was carried on to determine possible significant effects on Borg scale caused by the listed factors: significant effect caused by LI ($F=8.12$, $p=0.01$)., significant effect caused by subjects ($F=22.11$, $p<0.001$).

VAS during each minute of lifting for LBPs is reported in the **Figure 5.26.**

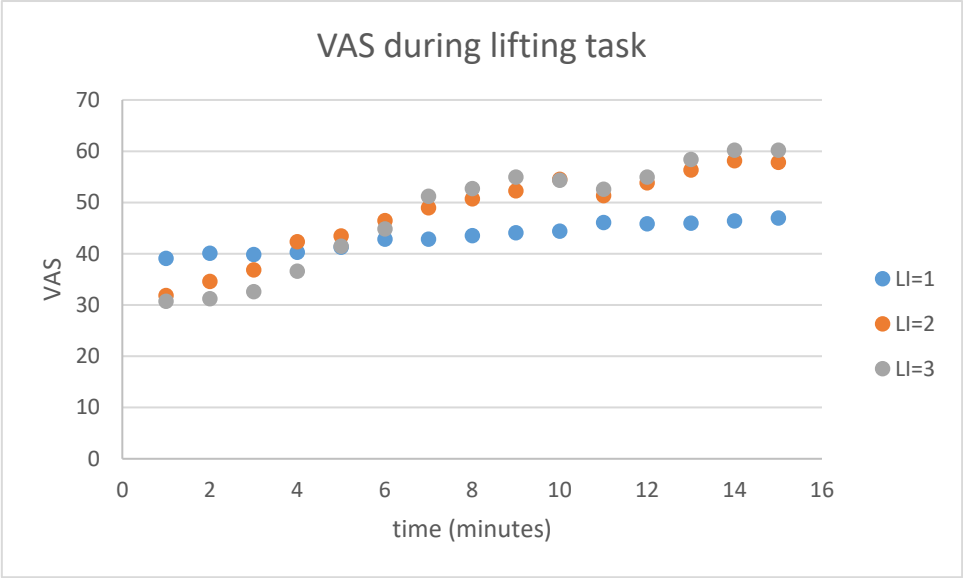

Figure 5.26. *The mean value of pain scale score of the LBP group at each minutes during 15 minutes of lifting task. VAS, visual analogue scale (0-100).*

5.3.2 Kinematic Angles

Figure 5.27 shows the RoM of Trunk for the 2 groups during the lifting tasks:

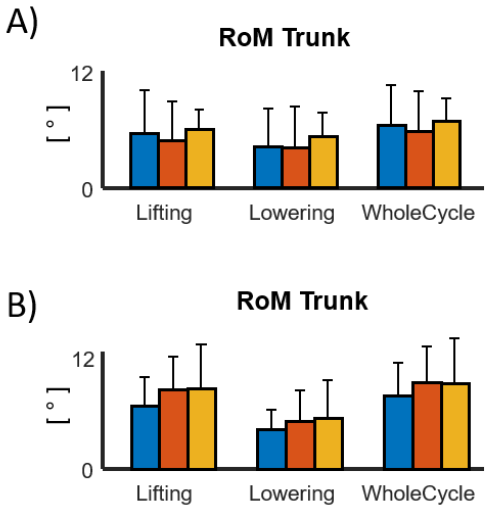

Figure 5.27. *Results in LBP subjects (A) and Healthy subjects (B).*

5.3.3 RMS of acceleration and Jerk

Figure 5.28 shows the means and standard deviation values of RMS of acceleration and jerk for each IMU and for each LI considering lifting cycles, lowering cycles and whole cycles (lifting+lowering) for both Controls (A) and LBPs (B).

A three-way ANOVA test with LI, cycles (Lifting, Lowering and Whole Cycle) and subjects (LBP vs Control) as factors was carried on to determine possible significant effects on each parameter caused by the listed factors. Post-hoc analysis with Bonferroni's corrections were performed when significant differences were observed in the ANOVA results. The statistical significance was set for p values < 0.05.

Results show: significant effect caused by subjects ($p<0.05$) for each considered parameter except for RMS_{Acc_y} of Head; significant effect caused by LI ($p<0.05$) for each considered parameter except for RMS_{Acc_z} of Head and Upper Spine, for RMS_{Acc_x} of Lower Spine and Pelvis and for $RMS_{Acc\_magnitude}$ of Pelvis. Furthermore, results show: significant effect caused by phase ($p<0.05$) for RMS_{Acc_x} of Upper Arm and Forearm; for RMS_{Acc_y} of Upper Arm, Forearm and Load; for RMS_{Acc_z} of Lower Spine, Upper Arm, Forearm and Load; for $RMS_{magnitude}$ of Upper Arm, Forearm and Load; for RMS_{jerk} of Head, Upper Spine, Arm, Forearm and Load.

The significant differences of post hoc analysis between the pair of lifting conditions (LI) are shown in **Figure 5.28.**

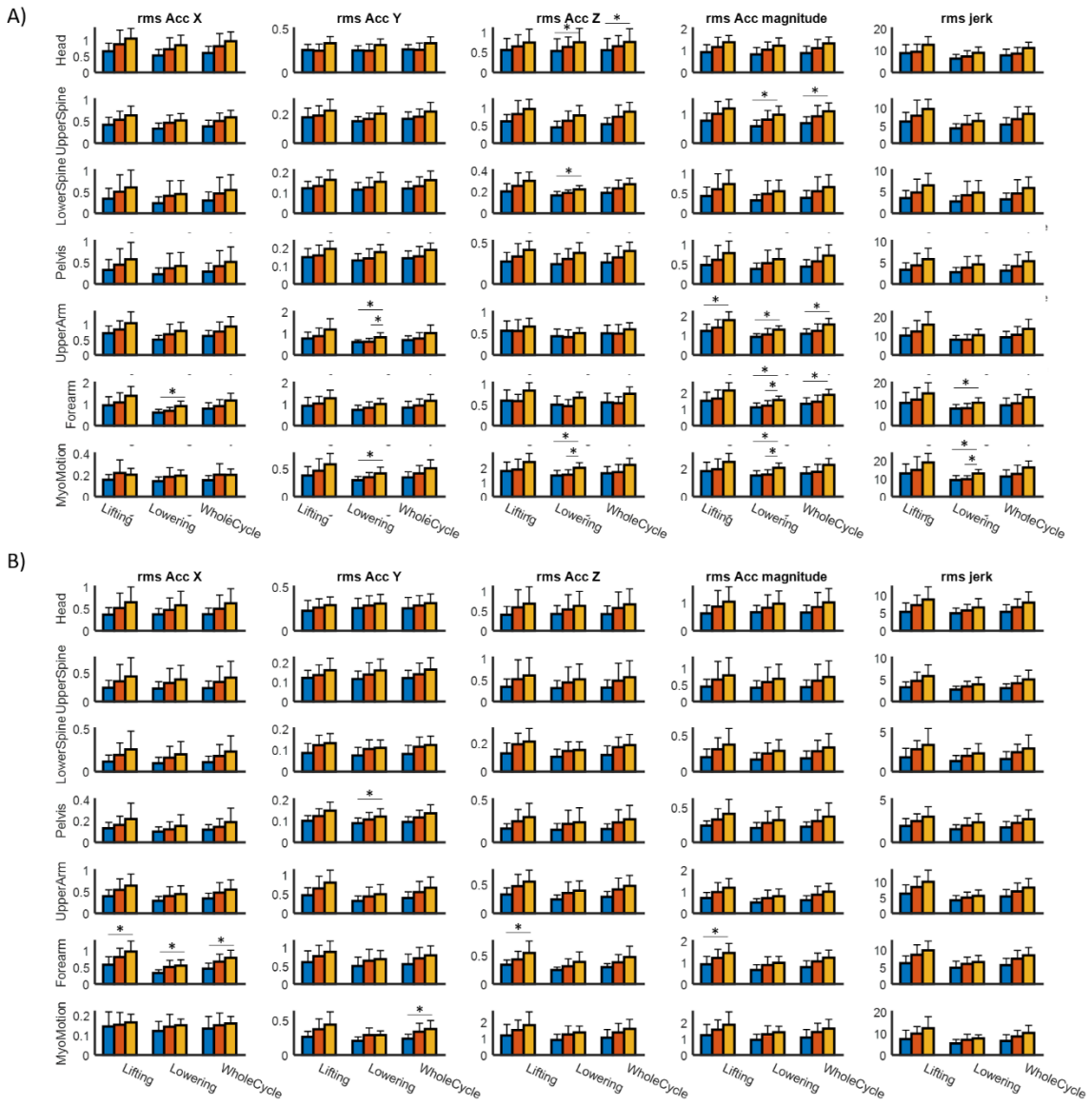

***Figure 5.28**. Mean and standard deviation values of RMS of acceleration and jerk for each IMU and for each LI considering lifting cycles, lowering cycles and whole cycles in HS (A) and in LBP (B).*

5.3.4 Bipolar sEMG

5.3.4.1 Lifting: mean in each minute normalized with the value in the first minute

Time domain features

Since no statistically significant differences were found between the right and left muscles in any of the sEMG features ($p > 0.05$), the following results are referred considering the two side togheter.

Figure 5.29 shows the means and standard deviation values of RMS for HS (A) and LBP (B) of ESL and LD muscles for each LI considering lifting cycles, lowering cycles and whole cycles (lifting+lowering).

Figure 5.29. Mean and standard deviation values of RMS for HS (A) and LBP (B) of ESL and LD for each LI considering lifting cycles, lowering cycles and whole cycles. *statistical significance.

Figure 5.30 shows the means and standard deviation values of RMS for HS (A) and LBPs (B) of RAS and EO muscles for each LI considering lifting cycles, lowering cycles and whole cycles (lifting+lowering).

These values are the mean during each minute normalized by the mean in the 1st minute of lifting task.

Three-way ANOVA showed significant effects of multiple factors on each parameter (RMS, ARV, Max for each muscle and MNF, MDF for ESL and LD) considering LI ($p < 0.05$), on RMS, ARV and Max of ESL and LD considering phase ($p < 0.05$) and on ARV for LD, RAS and EO, Max of ESL and OE, MNF and MDF of LD considering subjects ($p < 0.05$).

The statistical significances of post-hoc analiysis are reported on **Figures 5.29** and **5.30.**

Figure 5.30. *Mean and standard deviation values of RMS for HS (A) and LBP (B) of RAS and EO for each LI considering lifting cycles, lowering cycles and whole cycles. *statistical significance.*

5.3.5 HD sEMG

5.3.5.1 MVC pre and post lifting tasks

RMS, MNF, Entropy, CV RMS, Correlation Coefficient, x and y coordinate of baricenter, CV Torque during 50% of MVC for each LI and for both groups are shown in **Figure 5.31.**

Three-way ANOVA showed no significant effects of multiple factors on each parameter RMS, MNF, Entropy, CV RMS, Correlation Coefficient, x and y coordinate of baricenter, CV Torque considering LI, considering time and subjects ($p > 0.05$).

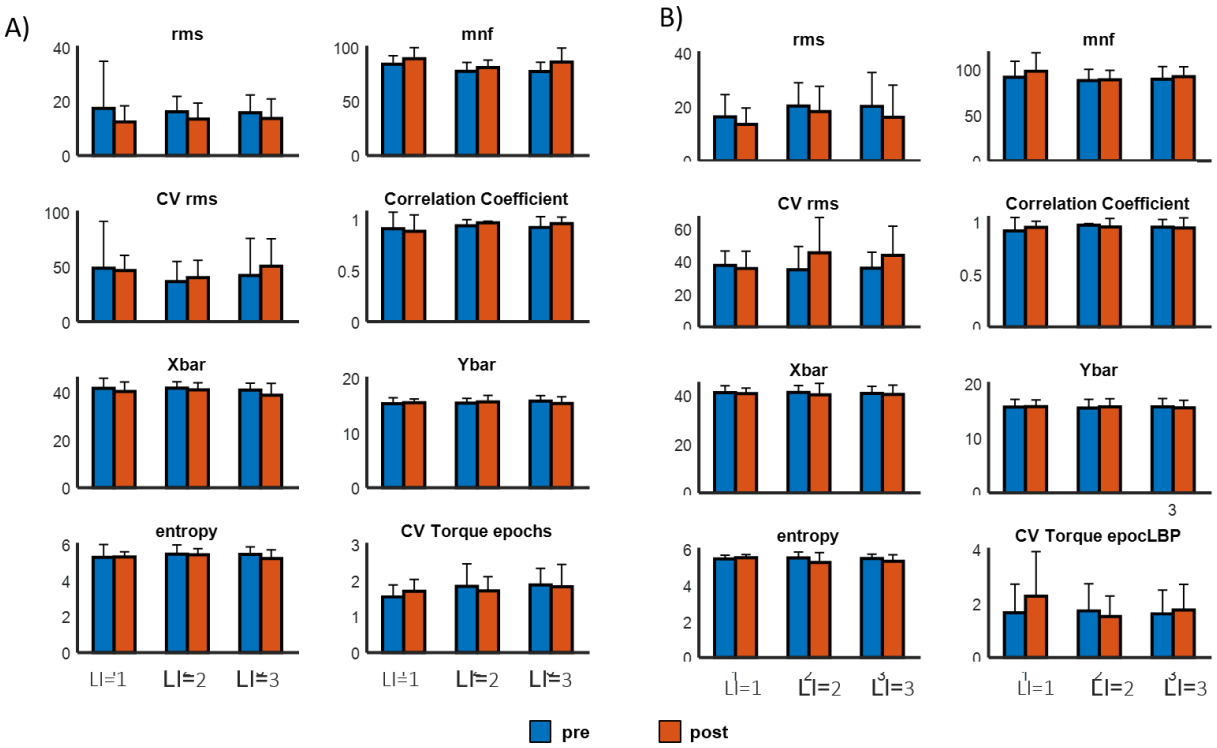

Figure 5.31. HD sEMG parameters for Erector Spinae Muscles in Healty subjects (A) and LBPs (B).

5.4 DISCUSSIONS

The preliminary results of this study show that most of the calculated indexes, both kinematic and sEMG, are significantly affected by changes in LI. Particularly, it is possible to distinguish the lower and higher level of risk (LI=1 and LI=3) while it is not always possible to discriminate the medium level (LI=2) from the other two.

Furthermore, the results show that it is possible to see differences between HS and LBPS considering both kinematic and sEMG parameters.

Regarding LBPs for sEMG analisys it is important take into account that the assessment of MVC is a real issue in this population [32] as patients are less prone to make maximal force exertion due to pain. We tried to encourage the participant to make the maximal possible effort and we repeated two times the execution of each iMVC to consider the maximum effort performed.In the future, the machine-learning techniques (see **Figure 5.32**) will be used to estimate the biomechanical risk in terms of LI starting with kinematic and sEMG features but also to distinguish LBP and HS. This approach could lead to a reliable biomechanical risk classification related to lifting tasks.

Furthermore, considering that there is a gender differences in the prevalence of WMSD [33], further analysis could be done to see if there are any differences in the gender from a biomechanical point of view.

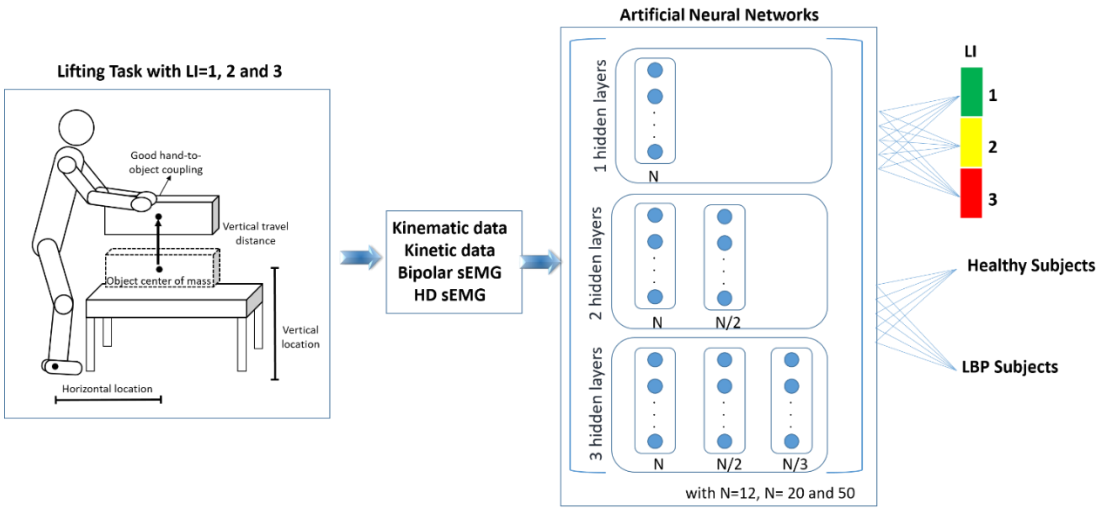

Figure 5.32. *Machine learning approach.*

BIBLIOGRAPHY

1. Waters TR, Putz-Anderson V, Garg A, Fine LJ. 1993. “Revised NIOSH equation for the design and evaluation of manual lifting tasks”. Ergonomics 36 (7), 749e776.
2. Waters TR, Putz-Anderson V, Garg A. 1994. “Applications Manual for the Revised NIOSH Lifting Equation”. U.S. Department of Health and Human Services, Cincinnati, OH.
3. Saunders S, Rath D, Hodges P. 2004. “Postural and respiratory activation of the trunk muscles changes with mode and speed of locomotion”. Gait Posture, 20:280–90.
4. van der Hulst M, Vollenbroek-Hutten M, Rietman J, Schaake L, GroothuisOudshoorn K, Hermens H. 2010. “Back muscle activation patterns in chronic low back pain during walking: a ‘‘guarding’’ hypothesis”. Clin J Pain, 26:30–7.
5. Hodges P, Moseley G, Gabrielsson A, Gandevia S. 2003. “Experimental muscle pain changes feedforward postural responses of the trunk muscles”. Exp Brain Res,151:262–71.
6. Jones S, Henry S, Raasch C, Hitt J, Bunn J. 2012. “Individuals with non-specific low back pain use a trunk stiffening strategy to maintain upright posture”. JElectromyogr Kinesiol, 22:13–20.
7. Falla D, Gizzi L, Tschapek M, et al. 2014. “Reduced task-induced variations in the distribution of activity across back muscle regions in individuals with low back pain”. Pain 155, 944–953.
8. Brazier JE, Harper R, Jones NM, O'Cathain A, Thomas K J, Usherwood T, & Westlake L. 1992. “Validating the SF-36 health survey questionnaire: new outcome measure for primary care”. BMJ, 305(6846), 160-164.
9. Lovibond SH, & Lovibond PF. 1995. “Manual for the depression anxiety stress scales”. Sydney, N.S.W.: Psychology Foundation of Australia.
10. Booth M. 2000. “Assessment of physical activity: An international perspective”. (vol 71, pg 114, 2000). Res Q Exerc Sport, 71(3), 312-312.
11. Osman A, Barrios FX, Kopper BA, Hauptmann W, Jones J, & O'Neill E. 1997. “Factor structure, reliability, and validity of the Pain Catastrophizing Scale”. J Behav Med, 20(6), 589-605.
12. Fairbank JC, & Pynsent PB. 2000. “The Oswestry Disability Index”. Spine (Phila Pa 1976), 25(22), 2940-2952; discussion 2952.
13. Waddell G, Newton M, Henderson I, Somerville D, & Main C J. 1993. “A Fear-Avoidance Beliefs Questionnaire (FABQ) and the role of fear-avoidance beliefs in chronic low back pain and disability.” Pain, 52(2), 157-168.
14. Vlaeyen JW, Kole-Snijders AM, Boeren RG, & van Eek H 1995. “Fear of movement/(re)injury in chronic low back pain and its relation to behavioral performance”. Pain, 62(3), 363-372.
15. Martinez-Valdes E, Laine CM, Falla D, Mayer F, Farina D. 2016. “High-density surface electromyography provides reliable estimates of motor unit behavior”. Clin Neurophysiol., 127(6):2534-41.
16. Nintendo Wii. (2011) Date accessed online: October 19, 2011) http://www.nintendo.com/wii/console/accessories/balanceboard.
17. Barbero M, Merletti R, Rainoldi A. 2012.”Atlas of Muscle Innervation Zones: Understanding Surface Electromyography and Its Applications”, New York, Springer.
18. Hermens HJ, Freriks B, Disselhorst-Klug C, Rau G. 2000. “Development of Recommendations for SEMG Sensors and Sensor Placement Procedures”. J Electromyogr Kinesiol 10 No. 5, 361–374.
19. Sanderson A, Martinez-Valdes E, Heneghan NR, Murillo C, Rushton A, Falla D. “Variation in the spatial distribution of erector spinae activity during a lumbar endurance task in people with low back pain”. J Anat. 2019 Jan 21. doi:10.1111/joa.12935.
20. Fazio P, Granieri G, Casetta I, Cesnik E, Mazzacane S, Caliandro P, Pedrielli F, and Granieri . 2013. “Gait measures with a triaxial accelerometer among patients with neurological impairment,” J. Neurol. Sci., vol. 34, no. 4, pp. 435-440.
21. Butler HL, Newell R, Hubley-Kozey CL, Kozey JW. 2009. “The Interpretation of Abdominal Wall Muscle Recruitment Strategies Change when the Electrocardiogram (ECG) is Removed from the Electromyogram (EMG).” J Electromyogr Kinesiol. 2009; 19(2): 102–113. http://doi:10.1016/j.jelekin.2007.10.004.
22. Batschelet E. 1981. “Circular Statistics in Biology”. Academic.
23. Ranavolo A, Mari S, Conte C, Serrao M, Silvetti A, Iavicoli S, Draicchio F. 2015. “A new muscle co-activation index for biomechanical load evaluation in work activities”. Ergonomics 58 (6), 966e979.
24. Farina D, Merletti R. 2000. “Comparison of algorithms for estimation of EMG variables during voluntary isometric contractions”. J Electromyogr Kinesiol.10(5): 337-349. Review.

25. Merletti R, Knaflitz M, De Luca CJ. 1990. “Myoelectric manifestations of fatigue in voluntary and electrically elicited contractions”. J Appl Physiol 69:1810–20.
26. Madeleine P, Leclerc F, Arendt-Nielsen L, Ravier P, Farina D. 2006. “Experimental muscle pain changes the spatial distribution of upper trapezius muscle activity during sustained contraction”. Clin Neurophysiol, 117(11):2436-45.
27. Falla D, Cescon C, Lindstroem R, et al. 2017. “Muscle pain induces a shift of the spatial distribution of upper trapezius muscle activity during a repetitive task: a mechanism for perpetuation of pain with repetitive activity?” Clin J Pain 33,1006–1013.
28. Abboud J, Nougarou F, Page I, et al. 2014. “Trunk motor variability in patients with non-specific chronic low back pain”. Eur J Appl Physiol 114, 2645–2654.
29. Welch P. 1967. “The use of fast Fourier transform for the estimation of power spectra: a method based on time averaging over short, modified periodograms”. IEEE Transactions on audio and electroacoustics,
30. Farina D, Leclerc F, Arendt-Nielsen L, Buttelli O, Madeleine P. 2008. “The change in spatial distribution of upper trapezius muscle activity is correlated to contraction duration”. J Electromyogr Kinesiol, 18(1):16–25.
31. Watanabe K, Kouzaki M, Merletti R, Fujibayashi M, Moritani T. 2012. “Spatial EMG potential distribution pattern of vastus lateralis muscle during isometric knee extension in young and elderly men”. J Electromyogr Kinesiol. 22(1):74-9. doi: 10.1016/j.jelekin.2011.09.010.
32. van Dieën JH, Selen LP, Cholewicki J. Trunk muscle activation in low-back pain patients, an analysis of the literature. J Electromyogr Kinesiol. 2003 Aug;13(4):333-51.
33. Nordander, C., Ohlsson, K., Balogh, I., Rylander, L., Palsson, B., & Skerfving, S. (1999). Fish processing work: The impact oftwo sex dependent exposure profiles on musculoskeletal health. Occupational and Environmental Medicine, 56, 256-264.

CHAPTER VI

6. BIOMECHANICAL ASSESSMENT IN WORKS ASSOCIATED TO WRNULD

Epidemiological and biomechanical evidence suggest that static neck and shoulder posture or forward head posture, such as that frequently assumed by office workers, as a possible risk factor in work-related neck and upper limb disorders (WRNULD) spread [1]. These disorders are mainly caused by increasing computer use and use of touch screen devices which may be used in various non-traditional workstations and postures [2].

In this chapter, a study on the biomechanics of some activities related to WRNULD is reported.

In this chapter, text and figures have been taken from or adapted from the articles "Comparison of two post office workstation layouts by means of an optoelectronic motion analysis system" [Applied Human Factors and Ergonomics. AHFE 2017*]*, "Analisi Cinematica di una postazione di interfaccia cliente/operatore" [2016, XI Congresso Nazionale SIE Napoli], and "Effect of different smartphone uses on posture while seating and standing" [2018, IEEE International Symposium on Medical Measurements & Applications] which were co-authored by me.

6.1 STUDY N°1: COMPARISON OF TWO POST OFFICE WORKSTATION LAYOUTS BY MEANS OF AN OPTOELECTRONIC MOTION ANALYSIS SYSTEM

Notwithstanding the technological evolution and digitalisation of many operations, which, nowadays, can be carried out through our smartphones, some public services (i.e. banks, post offices, private postal services, public institution help desks, shops, etc.) cannot be completely digitalised. In most cases, customer/operator interfaces have specific short-term functional

requirements for the customer, not taking into account the long-term postural needs of the operators. Excessive digitalisation has also led to a paradox: the amount of equipment has increased at the workstation, thus reducing the already limited availability of space at the traditional workstations. Various guidelines and checklists [3-6] underline the importance of correct positioning for the most frequently used equipment, allowing easy access for the operator. In the services sector (banks, shops, supermarkets, etc.), when designing a workstation, both the movements related to the use of the various equipment (POS, scales, scanners, cash, monitors etc.) as well as the movements related to customer interaction shall be considered. Every modification to a workstation and equipment affects not only the performance, but also the biomechanical risk. Sengupta [7] noted that energy expenditure was closely related to the reach zone breadth (reach envelope).

Several studies have investigated the reach envelope under static conditions but without taking trunk movements into account [7-11]; more recent studies have also considered dynamic conditions [12]. This study aims at comparing two customer/operator interfaces: (1) the operator is sitting in front of the customer; (2) the operator is sitting at a 45° angle to the customer, in line with the monitor and keyboard. For this comparative study, starting with a workstation prototype to analyse, some modifications were suggested, whose efficacy was assessed through a motion analysis system.

6.1.1 Materials and methods

This study focuses on the two most frequent tasks, which appear to be also the most critical ones from a biomechanical point of view: (1) payment of a bill (2) weighing and taking payment for sending a registered letter. For greater ease of analysis, the two tasks were broken down into the following sub-tasks. Task 1 was broken down as follows: (1a) withdrawal of the bill by the customer and put on the scanner; (1b) typing data and picking up the bill from the scanner; (1c) taking the money from the customer and typing in the amount; (1d) getting the change (banknotes and coins) and the bill and returning it to the customer. Task 2 was broken down as follows: (2a) taking the

customer's envelope and placing it on the scales; (2b) picking up and scanning the tracking form and placing it on the printer; (2c) removing the envelope from the scales and inserting/removing it from the franking machine and placing it in the outgoing post box (2d) taking the receipt from the printer, sticking the receipt to the envelope and placing the letter in the outgoing post box.

For each sub-task, the Range of Motions (RoM) for the trunk and the shoulders in three spatial planes (frontal, sagittal, transverse), the elbows extension and the head torsion were calculated. The chair rotation angle, in respect to the table, was also measured.

Analysis of two different working desk types was made:

(1) Front-facing positioning of the operator in respect to the customer, leaving spaces and equipment placement unaltered, as during daily operations, with the original counter.

(2) 45° positioning of the operator in respect to the customer, made possible by the addition of a triangular structure connecting the working desk and a board of extended size on the left side of the operator.

The images below illustrate, respectively, the operator's starting position for front-facing positioning (**Figure 6.1**) and at 45° (**Figure 6.2**) at the modified workstation.

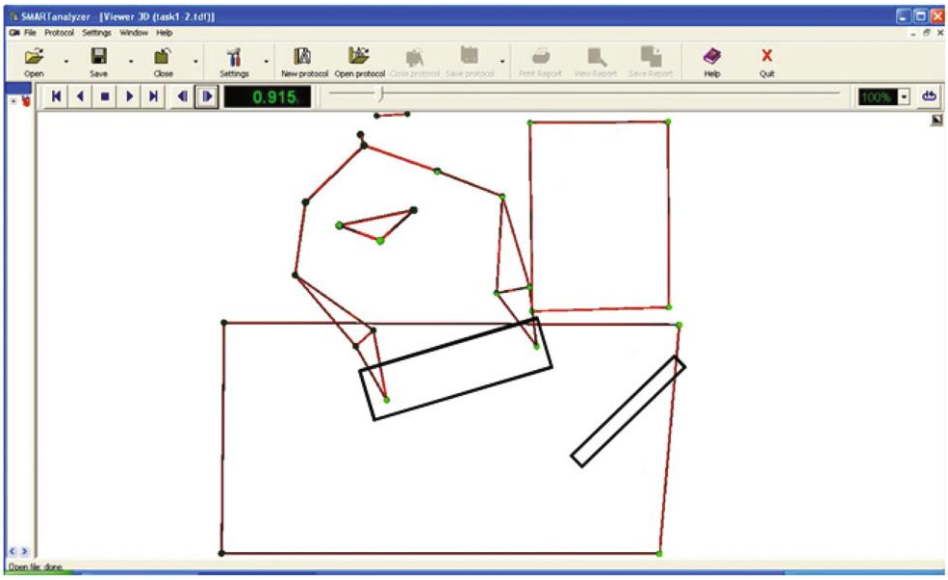

Figure 6.1. *The image shows a kinematic reconstruction of the operator's starting position at the unaltered workstation. The rectangles with a darker border represent the position of the monitor and keyboard (the latter are not to scale).*

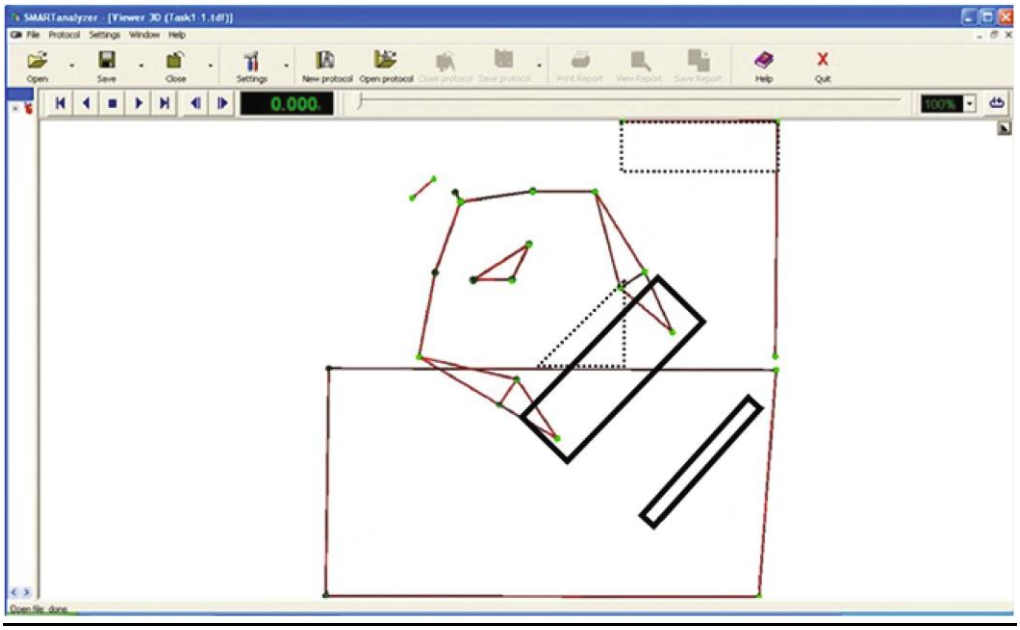

Figure 6.2. *The image shows a reconstruction of the operator's starting position at the modified workstation. For this, the operator is aligned with the keyboard and monitor (the rectangles with the darker borders are not to scale in this reconstruction). The areas with dashed borders represent the modifications made to the workstation addition of a triangular part to align the monitor and keyboard and to allow forearm support together with lengthening the board to allow equipment placement (not to scale in this reconstruction).*

6.1.1.1 Participants

Four workers with more than 5 years of experience in the activity sector participated in the study. Their average age was 49 (±5.2), an average height of 177 cm (±3.9) and average weight of 81 kg (±3.1). None of the participants had ever suffered from musculoskeletal disorders.

6.1.1.2 Equipment

An optoelectronic system for the kinematic motion analysis was used (SMARTDX6000, BTS, Milan, Italy) [13], consisting of eight infrared cameras (sampling frequency 340 Hz), for recognising passive reflective markers coated with aluminium dust and positioned in specific anatomical landmarks in accordance with Rab protocol [14]. Other markers were positioned on the two temporal regions, in the centre of the forehead and on the edges of the chair, in order to investigate trunk and head torsion.

6.1.1.3 Detailed Description of the Analysed Sub-tasks

Bill Payment Task

- Task 1a. Starting with their hands on the keyboard, they take the bill, check the bill, place it on the scanner and return hands to the keyboard;
- Task 1b. Starting with their hands on the keyboard, they type 08081959, two tabs and send to the numeric keypad, wait two seconds, take the bill from the scanner and put it in front of the keyboard, return hands to the keyboard;
- Task 1c. Starting with their hands on the keyboard they take the customer's money, check the money, put the money on the keyboard, type 50, tab and send on the numeric keypad, return hands to keyboard;
- Task 1d. Starting with their hands on the keyboard and the bill in front of the keyboard, take a banknote from the draw to the furthest right, move the banknote to the left, take the change (20 cent more) from the till with the right hand and pass it to the left, take the bill with the right hand, pass the change and the bill to the right, give them back to the customer, return hands to the keyboard.

Registered Letter Acceptance Task.

- Task 2a. Starting with their hands on the keyboard, they take the envelope from the customer with the right hand, pass the envelope to the left hand and place it on the scales, return hands to the keyboard;
- Task 2b. Starting with their hands and the registered letter in front of the keyboard, take the form with their right hand, place the form on the scanner with the right hand and put it in the right hand side of the printer;

- Task 2c. Starting with their hands on the keyboard, take the envelope from on top of the scales with their left hand and put it in the left hand side of the franking machine, take the envelope from the right hand side of the franking machine with the right hand, pass the envelope to the left hand and place it in the box, return hands to the keyboard;
- Task 2d. Starting with their hands on the keyboard, take the return receipt from the printer, detach the return receipt tabs with the right hand, stick the return receipt to the envelope with both hands, take the envelope with the left hand and put it in the box, return hands to the keyboard.

6.1.1.4 Kinematic Analysis

Following a frame by frame reconstruction procedure, to assign each track the respective marker (Smart Tracker, BTS, Milan, Italy), the acquired data was processed using Analyzer software (Smart Analyzer, BTS, Milan, Italy).

The movement always started from the same position (sitting in front of the customer in position 1 in front of the monitor in position 2). The RoMs were calculated for: trunk torsion, flexion and lateral bending; abduction, horizontal abdo-adduction and flexion-extension of the shoulders; elbow extension and head torsion. The chair rotation angle, in respect to the table, was also measured. The kinematic signals were finally processed using a low pass filter with 5 Hz frequency. Five tests were carried out on each sub-task.

6.1.1.5 Statistical Analysis

The statistical analysis was performed using SPSS 17.0 software (SPSS Inc., Chicago, IL, USA). For each RoM, the average and standard deviation were calculated, to which the Student t-test was applied for paired data. P-values lower than 0.05 ($p < 0.05$) were considered statistically significant.

6.1.2 Results

Below are the results of the kinematic analysis of each investigated subtask, were a statistically significant difference was reported ($p < 0.05$).

Task 1a: complete torsion (trunk + head) remained essentially unaltered (about 37° overall), but differently distributed. The modified workstation allowed for minor torsion of the trunk (10.5° Vs 22.6°), but higher torsion of the head (27.5° Vs 14.9°). The modified workstation allowed for a reduced RoM value for the right shoulder in all three of the spatial planes: abduction (41.8° Vs 54.1°), horizontal abdo-adduction (28.4° Vs 33.2°) and flexion-extension (55.1° Vs 61.8°). Moreover, at the modified workstation the trunk torsion and lateral bending values were lower (17.4° Vs 24.6°), (26.7° Vs 37.4°).

Task 1b: The modified workstation allowed for reduced rotation of both the trunk (value of 11.1° Vs 17.2°) and head (7.9° Vs 12.9°). Statistically significant reductions were also noted in flexion (4.8° Vs 13.7°) and lateral bending (11.2° Vs 31.6°), in the right shoulder (39.9° Vs 59.2°) and the left shoulder (10.6° Vs 14.5°) flexion, abduction of the right shoulder (33.5° Vs 49.9°), horizontal abdo-adduction of the right shoulder (26.7° Vs 38.6°) and left shoulder (9.1° Vs 19°) and left elbow extension (20.1° Vs 25.6°). Finally, the modified position allowed for reduced chair rotation (value of 2.2° Vs 6.6°).

Task 1c: This task was almost exclusively carried out with the operator's right arm. Overall, the modified workstation showed high rotation values (trunk and head) in comparison to the original position (33.2° Vs 27.5°). Similarly, to what reported for task 1a, in this task the operators adopted a different motor strategy when rotating. In fact, the modified workstation showed lower values of trunk torsion (6.9° Vs 11°), but higher head torsion values (26.3° Vs 16.5°). The modified workstation also showed lower values for trunk flexion (4.8° Vs 13.7°) and trunk lateral bending (11.2° Vs

31.6°), right shoulder flexion (38.1° Vs 50.4°), right elbow extension (63.4° Vs 93°), right shoulder abduction (33.5° Vs 49.9°) and finally, right shoulder horizontal abdo-adduction (26.7° Vs 38.6). For this task, chair rotation was lower in the unaltered workstation (1.8° Vs 5.3°).

Task 1d: This task actively involved both upper limbs. Here, the modified workstation showed higher chair rotation values (18.6° Vs 15.4°) but lower overall torsion values for body parts, both for the trunk (21.6° Vs 33.8°), and the head (26.7° Vs 34.9°). The changed position showed reduced RoM and reduced abduction values for both shoulders (right 47.5° Vs 62.3° and left 7.9° Vs 12.9°), reduced horizontal abdo-adduction for the right shoulder (43.2° Vs 61.7°) and left elbow extension (39.2° Vs 52.3°). A significant reduction was also reported, although not statistically significant, of the extension of both elbows. Flexion and trunk lateral bending remained substantially unchanged.

Task 2a: the task in the modified workstation showed a statistically significant reduction in head torsion (27.8° Vs 33.5°), extension of both elbows (right 56.6° Vs 83.3°; left 47.1° Vs 62.7°), right shoulder flexion (31.7° Vs 50.8°) and horizontal abdo-adduction of the right shoulder (23.7° Vs 46.9°). The unaltered workstation showed lower statistically significant values of left shoulder abduction (30.5° Vs 41.3°). The modifications made to the workstation did not lead to statistically significant differences in the RoMs related to trunk, in any of the three spatial planes for this task.

Task 2b: Contrary to those previously described, this task was carried out entirely on the right side of the operator. The modifications introduced produced an overall increase in rotation (48.9° Vs 42°) trunk torsion was reduced in the modified workstation (9.9° Vs 29.3°), but head rotation was significantly increased (39.1° Vs 12.7°).

In this task, chair rotation was reduced in the modified workstation, although slightly, (4.3° Vs 7.7°). The modified workstation also showed higher RoM values for the operator's right side, in particularly for elbow extension (84.8° Vs 58.6°), shoulder flexion (69.1° Vs 48.2°) and shoulder

abduction (43.9° Vs 20.2°). However, the modified workstation showed reduced RoM values for horizontal abdo-adduction of

the right shoulder (46° Vs 61.8°).

Task 2c: This task was carried out exclusively on the operator's left side. The modified workstation showed lower values for chair rotation (32.2° Vs 50.2°), trunk rotation (16.2° Vs 21.5°) and trunk lateral bending (35.2° Vs 54.5°) and right elbow extension (51.7° Vs 60.9°). However, the modified workstation showed higher values of flexion for shoulders (right 39.6° Vs 28°; left 60.8° Vs 38.8°), left shoulder abduction (44.2° Vs 34.9°) and left elbow extension (70.6° Vs 63°).

Task 2d: In this task – unlike all the abovementioned tasks – the operator moved on both sides of the workstation. The modified workstation showed high RoM values with regards to trunk torsion (23.1° Vs 16.4°) and left shoulder flexion (35.4° Vs 26.8°), but reduced RoM values for chair rotation (18.1° Vs 39.3°), trunk lateral bending (30.5° Vs 50°), left shoulder abduction (12.5° Vs 19°) and horizontal adduction of the right shoulder (26° Vs 35.7°). The modified workstation showed higher values, although not statistically significant, in terms of extension for both elbows (right 63.7° Vs 57.2°; left 72.2° Vs 69°).

Tables 6.1, 6.2, 6.3, 6.4, 6.5 and 6.6 summarise the abovementioned results, along with relevant statistical analysis (statistically significant differences $p < 0.05$ are reported in bold) for chair rotation and for each movement under investigation.

Task	Chair rotation		
	Front facing	45°	p
1a	4.2 ± 0.9	4.3 ± 0.9	0.807
1b	6.6 ± 1.9	2.2 ± 0.4	**<0.001**
1c	1.8 ± 0.4	5.3 ± 3.7	**0.008**
1d	15.4 ± 4.2	18.6 ± 1.6	**0.037**
2a	3.8 ± 2.8	3.1 ± 0.8	0.457
2b	7.7 ± 2	4.3 ± 2.1	**0.002**
2c	50.2 ± 8.7	32.2 ± 7.8	**0.001**
2d	39.3 ± 8	18.1 ± 6.2	**<0.001**

Table 6.1. *The table shows the average chair rotation (±SD) achieved relating to the desk and the relevant statistical analysis for each of the eight sub-tasks analysed.*

Task	Head torsion		
	Front facing	45°	p
1a	14.9 ± 1.2	27.5 ± 2.7	**<0.001**
1b	12.9 ± 1.8	7.9 ± 1.4	**<0.001**
1c	16.5 ± 2.2	26.3 ± 2.6	**<0.001**
1d	34.9 ± 3.2	26.7 ± 8.7	**0.012**
2a	33.5 ± 2.9	27.8 ± 2.2	**<0.001**
2b	12.7 ± 1	39 ± 1.1	**<0.001**
2c	41.3 ± 3.7	41.7 ± 3.1	0.796
2d	41 ± 13.1	42.8 ± 2.1	0.673

Table 6.2. *The table shows the average RoMs (±SD) achieved for head torsion and the relevant statistical analysis for each of the eight sub-tasks analysed.*

Task	Trunk flexion			Trunk lateral bending			Trunk torsion		
	Front facing	45°	p	Front facing	45°	p	Front facing	45°	p
1a	24.6 ± 3.5	17.4 ± 3.3	**<0.001**	37.4 ± 2.1	26.7 ± 4.4	**<0.001**	22.6 ± 1.5	10.5 ± 1.3	**<0.001**
1b	13.7 ± 4.7	4.8 ± 0.9	**<0.001**	31.6 ± 2.8	11.2 ± 2.7	**<0.001**	17.2 ± 2.7	11.1 ± 1.1	**<0.001**
1c	22.3 ± 3.7	15.9 ± 1.8	**<0.001**	31.6 ± 6.1	22.2 ± 2.7	**<0.001**	11 ± 1.9	6.9 ± 1.7	**<0.001**
1d	29 ± 3.3	27.7 ± 10.4	0.711	34.5 ± 2.6	28.3 ± 10	0.0074	33.8 ± 2.8	21.6 ± 7.3	**<0.001**
2a	19.2 ± 2.7	19.8 ± 3.2	0.656	31.2 ± 2.5	31.4 ± 3	0.873	11.3 ± 1.8	10.1 ± 1.8	0.153
2b	8.5 ± 1.8	7.2 ± 3.3	0.289	17.4 ± 2.7	17.5 ± 4.2	0.950	29.3 ± 1.5	9.9 ± 1.1	**<0.001**
2c	35.4 ± 4.1	32.6 ± 5.8	0.229	54.5 ± 5.5	35.2 ± 3.4	**<0.001**	21.5 ± 1.5	16.2 ± 3.4	**<0.001**
2d	25.8 ± 8.6	19.9 ± 4.6	0.072	50 ± 14.7	30.5 ± 5.5	**0.001**	16.4 ± 5.3	23.1 ± 2.4	**0.002**

Table 6.3. *The table shows the average RoMs (±SD) achieved for the three spatial planes of the trunk and the relevant statistical analysis for each of the eight sub-tasks analysed.*

Task	Trunk flexion			Trunk lateral bending			Trunk torsion		
	Front facing	45°	p	Front facing	45°	p	Front facing	45°	p
1a	54.1 ± 2.2	41.8 ± 2.8	**<0.001**	33.2 ± 4.5	28.4 ± 2.8	**0.010**	61.8 ± 3.8	55.1 ± 14.7	**0.003**
1b	49.9 ± 4.4	33.5 ± 2.1	**<0.001**	38.6 ± 5	26.7 ± 2.6	**<0.001**	59.2 ± 4	39.9 ± 2.9	**<0.001**
1c	48 ± 2.9	32.7 ± 3.1	**<0.001**	23.1 ± 5.4	17.5 ± 2.5	**0.008**	50.4 ± 3.8	38.1 ± 5.2	**<0.001**
1d	62.3 ± 3.3	47.5 ± 16.1	**0.011**	61.7 ± 4.8	43.2 ± 14.7	**0.001**	47.8 ± 2.6	46.5 ± 15.7	0.799
2a	37.5 ± 5.8	34 ± 4.3	0.143	46.9 ± 6.3	23.7 ± 4.5	**<0.001**	50.8 ± 4.1	31.7 ± 2.8	**<0.001**
2b	20.2 ± 2.8	43.9 ± 2.6	**<0.001**	61.8 ± 3.3	46 ± 3.3	**<0.001**	48.2 ± 2.5	69.1 ± 2	**<0.001**
2c	14.8 ± 2.3	16.2 ± 4.7	0.409	44 ± 4.9	46.1 ± 8.7	0.514	28 ± 3	39.6 ± 5.5	**<0.001**
2d	20.5 ± 6.5	21.3 ± 2.8	0.725	35.7 ± 9.6	26 ± 4.4	**0.009**	24.6 ± 6.8	26.7 ± 3	0.383

Table 6.4. *The table shows the average RoMs (±SD) achieved for the three spatial planes of right (R) shoulder and the relevant statistical analysis for each of the eight sub-tasks analysed.*

Task	L shoulder abduction			L shoulder horizontal abdadduction			L shoulderflexion		
	Front facing	45°	p	Front facing	45°	p	Front facing	45°	p
1a	7.6 ± 1.6	12.4 ± 2.7	**<0.001**	25.8 ± 6.2	21.8 ± 6	0.159	14.4 ± 3.5	16.7 ± 3.9	0.182
1b	7.3 ± 4	7.6 ± 1	0.879	19 ± 3.5	9.1 ± 1.2	**<0.001**	14.5 ± 2.8	10.6 ± 1.3	**0.001**
1c	9.5 ± 2.1	12.5 ± 3.3	**0.026**	19.1 ± 3.4	20.3 ± 3.2	0.427	17.4 ± 3	25.8 ± 3.5	**<0.001**
1d	12.9 ± 3.2	7.9 ± 2.8	**0.002**	50.9 ± 2.8	42.2 ± 14.3	0.075	33.9 ± 3	28.4 ± 9.9	0.110
2a	30.5 ± 11.2	41.3 ± 4.5	**0.011**	42.5 ± 17.6	36.4 ± 4	0.299	25.1 ± 9.9	27.6 ± 2.4	0.448
2b	10.6 ± 1.9	5.5 ±1.2	**<0.001**	20.8 ± 1.2	17.4 ± 5.3	0.063	11.4 ± 2.1	11.3 ± 5.4	0.957
2c	34.9 ± 3.8	44.2 ± 2.9	**<0.001**	49.3 ± 3.1	49.5 ± 4.2	0.905	38.8 ± 6	60.8 ± 6.9	**<0.001**
2d	19 ± 7.1	12.5 ± 1.7	**0.012**	39.5 ± 11	46.9 ± 2.8	0.054	26.8 ± 8.1	35.4 ± 4.7	**0.009**

Table 6.5. *The table shows the average RoMs (±SD) achieved for the three spatial planes of left (L) shoulder and the relevant statistical analysis for each of the eight sub-tasks analysed.*

Task	R Elbow Extension			L Elbow Extension		
	Front facing	45°	P	Front facing	45°	p
1a	94.9 ± 6.8	94.8 ± 6.9	0.974	36.3 ± 5.7	32 ± 3.4	0.055
1b	69.1 ± 5	68.9 ± 4.9	0.929	25.6 ± 6.2	20.1 ± 3	**0.021**
1c	93 ± 2.3	63.4 ± 3.5	**<0.001**	35.8 ± 4.1	27.8 ± 3.5	**<0.001**
1d	109.7 ± 7.7	103 ± 34.6	0.558	52.3 ± 7.9	39.2 ± 13.5	**0.016**
2a	83.3 ± 6.4	56.6 ± 11.4	**<0.001**	62.7 ± 10.8	47.1 ± 5.5	**<0.001**
2b	58.6 ± 3.8	84.8 ± 3.2	**<0.001**	22.4 ± 4.7	17.5 ± 5.8	0.053
2c	6.9 ± 7.6	51.7 ± 5.2	**0.005**	63 ± 2.6	70.6 ± 6.9	**0.004**
2d	57.2 ± 17	63.7 ± 5.1	0.262	69 ± 22.8	72.2 ± 9	0.685

Table 6.6. *The table shows the average RoMs (± SD) achieved for extension of both of the elbows and the relevant statistical analysis for each of the eight sub-tasks analysed.*

6.1.3 Discussions and conclusions

The changes made to the workstation, especially the introduction of a connecting board allowing for the alignment of the operator with the monitor and keyboard, appeared to bring improvement in the sub-tasks 1a, 1b, 1c 1d and 2a, which is in those where the operator carried out operations mainly in the central and left side of the workstation and involved interaction with customers. According to the data provided to us, these tasks are among those most frequently performed by operators. In particular, the RoMs for lateral bending and flexion were reduced, while as regards rotation, it was noticed that the workers adopted a different motor strategy, which provided for a broader movement of the head rather than the trunk. This change appeared to lead to a worsening in the case of sub-tasks 2b and 2c. In fact, in sub-task 2b, the re-design intervention moved the operator further away from the right side of the workstation, where the printer was located, thus leading to an increase of ROMs for elbow extension, as well as for right shoulder flexion

and abduction. Nevertheless, according to the data provided to us, this subtask resulted in being the least frequent among those actually performed. Meanwhile, in subtask 2 the change lead to a worsening for upper limb movements, in that the operator, in order to place the envelope on the scales/franking machine, had to raise their shoulder and extend their elbow further because of the machine overall size. However, the alteration involved improvements to the transverse plane resulting in reduced chair rotation and reduced trunk torsion. The modifications to the workstation in sub-task 2d, the only one involving actions performed on both sides of the operator, resulted in advantages and disadvantages. In fact, the RoM values were reduced in regard to trunk lateral bending, left shoulder abduction and right shoulder horizontal abdo-adduction, but were greater for trunk torsion and right shoulder flexion. However, the increase in trunk torsion by 6.7° was largely offset by the reduction in chair rotation by 21.2°.

The activities carried out in the laboratory showed the need to remove the solid metal footrest fixed and permanently joint to the counter because it interfered with the base of the operator's chair.

As a conclusion, the change in the working desk, made with the introduction of a board joined to the original straight working desk, allowed the operator to align with the monitor and keyboard as well as providing adequate support for the forearms while typing, that, according to published data [15], also allowed for muscle engagement reduction while typing on the keyboard. The change appeared to bring improvement for most of the sub-tasks investigated, both in terms of trunk torsion and lateral bending, as well as in terms of interaction with the equipment located on the left side of the workstation. The flexion-extensions were also reduced in both upper limbs and trunk during customer interaction. Conversely, the change appeared to lead to worsening, when the operator worked on the right side of their workstation.

To reduce overall head and trunk rotation, it would be appropriate to provide the operator with a seating that allows the operator to rotate the seating plan rather than their trunk and/or head.

Furthermore, it would be useful to provide a chair that allows for an easy transition between sitting and standing positions. This is in view of the fact that, from the information supplied to us, when working at the counter the operator often stands up (for example, taking forms from the cabinets, photocopying, picking up/consulting documents, processing manager requests, etc.) and moves therefore from sitting position.

Finally, it would be appropriate to provide the workstation with devices that are less cumbersome as possible, to allow them to be better distributed on the working desk.

This arrangement would lead to a better interaction of the worker with the equipment and would allow for a greater availability of space, thus providing a more correct positioning of the operator at the workstation.

One limitation of this study is the presence of a very small sample: only four participants took part in the experiments. To strength the obtained results more analysis should be done.

6.2 STUDY N°2: EFFECT OF DIFFERENT MOBILE DEVICE USES ON POSTURE WHILE SEATING AND STANDING

In the last twenty years the use of mobile handheld devices, including touchscreen smartphone, tablet and keypad phones, has grown exponentially, for both adolescents and adults. Recent surveys have shown that the users spend approximately more than three hours daily [16] on their mobile device to text, read e-mail, surf the internet and game (excluding voice activities). These data are expected to continue to increase in the next years showing an important social change: due to their portability and simplicity of use, these devices are recently introduced in education, in healthcare and in various working environments.

The effect of an intensive and daily use of mobile hand-held devices – smartphones and tablets, in particular – on one's health is still a matter of research: while several reviews [17-18] have deeply investigated the association between electromagnetics field exposure and some non-specific

symptoms such as fatigue, sleep disturbance, headache and earache, few studies have targeted the relationship between the daily use of smartphones and modifications to motor outcomes (such as alterations of gait patterns while walking [19]); in particular, posture taken during touch-screen device use has been investigated, and the potential associated risks to develop musculoskeletal complaints and disorders [20-21]. Moreover, since children extensively use digital devices, the topic regarding possible alterations to the development of motor and stance control mechanisms [22-24] is worth being investigated.

Most studies in this research area make use of questionnaires to evaluate self-reported pain, discomfort at the neck, at the shoulder and at the upper extremity and muscle fatigue. Among these, Berolo et al. [16] used a questionnaire to collect some self-reported measures of smartphone use and symptoms of pain on a population of university students and observed a relationship between the use of a mobile device and some symptoms of the upper extremity and neck. Hakala et al. [25] found that the use of the smartphone for more than five hours daily was associated with neck-shoulders pain, while the effect of sustained static postures and repetitive movements of the finger has been investigated by Barr et al. [26]. Xie and colleagues [27] showed that the participants felt a neck discomfort after using a smartphone for more than ten minutes when they were sitting.

While several studies have been based on kinematic analysis of some tasks to deal with a functional assessment (see for example [28]), the musculoskeletal exposure of head and trunk districts has been rarely studied through mathematical models or laboratory measurements (e.g. motion analysis systems, electro-goniometers): Hansraj [29] developed a mathematical model to simulate the effect of the neck tilt on the cervical spine, and showed that the equivalent weight suffered by the spine depends on the neck angle, so becoming a potential cause of cervical pathology. Lee et al. [30], evaluated head flexion during common smartphone tasks showing that the messaging produced the highest effect on the neck tilt. Guan et al. [31] investigated gender differences in the

cervical posture when using mobile phone. Ning et al. [32] explored the kinematics of the cervical spine while typing and showed a high level of risk to develop neck pain. Other experimental studies have also shown the postural difference between natural standing and the posture assumed while focussing upon the smartphone. Only one study analysed head flexion while using a smartphone in sitting compared to standing [33] and indecisive results have been found about the effect of the task on the neck and trunk posture.

The limited evidence regarding the relationship between mobile handheld device and musculoskeletal symptoms and exposures, due to few studies, does not permit the development of clinical management and ergonomics guidelines to facilitate prevention strategies. In this context, the present research main purpose is to assess, through laboratory sessions, the alteration of neck and trunk postures during smartphone use.

6.2.1 Materials and methods

6.2.1.1 Participants

Fifteen healthy subjects aged between 21 and 25 years were recruited in this study (height: 1.68 ± 0.5 m, weight: 71± 4.2 kg). The subjects had no history of musculoskeletal disorders and they have been using the smartphone for at least 6 years. All participants provided informed written consent before taking part in the study, which complied with the Helsinki Declaration and had local ethics committee approval (Ethics Committee of the Applied Electronics Section of the Department of Engineering).

6.2.1.2 Experimental set-up and procedure

An optoelectronic motion analysis system (SMART-DX 6000 System, BTS, Milan, Italy) consisting of eight infrared cameras (sampling frequency 250 Hz) was used to track the movements of four spherical markers (15 mm in diameter) covered with aluminum powder reflective material, placed over prominent anatomical bony landmarks according to the International Society of Biomechanics

recommendations [34]. The markers were attached using double-adhesive tape in such a way as to prevent them from falling out of place during the test. In detail, the markers were placed over the cutaneous projections of the spinous processes of the seventh cervical vertebra (C7), sacrum, right cyclops and right tragus (see **Figure 6.3**).

A calibration procedure was executed before the first data capture was performed. Spatial accuracy in the reconstruction of the markers 3-D position was 0.2 mm in the x, y and z dimensions. A global reference system was adopted in accordance with [34].

Before formal measurements were started, each subject answered a questionnaire concerning both demographic and anthropometric data and to assess the daily use of the smartphone. In particular, it has been requested: 'On average, how long do you use a smartphone daily? (less than 3 h; between 3 and 4 h; more than 4 h)'; 'Sort the activities carried out with the smartphone in order of frequency use from 1 to 4 (Messaging, Surfing, Gaming, Watching Video)'.

Participants were instructed as follows: they were asked to use the smartphone in a natural way performing a set of activities with the smartphone. All the subjects were right-handed and used their own smartphone with their right hand. The same device was used for the all the experimental sessions. Thus, all the required applications were already installed on the smartphone, and were well known by the subjects, thus no familiarization for the activities was needed. The following activities were administered randomly, and they were performed both while standing and while seating:

1. maintain posture in static conditions with no additional concurrent activities (*Baseline*)
2. use an instant messaging app (WhatsApp), answering to general knowledge questions asked by the experimenter (*Messaging*)
3. surf on a specific page of a social network *(Surfing*)
4. play a game on the smartphone (*Gaming*)

5. watch a video (*Video watching*)

Baseline tasks lasted 30 seconds, while the other tasks lasted 120 seconds. To avoid muscle fatigue, the tasks were separated by 1-min rest periods. After the end of the experiment, each subject was asked if he/she feelt neck and/or shoulder pain during the experiment.

6.2.1.3 Data acquisition and processing

After each acquisition performed by Smart Capture (BTS, Milan, Italy), three-dimensional marker trajectories were reconstructed using a frame-by-frame tracking system and a label to each marker was assigned. Data were processed using SMART Analyzer software and Matlab software. After a low pass filtering at 10 Hz of kinematic data, the following angles were extracted:

- Neck flexion-extension angle (NA): angle between the horizontal plane passing through the marker placed on the seventh cervical vertebra subtended to the horizontal and the straight line passing through the markers placed in the seventh cervical vertebra and in correspondence with the tragus
- Cranio-cervical angle (CCA): angle between the vector passing through the markers placed on the Tragus and on the Cyclops and the vector pointing from Tragus and C7.
- Trunk angle (TA): angle between the line passing through the markers placed on the seventh cervical vertebra and on the sacrum and the vertical (Y) coordinate of the laboratory reference system

For each condition and trial, the average value of each angle was computed; the percentage variation with respect to the baseline condition was calculated as in the following:

$$angle\_\mathrm{var}\% = 100 \times \frac{Angle_{baseline} - Angle_{activity}}{Angle_{baseline}} \quad (1)$$

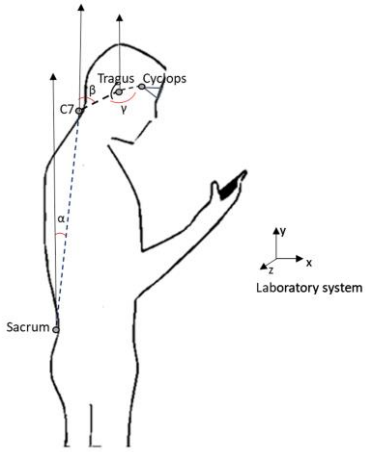

Figure 6.3. *Markers placements: Sacrum, C7, Tragus and Cyclops. Kinematics angles: α (trunk angle), β (neck angle), γ (cranio-cervical angle)*

6.2.1.4 Statistical analysis

Descriptive statistics were calculated for all the extracted parameters. To verify the normal distribution of data Kolmogorov-Smirnov test was done. All the parameters were then considered separately as dependent variables for a two-way ANOVA test considering Activity (Gaming, Messaging, Surfing, Video Watching) and Posture (Seat, Stand) as main factors and their interaction (Activity x Posture). Post-hoc analyses (with Bonferroni's corrections) were performed when significant differences were found. The level of significance was set at $p<0.05$.

6.2.2 Results

Results obtained from statistical analysis showed an overall significant effect of the Activity ($p=0.007$, $F=4.25$) only for the NA%, while no difference was found for CCA% and TA%. Instead an overall effect was found for the Posture in all the parameters (NA% $p<0.001$, $F=51.1$; CCA% $p<0.001$, $F=21.52$; TA% $p<0.001$, $F=59.71$). No significant effect was found for interaction between Posture and Activity factor for NA%, CCA% and TA% ($p>0.05$).

The post hoc analysis on NA% has shown a significant difference in Gaming vs Messaging ($p=0.02$, $F=6.52$), Gaming vs Video_Watching ($p=0.008$, $F=9.56$) and Surfing vs Video_Watching ($p=0.007$

F=9.76) during Stand. Instead during Seat a significant difference was found in Gaming vs Video_Watching ($p<0.001$, F=27.31) and Messaging vs Video_Watching ($p=0.03$, F=6.1).

As it is shown in **Figure 6.4**, in both postures, the percentage variation of the neck angle with respect to the baseline condition is greater when an activity with a major cognitive load is performed (Gaming vs Video_Watching).

The statistical analysis showed significant differences in NA% between the postures for all the activities. In particular: Gaming ($p=0.005$, F=10.28), Messaging ($p=0.003$, F=12.09), Surfing ($p=0.04$, F=4.73), Video Watching ($p=0.003$, F=12.4). For all activities, NA% is greater when the subjects are seated than when they are standing (See **Figure 6.4**).

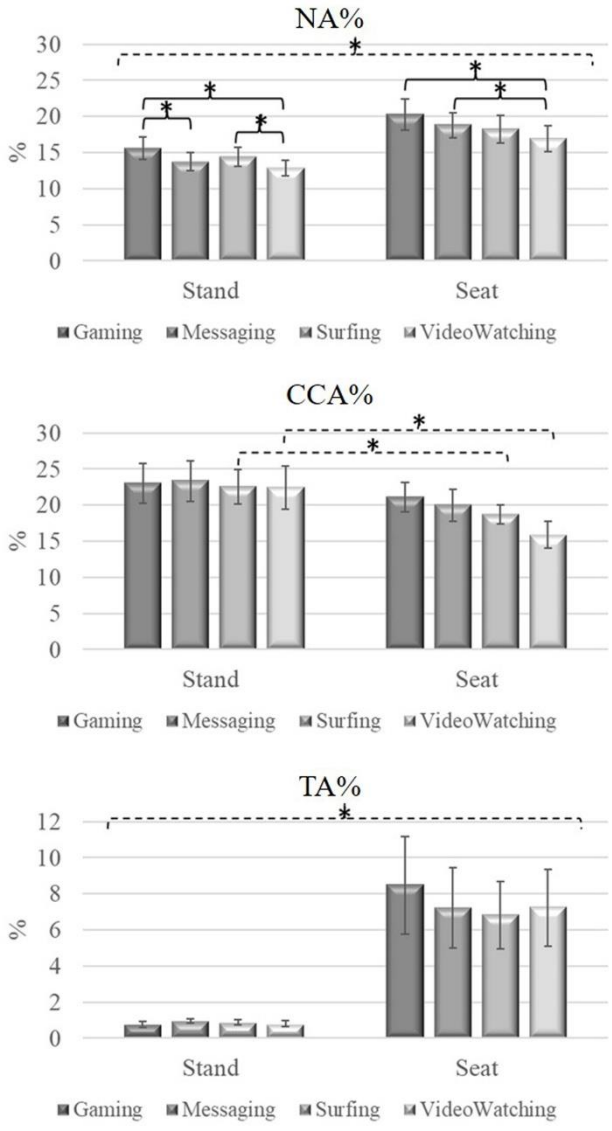

Figure 6.4. *Mean±standard error of the angle_var with respect to the baseline condition is shown for each activity in both posture condition. Significance is reported as *(p<0.05). In Neck_angle_var and Trunk_angle_var --* indicates significance difference among all activities.*

For CCA% a significant difference is shown only for Surfing (p=0.03, F=5.25) and Video Watching (p=0.004, F=11.64). Instead, for TA% a significant difference is showed for all the activities: Gaming (p=0.01, F=8.22), Messaging (p=0.01, F=8.28), Surfing (p=0.007, F=9.94) and Video_Watching (p=0.008, F=9.48) showed a significant increase of the mean values when the activities were performed while sitting (See **Figure 6.4**).

Results of the questionnaire highlighted that two thirds of the sample use the smartphone for more than 3 hours in a day; all participants chose messaging as the most performed activity during the day, and the majority of them reported neck pain during the experiment. The details of the answers are given in **Table 6.7**.

Hours of daily use				
< 3h		***>3h ^ <4h***		***>4h***
33.3%		40%		26.7%
Scores	**Activity preference**			
	Gaming	***Messaging***	***Surfing***	***Video Watching***
I	———	100%	———	———
II	20%	———	53.3%	26.6%
III	———	———	———	53.4%
IV	80%	———	46.7%	20%
Neck and/or shoulder pain during experiment				
Yes		***No***		
66.7 %		33.3%		

Table 6.7. *Summary of questionnaire answers.*

6.2.3 Discussions and conclusions

The goal of this study was to evaluate the effect of smartphone use on neck and trunk kinematics, considering four different daily activities performed both standing and sitting.

With respect to the neutral condition, the percentage of variation of neck and trunk posture varied significantly between the two different postures (Stand, Seat). A clear increase of the neck and trunk angles when the subjects used the smartphone in a sitting position regardless of the performed activities was reported: in particular, with respect to standing, while sitting the percentage variation of both neck and trunk angles increased in average by 4.6% and 6.6% respectively. This evidence could depend on the incorrect posture taken by the subjects when using the smartphone while sitting: in fact, all of them tended to bend the trunk forward by resting their elbows on their knees. Instead, cranio-cervical angle varied slightly only during surfing and video watching, with a decrease of the angle value when sitting. This angle appears to be only partially influenced by the activities performed and by the posture taken during smartphone use.

If on the one hand both trunk and neck angles are influenced by the posture taken by the participants, on the other one only the neck angle is influenced by the performed activity: among the four activities, gaming caused the largest neck flexion (15.6% stand, 20.3% seat), and video watching caused the smallest one in both standing and sitting. The analysis suggests that an activity involving subject's attention affects the neck kinematics more than a passive activity, like watching a video.

From the administered questionnaire, it emerged that the messaging activity is the activity most frequently carried out during daily life. Lee at al. [30] have shown that text messaging could cause neck pain symptoms in heavy smartphone users. By looking at our results, it comes to light that when the subjects stand, neck angle variations are comparable with those while watching videos and surfing, while when they seat, the values are significantly higher. This evidence could suggest that the alteration of the neck angle during text messaging may not primarily depend on the performed activity but rather on the posture conditions.

In this research almost 40% of the participants use the smartphone for more than three hours in a day, and at the end of the experimental session the 66.7% of the participants felt neck pain. This could be interpreted as follows: a) the prolonged use of the smartphone alters the kinematics of the neck and of the trunk; b) the performed activity influences the neck posture: in particular, the activities with a greater cognitive load, like gaming, determine a major alteration with respect to a passive activity (video watching). The study of correlation between the questionnaire data and the postural parameters will be one of the next step of the research, considering a large sample of subjects.

These results could underline the importance of ergonomics interventions in work and school environments where smartphones and tablets are used daily, to monitor the posture flexion and to reduce the potential biomechanical symptoms.

With the aim to define ergonomics guidelines to facilitate prevention strategies, future research should include recording cervical muscle activity, to better understand the relationship between kinematics and muscle activity, pain and biomechanics risks associated with long-term smartphone use.

BIBLIOGRAPHY

1. Szeto GP, Straker L, Raine S. A field comparison of neck and shoulder postures in symptomatic and asymptomatic office workers. Appl Ergon. 2002 Jan;33(1):75-84.
2. Toh SH, Coenen P, Howie EK, Straker LM. The associations of mobile touch screen device use with musculoskeletal symptoms and exposures: A systematic review. PLoS One. 2017 Aug 7;12(8):e0181220. doi: 10.1371/journal.pone.0181220.
3. NIOSH: Public Health Service. NIOSH Publications on Video Display Terminals (Revised). NIOSH, Cincinnati, OH (1991)
4. OSHA, Department of Labor, Working Safely with Video Display Terminals (1997)
5. SUVA: Il lavoro al videoterminale informazioni dettagliate per specialisti e non (2003)
6. INAIL: Il Lavoro al videoterminale. A cura di Barbara Manfredi. Stampato dalla Tipolitografia INAIL di Milano (2010). ISBN 978-88-7484-169-1
7. Sengupta, A.K., Das, B.: Determination of worker physiological cost in workspace reach envelopes. Ergonomics 47, 330–342 (2004)
8. Roth J.T., Ayoub M.M., Halcomb C.G.: Seating console and workplace design: seated operator reach profiles. In: Proceedings of the Human Factors Society, 21st Annual Meeting, pp. 83–87 (1977)
9. Haslegrave, C.M.: Characterizing the anthropometric extremes of the population. Ergonomics 29, 281–301 (1986)
10. Das, B., Behara, D.N.: Determination of the normal horizontal working area: a new model and method. Ergonomics 38, 734–748 (1995)
11. Sengupta, A.K., Das, B.: Maximum reach envelope for the seated and standing male and female for industrial workstation design. Ergonomics 43, 1390–1404 (2000)
12. Holman, G.T., Davis, J., Maghsoodloo, S.: The effects of dynamic movement on seated reach arcs. Ergonomics 51, 691–701 (2008)
13. Ferrigno, G., Pedotti, A.: ELITE: a digital dedicated hardware system for movement analysis via real-time TV signal processing. IEEE T. Bio-Med. Eng. 32, 943–950 (1985)
14. Rab, G., Petuskey, K., Bagley, A.: A method for determination of upper extremity kinematics. Gait Posture 15, 113–119 (2002)
15. Cook, C., Burgess-Limerick, R., Papalia, S.: The effect of upper extremity support on upper extremity posture and muscle activity during keyboard use. Appl. Ergon. 35(3), 285–292 (2004)
16. S. Berolo, RP. Wells, and B.C. Amick III, "Musculoskeletal symptoms among mobile hand-held device users and their relationship to device use: a preliminary study in a Canadian university population," Applied Ergonomics vol. 42, no.2, pp.371-378, 2011.
17. E. Valentini, G. Curcio, F. Moroni, M. Ferrara, L. De Gennaro, M. Bertini, “Neurophysiological effects of mobile phone electromagnetic fields on humans: a comprehensive review,” Bioelectromagnetics, vol. 28, no. 6, pp. 415-432, 2007.
18. M. Röösli, P. Frei, E. Mohler, K. Hug, “Systematic review on the health effects of exposure to radiofrequency electromagnetic fields from mobile phone base stations,” Bulletin of the World Health Organization, vol.88, no. 12, pp. 887-896, 2010.
19. C. Caramia, I. Bernabucci, C. D'Anna, C. De Marchis, M. Schmid, “Gait parameters are differently affected by concurrent smartphone-based activities with scaled levels of cognitive effort,” PloS one, vol.12, no. 10, 2017.

20. Y. Xie, G. Szeto, J. Dai, “Prevalence and risks factors associated with musculoskeletal complaints among users of mobile handheld devices: A systematic review,”, Applied Ergonomics, vol. 59, pp. 132-142, 2017
21. S.H Toh, P. Coenen, E.K Howie, L.M Straker, “The associations of mobile touch screen device use with musculoskeletal symptoms and exposures: A systematic review,”Plos one, vol. 12, no. 10, 2017.
22. C. D’Anna, M. Schmid, A. Scorza, SA Sciuto, L. Lopez, S. Conforto, “Time-to-boundary function to study the development of upright stance control in children,” Open Biomedical Engineering Journal, vol.11, pp. 49-58, 2017.
23. M. Schmid, S. Conforto, L. Lopez, T. D'Alessio, “Cognitive load affects postural control in children,” Experimental Brain Research, vol. 179, no. 3, pp. 375-385, 2007.
24. M. Schmid, S. Conforto, L. Lopez, P. Renzi, T. D'Alessio, “The development of postural strategies in children: A factorial design study,” Journal of NeuroEngineering and Rehabilitation, vol. 2, no. 29, 2005.
25. P.T. Hakala, A.H. Rimpela, L.A. Saarni, J.J. Salminen, “frequent computer- related activities increase the risk of neck- sholulder and low back pain in adolescents,” Adolescent health, vol. 16, no.5, pp.536-541, 2006.
26. A.E. Barr, M.F. Barbe, B.D. Clark, “Work-related musculoskeletal disorders of the hand and wrist: epidemiology pathophysiology, and sensorimotor changes,” J. Orthp. Sports Phys. Ther., vol.34, no. 10, pp. 610-627, 2004.
27. Y. Xie, G.P. Szeto, J. Dai, P. Madeleine, “A comparison of muscle activity in using touchscreen smartphone among young people with and without chronic neck-shoulder pain,” Ergonomics, vol.59, no.1, pp. 61-72, 2016.
28. C. D'Anna, A. Scorza, M. Schmid, F. Orsini, A.S. Sciuto, S. Conforto, S. Scena, “A preliminary study on the validation of an automatic measurement method for functional reach assessment by stereophotogrammetry,” 2017 IEEE International Instrumentation and Measurement Technology Conference, Proceedings, 2017.
29. K.K. Hansraj, "Assessment of stresses in the cervical spine caused by posture and position of the head," Surg Technol Int, vol. 25, pp. 277-9, 2004.
30. M. Lee, et al., “The effects of smartphone use on upper extremity muscle activity and pain threshold,” Journal of physical therapy science, vol. 27, no. 6, pp. 1743-1745, 2015.
31. X. Guan et al., “Gender difference in mobile phone use and the impact of digital device exposure on neck posture,” Ergonomics, vol. 59, no.11, pp. 1453-1461, 2016.
32. X. Ning, Y. Huang, B. Hu, A.D. Nimbarte, “Neck kinematics and muscle activity during mobile device operations,” International Journal of Industrial Ergonomics, vol. 48, pp. 10-15, 2015.
33. S. Lee, H. Kang, G. Shin, “Head flexion angle while using a smartphone,” Ergonomics, vol. 58, no.2, pp. 220-226, 2015.
34. G. Wu et al., “International Society of Biomechanics. ISB Recommendation on Definitions of Joint Coordinate Systems of Various Joints for the Reporting of Human Joint Motion. Part II. Shoulder, Elbow, Wrist and Hand,” J Biomech, vol. 38, no. 5, pp. 981–992, 2005.

CHAPTER VII

7. SEMG FEATURES IN WRULD: MUSCLE ACTIVITY DETECTION IN WEAK AND NOISY MYOELECTRIC SIGNALS

The muscles involved in work activities associated with use of computer and touch screen devices are often difficult to analyze because these muscles are weak and noisy myoelectric signals. Indeed, the detection of skeletal muscle activation is a critical issuein myoelectric signal (EMG) processing for clinical [1], motorcontrol [2], ergonomics [3] and sports applications [4]. Different approaches were developed to estimate EMG onset–offset based on several automatic computer-based algorithms, including: single-threshold [5] and double-threshold [6] detection, adaptive threshold method [7], advanced statistical procedures [8], artificial neural network [9] and fuzzy logic [10] techniques. Unfortunately, these methods often fail when the muscle activity is recorded by damaged (i.e amputation) [11], pathological muscles (i.e myopathology) [12, 13], or in ergonomics studies, when looking at prolonged low-level sustained contractions (i.e. shoulder/neck muscles activity during computer work or upright stance) [14]. In these situations, the signals are weak and noisy, therefore they are characterized by a low activity level due to low firing rate, low number of motor units recruited, low activation threshold and very low signal-noise ratio (SNR) [15].

For these weak and noisy EMG signals, several approaches have been recently proposed to improve SNR and to minimize erroneous onset detection [16]: Xu et al. [17] developed an adaptive algorithm for the determination of the onset and offset of the muscle contractions based on the generalized likelihood ratio test(GLR); Merlo et al. [15] proposed a time-frequency analysis to identify the single motor unit activation potentials in noisy EMG, as they used the continuous wavelet transform (CWT), permitting to detect the intervals of activation through an optimal

threshold definition when the SNR is low (2 dB); Zhang and Zhou [18], instead, proposed an analysis based on Sample Entropy to distinguish the EMG signal from spurious background spikes. A method based on the non-linear properties of the Teager- Kaiser energy (TKE) operator, applied to surface EMG signal, was proposed for the first time by Liet al [16] considering simultaneously the amplitude and the instantaneous frequency of the signal: it improves SNR and favours a morerobust detection of the onset muscle activity. This method was perfected by Yang et al. [19] applying a filtering method that is borrowed from an advanced image enhancement technique in the TKE domain. Solnik and colleagues [20] compared the results obtainedby the application of the TKE with the three more-used classi-cal onset methods for detection (visual detection, threshold-based method and approximated generalized likelihood-ratio), showing that the application of TKE operator in signal conditioning significantly reduces the mean detection error with respect to the classical methods. However, all the mentioned methods depend, either fully (i.eGLR) or partially (i.e TKE or CWT), on the amplitude characteristicsof the weak EMG signal, and their performance often depends on the SNR level; this detrimentally affects the detection performance when SNR is less than 10 dB.

In this context, during my PhD project, I focused the attention on weak and noisy EMG signals, typical of some work activities (i.e. use of computer and mobile touch screen devices by office workers) proposing 2 methods tested on simulated signals, to detect muscle activation of these signals.

In this chapter, text and figures have been taken from or adapted from the articles “Using the frequency signature to detect muscular activity in weak and noisy myoelectric signals” [2019, *Biomedical Signal Processing and Control]*, “Generalization of a wavelet-based algorithm to adaptively detect activation intervals in weak and noisy myoelectric signals” [2020, *Biomedical Signal Processing and Control*], and “Muscle activity detection in pathological, weak and noisy

myoelectric signals" [2018, IEEE International Symposium on Medical Measurements & Applications] which were co-authored by me.

7.1 STUDY N°1: USING THE FREQUENCY SIGNATURE TO DETECT MUSCULAR ACTIVITY IN WEAK AND NOISY MYOELECTRIC SIGNALS

The aim of this work is to introduce a method based only on the frequency characteristics of the weak and noisy EMG to detect muscular activity.

Indeed, to date, despite the frequency analysis of the EMG is widely used to track muscular changes and to evaluate muscle fatigue [21,22], the possibility to extract the intervals of muscular activity only from the changes in frequency domain was only partially investigated: to our knowledge only one preliminary study was proposed in the literature, which uses frequency characteristics such as zero-crossings and mean instantaneous frequency to detect the muscular activity of a real EMG signal, by an empirical threshold approach [23].

In this work the aim is to evaluate the possibility to extract the intervals of muscular activation in weak and noisy signals, where amplitude-based parameters display a reduced efficacy driven by the low SNR characteristics, leveraging on frequency features only. In particular, we developed a cluster-based algorithm which is based on the extraction of the number of zero-crossings and the mean instantaneous frequency [23], which we can comprehen-sively denote as frequency signature. This kind of approach to muscle activity detection allows to overcome the problems related to the definition of empirical thresholding, which in turns makes comparisons of results among different operators and laboratories harder. The algorithm was validated on a set of simulated EMG signals and the performance was assessed showing good results in terms of detection and robustness with respect to both noise level and implementation settings.

7.1.1 Materials and Methods

7.1.1.1. EMG simulated signals

The EMG signals were simulated using an EMG simulation soft-ware based on the model developed by Hamilton-Wright andStashuk [24,25]. The details of the theoretical bases of the EMG modelling method can be found in [24,25]. The EMG signals were supposed to be generated from a small muscle (100 motor units) with low firing rate (10 pps). The muscular contraction was generated in terms of percentage of the maximum voluntary contraction (5% MVC). The maximum recruitment threshold was set at 50% of the Motor Unit Action Potential(MUAP) and a neurological jitter with a variance of 25 μs wasinserted according to Yang et al. [19]. The main configurationparameters to generate the EMG signal are shown in **Table 7.1**.

Parameters	*Value*
Electrode Type	concentric needle
Needle Position X/Y/Z	[0 0 15] mm
Number of MUs	100
Contraction Level	5%
Jitter (variance)	25 μs
Muscle fiber density	10.0/mm2
Area of 1 muscle fiber	0.0025 mm2
Min/Max MU diameter	2.0/8.0 mm
Firing rate	10pps
Sampling Frequency	31250 Hz

Table 7.1. *Parameter configuration for generating the EMG signals.*

Segments of EMG signals were simulated: each segment wasconstituted by a 2 s long coloured Gaussian noise realization (obtained by filtering white Gaussian noise in the range 10 Hz-10 kHz) to which the simulated muscular activity (lasting 1 s) was added with onset instants randomly varying from 0 to 1 s in orderto randomise the onset in the data set. The power of the noise waschanged to obtain four levels of SNR (2 dB, 4 dB, 6 dB, 8 dB), whose values were chosen, following Merlo et al. [15], to obtain weak and noisy simulated signals, for each SNR level. A total of 320 trials (8 EMG

signals x 4 SNR x 10 noise replicas) of artificial EMG were generated. An exemplary trial is illustrated in **Figure 7.1**.

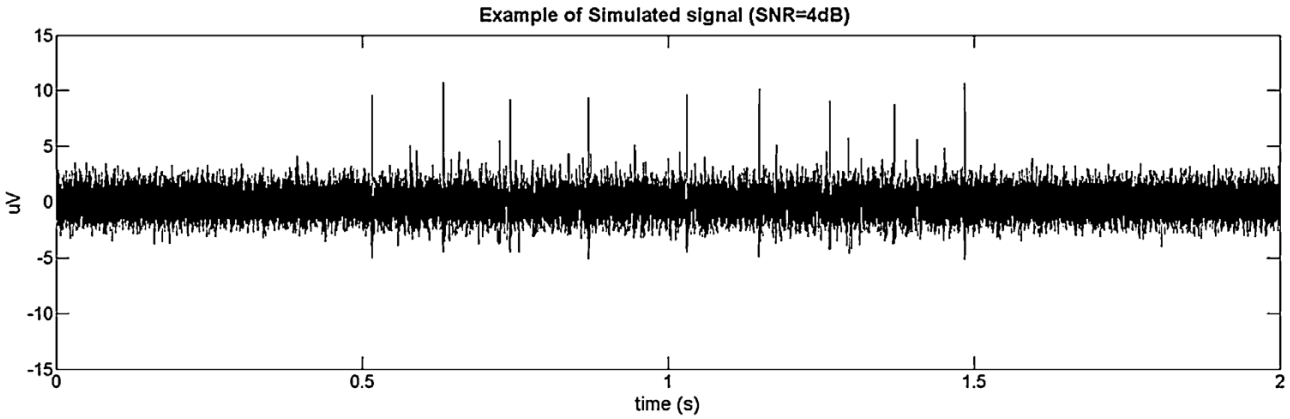

Figure 7.1. *Example of simulated EMG (SNR = 4 dB).*

7.1.1.2 Algorithm design to detect muscular activity

The algorithm extracts the number of zero-crossings and the mean instantaneous frequency estimated by Hilbert transform [22,28], which are frequency characteristics of the EMG signal [27], and uses these parameters to build a function which will be then fedto a cluster-based technique to classify activation and no-activationphases of the muscular signals. The flow diagram of the algorithm is showed in **Figure 7.2**.

Three principal steps were involved in the analysis:

a. The original simulated EMG time series (EMG(t)) was segmented into a series of overlapped analysis windows with a windowlength from 200 to 3000 samples (6.4 to 96 ms) with steps of 200 samples (6.4 ms), and four window overlaps (0%, 25%, 50%,75%).
b. For each segment the number of times that the signal crosses the zero line (number of zero-crossings, NZC), the number of times that the signal crosses the line of the standard deviation (number of standard deviation-crossings, NSDC) [23], and the mean instantaneous frequency (MIF) were calculated and processed following the equation below.The MIF was calculated using the Hilbert transform, and it was divided by the mean instantaneous frequency calculated in absence of activity (MIFno act, noise only).

$$s(t) = \left(\frac{NZC_j * NSDC_j}{2}\right) * \frac{MIF_j}{MIF_{j_{no\_act}}} \quad \text{for j=1....number of windows}$$

An example of the original simulated signal and of the *s(t)* function is showed in **Figure 7.3.**

c. To detect the muscular activation, the k-means clustering approach was applied (as in Lloyd's algorithm) to *s(t)*. The algorithm follows an iterative procedure in which the number of clusters was a priori set to two (activity /no_activity).

   The k-means algorithm follows the following steps:

   1. Initialization: initial estimation of C centroids randomly generated
   2. Data assignment: each input data point is assigned to a cluster based on the:

$$V_i = argmin_{c_i \in C} \left|\left|s_n - c_i\right|\right|^2$$

$$i = 1{:}\,2 \qquad C = \{c_1,\ c_2\} \qquad n = 1{:}\,length\ (s(t))$$

   3. Centroid update: the centroids are recomputed, taking the mean of all data points to that centroid's cluster:

$$c_i = \frac{1}{|S_i|} \sum_{s_i \in V_i} s_i$$

      The algorithm iterates between the last two steps (2-3) until the sum of the distances is minimized.

   4. Output: A 1-dimensional vector containing the clustering classification was stored to detect the muscular activity: zero= "no-activity", one= "activity".
   5. Activity detection: after the clustering, the events assigned to the cluster "activity" and separated by a temporal distance higher than 100 ms (inverse of the firing rate 10 pps) were considered as not representative of a muscular activation, and thus attributed to the "no_activity" cluster. The same was applied if spurious events of no_activity within an activity phase were separated of more than 100 ms.

Therefore, the onset (t_{onset}) and offset (t_{offset}) times were detected: the first was defined as the first instant in which the data sample was classified to belong to the cluster "activity", the second as the last.

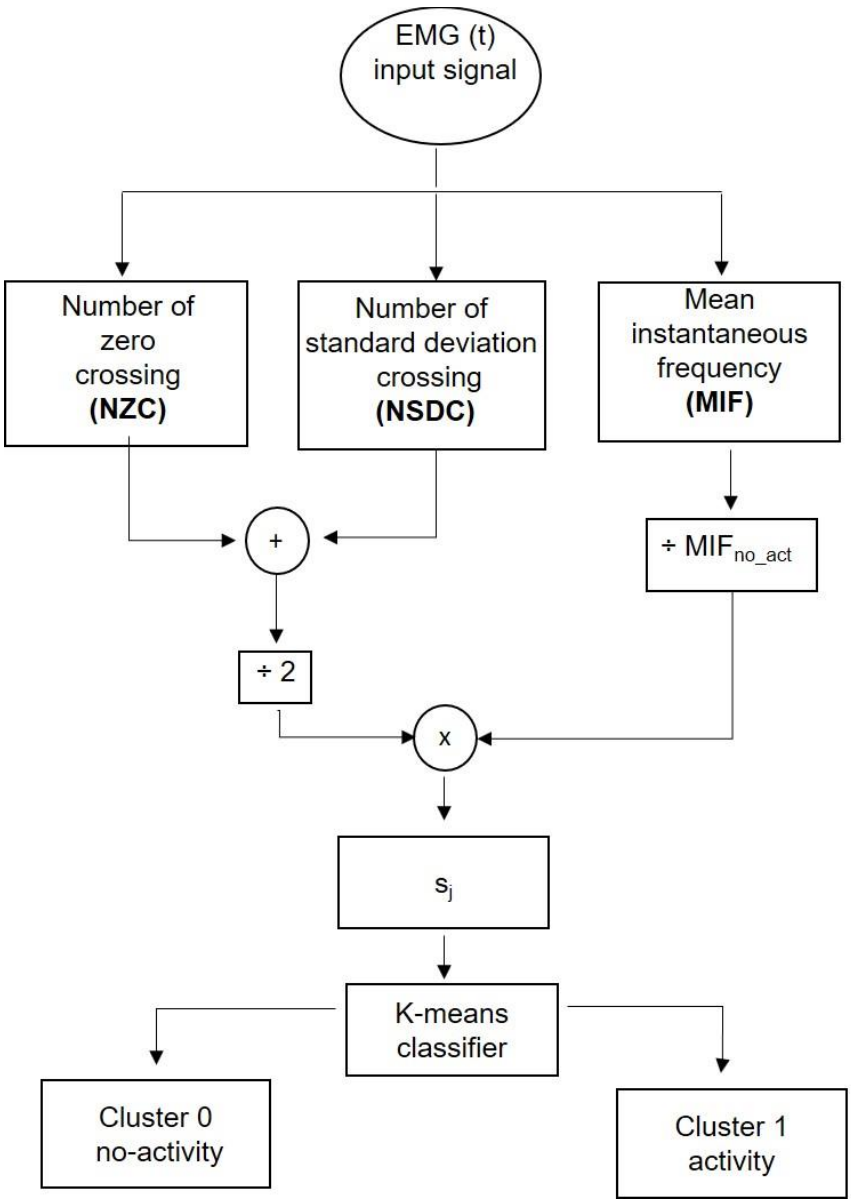

Figure 7.2. *Flow diagram of the algorithm.*

An example of the output of the complete algorithm is showed in **Figure 7.3.**

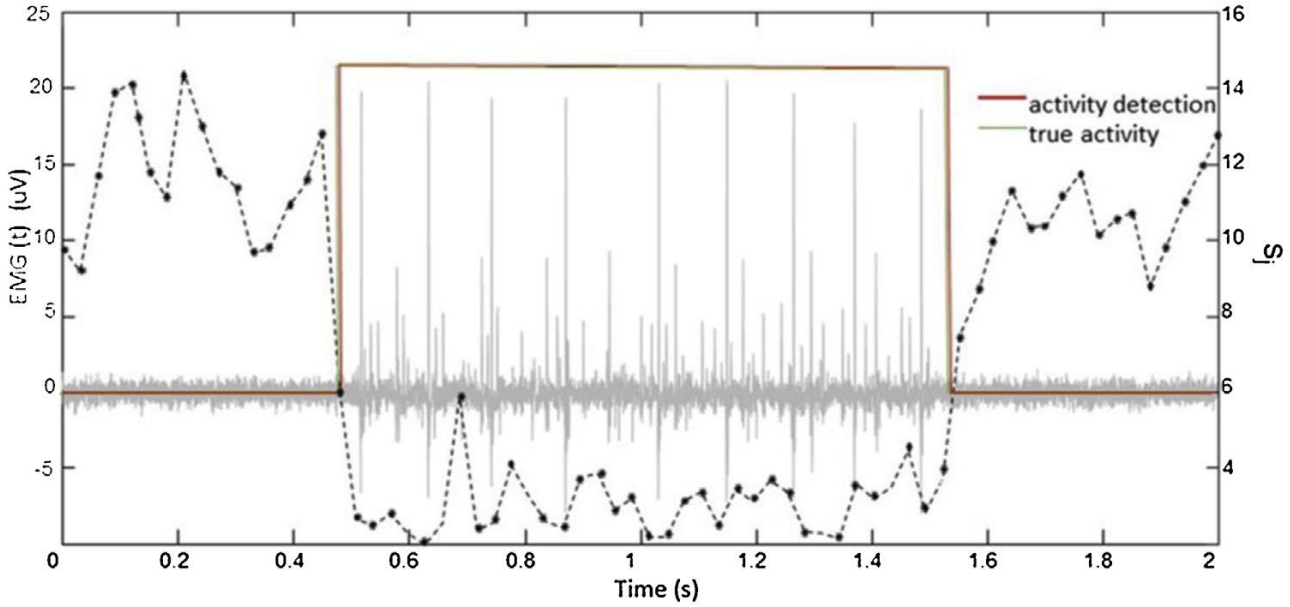

Figure 7.3. *An example of the algorithm is showed on the same graph: EMG simulated signal (gray bold line), s(t) function (black dashed line), activity detection interval (redline) and true activity (green line).*

7.1.1.3 Performance algorithm evaluation

To investigate the effect of the window length, the overlap, and the SNR level, respectively, on the algorithm performance, three performance parameters were calculated, and listed as in the following:

- τ (ms) bias in onset detection defined as the absolute difference between the detected onset time, and the true onset/offset time, was calculated:

$$\tau = |t_{onset} - t_{true_{onset}}|$$

- t_{error} (%) the percentage of the error time detection defined as the absolute difference between the time interval in which the activity was detected and the real interval of EMG activity (t_{true}):

$$t_{error} = \Delta t_{true} - |t_{offset} - t_{onset}| x100$$

in which Δt_{true} is the real interval of muscular activity.

- F1score percentage, as a measure of accuracy, was calculated as following:

$$F1_{score} = 2 * \frac{precision \cdot recall}{precision + recall}\ x\ 100$$

in which *recall* is calculated as the ratio between the number of true positives (TP) and the sum of TP and the number of false negatives (FN); TP and FN were calculated on a sample by sample basis with respect to the s(t) function:

$$recall = \frac{TP}{TP + FN}$$

and *precision* as the ratio between the TP and the sum of the TP and false positives (FP):

$$precision\ = \frac{TP}{TP + FP}$$

7.1.1.4 Statistical analysis

For each parameter, descriptive statistics was calculated (mean ± standard deviation) and statistical analysis was done: to verify the normal distribution of data, Kolmogorov-Smirnovtest was done. Bias and error time (τ, t_{error}) parameters werethen considered separately as dependent variables for a 3-way ANOVA test considering window length (win200, win400,win600,win800, win1000, win1200, win1400, win1600, win1800,win2000, win2200, win2400, win2600, win3000), overlap (0%, 25%, 50%, 75%) and SNR (2 dB, 4 dB, 6 dB, 8 dB) as main factors; the two-way interactions (window length x overlap, window length x SNR,overlap x SNR) were also analysed.To check the effect of the window length, SNR and overlapping,one-way repeated measures ANOVA test and post-hoc analysis(with Bonferroni's corrections) were performed. The level of significance was set at $p < 0.01$.

7.1.2 Results

For both τ and t_{error} the statistical analysis has shown a global effect for window length, overlap, SNR and the interaction between window length and overlap, between window length and SNR and between overlap and SNR. The statistical values are reported in the following **Table 7.2.**

	bias (τ)	error_time (t_{error})
Window length	F=19.98; *p < 0.01	F=12.69; *p < 0.01
Overlap	F=761.69; *p < 0.01	F=124.32; *p < 0.01
SNR	F=60.94; *p < 0.01	F=56.88; *p < 0.01
Window length x Overlap	F=19.12; *p < 0.01	F=10.67; *p < 0.01
Window length x SNR	F=1.83; *p < 0.01	F=3.14; *p < 0.01
Overlap x SNR	F=7.34; *p < 0.01	F=6.42; *p < 0.01

Table 7.2. *Three-way ANOVA test results: F-values and p values for bias (τ) and error time (t_{error}) considering window length, overlap and SNR as main factors. The level of significance was fixed as *p < 0.01.*

7.1.2.1 Effect on bias (τ)

The mean and the standard deviation values of the bias for each SNR and window length are shown in **Figure 7.4**, with each subplot representing a different level of overlap. For all the levels of overlapping, the decrease in the bias valuesas the SNR increases for all the window lengths is statistically significant ($p < 0.01$). In particular, for all overlap levels, the statistical difference is mainly due to the difference between very low value of SNR (2 dB) and the remaining ones (4 dB, 6 dB, 8 dB) for all windows lengths except for the larger window (3000 samples).The comparison among the different values of window length was done considering each level of SNR and the results have shownsignificant effect of the factor for all the levels of overlap ($p < 0.01$). For 0% of overlap the length of the window influences the biasvalues with a significant decrease as the window length increases. No significant difference is shown among the values of window length greater than 1600 samples for all SNR, with mean bias values between 60–100 ms. For 25% of overlap no significant difference is shown for window lengths between 1200 and 2000 samples for levels of SNR greater than 2 dB, with the bias values between 60 and 100 ms. Significant difference is shown only for window lengths greater than 2400 samples with very high mean bias values between 120–200 ms. Instead, for 50% of overlap the significant difference among the different window lengths resulted

for windows smaller than 1000 samples ($p < 0.01$) for very low SNR (2 dB); no significant difference resulted for window lengths greater than 800 samples for the remaining SNR levels.

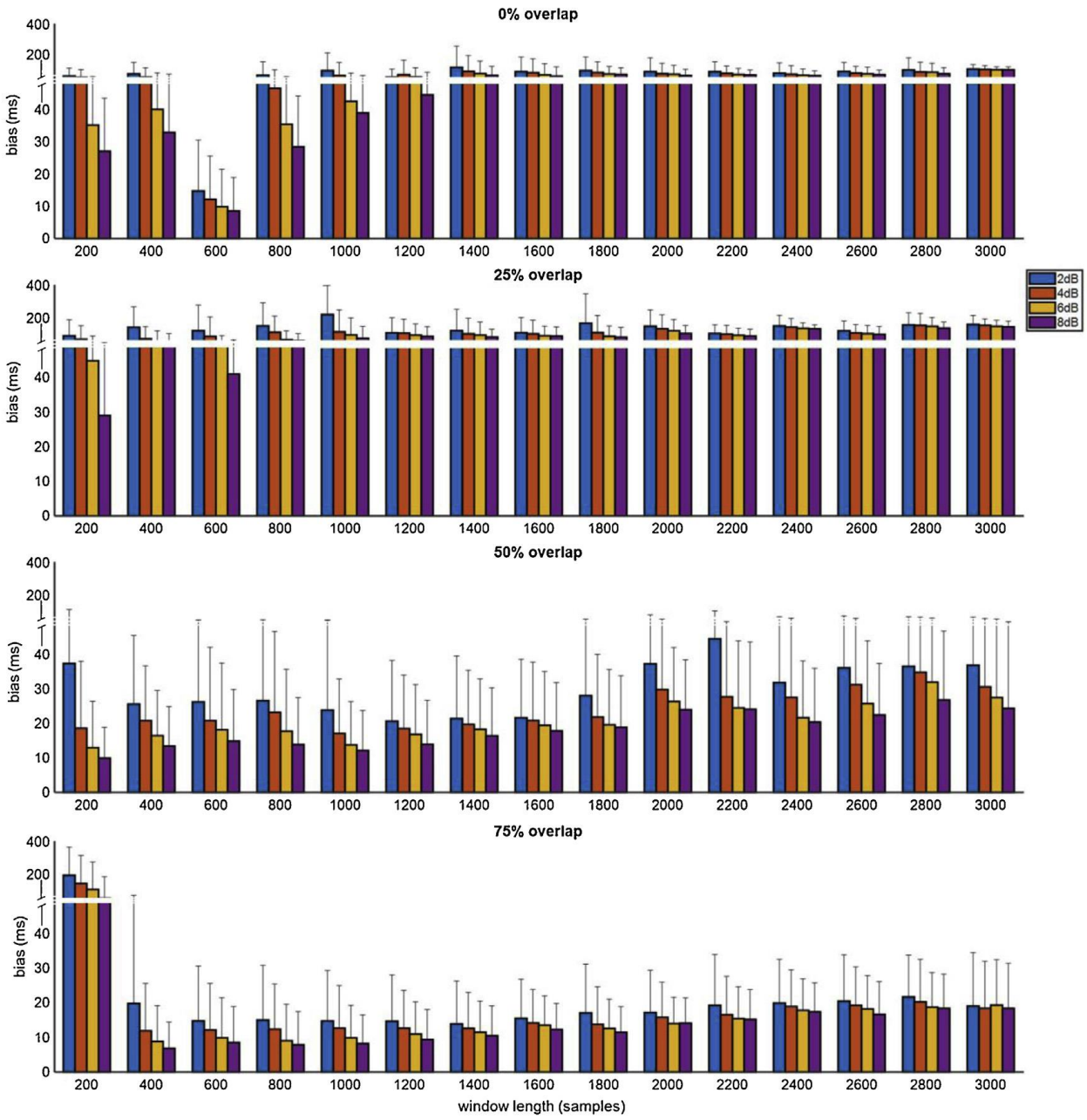

Figure 7.4. *Mean and std of bias for each overlap (0%, 25%, 50% and 75%), SNR level (2 dB, 4 dB, 6 dB, 8 dB) and window length.*

For window lengths between 200 and 1600 samples, instead, the bias values stabilize at 15 ± 3 ms for all SNR levels. For 75% of overlap the significant difference for bias is showed only for window lengths smaller than 400 samples ($p < 0.01$), while the statistical analysis has shown no significant

effect for windows bigger or equal to 600 samples, with a stabilization of the bias values for window lengths greater or equal to 800 samples (τ= 12 ± 4 ms). In general, the bias values obtained for all overlapping configurations are well below the corresponding results obtained by implementing the detection technique introduced in [23] (τ= 191 ± 94 ms).

7.1.2.2 Performance parameter: F1 score analysis

For all the levels of overlap the mean and the standard deviation values of the t_{error} for each SNR and window length are shown in **Figure 7.5**. The results of the statistical analysis have shown a significant effect of SNR for 0% and 25% of overlap for all the values of window length ($p < 0.01$), highlighting a decreasing trend for t_{error} at the increase of SNR. In particular, the statistical effect for window length greater than 1000 samples is essentially due to the significant difference between very low negative SNR (2 dB) and the remaining ones (4 dB, 6 dB, 8 dB). Considering 50% of overlap no significant effect of SNR factor is present in window lengths larger than 1600 samples; significant effect ($p < 0.01$), with a decrease of the mean value at an increase of SNR, is showed for window lengths between 200 and 1000 samples. The results highlighted that with the increase of the window length the significant effect is essentially due to the difference among 2 dB and the remaining SNR levels. In the same way for 75% of overlap forwindow lengths smaller than 1200 samples the effect is determined by the difference among the very low negative SNR value and the main ones. No significant effect of SNR is showed for window between 1200 and 2600 samples. Considering the effect of the window length on the parameter, for all the levels of overlapping and for SNR higher or equal to 2 dB, the results have shown no significant difference among the window lengths larger than 1000 samples. Comparing the t_{error} mean values for all the overlapping levels, for window length values not affected by SNR, minimum values (2–3%) are highlighted for 50% of overlap and window length larger than 1400 samples. These values are very good, also if compared against the ones obtained with the method proposed in [23] (average t_{error} = 34%).

7.1.2.3 Performance parameter: F1 score analysis

The median of the F1 score is reported in the **Figure 7.6**, for each overlap, SNR and window length. The analysis of the results showed that the algorithm accuracy depends on the level of overlap and on the window length. In particular, except for the 25% of overlap, the accuracy improves increasing the length of the window and it is in the range between 90 and 100%. For 50% and 75% of overlap and for window length greater than 1200 samples the F1 score values are between 93% and 98%.

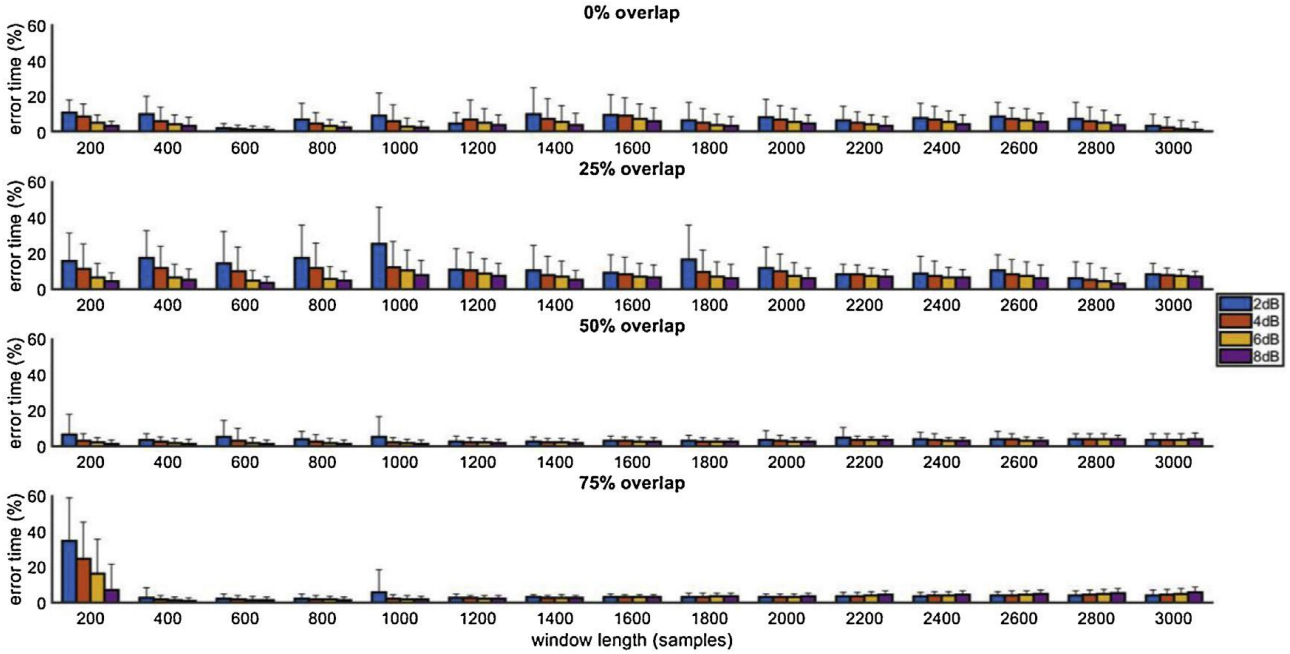

Figure 7.5. *Mean and std of* t_{error} *for each overlap (0%, 25%, 50% and 75%), SNR level (2 dB, 4 dB, 6 dB, 8 dB) and window length.*

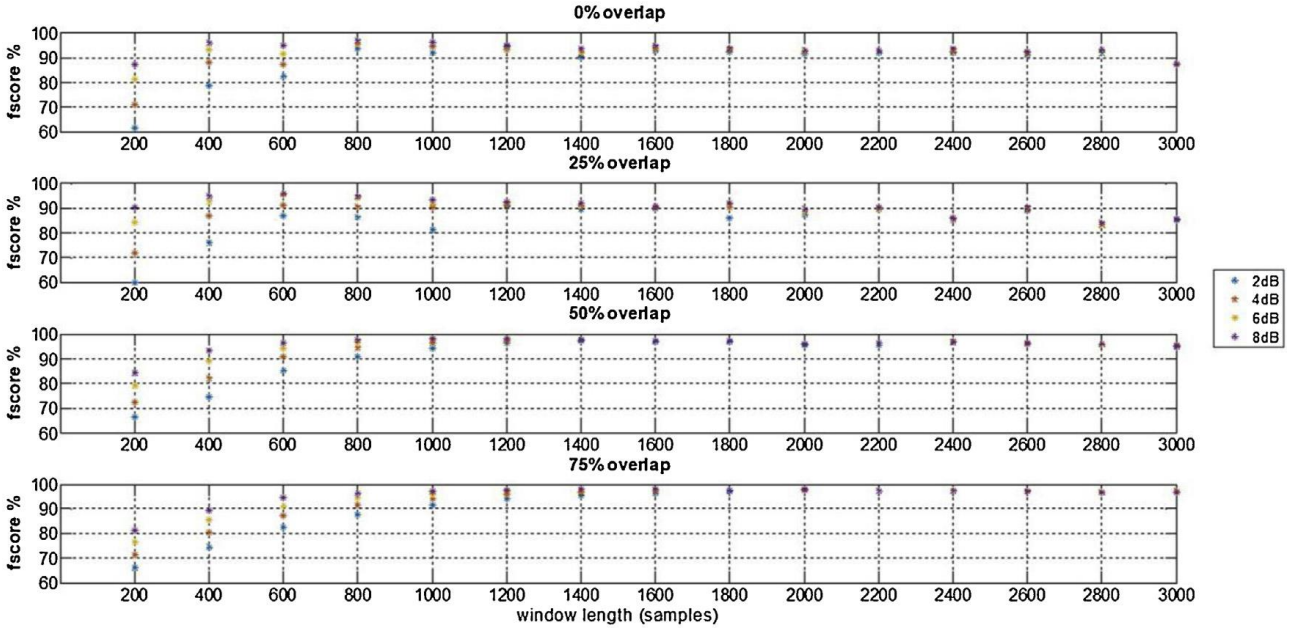

Figure 7.6. *Median values of the F1score for each overlap, SNR level and window length.*

7.1.3 Discussions and Conclusions

The detection of the muscular activity in signals characterized by low amplitude and low signal-to noise ratio is a challenge in biomedical data processing for application in different fields such as prosthesis control and ergonomics. To date the main approaches proposed to detect muscular activity are essentially based either on the amplitude or on the combination of both frequency and amplitude characteristics of the signals, and their performance are strictly related to the SNR level. Therefore, when the electromyographic signal is very weak and noisy the accuracy in the muscular detection decreases for almost all the published techniques and often is not satisfactory. This study shows how the latter limitation can be overcome. The proposed algorithm works on the frequency characteristics of the weak and noisy EMG signals, essentially disregarding the amplitude charac-teristics, and is able to extract, with a good accuracy the onset and the percentage time of activation, regardless of the signal-to noise ratio. The detection is obtained by combining the extraction of the frequency features to a clustering approach without the need of using a thresholding procedure. This latter feature plays a relevant role, as it is also underscored by the higher performance, in terms of temporal accuracy, of the method introduced in this study, as

compared to the activity detection introduced in [23], which uses frequency characteristics only, as well.

The analysis of the results, obtained by a set of simulated EMG signals with different levels of very low SNR, has highlighted a critical aspect, to study in deep, related to the implementation settings. In particular, it is important to examine how the window length and the overlap can influence the algorithm performance. The results show that both bias and time error can be improved by properly setting the window length and the overlap. In particular, window overlap determines an improvement of the algorithm performance, obtaining the best results for overlap between the 50% and 75%. As it happens in other time-frequency techniques [26], the overlap of the windows increases the number of observations and favours the timing detection accuracy (the function used for the detection is calculated over a greater number of samples). At this level of overlapping the best performance are for a window length of 1000 samples for 50% of overlap and of 800 samples for 75%, with bias values of about 13 ms and 8.5 ms, error in time detection of 1.5% and 2%, and accuracy of 96% and 98%, respectively. Considering the effect of the SNR levels for each window length and each overlap, the results show that for overlapping lower than 50% the difference in performance among the lower level of SNR (2 dB) and the remaining levels persists for all the window lengths, while this effect disappears for 50% and 75% of overlap when window lengths are larger than 30 ms and 25 ms, respectively.The obtained performance is satisfactory in the simulated conditions, with levels of bias well below 50 ms even under noisy conditions. The independence from the SNR level is also an important element that will favour the application of this technique in real situations characterized by weak signals such as the ones recorded, even by using sEMG, during sustained and prolonged activities (for instance, the upper trapezius activity during computer use), or from damaged and pathological muscles (i.e. limb muscle after an amputation). Future work will be devoted to i) improve the independence of the algorithm from the operator settings by adapting

the window size on the statistical characteristics of the signal, and ii) validate the technique on real signals by implementing ad-hoc experimental protocols (i.e. EMG signals acquired simultaneously to kinematic information to be used as a biomechanical reference for muscular onset detection). Some further investigations could study the effect of combining differently the frequency features used as input for the clustering and even comparing performance obtained by different classifiers.

7.2 STUDY N°2: AN ADAPTIVE WAVELET-BASED ALGORITHM TO DETECT MUSCLE ACTIVITY IN WEAK AND NOISY SIGNALS

The aim of this study is to present an approach for estimating the timing of muscular activation in weak and noisy myoelectric signals (EMG) starting from a method introduced in literature by Merlo and colleagues [15]. The work authored by Merlo and colleagues [15] has drawn the attention of the scientific community, as the method therein proposed showed accurate timing performance for low SNR values (i.e. around 2 dB). In that method, muscle activity is recognized by detecting the presence of activity in the EMG signal through the Continuous Wavelet Transform (CWT). In particular, a detection threshold is defined based on the statistical properties of an initial reference window where no muscular activity is hypothesized. This makes the algorithm unsuitable in cases when it is not guaranteed that myoelectric signals start without a muscular activation. Moreover, the method requires to calculate and to process all the wavelet decomposition levels with a relevant computational burden.

In this manuscript we want to generalize this approach. In particular, the threshold for the detection is determined iteratively based on the estimation of the SNR. With this addition the algorithm can be used also in conditions where muscular activity is present in the reference window. Moreover, by introducing a stopping criterion for the number of decomposition levels it would be possible to reduce the computational burden.

Given the rather promising results of the original formulation of the CWT-based scheme on weak and noisy signals, we will test whether the modifications coming from this adaptive approach maintain (or possibly improve) the performance in that class of signals. To evaluate and compare the performance of the method against traditional threshold-based methods and the original formulation of the technique, both simulated and semi-synthetic EMG signals were used, as detailed in the following section.

7.2.1 Materials and Methods

7.2.1.1 Synthetic EMG dataset

Very weak and noisy myoelectric signals have been simulated by a software based on the EMG mathematical model developed by Hamilton-Wright and Stashuk [25]. The simulation software allows the management of several parameters [30] whose values in this work are shown in **Table 7.3**.

Parameters	*Value*
Electrode Type	concentric needle
Needle Position X/Y/Z	[0 0 15] mm
Number of MUs	100
Contraction Level	5%
Max Recruitment Threshold	50%
Jitter	25 μs
Muscle fiber density	10.0/mm2
Area of 1 muscle fiber	0.0025 mm2
Min/Max MU diameter	2.0/8.0 mm
Firing rate	12pps
Sampling Frequency (F_c)	31250 Hz
EMG Bandwidth	10-10kHz
Activity Duration (RAD)	1s

Table 7.3. *All parameters for simulating the EMG signal by a generation software based on an EMG mathematical models.*

To simulate weak static muscular contractions (**Figure 7.7**) – weakness is associated with a very low percentage (e.g. 5%) of the maximum voluntary contraction – we have chosen, as the source of the activity, a small muscle characterized by: 100 motor units, firing rate of 12 pulses per second (pps), 50% as the percentage of the maximum recruitment threshold, 25 μs as the variance of the neurological jitter [19].

The signals used for assessing the algorithm were built in order to evaluate the performance with respect to the detection of the activity onset by varying the SNR values.

In particular, eight runs of the simulator were done to simulate eight different weak muscular contractions lasting 1 second. Then each of the latter contractions was used to build a set of simulated signals as in the following (see **Figure 7.7** b):

- 10 independent coloured Gaussian noise realizations (obtained by filtering white Gaussian noise in the range 10 Hz-10 kHz), lasting 2 seconds, were generated. Each of the realizations was differently magnified in order to obtain seven different values of the variance and then seven different levels of SNR (-2dB, 0dB, 2dB, 4dB, 6dB, 8dB, 10dB) in the final dataset;
- the synthetic weak static muscular contraction was superposed to the previous 60 noise realizations and, in particular, it was located from 0.5 s to 1.5 s, so simulating a contraction both preceded and followed by a rest phase lasting 0.5 seconds.

In sum a total of 560 trials (8 EMG x 10 noise replicas x 7 SNR) of artificial EMG simulated signals were processed. The real activity duration (*RAD*) is one second, while the entire signal (Signal Duration) lasts two seconds.

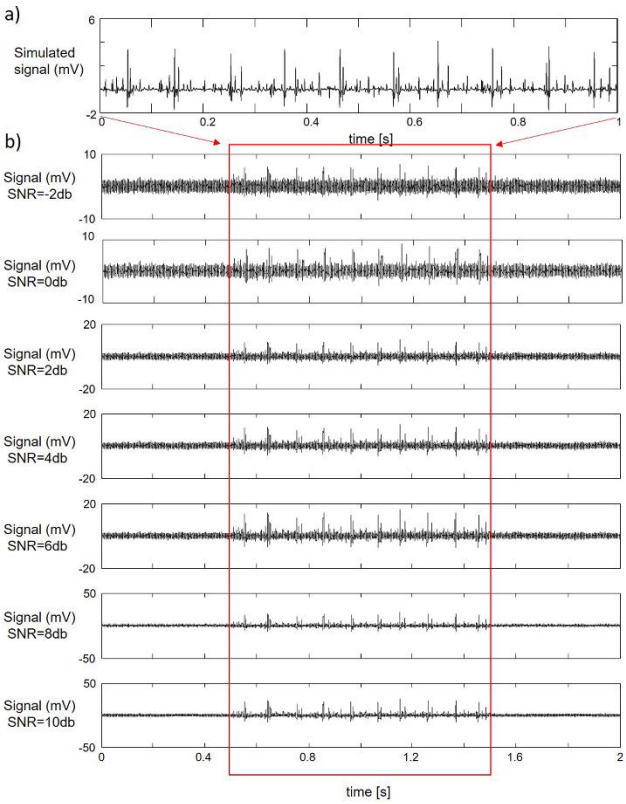

Figure 7.7. *a) A trial of 1 second simulated muscular activity generated by the generation software. b) The simulated EMG signals obtained by superposing the muscular activity (from 0.5s to 1.5s) represented in a) to a 2 seconds long white Gaussian noise realization with varying power to obtain the following values of SNR (SNR=-2dB, SNR=0dB, SNR=2dB, SNR=4dB, SNR=6dB, SNR=8dB, SNR=10dB).*

7.2.1.2 Semi-synthetic EMG dataset

The algorithms were also tested on a set of 280 semi-synthetic EMG signals generated from real EMG signals published by [31].

In particular, to generate each semi-synthetic EMG signal, we carried on the following operations:

1) a 6-s long sequence of coloured noise was synthetically generated, according to the same procedure described in the previous section;
2) three different sections of muscular activations were extracted from the recorded signals taken from the database;
3) the sections were added to the synthetic coloured noise, at different temporal intervals, so to create 3 different activation intervals.

This procedure was repeated 40 times by considering all the possible combinations of 10 different realizations of coloured noise and 4 real signals extracted from the database. The entire dataset of semi-synthetic EMG signals was then generated by considering the 7 different levels of SNR (-2dB, 0dB, 2dB, 4dB, 6dB, 8dB, 10dB), summing thus at a total of 280 realizations.

7.2.1.3 Generalized CWT-based estimation of muscle activation

Continuous Wavelet Transform (CWT) [15] was applied to the EMG simulated signals s(t) to detect muscle activation. The CWT was defined as:

$$CWT(a,\tau) = \frac{1}{\sqrt{a}} \int_{-\infty}^{+\infty} s(t) w^* \left(\frac{t-\tau}{a}\right) dt$$

where ***w(t)*** is the prototype function called mother wavelet (Mexican Hat), $\boldsymbol{\tau}$ is a translation index, and $\boldsymbol{a}$ is a scale parameter that is related to the frequency content. From now on we will refer to the scale as the level of decomposition to better match better the iterative and discrete nature of the detection algorithm.

The detection algorithm is based on the following three steps that are also represented in a graphical way in **Figure 7.8**:

1) **Definition of the minimum level of decomposition a_{min}**: CWT is calculated from a=1 to a=a_{min}. Particularly, the level of decomposition a_{min} is determined automatically as follows: the power of the CWT coefficients is estimated on windows lasting 200 ms and the coefficient of variation (CV) is evaluated. The level of decomposition a_{min} is determined as the first level of decomposition presenting a CV value higher than a given threshold (0.1), chosen with experimental tests satisfying the detection for the lowest SNR (-2dB).
2) **Detection cycle** (see bold box in **Figure 7.8**):

i. For each iteration *i*, starting from the value a_{min} determined in the previous initialization step, an objective function $\eta(t)_i$ is calculated according to the following:

$$\boldsymbol{\eta}(\boldsymbol{t})_i = max\{CWT(a,t)\}_{a=a_{min}}^{i}$$

ii. $\boldsymbol{\eta}(\boldsymbol{t})_i$ is processed to extract power values calculated on windows lasting 200 ms [32]. The series of the power values allowed a first classification of the signal into *noise* and *signal+noise* contributions. The lowest value of the series is attributed to *noise* (P_n) so considering the relative window as the part of the signal characterized by noise only. The remaining signal is considered as containing a superposition of noise and signal and is used to calculate the *signal+noise* power (P_{s+n}). With these values the SNR for the first iteration of the algorithm is calculated.

iii. An inner cycle is then initialized, with a first-guess threshold (th_1) is estimated on the $\boldsymbol{\eta}(\boldsymbol{t})_i$ function as:

$$th_h = \gamma * max_\eta, \quad h = 1$$

where *h* is the current iteration of the algorithm, max_η is the maximum value contained in the window of $\boldsymbol{\eta}(\boldsymbol{t})_i$ used to estimate P_n, and γ is calculated as follows:

$$\gamma = \sqrt{\frac{P_s}{P_n}} = \sqrt{\frac{P_{s+n} - P_n}{P_n}}$$

where P_s is the power value evaluated as the difference between P_{s+n} and P_n.

iv. Each time sample of the vector $\boldsymbol{t}$ is classified as either a burst or interburst by using the following rule:

$$\boldsymbol{t}_{burst} = \boldsymbol{t} \mid \boldsymbol{\eta}(\boldsymbol{t})_i > th_h$$

$$\boldsymbol{t}_{interburst} = \boldsymbol{t} \mid \boldsymbol{\eta}(\boldsymbol{t})_i \leq th_h$$

v. After the detection process, the SNR estimation is updated by considering the burst-interburst classification obtained at step iv) as in [7].

vi. The relative difference between two consecutive SNR estimations is evaluated. If it is higher than 10^{-3} [18], the algorithm goes into a new iteration: h = h+1, th_h (equation 3) is updated, steps iv) and v) are repeated; if the relative difference between two consecutive SNR estimations is lower than 10^{-3}, the inner iteration cycle ends.

vii. Then the detection is refined by a post-processing manipulation as in [15] to reject or merge spurious transitions.

3) **Definition of the maximum level of decomposition** a_{max}: the level of decomposition is increased automatically up to a maximum value (a_{max}) (see **Figure 7.8** dotted line). The stop criterion of the outer cycle is based on convergence: for level of decompositions greater than a_{max} the detection outcome, and then the estimation of the muscular activity (Estimated Burst Duration, *EBD*), doesn't change significantly. To assess this convergence step, the relative duration of the estimated activation is used:

$$Duration_{Activity} = \frac{EBD}{Signal\ Duration}$$

If the difference between $Duration_{Activity}$ at the current iteration *i* and the value obtained at the previous iteration is higher than a given threshold (1%), the outer cycle iterates, while if it is lower, the outer cycle ends, and the maximum value of the level of decomposition (a_{max}) is determined.

An example of the detection procedure is shown in **Figure 7.9** for a trial of simulated EMG signal with SNR = 6db: panels 3b) and 3c) show the true (dotted line) and the estimated (solid line) activation intervals detected in correspondence to a_{min} and a_{max} level of decompositions, respectively. Panel 3d) shows the final outcome after processing step vii.

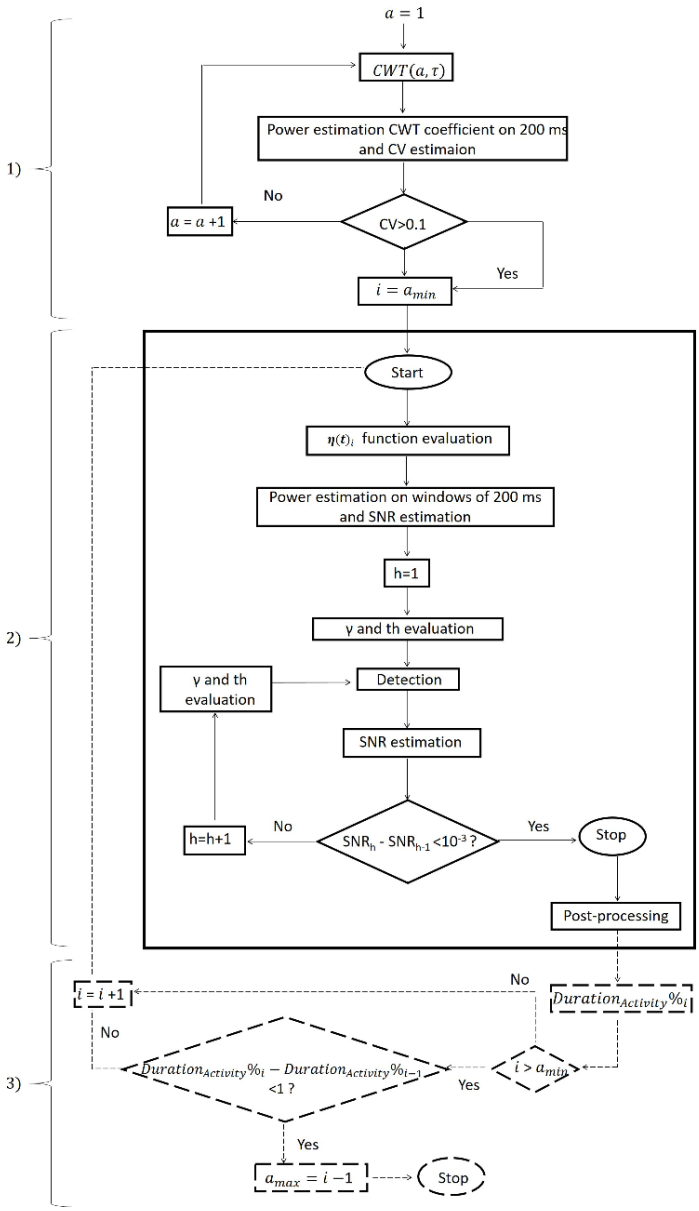

Figure 7.8. *Flow chart of muscle activity detection procedure.*

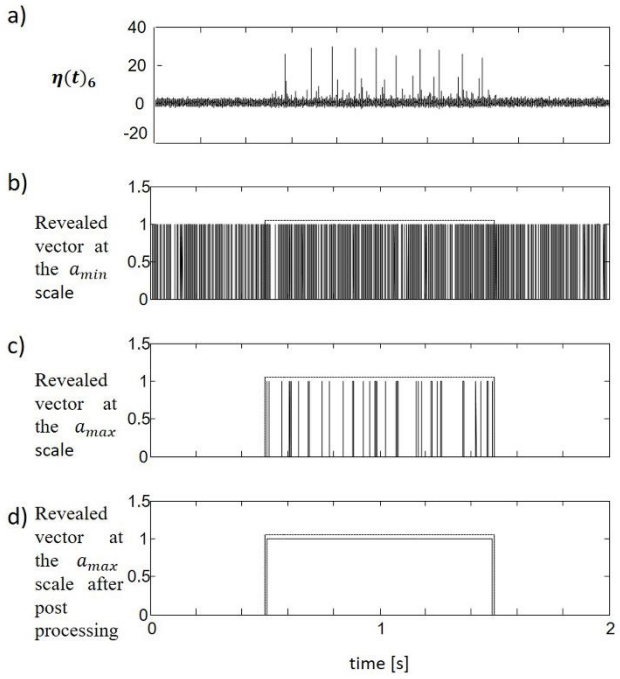

Figure 7.9. *Functions η(t) with range of a 3-6 (a), computed from a trial of simulated EMG signal with SNR=6db. The activation intervals estimated using the proposed method (solid line) at the a_{min} ((b)) and a_{max^x} level of decompositions (c)) and for a_{max} level of decompositions after post-processing (d)) and true activation intervals (dotted line).*

7.2.1.4 Evaluation of results

Results for simulated signals were evaluated in terms of:

- Bias on the onset ($Bias_{on}$) calculated as the difference (in milliseconds) between the true and the estimated onset of the EMG activity.
- Relative timing error of time of EMG activity ($RTE_{Activity}$): it is calculated as the magnitude of the difference between the duration of the nominal EMG activity (*RAD*) and the estimated burst duration *EBD* divided by the nominal duration:

$$RTE_{Activity} = \frac{|RAD - EBD|}{RAD}$$

- Accuracy calculated as follows:

$$accuracy = \frac{TP+TN}{TP+TN+FP+FN}$$

where TN and TP represent the true negatives and true positives. FN and FP are the false negatives and false positives.

In order to compare the performance of the proposed algorithm against techniques introduced in the literature, values of accuracy were calculated, on the same dataset, also for the estimation technique proposed in [16] (TKE), and for the original formulation of the CWT approach proposed by Merlo in [15]. For this latter case, the following parameters were used: the number of decomposition levels was set *a-priori* at 11; the threshold for timing detection was determined based on the variance of the first section of the signals (0.5 s), in the following defined denoted as reference window, hypothesized to be composed of noise only as in [15].

Then, to highlight possible improvements coming from the adaptive nature of the formulation proposed in this work, a further analysis on synthetic signals was also performed as in the following: for the dataset obtained with SNR = 2dB, we modified the amount of activity for the reference window, by adding interference signal, with varying levels of amplitude, leading to an Interference to Noise Ratio (INR_{window}) in the range (-14dB, 0dB). In this way it was possible to verify the robustness of both the original formulation of the method and that introduced in this study, when the hypothesis of absence of muscular activations in the reference window cannot be guaranteed.

7.2.2 Results

7.2.2.1 Synthetic EMG dataset

The results regarding the minimum and maximum level of decomposition (a_{min} and a_{max}) are dependent on SNR. Particularly, the a_{min} values resulted as 5, 5, 4, 4, 3, 3 and 3 for signals with SNR

equal to -2dB, 0dB, 2dB, 4dB, 6dB, 8dB and 10dB respectively. Instead, the a_{max} values were 10, 9, 8, 7, 6, 6 and 5 for signals with SNR equal to -2dB, 0dB, 2dB, 4dB, 6dB, 8dB and 10dB, respectively.

Table 7.4 shows the results in terms of $Bias_{on}$ in milliseconds: the rows represent the results for different a_{max} values, calculated as the mean and the standard deviation of 80 trials (8 simulated signals x 10 realizations of noise) for each SNR. The $Bias_{on}$ value decreases from a_{min} to a_{max} for each SNR value. The detections occur with a $Bias_{on}$ ranging from 8 ms (a_{max} = 5, SNR = 10dB) to 18 ms (a_{max} = 10, SNR = -2dB).

		SNR						
	a	-2dB	0dB	2dB	4dB	6dB	8dB	10dB
$Bias_{on}$ (M±SD) [ms]	3	-	-	-	-	504±2	503±3	500±4
	4	-	-	503±2	502±3	501±3	444±147	141±195
	5	504±1.9	502±3	463±95	384±194	232±209	51±130	8±9
	6	498±13	400±173	365±191	72±129	9±11	9±11	-
	7	416±152	255±214	45±98	10±11	-	-	-
	8	330±181	44±80	11±15	-	-	-	-
	9	102±151	12±16	-	-	-	-	-
	10	18±26	-	-	-	-	-	-
$RTE_{activity}$ (M±SD) [%]	3	-	-	-	-	99.9±0.3	99.9±0.4	98.7±4.6
	4	-	-	99.9±0.3	96.8±7.8	99.3.3±4.1	80.4.3±27.1	14.3±18.1
	5	99.9±0.4	97.3±7.2	88.9±23.1	71.6±36.3	41.1±32.1	3.9±2.6	3.3±1.7
	6	97.2±6.5	80.1±30.6	62.9±33.1	10.2±14.8	3.3±2	3.3±2	-
	7	79.8±27.5	44.9±33.9	6.3±6.7	3.4±2.1	-	-	-
	8	52.9±35.2	6.1±5.9	3.8±2.5	-	-	-	-
	9	17.1±17.9	3.7±2.6	-	-	-	-	-
	10	4.9±4.1	-	-	-	-	-	-
accuracy (M±SD) [%]	3	-	-	-	-	49.8±0.1	49.9±0.2	51±2.3
	4	-	-	49.9±0.1	51.9±3.9	50.6±2	60±13.5	91.7±9.1
	5	49.9±0.2	51.6±3.6	55.6±11	64.4±17.9	79.0±15.7	97.8±1.8	98.3±0.8
	6	51.7±3.2	59.9±14.7	68.5±16.3	94.3±7.3	98.3±1	98.3±1	-
	7	60.1±13	77.2±16.6	96.5±3.2	98.3±1	-	-	-
	8	72.9±16.8	96.5±3.1	98.1±1.2	-	-	-	-
	9	91.1±8.8	98.1±1.3	-	-	-	-	-
	10	97.5±2.0	-	-	-	-	-	-

Table 7.4. *The M±SD of 80 trials (8 simulated signals x 10 noise) of Bias on the onset ($Bias_{on}$), Relative timing error of EMG activity ($RTE_{activity}$) and accuracy for each* ***η(t)*** *and each SNR.*

Table 2 shows also the results concerning the $RTE_{Activity}$ with respect to the level of decomposition and the SNR. $RTE_{Activity}$ decreases with increasing values of the decomposition level, for every SNR value. At a_{max}, $RTE_{Activity}$ is less than 4% for all the SNR values (from 3.3% to

3.7%) with the exception -2dB (around 5%). Furthermore, in **Table 7.4** the values of accuracy obtained for the different levels of SNR and for each level of decomposition are reported.

The accuracy value becomes higher when the number of decomposition levels increases, and its maximum is independent from SNR. The values are around 98%.

7.2.2.2 Performance comparison

The comparisons between the gCWT method, the TKE method described in [16] and the traditional CWT method described in [15] were reported in terms of accuracy (see **Figure 7.9** for mean and standard deviation values). Mean and standard deviation were calculated, the normal distribution of the data was verified using Lilliefors test, and t-test was done to highlight the statistical difference between the methods. The level of significance was set at 0.05.

The accuracy was compared considering the last level of decomposition for each SNR.

The results of the method proposed in this study showed no significant difference from the original formulation (CWT) for all SNR values, while accuracy resulted significantly higher ($p<0.05$) than that displayed by TKE for all SNR values.

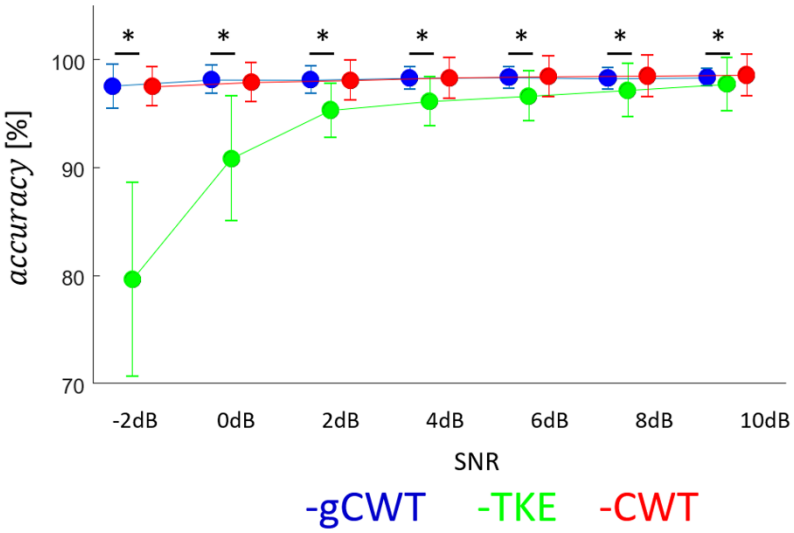

Figure 7.9. Performance comparison. *The M ± SD accuracy of proposed method and method of [25] and [29] for each* ***η(t)*** *and for each SNR. * statistically significance between gCWT and the other two methods (TKE and CWT).*

Results with Interference signals are reported in the **Figure 7.10**. The gCWT method introduced in this study displayed significantly better accuracy results than CWT for every INR level, with the exception INR =-14db.

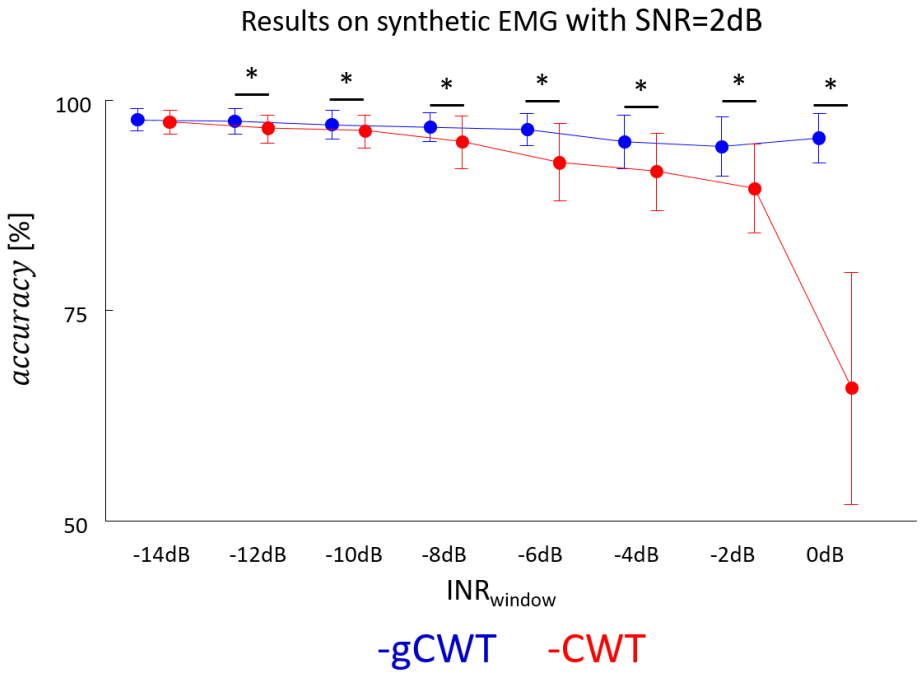

Figure 7.10. *The M ± SD accuracy of proposed method and method of [29] for SNR=2dB and for each INR (-14dB to 0dB).*

7.2.2.3 Results on semi-synthetic dataset

An exampe of the detection of muscular activation through gCWT on semi-synthetic EMG signals is showed in **Figure 7.11**.

The results obtained on semi-synthetic signals are reported in terms of accuracy in **Figure 7.12**; for each level of SNR the accuracy value is reported from a_{min} to a_{max}.

The results obtained on semi-synthetic signals showed an accuracy higher than 92% for all SNR levels except for -2dB. In particular, for SNR higher than 0 dB, the accuracy values stabilize around 96% for the maximum level of decomposition. Further, the number of the decomposition levels decreases when SNR increases, obtaining for SNR of 10 dB only three levels of decomposition. The accuracy results are showed in **Figure 7.12**.

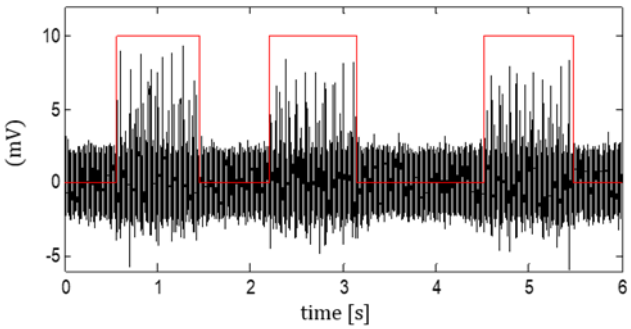

Figure 7.11. *An example of detection on semi-synthetic EMG (in black), in red the period of activation (SNR=2dB).*

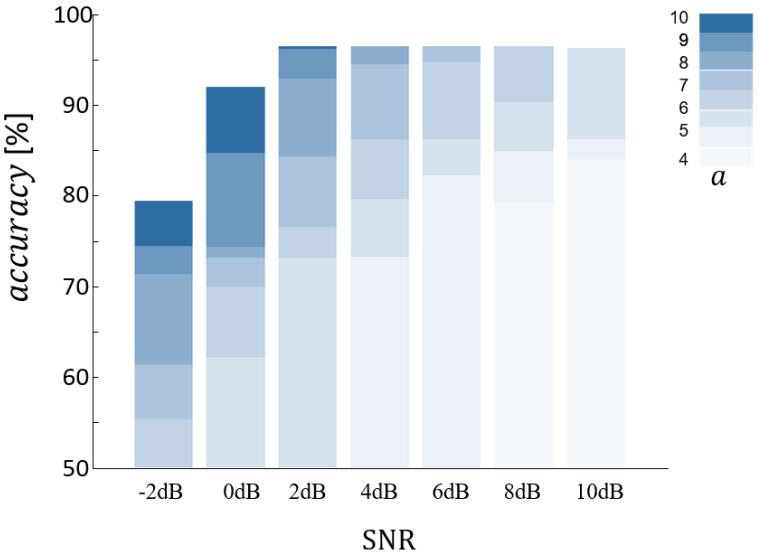

Figure 7.12. *The mean of 40 trials (4 semi-synthetic signals x 10 noise) of accuracy for each SNR and for each level of decomposition.*

7.2.3 Discussions and Conclusions

The detection of muscular activity, when this latter one is feeble and leads to weak and noisy EMG signals, represents a challenging task in biomedical signal processing, and techniques able to accurately solve this task can be useful in different fields of application.

The introduced algorithm takes advantage from the performance of the CWT-based technique in detecting muscle activity when SNR is low, as it is assented by the significant superior performance of both formulations of the algorithm with respect to TKE.

In particular, in terms of performance on synthetic signals, we want to stress the following points regarding the generalized algorithm: the bias is always lower than 18 ms and, for SNR higher than 4dB, it is around 10 ms; $RTE_{Activity}$ is independent from SNR and it is less than 5% for all the tested signals; accuracy is always higher than 97%. The obtained results are linked with the intrinsic nature of the CWT decomposition that, based on the observed shape correlation between MUAPs and wavelets, allows to be more sensitive to muscular activity and to minimize the detection inaccuracies associated with the presence of noise. The latter is an element of importance especially when dealing with weak and noisy signals. This aspect is confirmed by the results obtained on semi-synthetic weak and noisy EMG signals, where accuracy of the muscular detection is around 96% for SNR higher than 0 dB.

Moreover, the generalized algorithm can be implemented for real-time applications due to the reduced computational burden. The latter is reduced by optimizing the wavelet decomposition through a stopping criterion based on the convergence of the detection that prevents the need of calculating and processing all the decomposition levels. The optimization of the wavelet decomposition, indeed, allows the determination of the optimal values for both minimum and maximum level of decomposition. Choosing automatically the minimum level of decomposition guarantees the convergence of the procedure, while optimizing the maximum level reduces the computational burden and makes the results independent from the SNR.

Regarding the comparison with the traditional threshold-based estimation techniques, accuracy for these former ones vary as a function of the SNR level, and when the EMG signal is weak and noisy, the detection accuracy decreases, and it is often not satisfactory. In the case of CWT-based methods, this dependence is reduced [15], and the generalized algorithm introduced in this work takes advantage from this better performance. With the generalized formulation of the CWT-based technique, we were able to widen the applicability of the method to a class of signals where the

hypotheses required by the traditional method could not be met, in particular that of having no muscular activation to define the threshold. Indeed, the algorithm introduced in this study is based on an iterative and adaptive estimation of the signal to noise ratio that is used to assess the threshold for the activity detection. The threshold value is computed iteratively on the basis of a burst-interburst classification that is updated during the algorithm execution. This makes it possible for the generalized algorithm to work accurately not only when the SNR is low, but also when it is not directly possible to establish a reference to be used to manually define a threshold: this may happen in those experimental conditions where muscular activity is low, as the result of a reduced motor unit recruitment, or while operating in a noisy environment and in presence of physiological artifacts, or when recruitment cannot be accurately controlled, such as in the case of physical therapy sessions for people with reduced muscular strength.

Based on the previously described three elements (good accuracy across a broad range of SNR values, ability to work with no reference windows, reduced computational complexity), the algorithm is then a good candidate for a variety of applications where these conditions are important: for instance, in prosthetic control from myoelectric data coming from the residual muscular groups (where real-time is a need, EMG data may be weak and noisy, and control of absence of muscular activation is not always feasible). Future work will thus need to include experimentations for this class of conditions, and a specific analysis on the choice of the mother wavelet that would better capture the nature of the muscular activation.

BIBLIOGRAPHY

1. M.G. Benedetti, Muscle activation intervals and EMG envelope in clinical gaitanalysis, IEEE Eng. Med. Biol. Mag. 20 (6) (2001) 33–34.
2. H. Freund, Motor unit and muscle activity in voluntary motor control, Physiol.Rev. 63 (2) (1983) 387–436.
3. S. Kumar, Electromyography in Ergonomics, Routledge, 2017.
4. J. Vance, Jason, et al., EMG activity as a function of the performer's focus ofattention, J. Mot. Behav. 36 (4) (2004) 450–459.
5. P.W. Hodges, H.B. Bang, A comparison of computer-based methods for thedetermination of onset of muscle contraction using electromyography, Electroencephalogr. Clin. Neurophysiol. Mot. Control 101 (6) (1996) 511–519.
6. P. Bonato, T. D'Alessio, M. Knaflitz, A statistical method for the measurementof muscle activation intervals from surface myoelectric signal during gait, IEEE Trans. Biomed. Eng. 45 (1998) 287–299.
7. G. Severini, S. Conforto, M. Schmid, T. D'Alessio, Novel formulation of a doublethreshold algorithm for the estimation of muscle activation intervalsdesigned for variable SNR environments, J. Electromyogr. Kinesiol. 22 (6)(2012) 878–885.
8. J. Lee, H. Shim, H. Lee, Y. Lee, Y. Yoon, Detection of onset and offset time ofmuscle activity in surface EMGs using the Kalman smoother, in: WorldCongress on Medical Physics and Biomedical Engineering 2006 IFMBEProceedings, 2007, pp. 1103–1106.
9. A. Del Boca, C.P. Dong, Myoelectric signal recognition using fuzzy clusteringand artificial neural networks in real time. Neural networks, 1994, in: IEEEWorld Congress on Computational Intelligence, 1994.
10. F.H.Y. Chan, et al., Fuzzy EMG classification for prosthesis control, IEEE Trans.Rehabil. Eng. 8 (3) (2000) 305–311.
11. J. Silva, H. Winfried, C. Tom, MMG-based classification of muscle activity forprosthesis control. Engineering in medicine and biology society, 2004, IEMBS'04. 26th Annual International Conference of the IEEE Vol. 1 (2004).
12. E. Stålberg, P. Dioszeghy, Scanning EMG in normal muscle and inneuromuscular disorders, Electroencephalogr. Clin. Neurophysiol. PotentialsSect. 81 (6) (1991) 403–416.
13. C. De Marchis, M. Schmid, S. Conforto, An optimized method for tremordetection and temporal tracking through repeated second order momentcalculations on the surface EMG signal, Med. Eng. Phys. 34 (9) (2012)1268–1277.
14. G.M. Hagg, Interpretation of EMG spectral alterations and alteration indexesat sustained contraction, J. Appl. Physiol. 73 (4) (1992) 1211–1217.
15. A. Merlo, D. Farina, R. Merletti, A fast and reliable technique for muscleactivity detection from surface EMG signals, IEEE Trans. Biomed. Eng. 50 (3)(2003) 316–323.
16. X. Li, P. Zhou, A.S. Aruin, Teager–Kaiser energy operation of surface EMGimproves muscle activity onset detection, Ann. Biomed. Eng. 35 (9) (2007)1532–1538.
17. Q. Xu, et al., An adaptive algorithm for the determination of the onset andoffset of muscle contraction by EMG signal processing, IEEE Trans. NeuralSyst. Rehabil. Eng. 21 (1) (2013) 65–73.
18. X. Zhang, Z. Ping, Sample entropy analysis of surface EMG for improvedmuscle activity onset detection against spurious background spikes, J.Electromyogr. Kinesiol. 22 (6) (2012) 901–907.
19. D. Yang, Dapeng, et al., Accurate EMG onset detection in pathological, weakand noisy myoelectric signals, Biomed. Signal Process. Control 33 (2017)306–315.
20. S. Solnik, et al., Teager–Kaiser operator improves the accuracy of EMG onsetdetection independent of signal-to-noise ratio, Acta Bioeng. Biomech./Wroclaw Univ. Technol. 10 (2) (2008) 65.
21. R. Merletti, L. Conte, C. Orizio, Indices of muscle fatigue, J. Electromyogr.Kinesiol. 1 (1) (1991) 20–33.
22. S. Conforto, T. D'Alessio, Real time monitoring of muscular fatigue fromdynamic surface myoelectric signals using a complex covariance approach, Med. Eng. Phys. 21 (4) (1999) 225–234.
23. H.K. Hameed, Husamuldeen, et al., An amplitude independent muscle activitydetection algorithm based on adaptive zero crossing technique and meaninstantaneous frequency of the sEMG signal, in: Micro and Nanoelectronics(RSM), 2017 IEEE Regional Symposium on. IEEE, 2017.

24. A. Hamilton-Wright, D.W. Stashuk, EMG Generating Software, 2015.
25. A. Hamilton-Wright, D.W. Stashuk, Physiologically based simulation ofclinical EMG signals, IEEE Trans. Biomed. Eng. 52 (2005) 171–183.
26. L. Cohen, Time-frequency distributions-a review, Proc. IEEE 77 (7) (1989)941–981.
27. H. Göran, Electromyographic fatigue analysis based on the number of zerocrossings, Pflüg. Arch. 391 (1) (1981) 78–80.
28. H. Xie, Z. Wang, Mean frequency derived via Hilbert-Huang transform withapplication to fatigue EMG signal analysis, Comput. Methods ProgramsBiomed. 82 (2) (2006) 114–120 (2006).
29. R.M. Stude et al. “An algorithm for sequential signal estimation and system identification for EMG signals”, *IEEE Trans. Biomed. Eng*, vol. 3, pp. 285-295, 1984.
30. C. D’Anna et al., “Using the frequency signature to detect muscular activity in weak and noisy myoelectric signals”, *Biomed Signal Process Control*, vol. 52, pp. 69-76July 2019.
31. M. Nikolic, “Detailed Analysis of Clinical Electromyography Signals EMGDecomposition, Findings and Firing Pattern Analysis in Controls and Patientswith Myopathy and Amytrophic Lateral Sclerosis”, *Faculty of Health Science University of Copenhagen*, 2001.
32. P.M. Vieira et al., “An adapted double threshold protocol for spastic muscles”, *Conf Proc IEEE Eng. Med Biol Soc*, pp. 3630-3633, Aug. 2016.

CHAPTER VIII

8. GENERAL CONCLUSIONS

In the attempt to reduce the risk of work-related musculoskeletal disorders several methods have been developed, accepted by the international literature and used in the workplace. In the last years, the most innovative wearable technologies and electronic smart devices, without interfering with the work activities performed by workers, have been introduced to improve the biomechanical risk assessment adapting it to all the work conditions and overcoming the limits of the current standardized methods. Indeed, these devices allow the estimation of biomechanical risk in real-time providing a direct feedback to the end-user who would be constantly monitored directly while at work. In fact, the use of the recent implementations of wearable sensors for quantitative instrumental-based biomechanical risk assessments in the prevention of WMSDs is desirable also in view of the concerns regarding technical ISO standards on ergonomics and physical workloads [1].

In this thesis was underlined, among the others, that the risk assessment methods currently used for UL-WMSDs or WLBDs have different limitations that inhibit their applicability to all work activities. For these reasons instrumental-based tool will play an increasingly important role in both direct evaluations and in the rating of standard methods, also in consideration that several factors, implying work-related musculoskeletal disorders, interact at the same time. Therefore, it will be crucial to monitor all of them by using more than one method at the same time ensuring a more thorough evaluation of risk factors. On the other hand, a lot of attention must be paid because the use of more than one method can rapidly lead to unacceptably high costs for the practitioner, both from a time and money viewpoint [2, 3].

In this context, the technologies accredited to be used are without doubt inertial measurement units (IMUs), instrumented gloves and surface electromyography (sEMG) sensors,

although other new tools are appearing in research laboratories and the workplace. Among these, smart footwear-based wearable systems [4] will surely be useful because they will permit, by recording ground reaction forces through integrated tri-axial force sensors, an inverse dynamics analysis [5-7]. For their simplicity, vision-based tracking systems are also potentially useful for the rating of standardized methods as proposed for assessing the movements of workers within quick exposure check tools [8]. Wearable miniaturized sensors can monitor workers' motor behavior if individually placed on the body segments or embedded in elastic suits. The latter use is also the most probable because the research activity is working fast on the development of artificial muscles, materials able to reversibly contract, expand, and rotate due to an external stimulus [9-10]. These devices, that can be enriched by several material characteristics, textile layers, elastic components, diagonal and lateral seams and pneumatic mechanisms [11] are envisioned as actuators for silent, soft and compliant assistive devices [12] acting as force multiplier systems by helping workers to reduce their effort. These suits/devices can also embed miniaturized sensors which will also serve for their control through, for instance, effective feedforward anticipation mechanisms. Furthermore, numerous devices have been developed to support the trunk during dynamic lifting tasks. sEMG will allow the detection of the early preparatory muscle activities to classify muscle loading and to initiate appropriate device activation. It has been shown that preparatory muscle activity can be leveraged to identify the intent to lift a weight up to 100 ms prior to load-onset [13]. The reduction of the effort will also be guaranteed by highly adaptive production processes.

Although the use of new innovative technologies for biomechanical risk assessment is only at the beginning, the literature and our studies (see chapter 3-6) show that these instrumental approaches could be used to classify lifting tasks into low and high-risk categories. Particularly, this thesis dealt with wearable sensors, such as inertial measurement units, force platforms and surface

electromyography sensors, for biomechanical risk assessment during lifting tasks, which are strictly connected to work-related low-back disorders.

Particularly, in this work kinematic features (i.e. lifitng energy consumption or jerk) have been seen significantly change in relation to the risk levels. These kinematic features have been used as input variables of ANNs for the prediction of WLBDs during lifting tasks. This approach has been proved to be able to improve the biomechanical risk estimation suggesting that an IMU/Inertial sensor-based lifting recognition tool using LEC indices and designed according to the revised RNLE lends itself to the estimation of risk.

In another study of this thesis work, lifting tasks where analysed by using ANNs and sEMG features. The erector spinae longissimus was identified as the most sensitive trunk muscle with respect to changes in the lifting conditions based on the time and frequency sEMG features (max, average rectified value, mean and median frequency). Furthermore, sEMG features have been used as input variables of artificial neural network for the prediction of LBDs during lifting tasks: a multi-domain (time and frequency) approach proved able to improve the biomechanical risk estimation. These findings suggest the use of sEMG features to assess biomechanical risk associated.

The correlation between both kinematic and sEMG parameters and spinal load variables (force and moment) in the L5-S1 region suggests some promise in developing the IMU and/or sEMG based Lifting Risk Recognition Tool. Furthermore, these instrumental methods could be integrated with methods already used for biomechanical risk assessment (i.e. NIOSH protocol; [14-15]) or used when the standardized methods cannot be used due to the equation and parameters restrictions.

Moreover, the work also dealt with weak and noisy signals to allow to quantify the muscle attivity during some typical work activities that cause work-related neck and upper limb disorders (i.e. use of computer and mobile touch screen devices by office workers). Two methods tested on

synthetic and semisynthetic signals were developed so highlighting the possibility to identify the muscle activation also in these conditions.

From a technological point of view for the IMUs, if a high number of units is required for whole-body bio-mechanical studies in ergonomics, a high data transfer time could be required with both the Wi-Fi and Bluetooth protocols. Furthermore, IMUs fail to precisely measure translational motion and suffer from drift. Finally, IMUs can fail in the presence of magnetic fields in the workplace if they have embedded magnetic sensors. As regards limitations associated to sEMG, crosstalk muscle signals, electrode-skin impedance, noise and problems related to the electrode location, size, configuration and distance are the main critical factors [16]. To optimize the sEMG measures it is essential to use reference books such as the "*Atlas of Muscle Innervation Zones*" [17]. For both IMUs and sEMG sensors the energy consumption and the consequent battery discharge do not seem to be problems anymore, thanks to the long life of the most recent batteries.

Therefore, the use of new innovative technologies for biomechanical risk assessment is only at its initial stage, but this process seems to be unstoppable, as it is happening in all the other areas of medicine and beyond. Obviously, it will be necessary for any validation to follow evidence-based medicine/policy/legislation multistep scientific approaches by designing rigorous laboratory and epidemiologic studies, by replicating them by independent research groups and by systematically evaluating them through transparent review processes. I am however convinced that, even if such use should fail in ergonomic practice, the huge knowledge that will derive from its experimentation will allow the optimization of the current standardized methods or the developments of the new ones.

BIBLIOGRAPHY

1. Armstrong, T.J.; Burdorf, A.; Descatha, A.; Farioli, A.; Graf, M., Horie, S.; Marras, W.S.; Potvin, J.R.; Rempel, D.; Spatari, G.; Takala, E.P.; et al. Scientific basis of ISO standards on biomechanical risk factors. Scand. J. Work Environ. Health 2018, 44, 323–329.
2. Chiasson, M.E.; Imbeau, D.; Aubry, K.; Delisle, A. Comparing the results of eight methods used to evaluate risk factors associated with musculoskeletal disorders. Int. J. Ind. Ergon. 2012, 42, 478–488.
3. Peppoloni, L.; Filippeschi, A.; Ruffaldi, E. Assessment of task ergonomics with an upper limb wearable device. In Proceedings of the 22nd Mediterranean Conference on Control and Automation, Palermo, Italy, 16–19 June 2014.
4. Hegde, N.; Bries, M.; Sazonov, E. A Comparative Review of Footwear-Based Wearable Systems. Electronics 2016, 5, 48.
5. Moufawad, El.; Achkar, C.; Lenbole-Hoskovec, C.; Paraschiv-Ionescu, A.; Major, K.; Büla, C.; Aminian, K. Classification and characterization of postural transitions using instrumented shoes. Med. Biol. Eng. Comput. 2018, 56, 1403–1412.
6. Liu, K.; Liu, Y.; Yan, J.; Sun, Z. Nondestructive Estimation of Muscle Contributions to STS Training with Different Loadings Based on Wearable Sensor System. Sensors (Basel) 2018, 18, 971.
7. Liu, T.; Inoue, Y.; Shibata, K. A wearable ground reaction force sensor system and its application to the measurement of extrinsic gait variability. Sensors 2010, 10, 10240–10255.
8. Li, G.; Buckle, P. Evaluating Change in Exposure to Risk for Musculoskeletal Disordersea Practical Tool. HSE Books, Suffolk [Online]. 1999. 74p. CRR251. Available online: http://www.hse.gov.uk/research/crr_pdf/1999/crr99251.pdf (accessed on 27 October 2005).
9. Mirvakili, S.M.; Hunter, I.W. Artificial Muscles: Mechanisms, Applications, and Challenges. Adv. Mater. 2018, 30, doi:10.1002/adma.201704407.
10. Miriyev, A.; Stack, K.; Lipson, H. Soft material for soft actuators. Nat. Commun. 2017, 8, 596.
11. Furukawa, J.; Noda, T.; Teramae, T.; Morimoto, J. An EMG-Driven Weight Support System with Pneumatic Artificial Muscles. IEEE Syst. J. 2014, 10, 1026–1034.
12. Maziz, A.; Concas, A.; Khaldi, A.; Stålhand, J.; Persson, N.K.; Jager, E.W. Knitting and weaving artificial muscles. Sci. Adv. 2017, 3, e1600327.
13. Totah, D.; Ojeda, L.; Johnson, D.D.; Gates, D.; Mower Provost, E.; Barton, K. Low-back electromyography (EMG) data-driven load classification for dynamic lifting tasks. PLoS ONE 2018, 13, e0192938.
14. Waters TR, Putz-Anderson V, Garg A (1994) Applications Manual for the Revised NIOSH Lifting Equation. Cincinnati, OH: U.S. Department of Health and Human Services.
15. Waters TR, Putz-Anderson V, Garg A and Fine LJ (1993) Revised NIOSH Equation for the Design and Evaluation of Manual Lifting Tasks. Ergonomics 36 No. 7, 749–776.
16. Merletti, R.; Parker, P.J. Electromyography: Physiology, Engineering, and Non-Invasive Applications; Wiley-IEEE Press: Hoboken, NJ, USA, 2004.
17. Barbero, M.; Merletti, R.; Rainoldi, A. Atlas of Muscle Innervation Zones; Springer: Milan, Italy, 2012; ISBN 978-88-470-2462-5.

APPENDIX A: Reference Tables NIOSH protocoll

The Horizontal Multiplier, Vertical Multiplier, Distance Multiplier and Asymmetrical Multiplier (*Waters et al. 1993,1994*) are measured from the previous parameters (***Tables A.1, A.****2*).

MULTIPLIER		METRIC
Load constant	(LC)	23 kg
Horizontal Multiplier	(HM)	25/H
Vertical Multiplier	(VM)	1-(0.003|V-75|)
Distance Multiplier	(DM)	0.82+(4.5/D)
Asymmetrical Multiplier	(AM)	1-(0.0032A)
Frequency Multiplier	(FM)	*Table 4*
Coupling Multiplier	(CM)	*Table 5*

Table A.1. *Multipliers of lifting equation.*

H	HM
cm	
≤25	1.00
28	0.89
30	0.83
32	0.78
34	0.74
36	0.69
38	0.66
40	0.63
42	0.60
44	0.57
46	0.54
48	0.52
50	0.50
52	0.48
54	0.46
56	0.45
58	0.43
60	0.42
63	0.40
>63	0.00

V	VM
cm	
0	0.78
10	0.81
20	0.84
30	0.87
40	0.90
50	0.93
60	0.96
70	0.99
80	0.99
90	0.96
100	0.93
110	0.90
120	0.87
130	0.84
140	0.81
150	0.78
160	0.75
170	0.72
175	0.70
>175	0.00

D	DM
cm	
≤25	1.00
40	0.93
55	0.90
70	0.88
85	0.87
100	0.87
115	0.86
130	0.86
145	0.85
160	0.85
175	0.85
>175	0.00

A	AM
deg	
0	1.00
15	0.95
30	0.90
45	0.86
60	0.81
75	0.76
90	0.71
105	0.66
120	0.62
135	0.57
>135	0.00

Table A.2. *Horizontal, Vertical, Distance and Asymmetrical Multipliers of lifting equation.*

The Frequency Multiplier is defined by number of lifts per minute, the amount of time engaged in the lifting activity, and the vertical height of the lift from the floor. Lifting frequency (F) refers to the average number of lifts made per minute, as measured over a 15-minute period (**Table A.3**).

Frequency Lifts/min (F)	**Work Duration**					
	≤1 Hour		1<Hours≤2		2<Hours≤8	
	V<75 cm	V≥75 cm	V<75 cm	V≥75 cm	V<75 cm	V≥75 cm
≤0.2	1.00	1.00	0.95	0.95	0.85	0.85
0.5	0.97	0.97	0.92	0.92	0.81	0.81
1	0.94	0.94	0.88	0.88	0.75	0.75
2	0.91	0.91	0.84	0.84	0.65	0.65
3	0.88	0.88	0.79	0.79	0.55	0.55
4	0.84	0.84	0.72	0.72	0.45	0.45
5	0.80	0.80	0.60	0.60	0.35	0.35
6	0.75	0.75	0.50	0.50	0.27	0.27
7	0.70	0.70	0.42	0.42	0.22	0.22
8	0.60	0.60	0.35	0.35	0.18	0.18
9	0.52	0.52	0.30	0.30	0.00	0.15
10	0.45	0.45	0.26	0.26	0.00	0.13
11	0.41	0.41	0.00	0.23	0.00	0.00
12	0.37	0.37	0.00	0.21	0.00	0.00
13	0.00	0.34	0.00	0.00	0.00	0.00
14	0.00	0.31	0.00	0.00	0.00	0.00
15	0.00	0.28	0.00	0.00	0.00	0.00
>15	0.00	0.00	0.00	0.00	0.00	0.00

Table A.3. *Frequency Multiplier of lifting equation.*

Classification of the quality of the hand-to-object coupling: coupling quality is classified as good, fair, or poor. Based on the coupling classification and vertical location of the lift, the Coupling Multiplier is determined from **Table A.4** (Waters et al. 1993,1994).

Coupling Type	Coupling Multiplier	
	V<75 cm	V≥75 cm
Good	1.00	1.00
Fair	0.95	1.00
Poor	0.90	0.90

Table A.4. *Coupling Multiplier of lifting equation.*

APPENDIX B: Biomechanical evaluation during different activities

During my PhD, I collabored in the other research projects using the instrumentation and methodologies of movement analysis. From these collaborations, pubblications in 3 research areas have been obtained:

A. <u>Biomechanical analysis of subjects suffering from orthopedic diseases (subjects with amputation of the lower limbs):</u>

1) Human Movement Science: "Common and specific gait patterns in people with varying anatomical levels of lower limb amputation and different prosthetic components"; **T. Varrecchia**, M. Serrao, M. Rinaldi, A. Ranavolo, S. Conforto, C. De Marchis, A. Simonetti, I. Poni, S. Castellano, A. Silvetti, A. Tatarelli, L. Fiori, C. Conte, F. Draicchio; 2019.
2) XVIII Congresso SIAMOC Torino, 4-7 Ottobre 2017: "Analisi Cinematica del Cammino in Amputati per la Valutazione Funzionale della Stabilità Dinamica"; M. Guaitolini, C. De Marchis, M. Rinaldi, **T. Varrecchia**, G. Chini, A. Silvetti, M. Serrao, A. Ranavolo, M. Schmid, F. Draicchio, S. Conforto.
3) XVIII Congresso SIAMOC Torino, 4-7 Ottobre 2017: "Controllo motorio modulare dell'arto controlaterale nel cammino di amputati trans-femorali S. Ranaldi, C. De Marchis, M. Rinaldi, **T. Varrecchia**, A. Marchesi, A. Silvetti, M. Serrao, A. Ranavolo, M. Schmid, S. Conforto.
4) ISEK International Society of Electrophysiology and Kinesiology, University College Dublin, 29 Giugno-02 Luglio 2018 "Kinetic and kinematic patterns for prosthetic gait analysis"; S. Conforto, M. Serrao, **T. Varrecchia**, M. Rinaldi.

B. **<u>Biomechanical analysis during walking: healthy subjects and subjects suffering from neurological diseases:</u>**

1) Journal of Electromyografy and Kinesiology: "Global lower limb muscle coactivation during walking at different speeds: relationship between spatio-temporal, kinematic, kinetic, and energetic parameters"; T. Varrecchia, M. Rinaldi, M. Serrao, F. Draicchio, C. Conte, S. Conforto, M. Schmid, A. Ranavolo; 2018.
2) Clinical Biomechanics: "Increased lower limb muscle coactivation reduces gait performance and increases metabolic cost in patients with hereditary spastic paraparesis"; autori: **M. Rinaldi**, A. Ranavolo, S. Conforto, G. Martino, F. Draicchio, C. Conte, T. Varrecchia, F. Bini, C. Casali, F. Pierelli, M. Serrao; 2017.
3) PLOSONE: "Gait patterns in patients with hereditary spastic paraparesis""; M. Serrao, M. Rinaldi, A. Ranavolo, F. Lacquaniti, G. Martino, L. Leonardi, C. Conte, **T. Varrecchia**, F. Draicchio, G. Coppola, C. Casali, F. Pierelli; 2016.
4) XX Congresso SIAMOC Bologna 9-12 October 2019: "The role of trunk on human locomotion: damper, generator or perturbator?"; M. Rinaldi, **T. Varrecchia**, A. Ranavolo, F. Draicchio, S.F. Castiglia, F. Pierelli, M. Serrao.

5) XX Congresso SIAMOC Bologna 9-12 October 2019: “Artificial neural networks for staging the gait deficit in Parkinson disease”; **T. Varrecchia**, A. Ranavolo, M. Rinaldi, F. Draicchio, SF. Castiglia, F. Pierelli, C. Conte M. Serrao.
6) XX Congresso SIAMOC Bologna 9-12 October 2019: “Impairment of global lower limb muscle coactivation during walking in cerebellar ataxias”; L. Fiori, A. Ranavolo, **T. Varrecchia**, F. Draicchio, A. Tatarelli, C. Conte, C. Casali, M. Serrao.
7) XX Congresso SIAMOC Bologna 9-12 October 2019: “Gait harmonic structure of walking in patients with neurological gait disorders”; A. Tatarelli, A. Ranavolo, **T. Varrecchia**, F. Draicchio, L. Fiori, C. Conte, C. Casali, M. Iosa, M. Serrao.
8) 41st Annual International Conference of the IEEE Engineering in Medicine and Biology Society (EMBC), 2019; “Wearable-based temporal parameters of gait in circuitous routes under dual-task conditions”; C. Caramia, D. Bibbo, C. D’Anna, C. De Marchis, S. Ranaldi, **T. Varrecchia**, S. Conforto, M. Schmid.
9) ISPGR 2019 Edinburgh Scotland 30 Giugno-4 Luglio 2019; “Global lower limb coactivation during gait in patients with cerebellar ataxia”; M. Serrao, L. Fiori, **T. Varrecchia**, A. Tatarelli, A. Ranavolo, F. Draicchio, C. Conte, C. Casali.
10) XIX Congresso SIAMOC Firenze 3-6 Ottobre 2018; “Wearable sensor use for assessing walking dynamic balance in gait ataxia: comparisons between different stability indexes”; G. Chini, M. Serrao, A. Ranavolo, **T. Varrecchia**, C. Conte, C. Casali, F. Pierelli, F. Draicchio.
11) SIN XLIX Congresso SIN Roma, 27-30 Ottobre 2018: “The role of trunk in neurological gait disorders: damper, generator or perturbator?”; M. Rinaldi, M. Serrao, **T. Varrecchia**, C. Conte, A. Ranavolo, F. Draicchio, C. Casali, F. Pierelli.
12) SIN XLIX Congresso SIN Roma, 27-30 Ottobre 2018: “Global lower limb co-activation in patients with cerebellar ataxia”; **T. Varrecchia**, M. Serrao, L. Fiori, M. Rinaldi, A. Ranavolo, C. Conte, F. Draicchio, C. Casali, F. Pierelli.
13) SIN XLIX Congresso SIN Roma, 27-30 Ottobre 2018: “Gait harmonic structure of walking in patients with neurological gait disorders”; **T. Varrecchia**, M. Serrao, A. Tatarelli, M. Rinaldi, C. Conte, A. Ranavolo, F. Draicchio, C. Casali, F. Pierelli.
14) 48° Congresso SIN Napoli, 14-17 Ottobre 2017: “Predictors of gait improvement in patients with Parkinson's disease after rehabilitation”; G. Chini, M. Serrao, G. Caramanico, M. Rinaldi, **T. Varrecchia**, C. Conte, E. Sinibaldi, G. Monari, F. Pierelli.
15) 48° Congresso SIN Napoli, 14-17 Ottobre 2017: “Increased lower limb muscle coactivation and its relationship with gait performance and metabolic cost in patients with hereditary spastic paraparesis”; M. Rinaldi, M. Serrao, A. Ranavolo, C. Conte, **T. Varrecchia**, G. Chini, C. Casali, F. Pierelli.
16) 48° Congresso SIN Napoli, 14-17 Ottobre 2017: “Trunk-lower limb coordination pattern during gait in patients with ataxia”; C. Conte, P. Caliandro, C. Iacovelli, C. Casali, A. Ranavolo, G. Chini, M. Rinaldi, **T. Varrecchia**, L. Padua, F. Pierelli, M. Serrao.

C. <u>Degenerative diseases: return-to-work process:</u>

1) Cerebellum: “The working life of people with degenerative cerebellar ataxia”; A. Ranavolo, M. Serrao, T. Varrecchia, C. Casali, A. Filla, A. Roca, A. Silvetti, C. Marcotulli, B. M. Rondinone, S. Iavicoli, F. Draicchio; 2019.
2) 48° Congresso SIN Napoli, 14-17 Ottobre 2017: “The working life of people with degenerative cerebellar ataxia”; **T. Varrecchia**, A. Ranavolo, C. Casali, A. Filla, A. Silvetti, F. Pirelli, M. Rinaldi, C. Conte, G. Chini, A. Roca, C. Marcotulli, F. Draicchio, M. Serrao.

D. **Biomechanical analysis in the sport:**

1) European Journal of Sport Science: “Biomechanical characterization of the Junzuki karate punch: indexes of performance”; M. Rinaldi, Y. Nasr, G. Atef, F. Bini, T. Varrecchia, C. Conte, G. Chini, A. Ranavolo, F. Draicchio, F. Pierelli, M. Amin, F. Marinozzi, M. Serrao; 2018.